

# The Mechanics of Soils

An Introduction to Critical State  
Soil Mechanics

J. H. ATKINSON

*Department of Civil Engineering  
The City University, London*

P. L. BRANSBY

*Head, Materials Handling Division  
Warren Spring Laboratory*

**A.I.T. LIBRARY**

Thư viện tiếng Anh  
J. H. Atkinson



The English Language Book Society

**Some other ELBS low-priced editions**

Anderson, Leaver Alexander and Rawlings	<b>MATERIALS SCIENCE</b>	<i>Nelson</i>
Bishop and Henkel	<b>THE MEASUREMENT OF SOIL PROPERTIES IN THE TRIAxIAL TEST</b>	<i>Edward Arnold</i>
Blyth and de Freitas	<b>A GEOLOGY FOR ENGINEERS</b>	<i>Edward Arnold</i>
Case and Chilver	<b>STRENGTH OF MATERIALS AND STRUCTURES</b>	<i>Edward Arnold</i>
Chudley	<b>CONSTRUCTION TECHNOLOGY</b>	<i>Longman</i>
Coates, Coutie and Kong	<b>STRUCTURAL ANALYSIS</b>	<i>Nelson</i>
Craig	<b>SOIL MECHANICS</b>	<i>Van Nostrand Reinhold (U.K.)</i>
Duffin	<b>ELECTRICITY AND MAGNETISM</b>	<i>McGraw-Hill</i>
Fox and Mayers	<b>COMPUTING METHODS FOR SCIENTISTS AND ENGINEERS</b>	<i>Oxford University Press</i>
Jackson	<b>CIVIL ENGINEERING MATERIALS</b>	<i>Macmillan</i>
John	<b>INTRODUCTION TO ENGINEERING MATERIALS</b>	<i>Macmillan</i>
Kong and Evans	<b>REINFORCED AND PRESTRESSED CONCRETE</b>	<i>Nelson</i>
Lauder	<b>FOUNDATIONS</b>	<i>Macmillan</i>
Marshall and Nelson	<b>STRUCTURES</b>	<i>Pitman</i>
Neville	<b>PROPERTIES OF CONCRETE</b>	<i>Pitman</i>
Ryder	<b>STRENGTH OF MATERIALS</b>	<i>Macmillan</i>
Simons and Menzies	<b>A SHORT COURSE IN FOUNDATION ENGINEERING</b>	<i>Newnes-Butterworths</i>
Smith	<b>SOIL MECHANICS</b>	<i>George Godwin</i>
Todd	<b>STRUCTURAL THEORY AND ANALYSIS</b>	<i>Macmillan</i>
Tomlinson	<b>FOUNDATION DESIGN AND CONSTRUCTION</b>	<i>Pitman</i>

**Published by:**

**McGRAW-HILL Book Company (UK) Limited  
MAIDENHEAD · BERKSHIRE · ENGLAND**

**ISBN 07 084135 7**

**ELBS edition first published 1982**

**Copyright © 1978 McGraw-Hill Book Company (UK) Limited.  
All rights reserved. No part of this publication may be  
reproduced, stored in a retrieval system, or transmitted,  
in any form or by any means, electronic, mechanical,  
photocopying, recording, or otherwise, without the prior  
permission of McGraw-Hill Book Company (UK) Limited**

**PRINTED AND BOUND IN GREAT BRITAIN**

*To the Cambridge Soil Mechanics Group*



# CONTENTS

---

<b>Preface</b>	xiii
<b>Glossary of Symbols</b>	xv
<b>A Note on Units</b>	xix
<b>Chapter 1. An Introduction to Engineering Soils</b>	1
1-1 Introduction	1
1-2 Engineering materials and their behaviour	1
1-3 The meaning of 'engineering soil'	2
1-4 The occurrence of natural soils	3
1-5 Soil particle sizes, shapes, and gradings	4
1-6 Surface effects	5
1-7 Some basic relationships for soil	7
1-8 Specific volumes of sands and clays	10
1-9 Soil classification tests	10
1-10 Measurement of unit weight and water content	11
1-11 Measurement of particle size distribution	12
1-12 The Atterberg limit tests	12
1-13 Summary	14
<b>Chapter 2. Stresses and Strains in Soils</b>	15
2-1 Introduction	15
2-2 Normal stress and strain	15
2-3 Shear stress and strain	15
2-4 Soil as a continuum	18
2-5 Pore pressure and total stress	18
2-6 The principle of effective stress	20
2-7 The significance of effective stress	21
2-8 Examinations of the principle of effective stress	25
2-9 Discussion of the principle of effective stress	25
2-10 Increments of stress and strain	26
2-11 Summary	26
<b>Chapter 3. States of Stress and Strain in Soils</b>	28
3-1 Introduction	28
3-2 Two-dimensional states of stress	28
3-3 Mohr's circle of stress	29
3-4 Principal stresses and principal planes	30
3-5 Mohr's circles of total and effective stress	33

3-6	Two-dimensional states of strain – Plane strain	35
3-7	General plane strain deformations	35
3-8	Normal and shear strain	37
3-9	Representation of a state of strain	38
3-10	Pure shear strain and engineers' shear strain	38
3-11	Mohr's circle of strain	39
3-12	Principal planes and principal strains	41
3-13	Mohr's circles for increments of stress and strain	43
3-14	Relationships between states of stress and states of strain	43
3-15	Summary	44
<b>Chapter 4. Stress and Strain Paths and Invariants</b>		<b>45</b>
4-1	Introduction	45
4-2	Stress paths	45
4-3	Stress paths with $\sigma'_1:\sigma'_3$ and $\sigma_1:\sigma_3$ axes	47
4-4	Stress paths with $t':s'$ and $t:s$ axes	49
4-5	Invariants of stress	52
4-6	Stress paths with $q':p'$ or $q:p$ axes	54
4-7	Invariants of strain	56
4-8	Strain paths	57
4-9	Volumetric strains	59
4-10	Correspondence between parameters for stress and strain	61
4-11	Stress-strain behaviour of an ideal elastic soil	62
4-12	Summary	65
<b>Chapter 5. Laboratory Testing of Soils</b>		<b>67</b>
5-1	Introduction	67
5-2	Requirements of soil loading tests	67
5-3	Boundary conditions	68
5-4	Control of loading	70
5-5	Control of pore pressure and drainage	70
5-6	Classification of soil tests	71
5-7	The triaxial apparatus	74
5-8	The oedometer	80
5-9	The direct shear box	81
5-10	The simple shear apparatus	83
5-11	Summary	85
<b>Chapter 6. Flow of Water in Soils</b>		<b>86</b>
6-1	Introduction	86
6-2	Pore pressure and potential	87
6-3	Seepage velocity	88
6-4	Hydraulic gradient	90
6-5	Darcy's law	93
6-6	Seepage forces	94
6-7	Critical hydraulic gradient for vertical upward flow	95
6-8	Flow net for one-dimensional seepage	96

6-9	Two-dimensional seepage	99
6-10	Potential function $\Phi(x, z)$	101
6-11	Flow function $\Psi(x, z)$	101
6-12	Rate of flow through a flownet	102
6-13	'Square' flownets'	103
6-14	Boundary conditions	105
6-15	Construction of flownets by sketching	106
6-16	Other methods of solution	109
6-17	Seepage through anisotropic, layered, and non-uniform soils	110
6-18	Seepage through layered strata	110
6-19	Seepage through anisotropic soils	113
6-20	Seepage across a boundary between two soils	114
6-2i	Summary	116
<b>Chapter 7. Compression</b>		<b>118</b>
7-1	Introduction	118
7-2	Compression and consolidation – A simple model	118
7-3	Isotropic compression test	122
7-4	Back pressure	124
7-5	Secondary compression – Creep	124
7-6	Isotropic compression of clay	125
7-7	An idealization of isotropic compression of clay	125
7-8	Overconsolidation	127
7-9	Possible states of isotropic compression	128
7-10	Mathematical representation of isotropic compression	129
7-11	Isotropic compression of sand	132
7-12	One-dimensional compression – The oedometer test	134
7-13	Variation of $K_0$ in oedometer tests	136
7-14	One-dimensional compression of clay	136
7-15	One-dimensional and isotropic compression of clay	138
7-16	Coefficient of volume compressibility $m_v$	142
7-17	Compression index $C_C$ and swelling index $C_S$	142
7-18'	Summary	143
<b>Chapter 8. One-dimensional Consolidation</b>		<b>145</b>
8-1	Introduction	145
8-2	Theory of one-dimensional consolidation	145
8-3	Isochrones	147
8-4	Boundary conditions for one-dimensional consolidation	150
8-5	Time factor $T_v$	150
8-6	Average degree of consolidation $U_v$	150
8-7	Approximate solution for one-dimensional consolidation by parabolic isochrones	152
8-8	The exact solution for one-dimensional consolidation	157
8-9	Determination of $c_v$ from an oedometer test	160
8-10	Summary	166



**x CONTENTS**

<b>Chapter 9. Shear Testing</b>	<b>167</b>
9-1 Introduction	167
9-2 Shear testing apparatus	167
9-3 Simple tests in the triaxial apparatus	172
9-4 Typical test results	175
9-5 Patterns of behaviour; summary of main points	182
<b>Chapter 10. The Critical State Line and the Roscoe Surface</b>	<b>184</b>
10-1 Introduction	184
10-2 Families of undrained tests	184
10-3 Families of drained tests	185
10-4 The critical state line	189
10-5 'Drained' and 'undrained' planes	191
10-6 The Roscoe surface	196
10-7 The shape of the Roscoe surface	201
10-8 The Roscoe surface as a state boundary surface	206
10-9 Summary	208
<b>Chapter 11. The Behaviour of Overconsolidated Samples: The Hvorslev Surface</b>	<b>210</b>
11-1 Introduction	210
11-2 Drained tests	210
11-3 The Hvorslev surface	212
11-4 The critical state line	217
11-5 The complete state boundary surface	221
11-6 Volume changes and pore water pressure changes	228
11-7 Summary	233
<b>Chapter 12. The Behaviour of Sands</b>	<b>235</b>
12-1 Introduction	235
12-2 The critical state line for sand	238
12-3 Normalized plots	244
12-4 The effect of dilation	251
12-5 Consequences of Taylor's model	255
12-6 Summary	262
<b>Chapter 13. Behaviour of Soils Before Failure</b>	<b>263</b>
13-1 Introduction	263
13-2 Elastic and plastic deformations: the elastic wall	263
13-3 Calculation of elastic strains	266
13-4 Calculation of elastic strains for undrained loading in terms of total stresses	271
13-5 Essential plasticity theory	274
13-6 Plasticity for soils	278
13-7 Cam-clay	283
13-8 Summary	291

<b>Chapter 14. Routine Soil Tests and the Critical State Model</b>	<b>292</b>
14-1 Introduction	292
14-2 The Mohr-Coulomb failure criterion	292
14-3 One-dimensional compression	299
14-4 Undrained shear strength	304
14-5 General stress states	310
14-6 Pore pressure parameters for undrained loading	324
14-7 Variation of $c_u$ with depth	329
14-8 Interpretation of the index tests	336
14-9 Summary	342
<b>Chapter 15. Soil Parameters for Design</b>	<b>344</b>
15-1 Introduction	344
15-2 Choice of analysis methods	344
15-3 Choice of strength parameters	351
15-4 Wet and dry states	354
15-5 Residual strength	362
15-6 Material idealizations	362
15-7 The stress path method	364
15-8 Summary	366
<b>Chapter 16. Concluding Remarks</b>	<b>367</b>
<b>Index</b>	<b>369</b>

## CONSULTING EDITORS' FOREWORD

---

McGraw-Hill's *University Series in Civil Engineering* has been planned to make available to students and lecturers a number of textbooks that reflect the philosophy of the Consulting Editors and the Company, namely that the emphasis of engineering degree courses should be on the fundamental principles. Therefore, the primary aim of the books in the Series is to develop a sound understanding of the subject matters and an ability to apply the relevant scientific principles to the solution of engineering problems. Where familiarity with a Code of Practice or an empirical method is desirable, the technical background is explained, so that the student understands the *why* as well as the *what* and the *how* of the subject.

*The Mechanics of Soils*, by Atkinson and Bransby, is the first book in the Series. It explains in simple terms the theories of critical state soil mechanics and conveys a fundamental understanding of the mechanical behaviour of soils. It brings together in a unified manner much of what previously exists only in the form of lecture notes or technical papers, and serves also as a useful introduction to Schofield and Wroth's *Critical State Soil Mechanics*, published earlier by McGraw-Hill.

The Consulting Editors wish to thank their colleagues in the universities and industry for their valuable advice concerning the development of the Series. In particular, they wish to record the exemplary care and attention devoted to the Series by McGraw-Hill's Editor Stephen Wellings and his predecessor Ian Pringle.

F. K. KONG and R. H. EVANS

## PREFACE

---

This book is about the mechanical behaviour of soil when it is compressed, sheared, or when water flows through it. It covers the first half of the essential soil mechanics content of a degree course in civil engineering.

The book is based on material taught in undergraduate courses at Cambridge University for the past decade and this material in turn flows from fundamental research into theories of soil behaviour which has been in progress in Cambridge and elsewhere for over twenty years. The book concentrates on the mechanical behaviour of saturated soils; it does not cover the practical aspects of geotechnical engineering. Although the book is primarily aimed at students taking first degree courses in civil engineering, it should also appeal to postgraduate students wishing for a simple introduction to recent work on the stress-strain behaviour of soils.

Ours is a modern approach to soil mechanics, and our purpose in this book is to convey a fundamental understanding of the mechanical behaviour of soil. Our treatment is intended to be simple and essentially non-mathematical, and we develop our ideas of soil behaviour by observing the response of clay and sand soils to loading in laboratory tests. We believe that our approach to soil behaviour through the theories of critical state soil mechanics not only provides a simple and logical method of teaching the subject, but also forms the basis of rational design methods. Although the discussion of soil behaviour is developed against a critical state framework, we draw into our discussions at appropriate points the ideas of the Mohr-Coulomb strength and Terzaghi consolidation theories familiar in classical soil mechanics.

We are conscious that we have drawn a bold picture using a broad brush and perhaps a few of our interpretations may be controversial. Our concern, however, is to develop a simple framework of ideas within which we may view the mechanical behaviour of soil under a wide range of states of compression and shear. To do so we must make bold generalizations and we must accept that modifications of detail may be necessary to account for particular soil conditions found in nature. Our generalizations are of the kind familiar to engineers: for example, civil engineers are used to assuming that steel is an ideal elasto-plastic material or that concrete cannot sustain tensile stress.

As the book develops we will find that the concepts of consolidation, compression, yielding, and failure of soils can be drawn together into a single unifying framework. It is this unification of ideas which is the cornerstone of the critical state theories and which provides the foundation for a proper

understanding of soil behaviour. We hope that by adopting an essentially non-mathematical approach we are able to convey clearly the underlying simplicity of soil behaviour.

The first five chapters of the book introduce basic ideas concerning the nature of soil, states of stress and strain in soil, and laboratory testing techniques. The topics of seepage, compression, and consolidation are introduced in Chapters 6–8 and an extended discussion is given of the shear behaviour of clays and sands in Chapters 9–12. A distinction is made between elastic and plastic strains in Chapter 13, and a simple introduction given to the Cam-clay stress–strain theory for soil. This Chapter is intended as a link between this book and *Critical State Soil Mechanics* by Schofield and Wroth which includes a detailed mathematical treatment of the Cam-clay theory. The ideas discussed in Chapters 10–13 are related to routine testing and design in Chapters 14 and 15. The book closes with Chapter 16 which is intended, very briefly, to relate the topics discussed both to engineering practice and to current research work.

We assume that our readers are familiar with the basic principles of the mechanics of deformable bodies (including simple elasticity and plasticity theory), and the analysis of states of stress and strain using the Mohr's circle method. We assume also that, as part of an undergraduate course in soil mechanics, a student will have the opportunity of performing standard laboratory tests such as permeameter, shear box, triaxial, and oedometer tests, and determination of the Atterberg limits and gradings of soil samples.

We have adopted a nomenclature similar to that in *Critical State Soil Mechanics* by Schofield and Wroth, but with minor differences. In particular, we have used the name 'Roscoe surface' for the state boundary surface on the wet side of critical corresponding to the 'Hvorslev surface' on the dry side. This nomenclature follows standard usage in powder technology and acknowledges the part played by K. H. Roscoe and his colleagues A. N. Schofield and C. P. Wroth in extending the classic work of Rendulic and of Henkel.

We wish to acknowledge that the research which led to the theory of critical state soil mechanics was carried out by others and in particular by the late Professor K. H. Roscoe and his students and colleagues in the University Engineering Department, Cambridge. We consider ourselves fortunate to have been members of the Cambridge Soil Mechanics Group. We are grateful to all those, in Cambridge and elsewhere, with whom we have discussed the behaviour of soils and who have helped to clarify our ideas. We are particularly grateful to Dr C. P. Wroth, to Dr D. M. Wood, and to Dr D. M. Potts for reading and criticizing parts of our book and to Ruth Stock for typing our manuscripts. We, however, not they, are responsible for what is written.

March 1977

J. H. ATKINSON  
P. L. BRANSBY

## GLOSSARY OF SYMBOLS

---

$A$	activity
$A$	area
$A, B$	Skempton's pore pressure parameters
$B$	width or breadth
$C_U$	compression index
$C_S$	swelling index
$D_r$	relative density
$E'$	Young's modulus in terms of effective stresses
$E_u$	Young's modulus for undrained loading in terms of total stresses
$F$	force
$F_N$	normal force
$F_S$	shear force
$G'$	elastic shear modulus
$G_s$	specific gravity of soil grains
$H$	height, thickness
$H$	maximum drainage path
$K'$	elastic bulk modulus
$K'_s$	bulk modulus of soil
$K'_w$	bulk modulus of water
$K_0$	coefficient of earth pressure at rest
$LL$	liquid limit
$LI$	liquidity index
$N_d$	number of potential drops
$N_f$	number of flow channels
$P$	potential
$PL$	plastic limit
$PI$	plasticity index
$Q$	seepage flow (volume)
$Q$	force (on a footing)
$R_0$	overconsolidation ratio for one-dimensional compression
$R_p$	overconsolidation ratio for isotropic compression
$T_v$	time factor
$U_i$	average degree of consolidation
$V$	artificial velocity (of seepage flow)
$V_s$	seepage velocity
$V$	volume
$V_w$	volume of water
$V_s$	volume of soil grains

271 GLOSSARY OF SYMBOLS

- $W$  work  
 $W$  weight  
 $W_s$  weight of soil grains  
 $W_w$  weight of water  
 $Z$  depth below ground surface
- $a = [\sqrt{(10)/3}]q'$ , distance up the drained plane from  $q' = 0$   
 $a, b$  pore pressure parameters
- $a$  }  
 $b$  } coordinate axes ( $a =$  axial)  
 $c$  }
- $b$  width or breadth  
 $c'$  cohesion  
 $c_u$  undrained shear strength  
 $c_v$  coefficient of consolidation  
 $d$  differential operator  
 $e$  voids ratio
- $g$  }  
 $h$  } soil constants defining the Hvorslev surface
- $h$  (subscript) horizontal  
 $h$  height of water in a standpipe  
 $i$  hydraulic gradient  
 $i_0$  critical hydraulic gradient  
 $k$  coefficient of permeability  
 $\ln$  natural logarithm  
 $m_v$  coefficient of compressibility for one-dimensional compression  
 $n$  porosity  
 $p' = \frac{1}{3}(\sigma'_1 + \sigma'_2 + \sigma'_3)$   
 $p'_0$  equivalent pressure: value of  $p'$  at the point on the normal consolidation line at the same specific volume  
 $p'_0$  value of  $p'$  at the start of a drained test  
 $p'_t$  value of  $p'$  at failure  
 $p'_u$  value of  $p'$  at the point on the critical state line at the same specific volume
- $p = \frac{1}{3}(\sigma_1 + 2\sigma_2)$  }  
 $q = (\sigma_1 - \sigma_3)$  } stress parameters for  $\sigma_2 = \sigma_3$   
 $q' = (\sigma'_1 - \sigma'_3)$   
 $q'_t = (\sigma'_1 - \sigma'_3)_t$ , value of  $q'$  at failure  
 $q_u = q_t$  for undrained loading  
 $q$  flow rate  
 $r$  (subscript) residual ( $c'_r, \phi'_r$ )  
 $r$  (subscript) radial  
 $s$  length along a flowline  
 $s$  slope of an isochrone

- $s = \frac{1}{2}(\sigma_1 + \sigma_3)$   
 $t = \frac{1}{2}(\sigma_1 - \sigma_3)$  } stress parameters for plane strain  
 $s' = \frac{1}{2}(\sigma'_1 + \sigma'_3)$   
 $t' = \frac{1}{2}(\sigma'_1 - \sigma'_3)$   
*t* time  
*u* pore pressure  
 $u_t$  pore pressure at failure  
 $u_0$  steady-state pore pressure  
 $u_b$  back pressure  
 $\bar{u}$  excess pore pressure  
*v* (subscript) vertical  
*v* specific volume  
 $v_0$  initial specific volume  
 $v_t$  specific volume at failure  
 $v_x$  specific volume of isotropically overconsolidated soil swelled to  $p' = 1.0 \text{ kN m}^{-2}$   
 $v_{x_0}$  specific volume of one-dimensionally overconsolidated soil swelled to  $p' = 1.0 \text{ kN m}^{-2}$   
 $v_\lambda = v + \lambda \ln p'$ , specific volume on reference section  
 $v_{\lambda_0} = v_0 + \lambda \ln p'_0$ , value of  $v_\lambda$  at the start of loading  
*w* water content  
*w* width (of a footing)  
 $\left. \begin{array}{l} x \\ y \\ z \end{array} \right\}$  coordinate axes ( $z = \text{vertical}$ )  
 $\sigma'$  effective stress (e.g.  $\sigma'$ )  
 $\Gamma$  specific volume of soil at critical state with  $p' = 1.0 \text{ kN m}^{-2}$   
 $\Delta$  large increment of . . .  
*M* slope of critical state line when it is projected on to a constant volume plane  
 $M_0$  value of *M* for triaxial compression tests  
 $M_0$  value of *M* for triaxial extension tests  
*N* specific volume of isotropically normally consolidated soil at  $p' = 1.0 \text{ kN m}^{-2}$   
 $\Sigma$  sum of . . .  
 $\Phi$  potential function  
 $\Psi$  flow function  
 $\alpha$  angle  
 $\gamma$  engineers' shear strain  
 $\gamma$  unit weight  
 $\gamma_d$  dry unit weight  
 $\gamma_w$  unit weight of water  
 $\delta$  small increment of . . .



xviii GLOSSARY OF SYMBOLS

- $\varepsilon$  strain
- $\varepsilon_v = (\varepsilon_1 + \varepsilon_2 + \varepsilon_3)$ , volumetric strain
- $\varepsilon_s = \frac{2}{3}(\varepsilon_1 - \varepsilon_3)$ , shear strain for  $\varepsilon_2 = \varepsilon_3$
- $\varepsilon_y = (\varepsilon_1 - \varepsilon_2)$ , shear strain for plane strain
- $\theta$  angle
- $\kappa$  slope of overconsolidation line (negative)
- $\lambda$  slope of normal consolidation line (negative)
- $\mu$  coefficient of friction
- $\nu'$  Poisson's ratio
- $\nu'_u (= 0.5)$ , Poisson's ratio for constant volume (undrained) loading
- $\rho$  settlement
- $\sigma$  normal stress
- $\sigma_n$  normal stress
- $\sigma_{oct}$  octahedral normal stress
- $\sigma'_s$  seepage stress
- $\tau$  shear stress
- $\tau_{oct}$  octahedral shear stress
- $\phi'$  angle of internal friction
- $\phi'_o, \phi'_c$  angle of internal friction for triaxial extension and compression tests, respectively

## A NOTE ON UNITS

The S.I. system of units has been used throughout this book. The basic units of measurement are:

length m (metre),  
time s (second),  
force N (Newton);

multiples

kilo =  $10^3$ , e.g. kiloNewton, 1 kN =  $10^3$  N,  
mega =  $10^6$ , e.g. megaNewton, 1 MN =  $10^6$  N.

Some useful derived units are:

velocity  $\text{m s}^{-1}$ ,  
acceleration  $\text{m s}^{-2}$ ,  
stress or pressure  $\text{kN m}^{-2}$ ,  
unit weight  $\text{kN m}^{-3}$ .

Unit force (1 N) gives unit mass (1 kg) unit acceleration ( $1 \text{ m s}^{-2}$ ). The acceleration due to Earth's gravity is  $g = 9.81 \text{ m s}^{-2}$ ; hence, the force due to a mass of 1 kg at rest on Earth is 9.81 N.

Conversions from Imperial units:

1 ft = 0.3048 m,  
1 lbf = 4.448 N,  
1  $\text{lb}_f \text{ in}^{-2}$  = 6.895  $\text{kN m}^{-2}$ ,  
1  $\text{lb}_f \text{ ft}^{-3}$  = 0.157  $\text{kN m}^{-3}$ .



## AN INTRODUCTION TO ENGINEERING SOILS

### 1-1 INTRODUCTION

As a civil engineering material, soil is just as important as steel and concrete. It may be dug into, heaped up, or spread out in the construction of civil engineering works. All man made structures, except those which float or fly, are supported by natural soil or rock deposits, and many civil engineering structures, such as water-retaining banks, roads, and airfield pavements, are constructed from soil and rock materials.

Civil engineers are concerned with the design and construction of civil engineering works and are obliged to perform calculations which demonstrate the safety and serviceability of any new structure. But, before these calculations can be performed, the mechanical behaviour of engineering materials such as steel, concrete, and soil must be understood.

This book is concerned with the mechanical behaviour of engineering soils when they are sheared or compressed or when water flows through them. There are topics in soil mechanics that are relevant to allied subjects, for example, the strength of soil and the stability of soil slopes are of interest in geomorphology and theories of soil deformation and flow relate to the discharge of granular materials from storage bunkers and to materials handling. Consequently, although this book is written primarily from the point of view of the civil engineer concerned with the design of soil structures, there may be parts that are of interest to others.

### 1-2 ENGINEERING MATERIALS AND THEIR BEHAVIOUR

Engineering structures are required to support loads safely. These loads may be applied externally or they may be due to the weight of the structure itself. No material is perfectly rigid and any change in the loading must produce deflections and distortions in the structure; this is as true of a small machine component as it is of a large civil engineering structure. Engineering involves assessing the possibility of collapse and the deflections and distortions of the structure in service. The necessary links between load and stability and between load and distortion are usually found using physical

## 2 THE MECHANICS OF SOILS

theories for the mechanical behaviour of the materials in the structure and a knowledge of its geometry.

A physical theory for material behaviour, whether it be for soil, steel, concrete, foam rubber, sailcloth, or whatever, must describe adequately all the relevant aspects of the mechanical behaviour of the material and it must be arranged in such a way that real engineering problems may be solved. Since real materials do not behave in a simple way, it is usually fruitless to attempt to obtain a physical theory for material behaviour that is, at the same time, simple and exact; this is certainly true for soil. What we must aim for is a physical theory for the mechanical behaviour of soil which balances simplicity and truth; with a satisfactory physical theory engineering calculations are reasonably straightforward and the results of these calculations are sufficiently accurate for the particular purpose for which they are intended.†

The major objective of this book is to present physical theories which describe different aspects of soil behaviour. These theories are, of necessity, idealizations of the behaviour of the wide variety of soils met in civil engineering practice. Nevertheless, these physical theories are sufficiently accurate for many engineering purposes and for many soils; refinements and modifications can be incorporated into the theories to allow for special applications or for soils whose behaviour is not typical. The physical theories discussed in this book form the basis on which experienced engineers will superimpose their judgement, and so these theories must be well understood.

### 1-3 THE MEANING OF 'ENGINEERING SOIL'

Many people reserve the word 'soil' for the relatively thin surface covering capable of supporting plant life; to a civil engineer this material is known as topsoil and in many cases it is removed before any engineering work is started. Consequently it will be as well, at the outset, to define what is meant by an 'engineering soil' and, in particular, to distinguish between soil and rock.

For a definition of an engineering soil we may quote from Terzaghi and Peck (1948, p. 4):

Soil is a natural aggregate of mineral grains that can be separated by such gentle mechanical means as agitation in water. Rock, on the other hand, is a natural aggregate of minerals connected by strong and permanent cohesive forces. Since the terms 'strong' and 'permanent' are subject to different interpretations the boundary between soil and rock is necessarily an arbitrary one.

† The point is elaborated by Calladine (1969, pp. 5-10).

or from R. F. Scott (1963, p. 1):

In its most general sense, soil refers to the unaggregated or uncemented granular material consisting of both mineral and organic particles; . . . . In many materials classified by engineers as soils, cementing between grains may exist to some slight degree and therefore may contribute to the mechanical characteristics of the granular mass. This cementation should not be such as to cause the granular material to assume a hard, rocklike form, however, if the substance is to be classified as soil . . . .

These definitions are quite satisfactory as far as they go but they deal only with the composition of the solid part of soil and we must consider as well the fluid filling the pore spaces between the mineral grains. We will discover that the pressure in the pore fluid, which we will call the pore pressure, has a very important influence on the mechanical behaviour of soil. The pore fluid may be water or gas such as air or water vapour or a combination of these; if the pore spaces are completely filled with water the soil is known as *saturated*. In nature, the level of water in the ground is often close to the surface and, hence, most engineering soils are saturated, at least in temperate zones.

Throughout this book, unless we specifically state otherwise, we will consider only *saturated soils*.

#### 1-4 THE OCCURRENCE OF NATURAL SOILS

The natural cycle of weathering of the Earth's crust by mechanical or chemical agents, erosion, transportation, deposition, and compression by later sediments has been appreciated by geologists for many years (e.g., Holmes, 1965). The remainder of the cycle, that of loss of crustal material to the mantle and supply of fresh mantle material to the crust, has recently been explained by continental drift and plate tectonics (e.g., Hallam, 1973). That part of the geological cycle which includes weathering, deposition, and, up to a point, compression leads to the formation of engineering soils.

Under large compressions due to great depths of overlying sediment, soils may be altered to become what are known as rocks in the engineering sense; on the other hand, near to the Earth's surface rocks may weather *in situ* to form engineering soils. Most texts on soil mechanics and engineering geology discuss the place of soil in the geological cycle and deal with the formation of soils by deposition and compression of eroded rock or by the weathering of rock *in situ*.

Civil engineers may be concerned with naturally occurring soils in the design of slopes and foundations or may excavate and rework soils during construction of an embankment. In any case, whether the soil is undisturbed or reworked, the civil engineer will be concerned with the engineering behaviour of an uncemented, or only slightly cemented, aggregate of mineral grains with water contained in the pore spaces.

Since soils are formed by the weathering of rocks, the soil grains will consist of the basic rock-forming minerals or their products after chemical alteration. If rocks are only physically degraded by the motion of ice, water, or air, the soil grains will have the same composition as the parent rock; the size, shape, and texture of the mineral grains will depend primarily on the history of degradation, transportation, and deposition. When chemical changes occur, the basic rock-forming minerals may be changed to the clay minerals, of which the common ones are kaolinite, illite, and montmorillonite. The precise products of chemical alteration of soils and rocks depend more on the local conditions of climate and drainage than on the mineral composition of the parent rock. The physics and chemistry of the clay minerals and their importance in the manufacture of ceramics and in other common applications are covered in texts on clay mineralogy (e.g., Grim, 1962). For engineering purposes, the presence of only relatively small quantities of clay in a soil may have a substantial effect on its behaviour.

Engineers are concerned more with the mechanical behaviour of masses of soil than with the microscopic properties of individual grains; the chemical nature of the soil grains will not, therefore, be considered here. We shall, however, examine the range and variation of particle sizes and the effects of surface forces between grains on the behaviour of soil masses.

### 1-5 SOIL PARTICLE SIZES, SHAPES, AND GRADINGS

The range of particle sizes in engineering soils is very large. Several systems for the classification of particle sizes exist in current use; these are all basically similar and differ only in detail. The system proposed by the Massachusetts Institute of Technology and adopted in Britain and in the United States of America is shown in Table 1-1. As a general guide, individual sand-sized and coarser particles are visible to the naked eye, individual silt-sized particles are visible through an optical microscope, but not with the naked eye, while individual clay-sized particles can be seen only with electron microscopes.

Particle shapes differ considerably. Clay particles occur as very thin plates (perhaps only a few molecules thick) while silt, sand, and coarse-grained particles are more rotund.

It is important to appreciate that in the classification of particle sizes the words 'sand', 'silt', etc., are used to describe a particular range of particle sizes. However, a soil which is described as 'sand' may also contain lesser quantities of gravel, silt, and clay-sized particles. The distribution of particle sizes in a soil sample is conveniently shown as a grading curve on a particle size distribution chart; grading curves are usually S-shaped, as indicated in Fig. 1-1 which shows the grading curves for some typical engineering soils.

If the grading curve is flat and the soil sample contains a wide variety of

**Table 1-1 Particle size classification  
(after BS 1377 : 1975)**

Description	Diameter (mm)
Cobbles	> 60
Gravel	
Coarse	60-20
Medium	20-6
Fine	6-2
Sand	
Coarse	2-0.6
Medium	0.6-0.2
Fine	0.2-0.06
Silt	
Coarse	0.06-0.02
Medium	0.02-0.006
Fine	0.006-0.002
Clay	< 0.002

particle sizes the soil is known as *well graded*; if the curve is steep and one size predominates the soil is *poorly graded*.

The grading of a soil often reflects its origin. Soils deposited by rivers or by wind tend to be poorly graded while boulder clays and glacial tills deposited by ice tend to be well graded with a wide distribution of sizes.

## 1-6 SURFACE EFFECTS

The surface of a soil grain carries a negative electrical charge the intensity of which depends on the particular soil mineral and which may be modified by the presence of an electrolyte in the pore water. These surface charges give rise to interparticle forces in addition to those due to the self weight of the soil grains. For a given mineral and electrolyte, the magnitudes of the surface forces are proportional to the surface areas of the grains while the self weight forces are proportional to the volumes of the grains.

As particle sizes decrease, surface forces diminish with the square of the effective particle diameter whereas self weight forces diminish with the cube; consequently, the effects of surface forces are relatively more important in fine-grained than in coarse-grained soils.

For a given soil with a given pore water electrolyte, the relative importance of the surface forces may be described by the specific area of the soil. The specific area is defined as the total surface area of all grains in unit mass of soil. Table 1-2 lists typical values for the specific surface of the three common



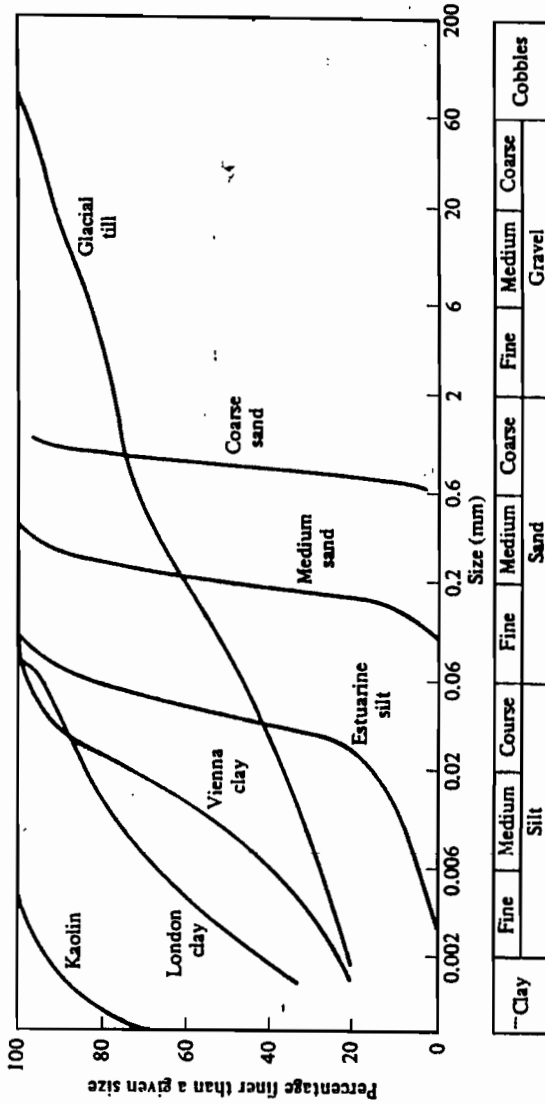


Figure 1-1 Grading curves plotted on a particle size distribution chart (after BS 1377 : 1975)

**Table 1-2 Approximate values for the specific surface of some common soil grains (after Mitchell, 1976)**

Soil grain	Specific surface (m <sup>2</sup> /g)
Clay minerals	
Montmorillonite	Up to 840
Illite	65-200
Kaolinite	10-20
Clean sand	~ 2 × 10 <sup>-4</sup>

clay minerals and of clean sand; the differences in the values of specific surface for sand and clay are very large. For engineering purposes the effects of surface forces in sands are negligible, but in clays they may play an important part in the behaviour of a soil mass.

## 1-7 SOME BASIC RELATIONSHIPS FOR SOIL

Many important mechanical properties of a soil – such as unit weight, strength, compressibility, and permeability – depend on the closeness of the packing of the mineral grains. The packing of the grains may be measured by the *voids ratio*, the ratio of the volumes of the void spaces and the mineral grains. In a saturated soil, the void spaces are completely filled with water and so the voids ratio may be expressed in terms of the *water content*, which is a property simply determined by weighing the soil and then drying it in an oven and reweighing. Voids ratio, unit weight, and water content may be related to each other and to the specific gravity of the mineral grains.

Figure 1-2 represents a sample of saturated soil with a volume  $V$  and weight  $W$ ; the sample contains only water and soil grains. The volume of the sample occupied by the soil grains is  $V_s$  and that occupied by the water-filled voids is  $V_w$ . The weight of soil grains and water in the sample may be calculated from the unit weight of water  $\gamma_w$  and the specific gravity of the grains  $G_s$ , as indicated in the diagram.

Water content, voids ratio, and unit weight are defined as follows:

$$\text{Water content, } w = \frac{\text{Weight of water}}{\text{Weight of soil grains}} = \frac{W_w}{W_s},$$

$$\text{Voids ratio, } e = \frac{\text{Volume of voids}}{\text{Volume of soil grains}} = \frac{V_w}{V_s},$$

$$\text{Unit weight, } \gamma = \frac{\text{Weight of sample}}{\text{Volume of sample}} = \frac{W}{V}.$$

	Volumes	Weights
Water	$V_w$	$W_w = \gamma_w V_w$
Soil grains	$V_s$	$W_s = \gamma_w G_s V_s$
Totals	$V$	$W$

Figure 1-2 Division of water and soil grains in saturated soils

From these and from Fig. 1-2 we obtain the basic relationships

$$e = wG_s \quad (1-1)$$

$$\gamma = \left( \frac{G_s + e}{1 + e} \right) \gamma_w \quad (1-2)$$

It is sometimes convenient, especially when considering unsaturated soils, to define a dry unit weight  $\gamma_d$ . This is the weight of the soil grains in a unit volume of the soil sample and  $\gamma_d$  may be found by putting  $W_w = 0$  in Fig. 1-2 giving

$$\gamma_d = \left( \frac{G_s}{1 + e} \right) \gamma_w \quad (1-3)$$

We will make considerable use later of the *specific volume*  $v$ , where  $v$  is defined as the volume of the soil sample containing unit volume of soil grains, as illustrated in Fig. 1-3. Then,

$$v = 1 + e \quad (1-4)$$

$$w = \frac{v - 1}{G_s} \quad (1-5)$$

$$\gamma = \left( \frac{G_s + v - 1}{v} \right) \gamma_w \quad (1-6)$$

	Volumes	Weights
Water	$V_w = v - 1$	$W_w = \gamma_w (v - 1)$
Soil grains	$V_s = 1$	$W_s = \gamma_w G_s$
Totals	$v$	$W = \gamma_w (G_s + v - 1)$

Figure 1-3 Specific volume of saturated soil

**Example 1-1** Calculation of water content and unit weight

A cylinder of undisturbed saturated soil is 38 mm in diameter and 78 mm long and its mass is 142 g. After oven drying, its mass is 86 g. Calculate the water content and unit weight of the soil.

$$\text{Mass of water} = 142 - 86 = 56 \text{ g,}$$

$$\text{Mass of dry soil} = 86 \text{ g.}$$

Hence,

$$\text{Water content, } w = \frac{56}{86} = 0.651$$

or

$$w = 65.1 \text{ per cent.}$$

$$\text{Weight of saturated soil} = 142 \times 9.81 \times 10^{-6} \text{ kN,}$$

$$\text{Volume of cylinder} = \frac{1}{4}\pi \times 38^2 \times 78 \times 10^{-9} \text{ m}^3.$$

Hence,

$$\text{Unit weight, } \gamma = \frac{\text{Weight}}{\text{Volume}}$$

$$\gamma = 15.75 \text{ kN m}^{-3}.$$

**Example 1-2** Calculation of specific volume and specific gravity

The water content of a sample of saturated soil is 65.1 per cent and its unit weight is  $15.75 \text{ kN m}^{-3}$ . Calculate the specific volume of the sample and the specific gravity of the grains.

From Eqs (1-5) and (1-6),

$$\frac{\gamma}{\gamma_w} = \left(1 - \frac{1}{v}\right) \left(\frac{1}{w} + 1\right),$$

i.e.,

$$\frac{15.75}{9.81} = \left(1 - \frac{1}{v}\right) \left(\frac{1}{0.651} + 1\right).$$

Hence,

$$\text{Specific volume } v = 2.72.$$

From Eq. (1-5) the specific gravity of the soil grains is

$$G_s = \frac{v-1}{w} = \frac{1.72}{0.651}.$$

Hence,

$$G_s = 2.65.$$

### 1-8 SPECIFIC VOLUMES OF SANDS AND CLAYS

The state of packing of the grains in a particular soil can be conveniently described by its current specific volume. The specific volume cannot be measured directly but it may be calculated from measurements of water content or unit weight from Eqs (1-1) or (1-2) and (1-4); for most common soils the specific gravity of the mineral grains lies between 2.65 and 2.75.

In coarser-grained sand and gravel soils, the specific surface of the grains is relatively small and surface forces are negligible compared with self weight forces; in soils such as these the grains will pack together in a fashion similar to the random packing of spheres. Uniform spheres may be packed in different ways but in the densest possible state the specific volume is 1.35 and in the loosest state the specific volume is 1.92. Commonly, sand soils exist in nature with specific volumes in the range  $v = 1.3$  to  $v = 2.0$ .

For a particular sand or gravel soil, it is convenient to define the relative density  $D_r$ , which is a measure of the state of packing of the grains in terms of the loosest and the densest possible states of packing. The relative density is given by

$$D_r = \frac{v_{\max} - v}{v_{\max} - v_{\min}}, \quad (1-7)$$

where  $v_{\max}$  and  $v_{\min}$  are the specific volumes corresponding to the loosest and densest states of packing and  $v$  is the current specific volume. Thus, when  $D_r = 1.0$  the soil is dense and strong; when  $D_r = 0$  the soil is loose and relatively weak.

In clays, on the other hand, the specific surface is relatively large and surface forces play an appreciable role in the arrangement of the clay plates during sedimentation. The structure of a natural clay deposited in an electrolyte (e.g., sea water) tends to be *flocculated* with many of the particle contacts edge to face. The structure of a clay deposited through fresh water tends to be *dispersed* with few particles in contact, most being separated by molecular water bound to the clay mineral. Nevertheless, in either case the specific volume of a clay soil may be relatively large. The specific volume of a recently sedimented clay will also depend on, among other things, the mineral composition of the clay. Montmorillonite clays with large specific surfaces may exist with specific volumes in excess of 10 while kaolinite clays with smaller specific surfaces are rarely found with specific volumes in excess of 3.0. With external loading, free water may be squeezed from the clay structure and the specific volume will be reduced substantially. Under relatively large engineering loadings the specific volume of a clay can be reduced to as little as  $v = 1.2$  and the clay plates tend to become parallel.

### 1-9 SOIL CLASSIFICATION TESTS

The mechanical behaviour of soil varies considerably and engineers have

found it convenient to devise a set of rapid and simple tests for classifying soils into groups which have similar engineering behaviour.

The factors primarily responsible for determining the mechanical behaviour of soil are grain size and mineralogy and the way in which the grains are packed together. The common classification tests provide rapid and relatively simple measurements of the grading of a soil sample, its unit weight and water content, and, where appropriate, its Atterberg limits. In addition, there are tests which involve rapid strength measurement of soil samples; these will be discussed in Chapter 14.

The common soil classification tests are specified in detail in the appropriate British and American standards (BS 1377: 1975 and ASTM Part II). The grading and Atterberg limits of a soil describe its character and, to some extent, the mineralogy of the clay present; the water content and unit weight provide measurements of the current state of a given soil and the way that the grains are packed together.

## 1-10 MEASUREMENT OF UNIT WEIGHT AND WATER CONTENT

The tests to determine the unit weight and water content are very simple. To measure the unit weight of a soil, an undisturbed sample is weighed and its volume measured; the unit weight is defined as

$$\gamma = \frac{\text{Weight of sample}}{\text{Volume of sample}} \quad (1-8)$$

For most common engineering soils the unit weight will be between 15 and 22 kN m<sup>-3</sup> depending on the voids ratio of the soil and whether or not it is saturated. If it is impossible to obtain an undisturbed sample of a soil its unit weight must be measured *in situ* by other means.

The water content of a soil is measured by weighing a sample before and after it is heated to 105 °C for sufficient time for it to reach constant weight; the water content is defined as

$$w = \frac{\text{Weight of water lost}}{\text{Weight of dry soil}} \quad (1-9)$$

The water content is often expressed as a percentage and we should note that  $w$  may exceed 100 per cent. It is worth remarking that in all soils some water exists as molecular water bound to the grains and this water will not be evaporated at 105 °C. Consequently, the water content test should be regarded more as an indexing or classification test than as an absolute measure of the quantity of water present in a soil sample.

### 1-11 MEASUREMENT OF PARTICLE SIZE DISTRIBUTION

The distribution of particle sizes in a soil sample is found by sieving and by sedimentation. The coarse particles are separated by passing the sample through a set of sieves and weighing the fraction retained on each sieve. The smallest practical sieve has an aperture size of approximately 0.075 mm, corresponding roughly to the division between silt and sand sizes. Particles passing this sieve are separated by sedimentation. The separation occurs because, by Stoke's law for the terminal velocity of a sphere sinking through a fluid, smaller particles settle more slowly than larger ones. Of course, soil particles are not spherical and so particles are classified as having the same diameter as spheres that settle at the same rate; the diameter is that of the equivalent sedimenting sphere. In contrast, for sieve analysis the diameter of the particles is defined by the aperture size of the sieve that just prevents the particles passing through.

The distribution of particle sizes in a soil sample is shown as a grading curve on a particle size distribution chart, as shown in Fig. 1-1.

### 1-12 THE ATTERBERG LIMIT TESTS

When a soil does not contain a substantial proportion of clay and its specific surface is relatively small, the grading and specific volume are often enough to classify the soil for engineering purposes. When, however, a soil contains a considerable quantity of clay, additional tests are necessary to classify the nature of the clay minerals and the importance of surface forces. The tests used for this purpose measure the Atterberg limits. The Atterberg limit tests are intended to investigate the clay minerals present in a soil and they are carried out on the fraction of the soil passing a 0.425 mm aperture sieve.

The Atterberg limit tests provide measurements of the water content of clayey soils at two strengths which are specified rather crudely. As the water content of a clay soil is raised, its strength falls; as the water content is reduced, so the soil strengthens. If the water content is large, the soil will become very weak and it will flow as a liquid; if, on the other hand, the water content is relatively small, the soil will become relatively strong, but it may be brittle and crumble on failure. The Atterberg limits measure the water content at which the soil becomes so weak that it is liquid-like and the water content at which it strengthens sufficiently to become brittle.

The precise points at which a clayey soil becomes liquid-like or becomes brittle are defined by the special conditions of the Atterberg limits tests. The liquid limit, at which the soil weakens and flows, is the water content at which a small slope in the sample collapses under the action of a standard shock caused by bumping the soil sample in a standard way. In the United Kingdom the preferred test to determine the liquid limit is now the cone

penetrometer test, in which a standard 30° cone causes failure as it penetrates a sample under its own weight. The plastic limit is determined by rolling a thread of the soil sample and adjusting its water content until the thread just splits and crumbles when its diameter is 3 mm; the failure of the thread of soil is similar to that observed in concrete samples subjected to the Brazil or split cylinder test.

The liquid limit ( $LL$ ) and the plastic limit ( $PL$ ) are the Atterberg limits: they are expressed as integers equal to the water contents in percentages at which the appropriate changes of behaviour occur. For example, if a soil just becomes liquid-like at a water content of  $w = 0.562$ , the liquid limit is 56. As we shall discuss in Chapter 14, it turns out, conveniently, that the strength of a soil at its plastic limit is very nearly one hundred times its strength at its liquid limit.

Three further index values may be obtained from the Atterberg limits:

$$\text{Plasticity index, } PI = LL - PL \quad (1-10)$$

is the range over which the soil remains plastic, as defined by the Atterberg limits. In soils containing little clay the  $PI$  will approach zero, while in a pure montmorillonite clay, the  $PI$  may exceed 500.

$$\text{Liquidity index, } LI = \frac{w\% - PL}{PI} \quad (1-11)$$

(where  $w$  is the water content) describes the current state of a soil in terms of its Atterberg limits. In the ground, soft, normally consolidated clays often have liquidity indices near 1.0 while in stiff, heavily overconsolidated clays the liquidity index will be near zero. In special circumstances, some clays (e.g., 'quick' clays) may have liquidity indices greater than 1.0.

$$\text{Activity, } A = \frac{PI}{\text{Per cent by weight of clay}} \quad (1-12)$$

is a measure of the plasticity index of the clay fraction in a particular soil sample containing both coarse and fine grains. The activity of a clay is related to the mineralogy of the clay grains and to the chemistry of the pore water.

### Example 1-3. Calculation of plasticity index, activity, and liquidity index

The Atterberg limits of a soil are  $LL = 74$ ,  $PL = 27$  and the soil contains 43 per cent by weight of clay. The water content of the soil is  $w = 65.1$  per cent. Calculate the plasticity index, activity, and liquidity index of the soil.

$$\begin{aligned} \text{Plasticity index, } PI &= 74 - 27, \\ PI &= 47. \end{aligned}$$



$$\text{Activity, } A = \frac{17}{16},$$

$$A = 1.09.$$

$$\text{Liquidity index, } LI = \frac{65.1 - 27}{47},$$

$$LI = 0.81.$$

### 1-13 SUMMARY

1. An engineering soil is an uncemented, or only slightly cemented, aggregate of mineral grains with a fluid filling the pore spaces.
2. The mineral grains consist of the basic rock-forming minerals or their products after chemical alteration. In a saturated soil, water completely fills the pore spaces; the pressure in the pore water is known as the pore pressure.
3. The character of a soil may be classified by its grading (particle size distribution) and by its Atterberg limits.
4. The current state of a soil may be described by its unit weight, its water content or by its specific volume. These are related by

$$w = \frac{v-1}{G_s}, \quad (1-5)$$

$$\gamma = \left( \frac{G_s + v - 1}{v} \right) \gamma_w. \quad (1-6)$$

### REFERENCES

- American Society for Testing and Materials. *Book of ASTM Standards, Part II*. ASTM, Philadelphia (published annually).
- British Standards Institution. *Methods of testing soils for civil engineering purposes*. BS 1377: 1975.
- Calladine, C. R. *Engineering Plasticity*. Pergamon Press, London, 1969.
- Grim, R. E. *Applied Clay Mineralogy*. McGraw-Hill, New York, 1962.
- Hallam, A. *A Revolution in Earth Sciences*. Oxford University Press, London, 1973.
- Holmes, A. *Principles of Physical Geology*. Nelson, London, 1965.
- Mitchell, J. K. *Fundamentals of Soil Behaviour*. Wiley, New York, 1976.
- Scott, R. F. *Principles of Soil Mechanics*. Addison-Wesley, Reading, Mass., 1963.
- Terzaghi, K., and Peck, R. B. *Soil Mechanics in Engineering Practice*. Wiley, New York, 1948.

## STRESSES AND STRAINS IN SOILS

### 2-1 INTRODUCTION

We will assume that our readers are familiar with the basic concepts of stress and strain whereby stress may be thought of as an intensity of loading and strain as a measure of deformation. These concepts are perfectly satisfactory for most engineering materials but, for soils, when the particle sizes may be relatively large, familiar ideas of stress and strain may need re-examination. In addition, we have to make allowance for pressures that may exist in the pore water and which may modify the stress in the soil; consideration of pore pressures leads on to the important *principle of effective stress*.

### 2-2 NORMAL STRESS AND STRAIN

Figure 2-1(a) shows a small cube of material of cross-sectional area  $\delta A$  and of height  $\delta Z$ . A load  $\delta F_N$  is applied across the cube in a direction normal to the area  $\delta A$  and the element elongates so that the new length is  $(\delta Z + \delta L)$  as shown in Fig. 2.1(b). Following conventional definitions of stress and strain, we define a normal stress  $\sigma$  and a normal linear strain  $\epsilon$  by

$$\sigma = - \lim_{\delta A \rightarrow 0} \frac{\delta F_N}{\delta A}, \quad (2-1)$$

$$\epsilon = - \lim_{\delta Z \rightarrow 0} \frac{\delta L}{\delta Z}. \quad (2-2)$$

Tensile stresses occur only rarely in soils and so the negative signs have been introduced into Eqs (2-1) and (2-2) in order that compressive stresses and compressive strains are positive quantities; this is usual practice in soil mechanics.

### 2-3 SHEAR STRESS AND STRAIN

If a load  $\delta F_S$  is applied across the cube in the plane of  $\delta A$ , the cube will

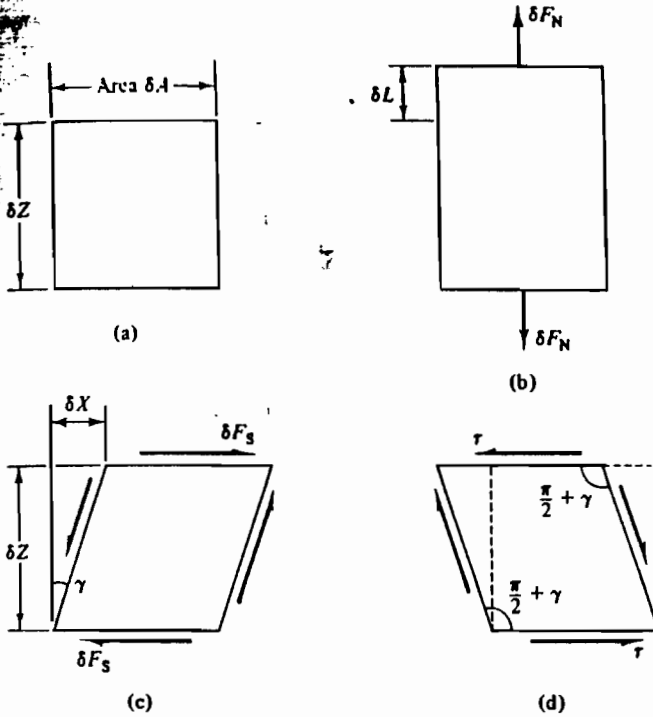


Figure 2-1 Stress and strain in an element. (a) Dimensions. (b) Normal stress and strain. (c) Shear stress and strain. (d) Positive shear

distort as initially vertical fibres rotate as shown in Fig. 2-1(c). The shear stress  $\tau$  and the shear strain  $\gamma$  are defined by

$$\tau = - \lim_{\delta A \rightarrow 0} \frac{\delta F_S}{\delta A} \tag{2-3}$$

$$\gamma = - \lim_{\delta Z \rightarrow 0} \frac{\delta X}{\delta Z} \tag{2-4}$$

Strictly, in Eq. (2-4) we should write  $\tan \gamma$  instead of  $\gamma$ , but the difference is negligible for small deformations. In Eqs (2-3) and (2-4) we follow conventional soil mechanics practice and introduce the negative signs so that positive shear stresses and positive shear strains are associated with increases in the angles in the positive quadrants of the element, as illustrated in Fig. 2-1(d).

The definition of shear strain in Eq. (2-4) is that usually taught to engineers and  $\gamma$  is known as engineers' shear strain. Later, in Chapter 3, we will discover that  $\gamma$  includes a component of rigid body rotation as well as a component of shear distortion and we will have to modify our definition of shear strain to make the analysis of states of strain possible. For the present,

however, we may continue to use Eq. (2-4) as a definition of engineers' shear strain.

**Example 2-1** Calculation of stress and strain

Loads  $M_1 = 30$  kg and  $M_2 = 10$  kg applied to the soil sample in Fig. E2-1 cause displacements  $\delta_1 = 0.9$  mm downwards and  $\delta_2 = 2.3$  mm to the right. The sides of the cubical sample are each 40 mm long. Calculate the normal stresses and strains and the shear stresses and strains in the sample.

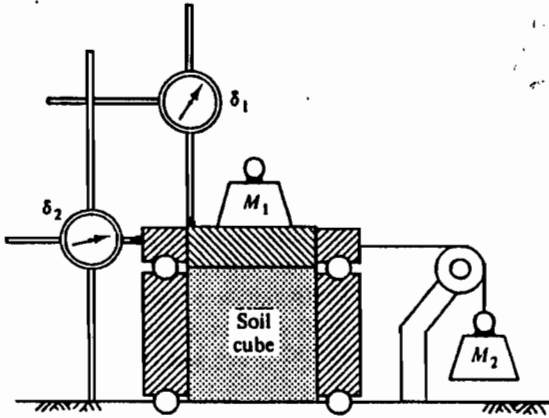


Figure E2-1

Referring to Fig. 2-1 and from Eqs (2-1) to (2-4), noting that the directions of  $M_1$  and  $\delta_1$  are such that  $\delta F_N = -M_1 g$  and  $\delta L = -\delta_1$ ,

$$\begin{aligned} \text{Normal stress, } \sigma &= -\frac{M_1 g}{A} = -\frac{30 \times 9.81}{(0.04)^2} \times 10^{-3}, \\ \sigma &= 183.9 \text{ kN m}^{-2}. \end{aligned}$$

$$\begin{aligned} \text{Shear stress, } \tau &= -\frac{M_2 g}{A} = -\frac{10 \times 9.81}{(0.04)^2} \times 10^{-3}, \\ \tau &= -61.3 \text{ kN m}^{-2}. \end{aligned}$$

$$\begin{aligned} \text{Normal strain, } \epsilon &= -\frac{\delta_1}{Z} = -\frac{-0.9}{40}, \\ \epsilon &= 0.0225. \end{aligned}$$

$$\begin{aligned} \text{Shear strain, } \gamma &= -\frac{\delta_2}{Z} = -\frac{2.3}{40}, \\ \gamma &= -0.0575. \end{aligned}$$

The sample deforms so that the angles in the positive quadrants decrease; hence, shear stresses and shear strains are negative.

## 2-4 SOIL AS A CONTINUUM

On the atomic scale, all materials have a particulate nature for they are constructed from the basic particles of matter, and, as we have seen, soils are particulate materials where the size of the particles may be much larger than atoms or even molecules. Because materials are particulate, we are not justified in taking the limits as  $\delta A$  and  $\delta Z$  approach zero since we will not know whether the elemental area  $\delta A$  or the elemental length  $\delta Z$  are centred on a particle or on a void space.

There are two possibilities for avoiding this difficulty. First, we may accept the particulate nature of materials and recognize that the basic definitions of stress and strain have little meaning. In this case we are obliged to investigate the distribution of interparticle contact forces and the relative movements of the particles.

Alternatively, we may approximate the behaviour of a particulate material to that of an ideal continuum. In a continuum all elements merge continuously into their neighbouring elements, infinitesimal elements have the same properties as the mass, and there are no difficulties in using Eqs (2-1) to (2-4) to define stresses and strains. There can be no such thing as a real continuum, because all materials, at least on the atomic scale, are particulate; a continuum is an imaginary material which has the same bulk behaviour as a real particulate material.

In most branches of engineering, materials are regarded as continua and stresses and strains are defined by equations like Eqs (2-1) to (2-4). This is generally so in soil mechanics as well, although a few workers adopt the particulate approach and examine the interactions between particles.

In this book we adopt the conventional continuum approach to soil mechanics. We will examine the behaviour of ideal continua whose properties are the same as soil in bulk and we define stresses and strains by equations like (2-1) to (2-4). This approach to the mechanics of soils is quite satisfactory so long as the dimensions of the particles are considerably smaller than the dimensions of the mass of soil (e.g., a test specimen) that we are examining.

## 2-5 PORE PRESSURE AND TOTAL STRESS

Although we will regard soils as ideal continua, we must not forget that, in reality, they are particulate materials and that water in the void spaces may be under some pressure. We must now examine whether any modifications are necessary to our ideas of a soil continuum to account for pore pressure.

An element of our ideal soil continuum will have a set of total stresses acting on the boundaries of the element and a pore pressure acting within the element. Following usual conventions, we write total normal and shear stresses as  $\sigma$  and  $\tau$ , respectively, and the pore pressure as  $u$ . As an example, Fig. 2-2 shows an element of soil at a depth  $Z$  below the surface of a soil mass; the soil to a depth  $Z_w$  is dry and has unit weight  $\gamma_d$ , while the rest of

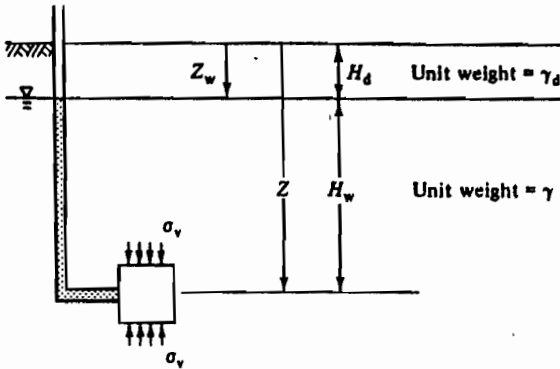


Figure 2-2 Stress and pore pressure in the ground

the soil is saturated with water and has unit weight  $\gamma$ . The relationships between  $\gamma$ ,  $\gamma_d$ , and other soil parameters have already been examined in Chapter 1. We may just note here that the unit weight of a soil is the weight of everything – mineral grains and water – contained in unit volume. If we regard the soil as composed of layers of thickness  $H_i$ , each of unit weight  $\gamma_i$ , the total vertical stress is

$$\sigma_v = \sum H_i \gamma_i \quad (2-5)$$

or, for the two layers in Fig. 2-2,  $\sigma_v = Z_w \gamma_d + (Z - Z_w) \gamma$ .

The total vertical stress is simply the intensity of loading due to the weight of all the material above the element.

If, as shown in Fig. 2-2, an open-ended standpipe is inserted into the ground, water will rise in the standpipe until the water pressure at the tip of the standpipe exactly balances the pore pressure in the saturated soil. Hence, the pore pressure  $u$  in the element in Fig. 2-2 is given by

$$u = H_w \gamma_w = (Z - Z_w) \gamma_w \quad (2-6)$$

#### Example 2-2 Calculation of vertical stress in the ground

The soil profile shown in Fig. E2-2 consists of 3 m of dense sand, unit weight  $\gamma = 17.5 \text{ kN m}^{-3}$  overlying saturated clay, unit weight  $15.75 \text{ kN m}^{-3}$ . The level of water in a standpipe driven into the clay to

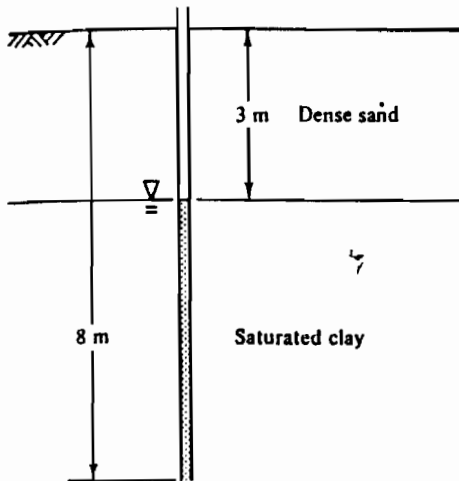


Figure E2-2

any depth coincides with the sand-clay interface. Calculate the total vertical stress and the pore pressure at a depth of 8 m below ground level.

$$\begin{aligned}\text{Total vertical stress, } \sigma_v &= \sum \gamma_1 H_1 = (17.5 \times 3) + (15.75 \times 5), \\ \sigma_v &= 131.25 \text{ kN m}^{-2}.\end{aligned}$$

$$\begin{aligned}\text{Pore pressure, } u &= \gamma_w H_w = 9.81 \times 5, \\ u &= 49.05 \text{ kN m}^{-2}.\end{aligned}$$

## 2-6 THE PRINCIPLE OF EFFECTIVE STRESS

For a soil subjected to a given total stress, it is intuitively obvious that the behaviour of the soil will, in some way, be dependent on the magnitude of the pore pressure.

The principle of effective stress determines the effect of a pore pressure on the behaviour of a soil with a given total stress. The principle is probably the single most important concept in soil mechanics and its importance cannot be overstated.

We begin with a simple statement of the principle of effective stress and we then proceed to examine some of the consequences.

The principle of effective stress was first stated in English by Terzaghi in 1936. The statement is in two parts, the effective stress is defined first.

The stresses in any point of a section through a mass of soil can be computed from the total principal stresses†  $\sigma_1$ ,  $\sigma_2$ , and  $\sigma_3$  which act at this point. If the voids of the

† We will assume for the present that our readers are familiar with principal stresses; they will be further discussed in Chapter 3.

soil are filled with water under a stress  $u$  the total principal stresses consist of two parts. One part  $u$  acts in the water and in the solid in every direction with equal intensity. It is called the neutral stress (or the pore pressure). The balance  $\sigma'_1 = \sigma_1 - u$ ,  $\sigma'_2 = \sigma_2 - u$  and  $\sigma'_3 = \sigma_3 - u$  represents an excess over the neutral stress  $u$  and it has its seat exclusively in the solid phase of the soil. This fraction of the total principal stress will be called the effective principal stress.

Thus, Terzaghi wrote the fundamental effective stress equation,

$$\sigma' = \sigma - u. \quad (2-7)$$

The prime in  $\sigma'$  is used to denote an effective stress and this is now conventional practice which will be followed in this book. It should be noted that some authors prefer to use  $\bar{\sigma}$  instead of  $\sigma'$ .

The second part of Terzaghi's statement defines the importance of the effective stress.

All measurable effects of a change of stress, such as compression, distortion and a change of shearing resistance, are exclusively due to changes in the effective stresses.

In engineering we are concerned with the compression, distortion, and strength of materials and so, when dealing with soil, we must always consider effective stresses and changes in effective stress.

## A.I.T. LIBRARY

### 2-7 THE SIGNIFICANCE OF EFFECTIVE STRESS

As stated by Terzaghi, the principle of effective stress is deceptively simple; nevertheless it is of extreme importance and must be understood properly. In order to illustrate the principle of effective stress we will consider three corollaries with corresponding examples.

**Corollary 1** The engineering behaviour of two soils with the same structure and mineralogy will be the same if they have the same effective stress.

**Example 2-3** Calculation of vertical effective stresses in estuarine and deep-sea sediments

Figure E2-3 shows elements of soil 1.0 m below the surface of (a) an estuarine sediment and (b) a deep-sea sediment. In the estuarine sediment, the water table is at the surface of the soil and the depth of water above the deep-sea sediment is 10<sup>4</sup> m. The unit weight of each sediment is



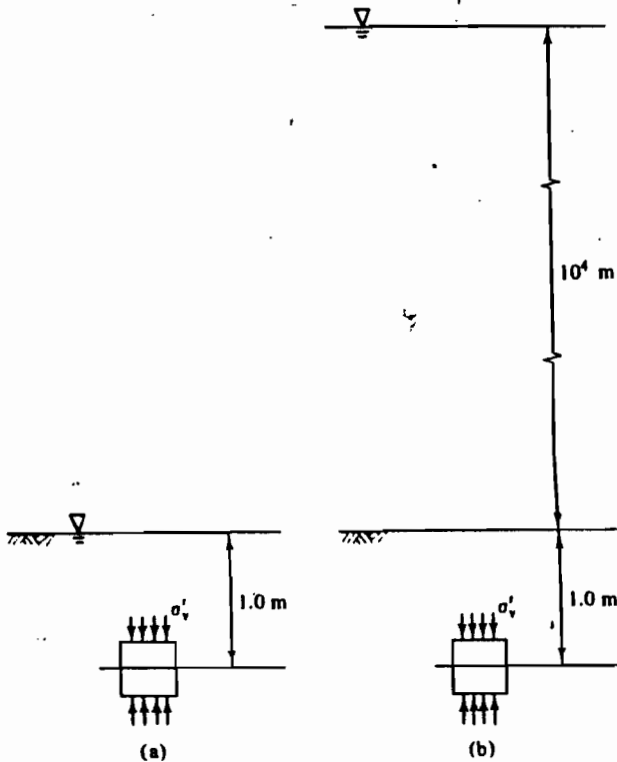


Figure E2-3 Vertical stresses in (a) estuarine and (b) deep-sea sediments

$17 \text{ kN m}^{-3}$  and the unit weight of sea water is  $10 \text{ kN m}^{-3}$ . Calculate the vertical effective stresses acting on each element.

(a) For the estuarine sediment,

$$\sigma_v = \sum H_i \gamma_i = 17.0 \times 1.0 = 17.0 \text{ kN m}^{-2},$$

$$u = H_w \gamma_w = 10.0 \times 1.0 = 10.0 \text{ kN m}^{-2},$$

$$\sigma'_v = \sigma_v - u = 17.00 - 10.0,$$

$$\sigma'_v = 7.0 \text{ kN m}^{-2}.$$

(b) For the deep-sea sediment,

$$\sigma_v = \sum H_i \gamma_i = (17.0 \times 1.0) + (10.0 \times 10^4) = 100\,017 \text{ kN m}^{-2},$$

$$u = H_w \gamma_w = 10.0 \times 10\,001 = 100\,010 \text{ kN m}^{-2},$$

$$\sigma'_v = \sigma_v - u = 100\,017 - 100\,010,$$

$$\sigma'_v = 7.0 \text{ kN m}^{-2}.$$

The effective stresses in the estuarine sediment and in the deep-sea sediment are the same and, provided that the structure and mineralogy of the sediments are the same, they will have the same engineering properties.

**Corollary 2** If a soil is loaded or unloaded without any change of volume and without any distortion there will be no change of effective stress.

**Example 2-4** Stresses and pore pressures in a constant volume isotropic loading test

Figure E2-4 illustrates a simple experiment. A cylindrical soil sample seated on a smooth base is sealed in a thin rubber membrane and enclosed in a vessel which is filled with a fluid. The fluid pressure applies an equal all-round total stress  $\sigma$  to the sample. The total stress  $\sigma$  and the pore pressure  $u$  may be changed independently and the dimensions of the sample observed by a set of displacement transducers such as A and B.

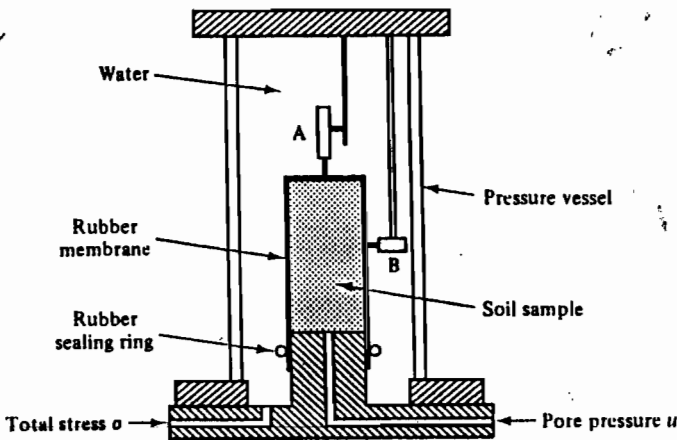


Figure E2-4 Constant volume isotropic compression test

At the start of a test the total stress is  $\sigma = 17 \text{ kN m}^{-2}$  and the pore pressure is  $u = 10 \text{ kN m}^{-2}$ . The total stress is raised to  $\sigma = 1000 \text{ kN m}^{-2}$  and the pore pressure changed simultaneously so that the transducers register no displacement of the sample; calculate the magnitude of the final pore pressure.

Since there has been no volume change or distortion of the soil the effective stress must remain constant.

At the start of the test,

$$\sigma' = \sigma - u = 17 - 10 = 7 \text{ kN m}^{-2};$$

at the end of the test,

$$\sigma' = \sigma - u = 1000 - u = 7 \text{ kN m}^{-2}.$$

Hence,

$$u = 1000 - 7,$$

$$u = 993 \text{ kN m}^{-2}.$$

**Corollary 3** Soil will expand in volume (and weaken) or compress (and strengthen) if the pore pressure alone is raised or lowered.

**Example 2-5** Effects of changes of pore pressure with constant total stress

Figure E2-5 illustrates a simple experiment; the apparatus is similar to that described in Ex. 2-4 except that now the volume of water entering or leaving the sample can be measured by means of a graduated vessel.

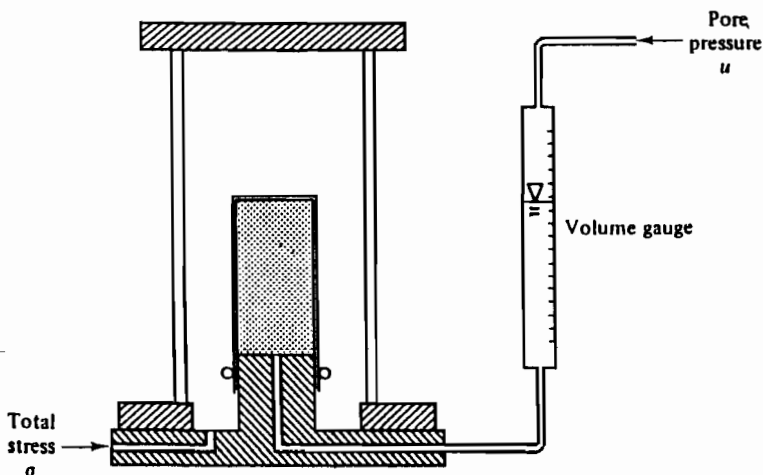


**Figure E2-5** Isotropic compression test

The total stress  $\sigma$  is held constant while the pore pressure  $u$  is changed and the change of volume of the sample observed.

At the start of the test,  $\sigma = 17 \text{ kN m}^{-2}$ ,  $u = 10 \text{ kN m}^{-2}$ . Hence,

$$\sigma' = 7 \text{ kN m}^{-2}.$$

The pore pressure  $u$  is raised to  $15 \text{ kN m}^{-2}$  while the total stress is held

constant; the level of water in the graduated vessel falls, indicating that the volume of the sample has increased.

At the end of the test,  $\sigma = 17 \text{ kN m}^{-2}$ ,  $u = 15 \text{ kN m}^{-2}$ . Hence,

$$\sigma' = 2 \text{ kN m}^{-2}.$$

If the *effective stress* is reduced then, as discussed in Chapter 7, the soil will swell (i.e., increase in volume) and, as discussed in Chapters 10 and 11, its strength will reduce. Conversely, if the effective stress is increased, the soil will compress and its strength will increase.

## 2-8 EXAMINATIONS OF THE PRINCIPLE OF EFFECTIVE STRESS

Because of its importance in soil mechanics, the principle of effective stress often assumes the status of a physical law and attempts are made to examine the principle theoretically. These examinations of the principle of effective stress, and of the physical meaning of effective stress, encounter difficulties when forces at interparticle contacts have to be expressed in the form of a stress; the problems are similar to those we encountered in defining the meaning of stress in a granular material.

However, if we examine Terzaghi's 1936 statement of the principle of effective stress, we note, first, that he does not assign any physical meaning to the effective stress other than 'it has its seat exclusively in the solid phase of the soil' and, second, that he limits the principle to 'all measurable effects'. Indeed, Terzaghi arrived at the principle of effective stress from the results of laboratory experiments and it is evident that he viewed the principle as a working hypothesis that was sufficiently accurate for practical engineering purposes.

Although most texts on soil mechanics examine the validity of the principle and the meaning of effective stress by considering the interparticle forces and the intergranular contact areas, there really is no need to do this, and the necessary assumptions are not always supported by experimental evidence. Detailed theoretical and experimental examinations of the principle of effective stress have been published by Skempton (1960) and by Bishop, Webb, and Skinner (1965) and no conclusive evidence has yet been found which invalidates Terzaghi's original postulate, at least for saturated soils at normal levels of engineering stress.

## 2-9 DISCUSSION OF THE PRINCIPLE OF EFFECTIVE STRESS

It is important that we should be clear about the principle of effective stress and its consequences. Intuitively, it is fairly obvious that, if the total stress or the pore pressure – or both – are varied, the behaviour of the soil will depend only on some *combination* of the two and not on the *individual*

values of total stress and pore pressure. The principle of effective stress states, quite simply, that the relevant combination of total stress and pore pressure is the difference  $(\sigma - u)$  and this difference is defined as the effective stress  $\sigma'$ . The principle goes further and states that *all* measurable effects of a change of stress are *exclusively* due to changes in the value of  $(\sigma - u)$ .

## 2-10 INCREMENTS OF STRESS AND STRAIN

It was convenient for our definitions of stress and strain in Secs 2-2 and 2-3 to consider loads applied to an element which was initially unstressed and unstrained. In general, however, we will be more concerned with additions of load causing changes in the states of stress and strain in elements which are already stressed and which have already suffered some strain. We must be careful, therefore, to distinguish between pre-existing states of stress and strain and increments of stress and strain.

We shall adopt the convention that pre-existing total and effective stresses are written as  $\sigma$  and  $\sigma'$ , respectively, while *small* additions of stress are written as  $\delta\sigma$  and  $\delta\sigma'$ , and, in the limit, as  $d\sigma$  and  $d\sigma'$ . If a succession of small increments of stress are applied so that a *large* change of stress occurs we will write

$$\Delta\sigma = \sum \delta\sigma = \int d\sigma, \quad (2-8)$$

where  $\Delta\sigma$  represents the large change in total stress.

A similar convention serves to distinguish between strain ( $\epsilon$ ), small strain increments ( $\delta\epsilon$ ), and large changes in strain ( $\Delta\epsilon$ ). An analogous notation is used for other variables.

## 2-11 SUMMARY

1. Soil is idealized as a continuum and normal and shear stresses and strains are defined, at the limits as  $\delta A$  and  $\delta Z$  tend to zero, as

$$\sigma = -\frac{\delta F_N}{\delta A}, \quad \tau = -\frac{\delta F_S}{\delta A},$$

$$\epsilon = -\frac{\delta L}{\delta Z}, \quad \gamma = -\frac{\delta X}{\delta Z}.$$

2. Compressive normal stresses and compressive normal strains are taken to be positive quantities. Positive shear stresses and positive shear strains are both associated with increases in the angles in the positive quadrants of elements.

3. The effective stress is defined as

$$\sigma' = \sigma - u. \quad (2-7)$$

4. 'All measurable effects of a change of stress, such as compression, distortion and a change of shearing resistance are exclusively due to changes in the effective stress.'

## REFERENCES

- Bishop, A. W., Webb, D. L., and Skinner, A. E. Triaxial tests on soil at elevated cell pressure. *Proc. 6th Int. Conf. Soil Mech. and Foundn Engng*, Vol. I, pp. 170-174, Montreal, 1965.
- Skempton, A. W. Effective stress in soils, concrete and rocks. *Proc. Conf. on Pore Pressure and Suction in Soils*, pp. 4-16. Butterworths, London, 1960.
- Terzaghi, K. The shearing resistance of saturated soil and the angle between the planes of shear. *Proc. 1st Int. Conf. Soil Mech. and Foundn Engng*, Vol. 1, pp. 54-56, Harvard, Mass., 1936.

## STATES OF STRESS AND STRAIN IN SOILS

## 3-1 INTRODUCTION

Every point within the idealized continuum which we use to represent a body of soil will be stressed, and it may have suffered some strain measured from a reference state. The stresses and strains in some directions may be known and we may wish to calculate the stresses and strains in other directions; in other words, we wish to analyse the states of stress and strain.

It is easiest to begin with the study of two-dimensional states of stress and strain. Accordingly, we will examine stresses and strains in a plane section through the soil and we will assume that these are independent of the stresses and strains normal to the section.

The simplest method of stress and strain analysis is to make use of the Mohr's circle construction. We will assume that our readers are familiar with the basic theory of Mohr's circles and we will not derive the analysis here; this is covered fully in many texts (e.g., Crandall, Dahl and Lardner, 1972, Chapter 4; Case and Chilver, 1971, Chapter 5). Instead we will describe briefly the application of Mohr's circles to states of stress and strain commonly met in soil mechanics and we will use this Chapter principally to define some parameters for stress and strain.

## 3-2 TWO-DIMENSIONAL STATES OF STRESS

If we imagine a small plane element such as OABC in Fig. 3-1(a), there will, in general, be normal and shear stresses on all four faces of the element. In the limit, as the element becomes very small, all the stresses act at the point O in the appropriate directions. The normal stress  $\sigma_x$  acts on planes OA and BC, the normals to which are parallel with the  $x$ -axis, and the shear stresses  $\tau_{zx}$  act on the same planes, but in a direction parallel with the  $z$ -axis. The directions of  $\sigma_x$  and  $\tau_{zx}$  are defined similarly.

Since the element is in equilibrium, it follows, by taking moments about any corner, that  $\tau_{zx} = \tau_{xz}$ . In soils, normal stresses will, in general, be compressive and the stresses marked in Fig. 3-1(a) are, therefore, positive quantities; the shear stresses marked in Fig. 3-1(a) are also positive quantities by the convention of Sec. 2-3.

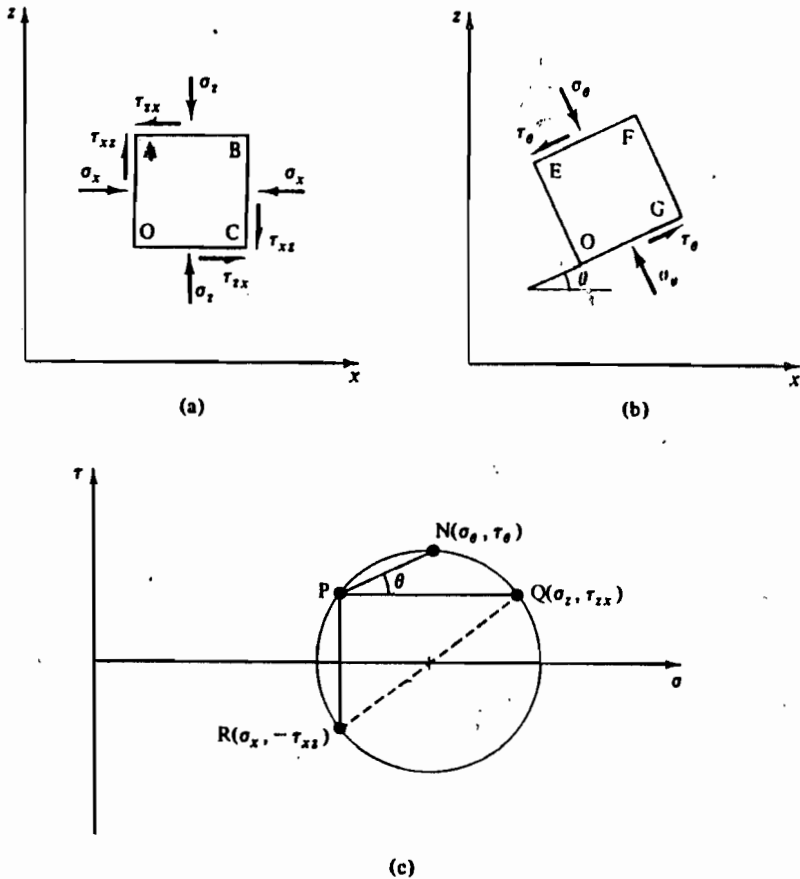


Figure 3-1 States of stress in two-dimensional elements and the corresponding Mohr's circle of stress

Suppose, for example, that the magnitudes of  $\sigma_x$ ,  $\sigma_z$ , and  $\tau_{xz}$  are known, and we wish to calculate normal and shear stresses ( $\sigma_\theta, \tau_\theta$ ) on some arbitrary plane at an angle  $\theta$  to the  $x$ -axis. If the element is rotated about  $O$  through an angle  $\theta$  to a new position  $O'E'F'G'$  in Fig. 3-1(b),  $\sigma_\theta$  and  $\tau_\theta$  will be the normal and shear stresses on the planes  $OG$  and  $E'F'$  at an angle  $\theta$  to the  $x$ -axis.

### 3-3 MOHR'S CIRCLE OF STRESS

The Mohr's circle of stress corresponding to the state of stress in Fig. 3-1(a) is shown in Fig. 3-1(c). The circle is plotted with axes  $\tau$  and  $\sigma$  and it passes through the points  $R (\sigma_x, -\tau_{xz})$  and  $Q (\sigma_z, \tau_{xz})$ . For plotting Mohr's circles,



and for this purpose *alone* we adopt the convention that counter-clockwise shear stresses are taken as positive quantities. Thus, the counter-clockwise shear stress  $\tau_{xz}$  in Fig. 3-1(a) is positive in Fig. 3-1(c) and the clockwise shear stress  $\tau_{zx}$  is negative. The Mohr's circle may be constructed, and hence the complete two-dimensional stress state defined, once the normal and shear stresses on any two planes are known.

There are several methods available for working with Mohr's circles to calculate the state of stress on other planes; we will employ the *pole method* to locate planes. The pole of a Mohr's circle is defined thus:

*if a line is drawn from the pole to a point on the circle where the stresses are  $\tau_t$  and  $\sigma_t$  then, in the  $(x, z)$  plane the line is parallel to the plane on which  $\tau_t$  and  $\sigma_t$  act.*

By reversing the definition we may draw the line QP (or the line RP) to locate the pole at P in Fig. 3-1(c). The line QP is parallel to the plane on which  $\sigma_x$  and  $\tau_{xz}$  act and is parallel with the  $x$ -axis in Fig. 3-1(a); similarly RP is parallel with the  $z$ -axis. We may now use the pole of the circle to calculate the state of stress on any plane through the material, and, in particular, the normal and shear stresses ( $\sigma_\theta, \tau_\theta$ ) on the plane EF in Fig. 3-1(b). The plane is at an angle  $\theta$  to the  $x$ -axis and, hence, in Fig. 3-1(c) we may draw PN at an angle  $\theta$  to PQ. The stresses at the point N are the stresses acting on the planes EF and OG in Fig. 3-1(b). By varying the arbitrary angle  $\theta$  between the planes EF and OG and the  $x$ -axis, we may calculate the stresses on any plane in Fig. 3-1(a) by drawing the corresponding line on Fig. 3-1(c).

### 3-4 PRINCIPAL STRESSES AND PRINCIPAL PLANES

There must always be two points where a Mohr's circle crosses the  $\sigma$ -axis. These points represent planes on which the shear stress is zero and the normal stress is either a maximum or a minimum. These planes are known as *principal planes* and the corresponding normal stresses as *principal stresses*.

Figure 3-2(b) is the Mohr's circle of stress corresponding to the state of stress in Fig. 3-1(a). The principal stresses  $\sigma_1$  and  $\sigma_3$  occur at T and S in Fig. 3-2(b) and we may locate principal planes (JK and OL, and JO and KL) in Fig. 3-2(a), where JK and OL are at an angle  $\theta_p$  (measured from Fig. 3-2(b)) to the  $x$ -axis. From the geometry of the Mohr's circle, the principal planes are orthogonal and so the directions of the principal stresses must also be orthogonal. In the limit, as the element OJKL becomes small, we observe only two orthogonal principal planes, OJ and OL.

It turns out that in three-dimensional stress analysis there will be three principal planes and three principal stresses. These will be denoted by  $\sigma_1, \sigma_2,$  and  $\sigma_3$ , and it is usual practice to define  $\sigma_1 > \sigma_2 > \sigma_3$ ;  $\sigma_1$  is the major principal stress,  $\sigma_2$  the intermediate, and  $\sigma_3$  the minor.

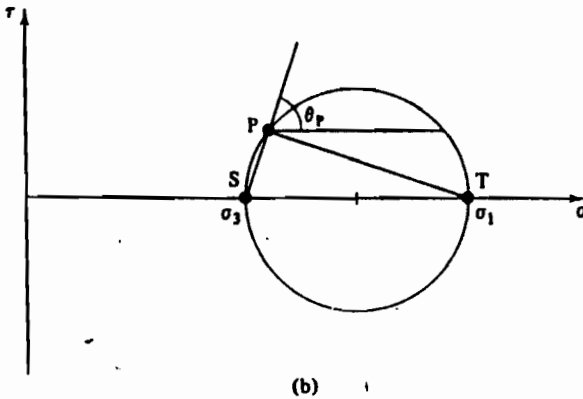
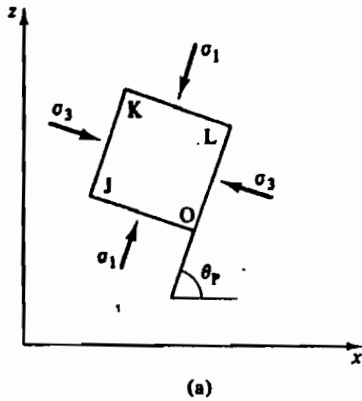


Figure 3-2 Principal planes and principal stresses

Thus, in summary, the major and minor principal stresses are the largest and smallest normal stresses in a given state of stress and they occur on two orthogonal planes which are free from shear stresses.

**Example 3-1 Mohr's circle of total stress**

In Fig. E3-1 the normal loads applied to the faces of a soil cube are  $F_1 = 45 \text{ kg}$  and  $F_2 = 30 \text{ kg}$  and the shear loads are  $F_3 = F_4 = 10 \text{ kg}$ . The sides of the soil cube are each 40 mm. Construct the Mohr's circle of total stress and find the magnitudes of the principal total stresses and the directions of the principal planes in the soil.

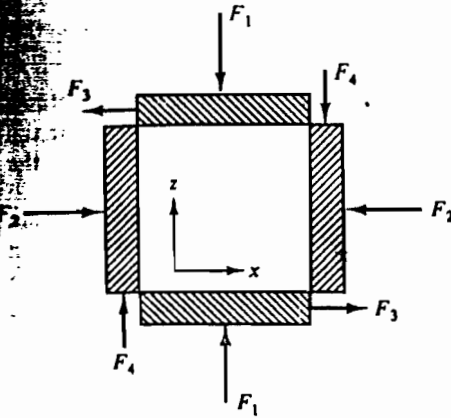


Figure E3-1

Defining axes  $(x, z)$  as shown in Fig. E3-1, and taking account of the directions of the forces, the total stresses are

$$\sigma_z = \frac{F_2 g}{A} = 183.9 \text{ kN m}^{-2},$$

$$\sigma_y = \frac{F_1 g}{A} = 275.9 \text{ kN m}^{-2},$$

$$\tau_{xz} = \tau_{zx} = \frac{F_3 g}{A} = 61.3 \text{ kN m}^{-2}.$$

The Mohr's circle of total stress is shown in Fig. E3-2: for plotting the Mohr's circle the counter-clockwise shear stress  $\tau_{xz}$  is plotted positively,

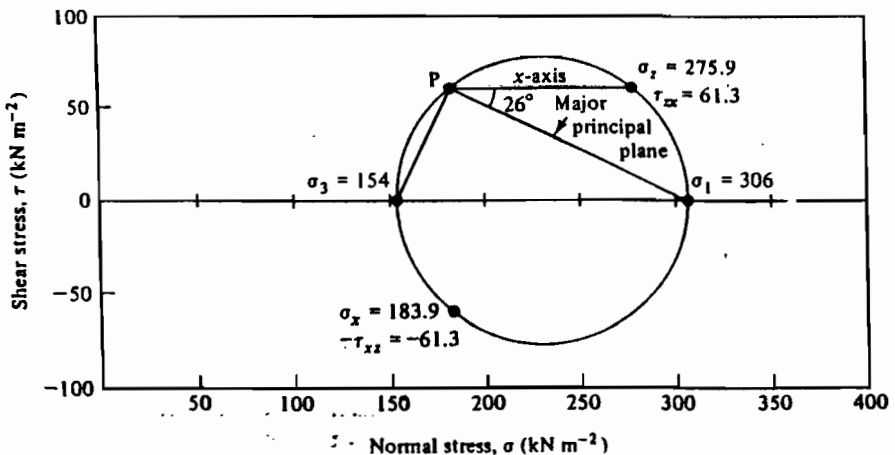


Figure E3-2 Mohr's circle of total stress

while the clockwise shear stress  $\tau_{xx}$  is plotted negatively. Scaling from the diagram, the principal total stresses are

$$\sigma_1 = 306 \text{ kNm}^{-2} \quad \text{and} \quad \sigma_3 = 154 \text{ kNm}^{-2}.$$

The pole of the Mohr's circle is located at P and the major principal plane makes an angle of  $26^\circ$  to the  $x$ -axis.

### 3-5 MOHR'S CIRCLES OF TOTAL AND EFFECTIVE STRESS

So far in considering stresses and Mohr's circles we have not differentiated between total and effective stress.

If the stresses acting on the faces of the element in Fig. 3-1(a) are total stresses, the corresponding Mohr's circle of total stress is shown in Fig. 3-1(c); this Mohr's circle is shown again as the right-hand circle in Fig. 3-3.

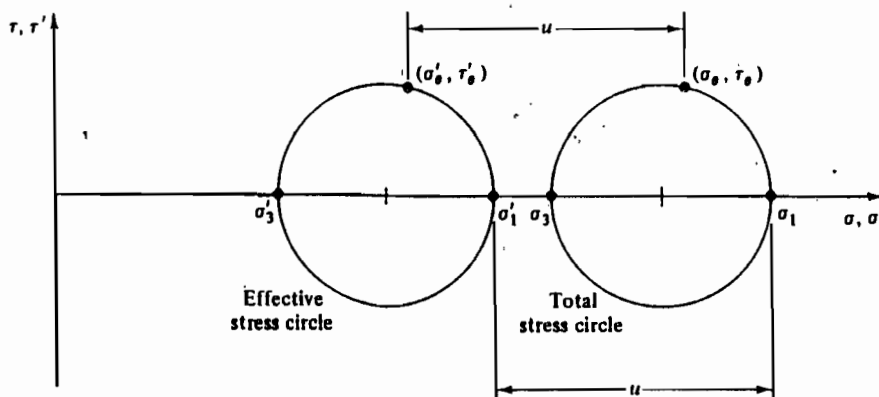


Figure 3-3 Mohr's circles of total and effective stress

The stresses  $\tau_\theta$  and  $\sigma_\theta$  are the total stresses acting on the planes EF and OG in Fig. 3-1(b). We will now assume that there is a pore pressure of magnitude  $u$  in the soil and we will construct the Mohr's circle of effective stress.

The principal effective stresses, given by Eq. (2-7), are

$$\sigma'_1 = \sigma_1 - u, \quad (3-1)$$

$$\sigma'_3 = \sigma_3 - u, \quad (3-2)$$

and the Mohr's circle of effective stress is shown as the left-hand circle in Fig. 3-3. The effective stress circle has the same diameter as the total stress circle and is separated from it by the pore water pressure. The stresses  $\tau'_\theta$  and  $\sigma'_\theta$  are the effective stresses acting on the same planes EF and OG in Fig. 3-1(b).

By examining the circles we note that

$$\tau'_\theta = \tau_\theta \tag{3-3}$$

$$\sigma'_\theta = \sigma_\theta - u. \tag{3-4}$$

Thus, for a given state of total stress, changes in pore pressure have no effect on the effective shear stresses, they alter only the effective normal stresses.

We may use the pole construction on the effective stress Mohr's circle to calculate the effective stresses on any plane in exactly the same way as we used the pole construction to calculate the total stresses.

**Example 3-2 Mohr's circle of effective stress**

The total stresses on the faces of a cube of soil are the same as those in the previous-example (Ex. 3-1) and the pore pressure is  $u = 50 \text{ kN m}^{-2}$ . Construct the Mohr's circle of effective stress.

Principal effective stresses are given by  $\sigma'_1 = \sigma_1 - u$  and  $\sigma'_3 = \sigma_3 - u$ . Hence,

$$\sigma'_1 = 256 \text{ kN m}^{-2} \text{ and } \sigma'_3 = 104 \text{ kN m}^{-2}.$$

The Mohr's circles of total and effective stress are shown in Fig. E3-3.

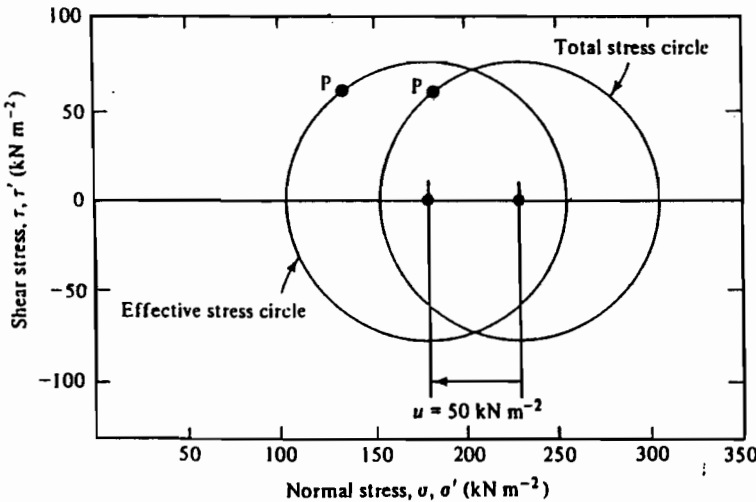


Figure E3-3 Mohr's circles of total and effective stress

The position of the pole in the Mohr's circle of effective stress is the same as in the Mohr's circle of total stress and the locations of the principal planes of total and effective stress in the soil are identical.

### 3-6 TWO-DIMENSIONAL STATES OF STRAIN – PLANE STRAIN

Just as we did with stress analysis, we will examine two-dimensional states of strain in order to keep the analysis simple. We will, therefore, examine the state of strain in the  $x : z$  plane and we will not consider strains in the direction normal to the plane.

There is a special case of a general three-dimensional state of strain which has practical importance in soil mechanics. This special case is when  $\epsilon_y = 0$  and it is known as plane strain; the conditions in the soil below a long wall or behind a long slope (Fig. 3-4) approximate closely to plane strain.

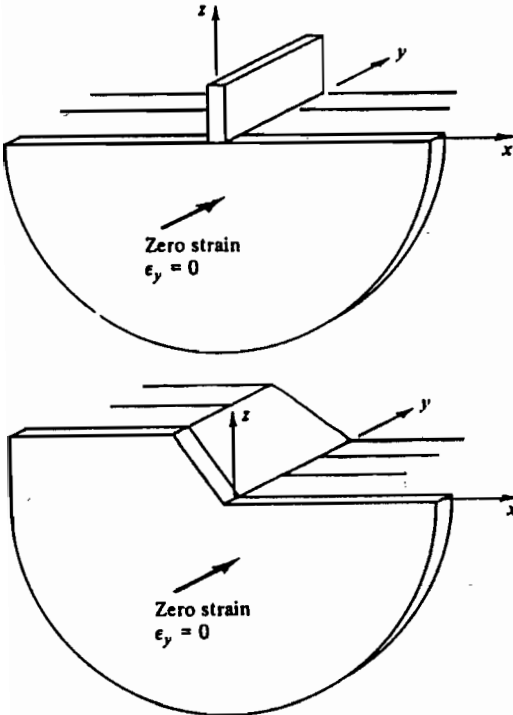
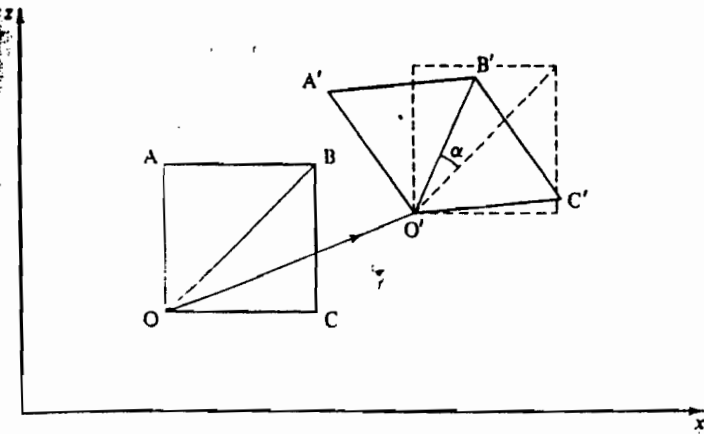


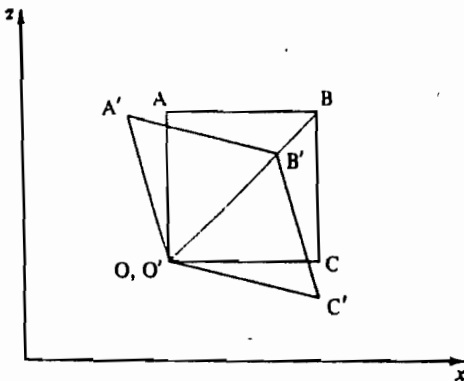
Figure 3-4 Illustrations of plane strain

### 3-7 GENERAL PLANE STRAIN DEFORMATIONS

Figure 3-5(a) shows a small element  $OABC$ , lying in the  $x : z$  plane which, as a result of some change in the state of effective stress, moves and distorts in plane strain (i.e.  $\epsilon_y = 0$ ) and takes up a new position  $O'A'B'C'$ . Before we



(a)



(b)

Figure 3-5 Components of deformation (a) Body displacement and rotation. (b) Strain and distortion

can investigate the state of strain in the element, it is necessary to separate components of body rotation and displacement from strains and distortions.

First, there has been a displacement of the element as a whole given by the vector  $OO'$ . Second, there has been a rotation of the element as a whole given by the rotation  $\alpha$  of the diagonal  $OB$  to  $O'B'$ . All other effects are due to normal and shear strains.

In order to examine the state of strain it is necessary to remove the components of rotation and displacement by rotating  $O'A'B'C'$  through  $-\alpha$  and moving it along the vector  $O'O$  so that  $O$  and  $O'$  coincide and  $OB$  and  $O'B'$  are collinear, as shown in Fig. 3-5(b). Shear strains and normal strains can now be distinguished. The strains are indicated in Fig. 3-6(a) which shows the distorted element  $O'A'B'C'$  from Fig. 3-5(b).

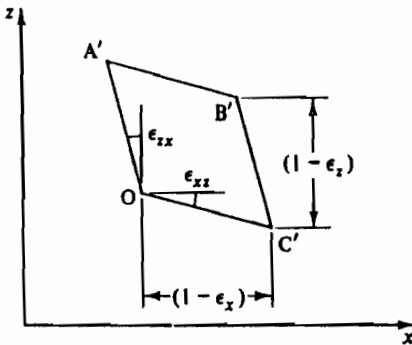
### 3-8 NORMAL AND SHEAR STRAIN

Normal strains defined by Eq. (2-2) are simply brought about by changes in the  $x$ - and  $z$ -dimensions of the element. If the sides of the element  $OABC$  were originally of unit length then, for small strains, the dimensions of the distorted element  $O'A'B'C'$  are

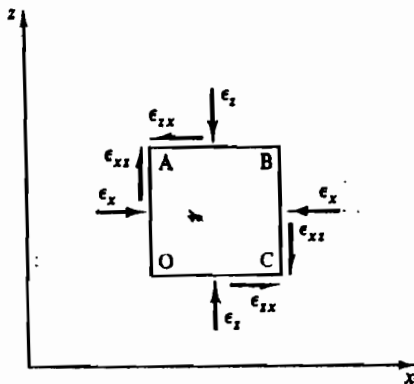
$$A'B' = C'O' = (1 - \epsilon_z),$$

$$A'O' = B'C' = (1 - \epsilon_x).$$

Shear strains  $\epsilon_{zx}$  and  $\epsilon_{xz}$  in Fig. 3-6(a) are brought about by rotations of the sides of the element which remain after the mean rotation  $\alpha$  of the element as a whole has been removed; from the geometry of Fig. 3-5(b) it follows that  $\epsilon_{zx} = \epsilon_{xz}$ . The index and sign notation adopted are such that a shear strain  $\epsilon_{zx}$  is associated with a shear stress  $\tau_{zx}$  and so positive values of  $\epsilon_{zx}$



(a)



(b)



and  $\epsilon_{xx}$  imply that the angle between the sides OA and OC increases. Thus, in Fig. 3-6(a), the shear strains are positive as defined in Sec. 2-3.

It is important to note that  $\epsilon_{xx}$  is a *pure shear strain* and it is not the same as the *engineers' shear strain*  $\gamma$  defined by Eq. (2-4); the point will be discussed further in Sec. 3-10.

### 3-9 REPRESENTATION OF A STATE OF STRAIN

The state of strain in the element OABC is shown in Fig. 3-6(a); this may be represented more simply by drawing the undeformed element as in Fig. 3-6(b) and marking normal and shear strains on the four faces.

Figure 3-6(b) is like Fig. 3-1(a), which shows the state of stress in an element, but we must be careful not to think of strains in quite the same way that we think of stresses. Although we may regard stresses as acting on individual planes, it is meaningless to try to imagine a strain on a plane. Thus, in Fig. 3-6(b),  $\epsilon_x$  and  $\epsilon_{xx}$  are the normal and shear strains in the material between the planes AO and BC.

### 3-10 PURE SHEAR STRAIN AND ENGINEERS' SHEAR STRAIN

Figure 3-7(a) shows the strained element O'A'B'C' of Fig. 3-6(a). The shear distortions of the element are  $\epsilon_{xx}$  and  $\epsilon_{yy}$ . If the element is rotated counter-clockwise about O' through an angle  $\epsilon_{xy}$ , we obtain Fig. 3-7(b), which is identical to Fig. 2-1(c) for  $\epsilon_x = \epsilon_y = 0$ . Comparing Figs 3-7(b) and 2-1(c), we have

$$\gamma_{yx} = \epsilon_{yx} + \epsilon_{xy}, \quad (3-5)$$

but

$$\epsilon_{xx} = \epsilon_{yy}, \quad (3-6)$$

therefore,

$$\gamma_{yx} = 2\epsilon_{xy}. \quad (3-7)$$

Alternatively, we may rotate the element clockwise about O' through an angle  $\epsilon_{yx}$  and we obtain Fig. 3-7(c). Comparing Figs 3-7(c) and 2-1(c), we have

$$\gamma_{xy} = \epsilon_{xy} + \epsilon_{yx}, \quad (3-8)$$

but

$$\epsilon_{yy} = \epsilon_{xx}, \quad (3-9)$$

therefore,

$$\gamma_{xy} = 2\epsilon_{yx}. \quad (3-10)$$

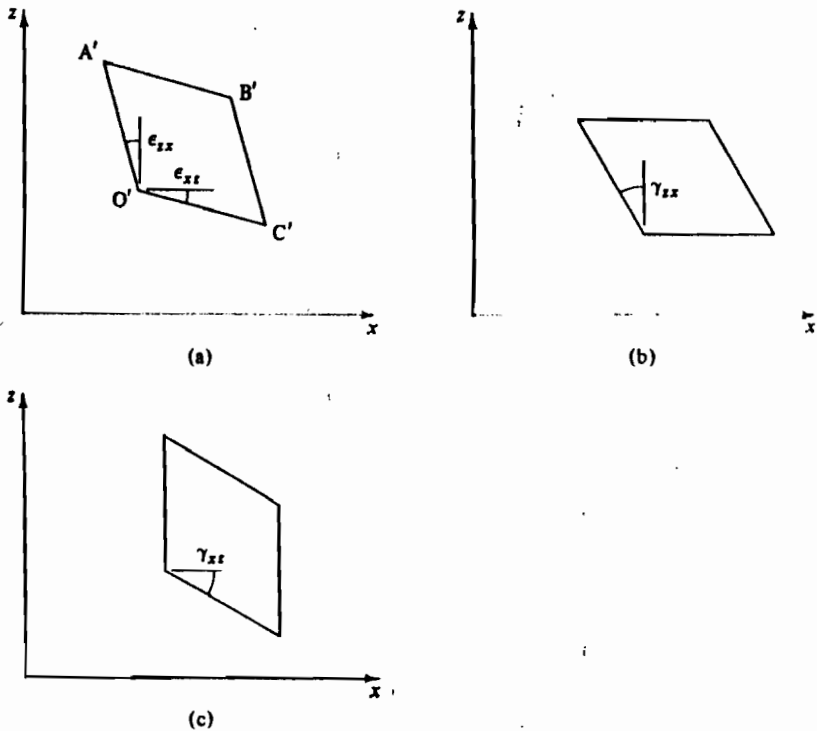


Figure 3-7 Pure shear strain and engineers' shear strain

Hence, engineers' shear strain is simply twice the pure shear strain; the engineers' shear strain  $\gamma_{xz}$  consists of a component of pure shear strain  $\epsilon_{xx}$  together with a numerically equal component of body rotation.

Engineers' shear strain is the change in the angle between two fibres embedded in the  $x : z$  plane which were originally at right angles to one another, as shown in Fig. 2-1(c). For the analysis of states of strain, however, it turns out that it is appropriate to work with the pure shear strains together with the normal strains. It is simplest, and conventional, to consider normal strains  $\epsilon_x$  and  $\epsilon_y$  associated with shear strains  $\frac{1}{2}\gamma_{xz}$  and  $\frac{1}{2}\gamma_{yz}$  and to plot Mohr's circles of strain with axes denoting normal strain  $\epsilon$  and pure shear strain  $\frac{1}{2}\gamma$  as shown in Fig. 3-8(c).

### 3-11 MOHR'S CIRCLE OF STRAIN

Figure 3-8(a) shows the state of strain in a small plane element OABC. If the strains  $\epsilon_x$ ,  $\epsilon_y$ , and  $\gamma_{xz}$  are known, we may wish to calculate the strains in the element OEF in Fig. 3-8(b) rotated through an angle  $\theta$  about O.

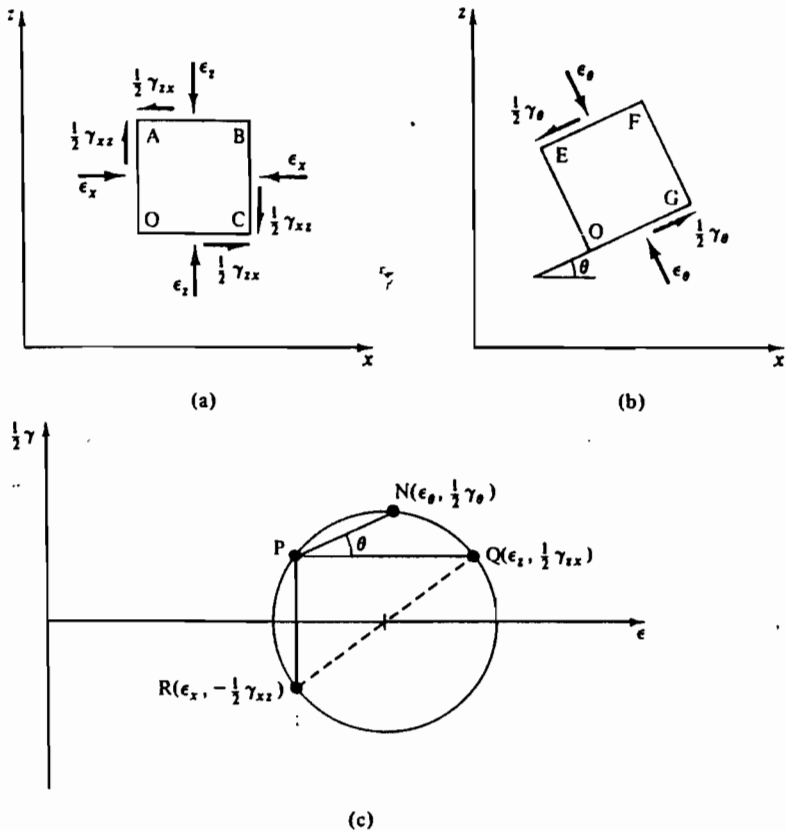


Figure 3-8 States of strain in two-dimensional elements and the corresponding Mohr's circle of strain

We make use of the Mohr's circle of strain in exactly the same way as that for stress.

The Mohr's circle of strain corresponding to the state of strain in Fig. 3-8(a) is shown in Fig. 3-8(c). The circle of strain is plotted on a diagram with axes  $\frac{1}{2} \gamma$  ( $=$  pure shear strain) and  $\epsilon$  ( $=$  normal strain) and is drawn to pass through the points R ( $\epsilon_x, -\frac{1}{2} \gamma_{xz}$ ) and Q ( $\epsilon_z, \frac{1}{2} \gamma_{xz}$ ), which represent the known strains. For plotting Mohr's circles of strain, and for this purpose *only*, we adopt the convention, compatible with that adopted for Mohr's circles of stress, that counter-clockwise shear strains are taken as positive. Hence the counter-clockwise shear strains  $\frac{1}{2} \gamma_{xz}$  in Fig. 3-8(a) are positive in Fig. 3-8(c) and the clockwise shear strains  $\frac{1}{2} \gamma_{xz}$  are negative.

In exactly the same way as for Mohr's circles of stress, we locate the pole at P by drawing RP or QP parallel with the planes OA or OC in Fig. 3-8(a). We may then draw PN at an angle  $\theta$  to PQ and the strains at N ( $\epsilon_\theta, \frac{1}{2} \gamma_\theta$ )

are the values of the respective strain components in the element OEF $G$  in Fig. 3-8(b).

### 3-12 PRINCIPAL PLANES AND PRINCIPAL STRAINS

There are two points where the Mohr's circle of strain crosses the  $\epsilon$ -axis. These points represent planes in the  $x : z$  plane across which the normal strain is either a maximum or a minimum and the shear strain is zero. These maximum and minimum normal strains are the principal strains  $\epsilon_1$  and  $\epsilon_3$  and the planes are principal planes. The magnitudes of  $\epsilon_1$  and  $\epsilon_3$  may be found from Fig. 3-9(b) and the directions of the principal planes, shown in Fig. 3-9(a), are fixed by the value of  $\theta_P$  determined from Fig. 3-9(b).

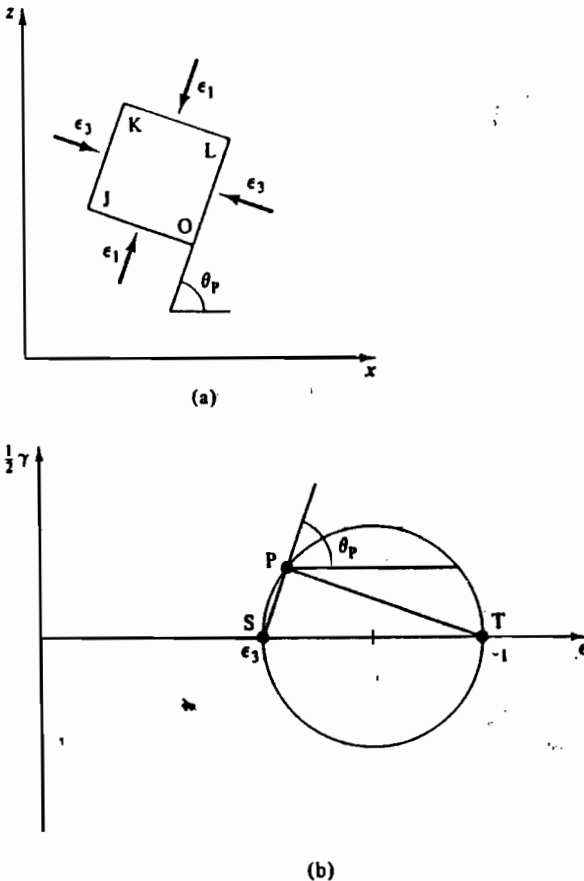


Figure 3-9 Principal planes and principal strains

Principal strains have the same meaning in strain analysis as principal stresses have in stress analysis. For general three-dimensional states of strain, there will be three principal planes and three principal stresses  $\epsilon_1 > \epsilon_2 > \epsilon_3$ ;  $\epsilon_1$  is the major principal strain,  $\epsilon_2$  the intermediate, and  $\epsilon_3$  the minor.

### Example 3-3 Mohr's circle of strain

Figure E3-4 shows a section of a 40 mm cube of soil OABC which is distorted in plane strain (i.e., zero strain out of the page) to O'A'B'C'. The coordinates of the corners of the distorted cube are A'(-2, 36), B'(41, 36), C'(43, 0), O'(0, 0). Construct the Mohr's circle of strain and find the magnitudes of the principal strains and the directions of the principal planes.

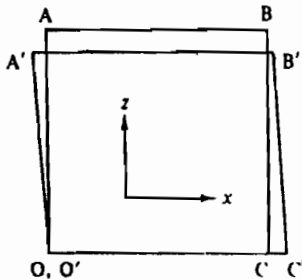


Figure E3-4

Defining axes ( $x, z$ ) as shown in Fig. E3-4, the normal and shear strains across the faces of the cube are

$$\begin{aligned}\epsilon_x &= -\frac{3}{40} = -0.075, \\ \epsilon_z &= +\frac{4}{40} = 0.100, \\ \gamma_{xz} &= \gamma_{zx} = +\frac{2}{40} = 0.050, \\ \epsilon_{xz} &= \epsilon_{zx} = \frac{1}{2}\gamma = 0.025.\end{aligned}$$

Note that  $\epsilon_x$  is a tensile strain and is, therefore, negative,  $\epsilon_z$  is a compressive strain and is, therefore, positive, and the shear strains  $\epsilon_{xz}$  and  $\epsilon_{zx}$  are positive because the angles in the positive quadrants of the cube increase.

The Mohr's circle of strain is shown in Fig. E3-5; for plotting the Mohr's circle, the counter-clockwise shear strain  $\epsilon_{xz}$  is plotted positively and the clockwise shear strain  $\epsilon_{zx}$  is plotted negatively. Scaling from the diagram, the principal strains are

$$\epsilon_1 = 0.104 \quad \text{and} \quad \epsilon_3 = -0.079.$$

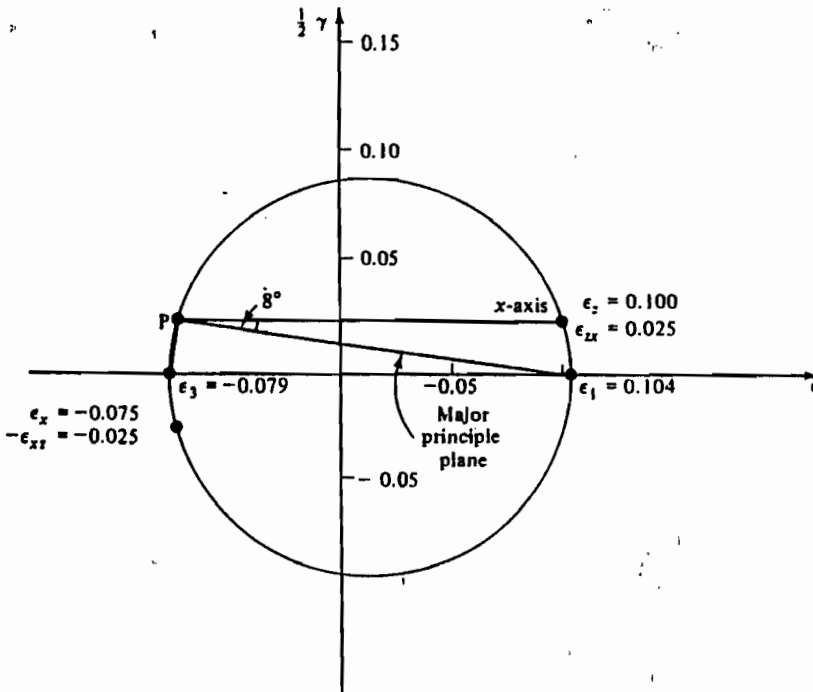


Figure E3-5 Mohr's circle of strain

The pole of the Mohr's circle is located at P and the major principal plane makes an angle of  $8^\circ$  to the  $x$ -axis.

### 3-13 MOHR'S CIRCLES FOR INCREMENTS OF STRESS AND STRAIN

Although we have considered Mohr's circles for states of stress and strain the analyses are equally applicable for *increments* of stress and strain.

### 3-14 RELATIONSHIPS BETWEEN STATES OF STRESS AND STATES OF STRAIN

Although the Mohr's circle of stress in Fig. 3-1(c) is similar to the Mohr's circle of strain in Fig. 3-8(c) and similar lettering has been used on each diagram, we have done this purely to bring out the similarities between stress analysis and strain analysis and it must not be assumed that the state of stress shown in Fig. 3-1(a) will give rise to the state of strain shown in Fig. 3-8(a).

The state of strain that occurs in a soil as a result of some state of stress depends on many factors and, in particular, on the special rules that govern the mechanical behaviour of soil. As engineers, we should be familiar with the theories of elasticity and plasticity. Both of these theories can relate stresses with strains (or strain increments) in loaded bodies, and they provide sets of rules for material behaviour under load. An important part of theoretical soil mechanics is to describe a set of rules governing the relationships between stresses and strains in loaded bodies of engineering soil.

### 3-15 SUMMARY

1. Mohr's circles may be used to analyse states of stress and of strain; a simple method of analysis is to use the pole construction.
2. Mohr's circles of total and effective stress have the same diameter and are separated by a distance equal to the magnitude of the pore pressure.
3. Pure shear strains such as  $\epsilon_{xz}$  must be distinguished from engineers' shear strains such as  $\gamma_{xz} (= 2\epsilon_{xz})$ .
4. Shear stresses are zero on principal planes of stress; shear strains are zero across principal planes of strain.

### REFERENCES

- Case, J. and Chilver, A. H. *Strength of Materials and Structures*. Edward Arnold, London, 1971.
- Crandall, S. H., Dahl, N. C., and Lardner, T. J. *An Introduction to the Mechanics of Solids*. McGraw-Hill Kogakusha, Tokyo, 1972.

## STRESS AND STRAIN PATHS AND INVARIANTS

### 4-1 INTRODUCTION

An element of soil, whether it is part of a laboratory test specimen or a soil structure, will experience changes in its state of stress and in its state of strain as the laboratory test progresses or as the structure is built and loaded in service. We have already seen how Mohr's circles may be employed to analyse the state of stress or the state of strain at a particular instant during the loading, but we may need to trace the history of the changes in the states of stress and strain.

If a perfectly elastic material is loaded or unloaded within its elastic range the behaviour of the material is dependent only on the initial and final states and is independent of the route taken during the loading or unloading. In contrast, soil behaviour is dependent not only on the initial and final states of stress but also on the way in which the states of stress and strain are changed and on the previous history of loading; we will need, therefore, to be able to trace the state of a soil element throughout its loading history.

### 4-2 STRESS PATHS

In a general cubical element of material, there are six independent stresses, i.e., three shear stresses and three normal stresses. If the element is rotated so that the faces become principal planes, the shear stresses on the faces vanish and the normal stresses become principal stresses. For a soil, the state of stress is completely defined by the three principal total stresses and their directions and the pore pressure; the three principal effective stresses may be calculated simply from Eq. (2-7).  $(\sigma' = \sigma - p)$

We may draw axes  $\sigma'_1$ ,  $\sigma'_2$ , and  $\sigma'_3$  as shown in Fig. 4-1 to define an effective stress space. The instantaneous state of effective stress in an element may be plotted as a point† in the effective stress space and the line joining all the points of instantaneous states of effective stress is defined as the *effective*

† The point represents only the magnitudes of the principal stresses: it does not record their directions and the stress path does not record any rotation of the principal planes.



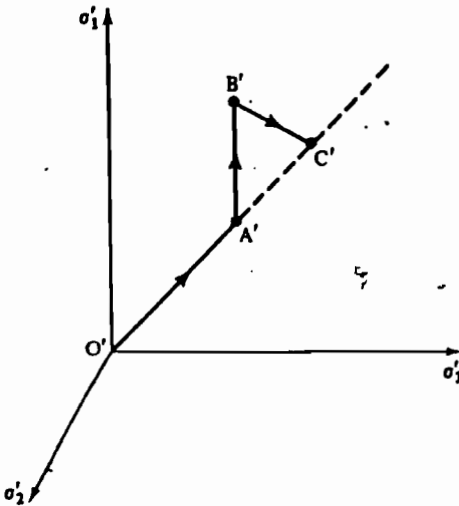


Figure 4-1 Stress path in a three-dimensional effective stress space

*stress path*. We could equally well define a total stress space with axes  $\sigma_1$ ,  $\sigma_2$ , and  $\sigma_3$  and plot a *total stress path*. It is often convenient to superimpose the total and effective stress axes. The total stress path and the effective stress path will then be separated by a distance representing the magnitude of the pore pressure.

In similar fashion we could also trace the history of the state of strain in an element by defining axes  $\epsilon_1$ ,  $\epsilon_2$ , and  $\epsilon_3$  and plotting a *strain path* as the line joining the instantaneous states of strain.

As an example we will consider the effective stress path illustrated in Fig. 4-1. The path represents a sequence of loading consisting of:

- O'A',  $\sigma'_1$ ,  $\sigma'_2$ , and  $\sigma'_3$  increased equally from zero;
- A'B',  $\sigma'_1$  increased,  $\sigma'_2$  and  $\sigma'_3$  held constant;
- B'C',  $\sigma'_2$  and  $\sigma'_3$  increased,  $\sigma'_1$  held constant.

If A'B' and B'C' represent equal increments of  $\sigma'_1$ , and of  $\sigma'_2$  and  $\sigma'_3$ , the point C' will lie on the projection of O'A'; the line O'A'C' is known as the *space diagonal*. The state of stress represented by a point on the space diagonal is isotropic (equal all-round) with  $\sigma'_1 = \sigma'_2 = \sigma'_3$ .

The method of plotting stress paths in three dimensions shown in Fig. 4-1 is rather cumbersome and the paths are not easy to follow or to manipulate. Under various circumstances we may select different axes to give simpler pictures of the history of loading of an element.

### 4-3 STRESS PATHS WITH $\sigma'_1:\sigma'_3$ AND $\sigma_1:\sigma_3$ AXES

It is sometimes convenient to ignore the intermediate principal stress  $\sigma'_2$  and plot effective stress paths in the two-dimensional effective stress plane  $\sigma'_1:\sigma'_3$ , as shown in Fig. 4-2. We may also superimpose the two-dimensional total stress plane  $\sigma_1:\sigma_3$  and plot total stress paths.

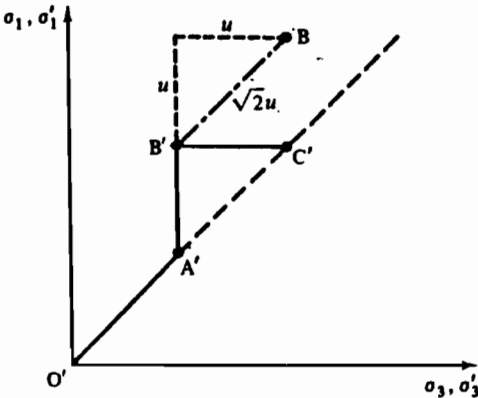


Figure 4-2 Stress path with  $\sigma'_1, \sigma'_3$ - and  $\sigma_1, \sigma_3$ -axes

In Fig. 4-2,  $O'A'B'C'$  is the same effective stress path as that shown in Fig. 4-1. If the pore pressure at  $B'$  has some value  $u$ , the point  $B$  represents the instantaneous total stress; by inspection, points of instantaneous total and effective stress are separated by  $\sqrt{(2)}u$  along lines inclined at  $45^\circ$  to the axes, as shown in Fig. 4.2.

#### Example 4-1 Stress paths with $\sigma_1:\sigma_3$ and $\sigma'_1:\sigma'_3$ axes

Table E4-1 records the variation of the total principal stresses and the pore pressure during a drained loading test on a sample of soil in which both the pore pressure  $u$  and the minor principal total stress  $\sigma_3$  were held constant and the sample was loaded by increasing the major principal total stress  $\sigma_1$ .

Table E4-1 Drained loading test

$\sigma_1$	$\sigma_3$	$u$	$\sigma'_1$	$\sigma'_3$
300	300	100	200	200
400	300	100	300	200
500	300	100	400	200
565	300	100	465	200
590	300	100	490	200

All stresses given in kiloNewtons per square metro.

Table E4-2 shows similar data from an undrained loading test in which the minor principal total stress  $\sigma_3$  was held constant and the pore pressure  $u$  changed as the soil responded to increases of major principal total stress  $\sigma_1$  without volume change.

Table E4-2 Undrained loading test

$\sigma_1$	$\sigma_3$	$u$	$\sigma'_1$	$\sigma'_3$
300	300	100	200	200
350	300	165	185	135
380	300	200	180	100
396	300	224	172	76
398	300	232	166	68

All stresses given in kiloNewtons per square metre.

For each test, plot total and effective stress paths using  $\sigma_1$ : $\sigma_3$  and  $\sigma'_1$ : $\sigma'_3$  axes.

Values for the major and minor principal effective stresses are simply calculated from Eq. (2-7) and values for  $\sigma'_1$  and  $\sigma'_3$  are given in the tables.

The required total and effective stress paths are shown in Fig. E4-1.

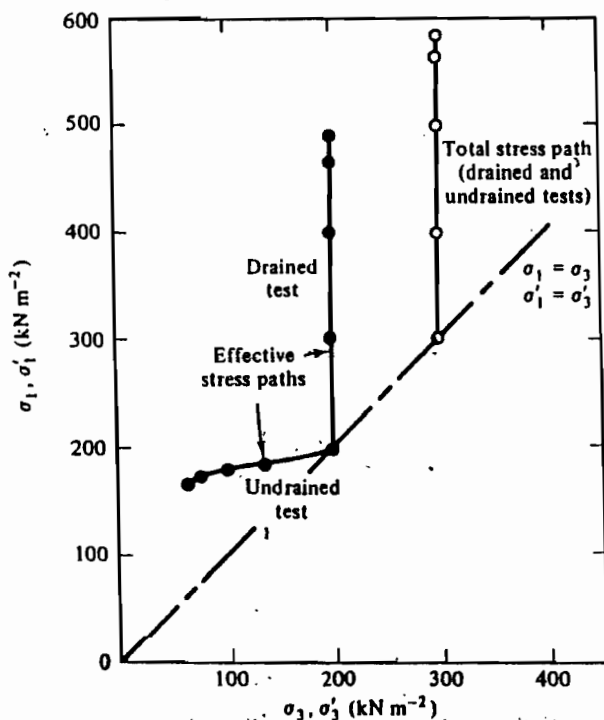


Figure E4-1 Stress paths for drained and undrained loading tests

4-4 STRESS PATHS WITH  $t':s'$  AND  $t:s$  AXES

The instantaneous two-dimensional state of stress may be represented by a Mohr's circle of stress as shown in Fig. 4-3. The position of the Mohr's circle and its size may be identified by the coordinates  $(s', t')$  of its apex  $M'$  and we could trace the loading of an element by plotting the path of  $M'$  on axes  $s'$  and  $t'$ . We could equally well consider total stresses and plot a total stress path on axes  $s$  and  $t$  by tracing the path of the apex of the Mohr's circle of total stress.

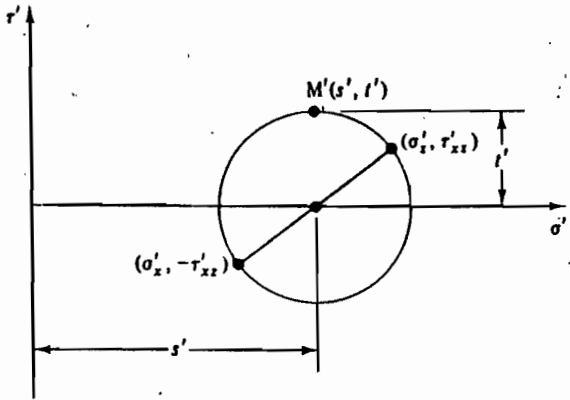


Figure 4-3 Definition of stress parameters  $t'$  and  $s'$

By inspection of Fig. 4-3, we see that  $t'$  is the radius of the Mohr's circle of effective stress and is equal to the maximum shear stress, while  $s'$  is the distance from the origin to the centre of the Mohr's circle of effective stress and is equal to the mean of  $\sigma'_x$  and  $\sigma'_y$ .

From the geometry of Fig. 4-3, and noting that the magnitude of  $\tau_{xx}$  and  $\tau_{xx}$  are equal, we have

$$t' = \frac{1}{2}[(\sigma'_x - \sigma'_y)^2 + 4\tau_{xx}^2]^{1/2}, \quad (4-1)$$

$$s' = \frac{1}{2}(\sigma'_x + \sigma'_y), \quad (4-2)$$

or, in terms of principal effective stresses,

$$t' = \frac{1}{2}(\sigma'_1 - \sigma'_2), \quad (4-3)$$

$$s' = \frac{1}{2}(\sigma'_1 + \sigma'_2), \quad (4-4)$$

In the same way, for total stresses we define

$$t = \frac{1}{2}(\sigma_1 - \sigma_2), \quad (4-5)$$

$$s = \frac{1}{2}(\sigma_1 + \sigma_2). \quad (4-6)$$

Simple calculation and use of the effective stress equation (2-7), then gives

$$t' = t, \tag{4-7}$$

$$s' = s - u, \tag{4-8}$$

and, if the total and effective stress paths are plotted with axes  $t:s$  and  $t':s'$  superimposed, the paths are separated horizontally by a distance equal to  $u$ , the pore pressure.

Figure 4-4 shows the stress path of Fig. 4-1 plotted with axes  $t':s'$ . To calculate the slopes of the parts A'B' and B'C' we may write Eqs (4-3) and (4-4) as

$$\delta t' = \frac{1}{2}(\delta\sigma'_1 - \delta\sigma'_3), \tag{4-9}$$

$$\delta s' = \frac{1}{2}(\delta\sigma'_1 + \delta\sigma'_3). \tag{4-10}$$

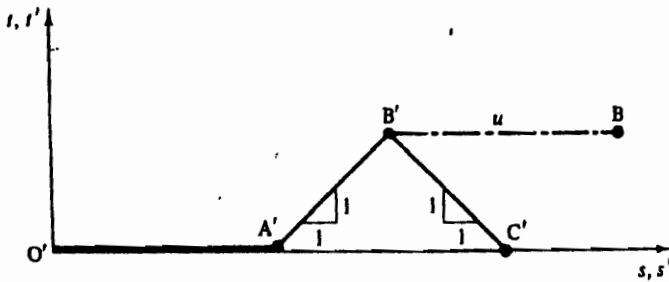


Figure 4-4 Stress paths with  $t', s'$ - and  $t, s$ -axes

For A'B'  $\delta\sigma'_3 = 0$  and  $dt'/ds' = 1$ , and for B'C'  $\delta\sigma'_1 = 0$  and  $dt'/ds' = -1$ . The point B represents the state of total stress corresponding to effective stresses at B' and so it is separated horizontally from B' by a distance equal to  $u$ , the pore pressure.

**Example 4-2. Stress paths with  $t:s$  and  $t':s'$  axes**

Plot total and effective stress paths using  $t:s$  and  $t':s'$  axes for the drained and undrained loading tests in Ex. 4-1.

**Table E4-3 Drained loading test**

$\sigma_1$	$\sigma_3$	$u$	$t$	$s$	$t'$	$s'$
300	300	100	0	300	0	200
400	300	100	50	350	50	250
500	300	100	100	400	100	300
565	300	100	133	433	133	333
590	300	100	145	445	145	345

All stresses given in kiloNewtons per square metre.

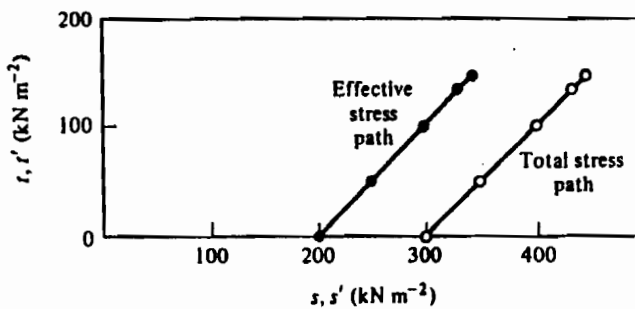
Values of  $t$  and  $s$  and of  $t'$  and  $s'$  may be found from the principal total stresses and pore pressures given in Tables E4-1 and E4-2, making use of Eqs (4-3) to (4-6) and the results are listed in Tables E4-3 and E4-4.

Table E4-4 Undrained loading test

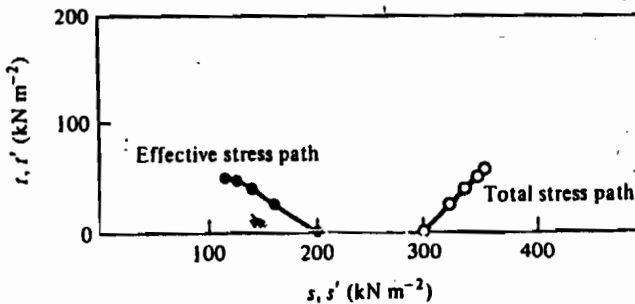
$\sigma_1$	$\sigma_3$	$u$	$t$	$s$	$t'$	$s'$
300	300	100	0	300	0	200
350	300	165	25	325	25	160
380	300	200	40	340	40	140
396	300	224	48	348	48	124
398	300	232	49	349	49	117

All stresses given in kiloNewtons per square metre.

The required total and effective stress paths are shown in Fig. E4-2.



(a)



(b)

Figure E4-2 Stress paths for (a) drained and (b) undrained loading tests

## 4.5 INVARIANTS OF STRESS

The parameters  $t'$  and  $s'$  (and  $t$  and  $s$ ) are rather special because, for a given state of stress, their values are independent of the arbitrary choice of the orientation of the reference axes. It is easy to see why this must be so; the two-dimensional state of effective stress in an element is described by a unique Mohr's circle of effective stress and the parameters  $t'$  and  $s'$  simply locate the apex of this unique circle. Parameters like  $\sigma'_x$ ,  $\sigma'_y$ , and  $\tau'_{xy}$ , which depend on the orientation of the reference axes as well as on the state of stress, are not entirely suitable on their own as measures of the stress state, because their magnitudes depend on the choice of axes. We would do better, at least for isotropic soils, to choose stress parameters which are independent of the choice of reference axes and which are unique for a given state of stress. As we have seen, the magnitudes of the parameters  $t'$  and  $s'$  do not depend on the choice of axes and, for this reason, they are appropriate measures of the state of stress for the two-dimensional stress states considered.

Stress parameters the magnitudes of which are independent of the choice of reference axes are usually known as *stress invariants*; they are invariant in the sense that their magnitudes do not change as the reference axes are varied. We should note, however, that the term 'stress invariant' is strictly reserved for parameters appropriate to general states of stress and, further, that the parameters  $t'$ ,  $s'$  are not entirely satisfactory as complete measures of a two-dimensional state of stress as the value of the intermediate principal stress  $\sigma'_2$  has been ignored. Nevertheless, use of the parameters  $t'$  and  $s'$  is often convenient when, for example, the value of the intermediate principal stress is not known.

We will not cover the theory of invariants here;† instead, we will only state that the octahedral normal effective stress  $\sigma'_{\text{oct}}$  and the octahedral shear stress  $\tau'_{\text{oct}}$  are invariants and these are defined by

$$\sigma'_{\text{oct}} = \frac{1}{3}(\sigma'_x + \sigma'_y + \sigma'_z), \quad (4-11)$$

$$\tau'^2_{\text{oct}} = \frac{1}{6}[(\sigma'_x - \sigma'_y)^2 + (\sigma'_y - \sigma'_z)^2 + (\sigma'_z - \sigma'_x)^2 + 6(\tau'^2_{xy} + \tau'^2_{yz} + \tau'^2_{zx})], \quad (4-12)$$

or, in terms of principal stresses,

$$\sigma'_{\text{oct}} = \frac{1}{3}(\sigma'_1 + \sigma'_2 + \sigma'_3), \quad (4-13)$$

$$\tau'_{\text{oct}} = \frac{1}{3}[(\sigma'_1 - \sigma'_2)^2 + (\sigma'_2 - \sigma'_3)^2 + (\sigma'_3 - \sigma'_1)^2]^{1/2}. \quad (4-14)$$

The corresponding octahedral total stresses are, similarly,

$$\sigma_{\text{oct}} = \frac{1}{3}(\sigma_1 + \sigma_2 + \sigma_3), \quad (4-15)$$

$$\tau_{\text{oct}} = \frac{1}{3}[(\sigma_1 - \sigma_2)^2 + (\sigma_2 - \sigma_3)^2 + (\sigma_3 - \sigma_1)^2]^{1/2} \quad (4-16)$$

† See, for example, Ford (1963), chapters 2 and 8.

and, by simple calculation, total and effective octahedral stresses are related by

$$\tau'_{oct} = \tau_{oct} \tag{4-17}$$

$$\sigma'_{oct} = \sigma_{oct} - u. \tag{4-18}$$

The meaning of the parameters  $\tau'_{oct}$  and  $\sigma'_{oct}$  is illustrated in Fig. 4-5.

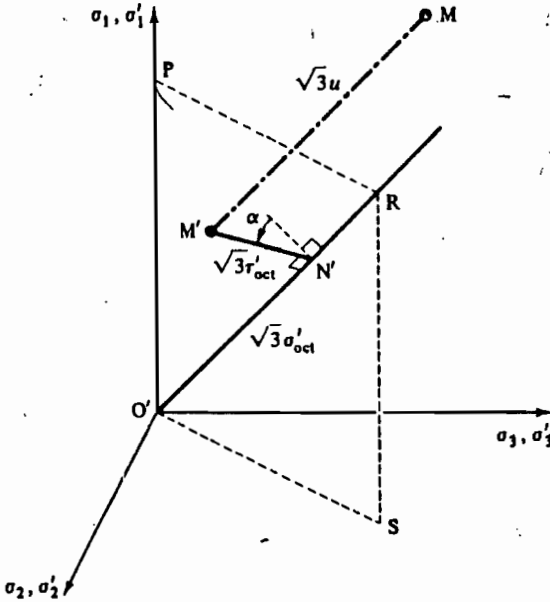


Figure 4-5 Representation of octahedral stress

The state of effective stress at  $M'$  may be described by a distance  $O'N'$  along the space diagonal  $O'R$  together with a distance  $N'M'$  normal to  $O'R$ ; the vector  $O'N'$  is equal to  $\sqrt{3}\sigma'_{oct}$  and the vector  $N'M'$  is equal to  $\sqrt{3}\tau'_{oct}$ . In order to describe the location of  $M'$  completely, we require a third invariant; this may conveniently take the form of an angle  $\alpha$  measuring the rotation of the vector  $N'M'$  from the plane  $OPRS$ . The state of total stress at  $M$  is equivalent to a state of effective stress  $M'$  plus a pore pressure  $u$ ; the vector  $M'M$  has magnitude  $\sqrt{3}u$  and is parallel to the space diagonal.

For the special case where  $\sigma'_3 = \sigma'_2$ , points such as  $M'$  and  $M$  plot in the  $OPRS$  plane with  $\alpha = 0$ . Also, for  $\sigma'_3 = \sigma'_2$ ,

$$\sigma'_{oct} = \frac{1}{3}(\sigma'_1 + 2\sigma'_2), \tag{4-19}$$

$$\tau'_{oct} = \frac{\sqrt{2}}{3}(\sigma'_1 - \sigma'_2). \tag{4-20}$$



To avoid the recurring  $\frac{1}{3}\sqrt{2}$  term, we will define new invariants  $q'$  and  $p'$ , where, for  $\sigma'_3 = \sigma'_2$ ,

$$p' = \frac{1}{3}(\sigma'_1 + 2\sigma'_2) = \sigma'_{\text{oct}}, \tag{4-21}$$

$$q' = (\sigma'_1 - \sigma'_2) = \frac{3}{\sqrt{2}} \tau'_{\text{oct}}. \tag{4-22}$$

For a general three-dimensional state of stress,  $q'$  and  $p'$  become

$$p' = \frac{1}{3}(\sigma'_1 + \sigma'_2 + \sigma'_3), \tag{4-23}$$

$$q' = \frac{1}{\sqrt{2}} [(\sigma'_1 - \sigma'_2)^2 + (\sigma'_2 - \sigma'_3)^2 + (\sigma'_3 - \sigma'_1)^2]^{1/2}, \tag{4-24}$$

and the third invariant  $\alpha$  will be non-zero. The corresponding total stress parameters are written

$$p = \frac{1}{3}(\sigma_1 + \sigma_2 + \sigma_3),$$

$$q = \frac{1}{\sqrt{2}} [(\sigma_1 - \sigma_2)^2 + (\sigma_2 - \sigma_3)^2 + (\sigma_3 - \sigma_1)^2]^{1/2}, \tag{4-26}$$

and simple calculation shows that the total stress and effective stress invariants are related by

$$p' = p - u, \tag{4-27}$$

$$q' = q. \tag{4-28}$$

Throughout the book we will be careful to distinguish  $q'$  from  $q$  and  $t'$  from  $t$ ; of course  $q' = q$  and  $t' = t$ , but, whenever we are considering effective stresses, we will write  $q'$  or  $t'$  and whenever we are considering total stresses we will write  $q$  or  $t$ .

#### 4-6 STRESS PATHS WITH $q':p'$ AND $q:p$ AXES

The invariants  $q'$  and  $p'$  may be used as axes for plotting effective stress paths. Figure 4-6 shows the stress path of Fig. 4-1; to calculate the slopes of

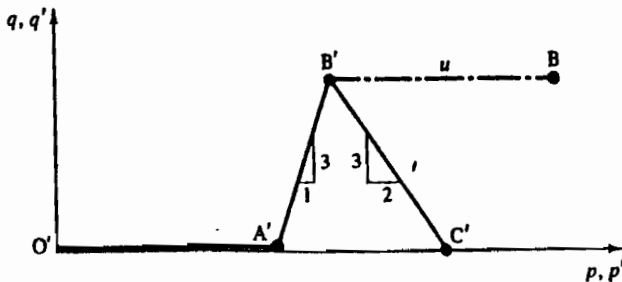


Figure 4-6 Stress paths with  $q', p'$ - and  $q, p$ -axes

the parts A'B' and B'C' we may write Eqs (4-21) and (4-22), which apply for the special case  $\sigma'_1 = \sigma'_2$ , as

$$\delta p' = \frac{1}{3}(\delta\sigma'_1 + 2\delta\sigma'_2), \tag{4-29}$$

$$\delta q' = (\delta\sigma'_1 - \delta\sigma'_2). \tag{4-30}$$

For A'B',  $\delta\sigma'_1 = \delta\sigma'_2 = 0$  and  $dq'/dp' = 3$  and, for B'C',  $\delta\sigma'_1 = 0$ ,  $\delta\sigma'_2 = \delta\sigma'_1$ , and  $dq'/dp' = -\frac{1}{3}$ . The point B represents the state of total stress corresponding to an effective stress state at B' together with a pore pressure  $u$ .

**Example 4-3** Stress paths with  $q:p$  and  $q':p'$  axes

Plot total and effective stress paths using axes  $q:p$  and  $q':p'$  for the drained and undrained loading tests in Ex. 4-1.

Values of  $q$  and  $p$  and of  $q'$  and  $p'$  may be found from the principal total stresses and pore pressures given in Tables E4-1 and E4-2 making use of Eqs (4-21), (4-22), (4-27), and (4-28). The results are listed in Tables E4-5 and E4-6.

**Table E4-5** Drained loading test

$\sigma_1$	$\sigma_2$	$u$	$q$	$p$	$q'$	$p'$
300	300	100	0	300	0	200
400	300	100	100	333	100	233
500	300	100	200	367	200	267
565	300	100	265	388	265	288
590	300	100	290	397	290	297

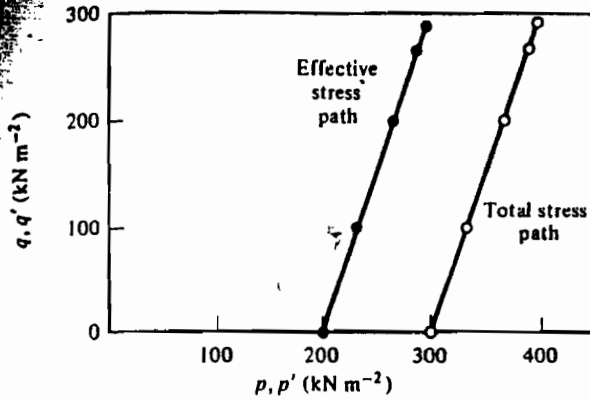
All stresses given in kiloNewtons per square metre.

**Table E4-6** Undrained loading test

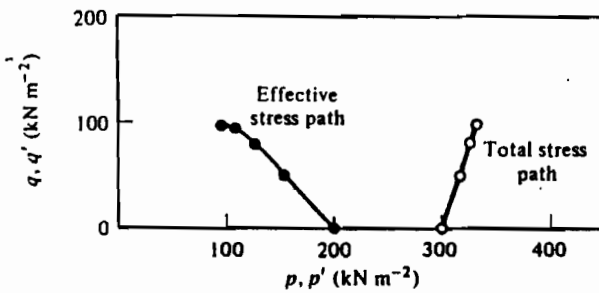
$\sigma_1$	$\sigma_2$	$u$	$q$	$p$	$q'$	$p'$
300	300	100	0	300	0	200
350	300	165	50	317	50	152
380	300	200	80	327	80	127
396	300	224	96	332	96	108
398	300	232	98	333	98	101

All stresses given in kiloNewtons per square metre.

The required total and effective stress paths are shown in Fig. E4-3.



(a)



(b)

Figure E4-3 Stress paths for (a) drained and (b) undrained loading tests

#### 4-7 INVARIANTS OF STRAIN

The history of strain in an element may be recorded by drawing axes  $\epsilon_1$ ,  $\epsilon_2$ , and  $\epsilon_3$ , and tracing a strain path as the line joining instantaneous states of strain; a strain path plotted in this way will appear like the stress path shown in Fig. 4-1. Alternatively, we may seek invariants of strain and use these as axes for plotting strain paths, but then we must take care that we select invariants of strain which correspond to those already chosen for stress.

The correct choice of strain invariants may be found by noting that, as an element of soil deforms under load, the work done by the external loads is invariant (i.e., the magnitude of the work is independent of the arbitrary choice of reference axes), and when corresponding stress and strain invariants are multiplied together the products must always equal the work done by the external loads. For the present, we will simply state our choice of invariants for plotting strain paths and we will perform the necessary checks that these correspond to the chosen stress invariants later.

### 4-8 STRAIN PATHS

In an element deforming in plane strain, one of the principal strains will be zero by definition and we need only consider normal and shear strains in two dimensions. The instantaneous state of strain may be represented by a Mohr's circle of strain as shown in Fig. 4-7. We may recall that Mohr's circles of strain are plotted with axes of normal strain and pure shear strain and that  $\epsilon_{xx} = \frac{1}{2}\gamma_{xx}$ , where  $\gamma_{xx}$  is the engineers' shear strain.

The position and size of the Mohr's circle may be defined by the coordinates of its apex M; we define parameters  $\epsilon_\gamma = 2 \cdot NM$  and  $\epsilon_v = 2 \cdot ON$  and, from the geometry of Fig. 4-7,

$$\epsilon_\gamma = [(\epsilon_x - \epsilon_z)^2 + 4\epsilon_{xz}^2]^{1/2}, \tag{4-31}$$

$$\epsilon_v = (\epsilon_x + \epsilon_z). \tag{4-32}$$

Since  $\epsilon_\gamma$  and  $\epsilon_v$  simply locate the position of M in Fig. 4-7, their magnitudes will not vary as the axes (x, z) are rotated.

In terms of principal strains,

$$\epsilon_\gamma = (\epsilon_1 - \epsilon_2), \tag{4-33}$$

$$\epsilon_v = (\epsilon_1 + \epsilon_2). \tag{4-34}$$

In defining  $\epsilon_\gamma$  and  $\epsilon_v$ , we introduced a factor of 2 so that the strain parameters ( $\epsilon_\gamma, \epsilon_v$ ) correctly correspond to the stress parameters ( $t', s'$ ). The inclusion of the factor 2 is convenient because  $\epsilon_\gamma$  and  $\epsilon_v$  have familiar meanings. We may show quite simply that

$$\epsilon_\gamma = \gamma_{max}, \tag{4-35}$$

$$\epsilon_v = -\Delta V/V, \tag{4-36}$$

where  $\gamma_{max}$  is the maximum value of engineers' shear strain and  $\Delta V$  is a small increase in a volume  $V$ . Thus  $\epsilon_v$  is simply the (compressive) volumetric strain.

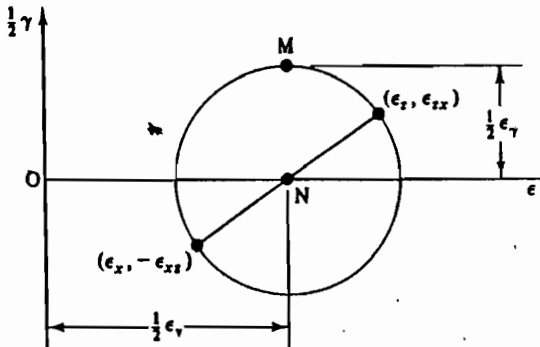


Figure 4-7 Definition of strain parameters  $\epsilon_\gamma$  and  $\epsilon_v$ .

The parameters  $\epsilon_\gamma$  and  $\epsilon_v$  may be used as axes for plotting strain paths; such strain paths will appear similar to the stress paths plotted with axes ( $t', s'$ ) as shown in Fig. 4-4. Use of the parameters  $\epsilon_\gamma$  and  $\epsilon_v$  when  $\epsilon_3 = 0$  is often very convenient; nevertheless, it must be appreciated that  $\epsilon_\gamma$  and  $\epsilon_v$  are *not* invariants, for their magnitudes depend on the choice of a reference axis aligned in the direction of zero strain. We must, therefore, examine the strain invariants which correspond with the stress invariants  $q'$  and  $p'$ .

The general state of strain in an element is defined completely by three direct strains ( $\epsilon_x, \epsilon_y, \epsilon_z$ ) and three shear strains ( $\epsilon_{xy}, \epsilon_{yz}, \epsilon_{zx}$ ), and we require combinations of these that are invariant. Without derivation, we will simply state that the octahedral normal strain  $\epsilon_{oct}$  and the octahedral shear strain  $\gamma_{oct}$  are invariant, where

$$\epsilon_{oct} = \frac{1}{3}(\epsilon_x + \epsilon_y + \epsilon_z), \quad (4-37)$$

$$\gamma_{oct}^2 = \frac{2}{3}[(\epsilon_x - \epsilon_y)^2 + (\epsilon_y - \epsilon_z)^2 + (\epsilon_z - \epsilon_x)^2] + \frac{2}{3}(\epsilon_{xy}^2 + \epsilon_{yz}^2 + \epsilon_{zx}^2). \quad (4-38)$$

There is an obvious similarity between octahedral stresses, defined by Eqs (4-11) and (4-12), and octahedral strains. Strictly, we should define a third strain invariant corresponding to  $\alpha$  in Fig. 4-5, but we have already dealt with strain paths for plane strain and, for axial symmetry,  $\alpha = 0$ .

If the axes are rotated so that the faces of the element are principal planes, Eqs (4-37) and (4-38) become

$$\epsilon_{oct} = \frac{1}{3}(\epsilon_1 + \epsilon_2 + \epsilon_3), \quad (4-39)$$

$$\gamma_{oct} = \frac{1}{\sqrt{3}}[(\epsilon_1 - \epsilon_2)^2 + (\epsilon_2 - \epsilon_3)^2 + (\epsilon_3 - \epsilon_1)^2]^{1/2}. \quad (4-40)$$

We must now find invariants of strain which correspond to the stress invariants  $q'$  and  $p'$  such that both together satisfy the work condition stated in Sec. 4-7. We will denote these invariants as  $\epsilon_\gamma$  and  $\epsilon_v$  and it turns out that

$$\epsilon_v = 3\epsilon_{oct}, \quad (4-41)$$

$$\epsilon_\gamma = \frac{1}{\sqrt{2}}\gamma_{oct}. \quad (4-42)$$

Thus,

$$\epsilon_v = (\epsilon_x + \epsilon_y + \epsilon_z), \quad (4-43)$$

$$\epsilon_\gamma^2 = \frac{2}{3}[(\epsilon_x - \epsilon_y)^2 + (\epsilon_y - \epsilon_z)^2 + (\epsilon_z - \epsilon_x)^2] + \frac{2}{3}(\epsilon_{xy}^2 + \epsilon_{yz}^2 + \epsilon_{zx}^2), \quad (4-44)$$

and, in terms of principal strains,

$$\epsilon_v = (\epsilon_1 + \epsilon_2 + \epsilon_3), \quad (4-45)$$

$$\epsilon_\gamma = \frac{\sqrt{2}}{3}[(\epsilon_1 - \epsilon_2)^2 + (\epsilon_2 - \epsilon_3)^2 + (\epsilon_3 - \epsilon_1)^2]^{1/2}. \quad (4-46)$$

It should be noted that, in Eqs (4-43) and (4-45), the invariant  $\epsilon_v$  is simply the volumetric strain as defined by Eq. (4-36) and, further, that by putting  $\epsilon_3 = 0$  for plane strain into Eq. (4-45) we recover Eq. (4-34).

The invariants  $\varepsilon_n$  and  $\varepsilon_v$  may be used as axes for plotting general three-dimensional strain paths; such paths will appear similar to the stress paths plotted with axes  $(q', p')$  as shown in Fig. 4-6.

For the special case, where  $\varepsilon_3 = \varepsilon_2$ , the strain invariants become

$$\varepsilon_v = (\varepsilon_1 + 2\varepsilon_2), \quad (4-47)$$

$$\varepsilon_n = \frac{2}{3}(\varepsilon_1 - \varepsilon_2). \quad (4-48)$$

#### 4-9 VOLUMETRIC STRAINS

The volumetric strain  $\varepsilon_v$  has appeared as an invariant and as an axis for plotting strain paths for general states of strain, for axial symmetry, and for plane strain. Volumetric strains play an important part in soil behaviour; they may be expressed and measured in a number of ways, and it is pertinent to examine these here.

If the volume  $V$  of an element of soil increases by  $\delta V$  as a result of some change of effective stress, the change in the volumetric strain is given by

$$\delta\varepsilon_v = -\delta V/V. \quad (4-49)$$

As usual we introduce the negative sign so that compressive strains are positive.

The volume  $V$  of a soil element is made up of a volume of water  $V_w$  and a volume of soil grains  $V_s$  as shown in Fig. 4-8(a). If the soil grains and the pore water are assumed to be incompressible, the volume of the element can only change if water is squeezed from, or drawn into, the soil element; thus,

$$\delta V = -\delta V_w, \quad (4-50)$$

where  $\delta V$  is the increase in the volume of the element and  $\delta V_w$  is the volume of water expelled. We may, therefore, calculate volumetric strains by measuring the quantity of water crossing the boundaries of a sample; such measurements are usually simple to arrange in laboratory tests.

The voids ratio, defined in Chapter 1, is  $e = V_w/V_s$  and, since the soil grains are incompressible (i.e.,  $\Delta V_s = 0$ ),

$$\delta e = \delta V_w/V_s.$$

Therefore,

$$\delta V = V_s \delta e \quad (4-51)$$

and, from Eq. (4-49),

$$\delta\varepsilon_v = -\frac{\delta V}{V} = -\frac{V_s \delta e}{V_s + V_w},$$

with the result that

$$\delta\varepsilon_v = -\frac{\delta e}{1+e}. \quad (4-52)$$

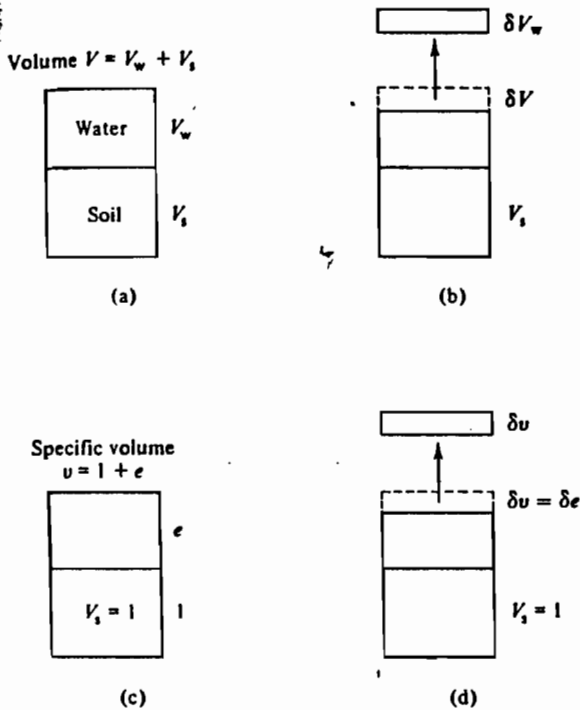


Figure 4-8 Volume changes in soils. (a) Volume of soil sample. (b) Volume change. (c) Specific volume. (d) Change of specific volume

The voids ratio is related to the water content and specific gravity of the soil grains by Eq. (1-1),  $e = wG_s$  and so

$$\delta e = G_s \delta w$$

and

$$\delta \varepsilon_v = -\frac{\delta w}{(1/G_s) + w}. \quad (4-53)$$

Volumetric strains may, therefore, be calculated from water content measurements.

In order that we may compare volume changes of different sized soil samples, it is convenient to introduce the specific volume  $v$ . The specific volume is defined as the volume of an element of soil containing unit volume of mineral grains, as indicated in Fig. 4-8(c); i.e.,  $V_s = 1$  and, from Chapter 1,

$$v = 1 + e. \quad (1-4)$$

If, due to some change of effective stress, the specific volume changes by  $\delta v$ , then

$$\delta v = \delta e$$

and

$$\delta \epsilon_v = -\frac{\delta e}{1+e} = -\frac{\delta v}{v} \tag{4-54}$$

### 4-10 CORRESPONDENCE BETWEEN PARAMETERS FOR STRESS AND STRAIN

We must now show that the stress and strain parameters have been chosen correctly by demonstrating that the products of corresponding parameters of stress and of strain correctly give the work done by the external loads.

First, we calculate the work done by the external loads and pressures per unit volume of soil. We consider an element with dimensions  $(a, b, c)$ , as shown in Fig. 4-9; the faces of the element are principal planes and the pore pressure has a constant value  $u$ . If, during a small time interval, the

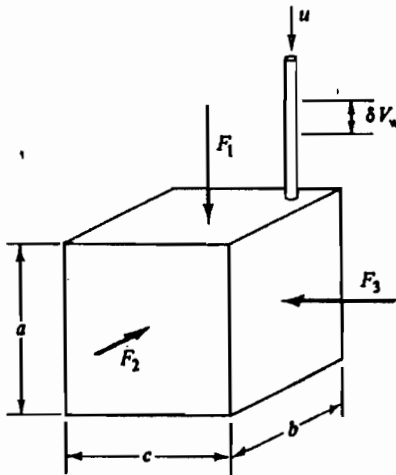


Figure 4-9 Diagram to illustrate the correspondence between invariants of stress and strain

dimensions of the element increase by  $\delta a$ ,  $\delta b$ , and  $\delta c$ , and the volume of water expelled is  $\delta V_w$ , then the work  $\delta W$  done by the external loads and pressures is given by

$$\delta W = F_1(-\delta a) + F_2(-\delta b) + F_3(-\delta c) - u\delta V_w \tag{4-55}$$

and, making use of Eq. (4-50), the work done per unit volume is

$$\frac{\delta W}{V} = \frac{F_1}{bc} \left( -\frac{\delta a}{a} \right) + \frac{F_2}{ca} \left( -\frac{\delta b}{b} \right) + \frac{F_3}{ab} \left( -\frac{\delta c}{c} \right) + u \frac{\delta V}{V}$$

Hence,

$$\delta W/V = \sigma_1 \delta \epsilon_1 + \sigma_2 \delta \epsilon_2 + \sigma_3 \delta \epsilon_3 - u \delta \epsilon_v \tag{4-56}$$



but  $u\delta\varepsilon_v = u(\delta\varepsilon_1 + \delta\varepsilon_2 + \delta\varepsilon_3)$  and, therefore,

$$\delta W/V = \sigma'_1 \delta\varepsilon_1 + \sigma'_2 \delta\varepsilon_2 + \sigma'_3 \delta\varepsilon_3 \quad (4-57)$$

The work done per unit volume may also be calculated in terms of the two-dimensional stress and strain parameters:

$$\delta W/V = t'\delta\varepsilon_\gamma + s'\delta\varepsilon_v \quad (4-58)$$

$$= \frac{1}{3}(\sigma'_1 - \sigma'_2)(\delta\varepsilon_1 - \delta\varepsilon_2) + \frac{1}{3}(\sigma'_1 + \sigma'_2)(\delta\varepsilon_1 + \delta\varepsilon_2)$$

$$= \sigma'_1 \delta\varepsilon_1 + \sigma'_2 \delta\varepsilon_2 \quad (4-59)$$

But for plane strain,  $\delta\varepsilon_3 = 0$  and Eq. (4-57) becomes

$$\delta W/V = \sigma'_1 \delta\varepsilon_1 + \sigma'_2 \delta\varepsilon_2 \quad (4-60)$$

Since Eqs (4-59) and (4-60) lead to identical expressions for  $\delta W/V$ , we have confirmed that the strain parameters  $\varepsilon_\gamma, \varepsilon_v$  are correctly associated with the stress parameters  $t', s'$  for conditions of plane strain.

The work done per unit volume may also be calculated in terms of the general three-dimensional stress and strain invariants as

$$\delta W/V = q'\delta\varepsilon_s + p'\delta\varepsilon_v \quad (4-61)$$

For the special case of axial symmetry, where  $\sigma'_2 = \sigma'_3$  and  $\varepsilon_2 = \varepsilon_3$ ,

$$q' = (\sigma'_1 - \sigma'_2), \quad (4-22)$$

$$p' = \frac{1}{3}(\sigma'_1 + 2\sigma'_2), \quad (4-21)$$

$$\delta\varepsilon_s = \frac{2}{3}(\delta\varepsilon_1 - \delta\varepsilon_2), \quad (4-62)$$

$$\delta\varepsilon_v = (\delta\varepsilon_1 + 2\delta\varepsilon_2), \quad (4-63)$$

and Eq. (4-61) becomes

$$\delta W/V = \sigma'_1 \delta\varepsilon_1 + 2\sigma'_2 \delta\varepsilon_2 \quad (4-64)$$

But, for axial symmetry,  $\sigma'_2 = \sigma'_3$  and  $\delta\varepsilon_2 = \delta\varepsilon_3$  and Eq. (4-57) becomes

$$\delta W/V = \sigma'_1 \delta\varepsilon_1 + 2\sigma'_2 \delta\varepsilon_2 \quad (4-65)$$

Thus we have confirmed that  $\varepsilon_s, \varepsilon_v$  are correctly associated with  $q', p'$  for conditions of axial symmetry.

#### 4-11 STRESS-STRAIN BEHAVIOUR OF AN IDEAL ELASTIC SOIL

In order to illustrate the importance of invariants it is useful to examine the behaviour of an ideal isotropic elastic material. In this context, isotropic means that the properties of the material are the same in all directions. We assume that our readers are familiar with the basic theory of elasticity as set out by, for example, Case and Chilver (1971, pp. 82-85). The ideal

material is taken to be like a soil in that it obeys the principle of effective stress, and, thus, strains must depend on effective, not total, stresses.

The stress-strain behaviour of this ideal soil-like material is given by the generalized form of Hooke's law:

$$\left. \begin{aligned} \delta \varepsilon_x &= (1/E') [\delta \sigma'_x - \nu' \delta \sigma'_y - \nu' \delta \sigma'_z], \\ \delta \varepsilon_y &= (1/E') [\delta \sigma'_y - \nu' \delta \sigma'_x - \nu' \delta \sigma'_z], \\ \delta \varepsilon_z &= (1/E') [\delta \sigma'_z - \nu' \delta \sigma'_x - \nu' \delta \sigma'_y], \\ \delta \gamma_{xy} &= (2/E')(1 + \nu') \delta \tau'_{xy}, \\ \delta \gamma_{yz} &= (2/E')(1 + \nu') \delta \tau'_{yz}, \\ \delta \gamma_{zx} &= (2/E')(1 + \nu') \delta \tau'_{zx}, \end{aligned} \right\} \quad (4-66)$$

where  $E'$  and  $\nu'$  are the Young's modulus and Poisson's ratio appropriate for changes of effective stress. The values of  $E'$  and  $\nu'$  are assumed to remain constant over small increments of stress and strain and, as the material is assumed to be linear elastic, Eqs (4-66) are also valid for large increments of stress  $\Delta \sigma'$  and of strain  $\Delta \varepsilon$ . Written in terms of principal stresses and principal strains, Eqs (4-66) become

$$\left. \begin{aligned} \delta \varepsilon_1 &= (1/E') [\delta \sigma'_1 - \nu' \delta \sigma'_2 - \nu' \delta \sigma'_3], \\ \delta \varepsilon_2 &= (1/E') [\delta \sigma'_2 - \nu' \delta \sigma'_3 - \nu' \delta \sigma'_1], \\ \delta \varepsilon_3 &= (1/E') [\delta \sigma'_3 - \nu' \delta \sigma'_1 - \nu' \delta \sigma'_2], \end{aligned} \right\} \quad (4-67)$$

since shear stresses and shear strains are zero on principal planes.

For the special case of axial symmetry, where  $\sigma'_2 = \sigma'_3$  and  $\varepsilon_2 = \varepsilon_3$ , Eqs (4-67) become

$$\delta \varepsilon_1 = (1/E') [\delta \sigma'_1 - 2\nu' \delta \sigma'_2], \quad (4-68)$$

$$\delta \varepsilon_2 = \delta \varepsilon_3 = (1/E') [\delta \sigma'_2(1 - \nu') - \nu' \delta \sigma'_1] \quad (4-69)$$

and, hence,

$$\delta \varepsilon_v = (\delta \varepsilon_1 + 2\delta \varepsilon_2) = \frac{(1 - 2\nu')}{E'} (\delta \sigma'_1 + 2\delta \sigma'_2) \quad (4-70)$$

or

$$\delta \varepsilon_v = \frac{3(1 - 2\nu')}{E'} \delta p'. \quad (4-71)$$

Similarly,

$$\delta \varepsilon_a = \frac{2}{3} (\delta \varepsilon_1 - \delta \varepsilon_2) = \frac{2(1 + \nu')}{3E'} (\delta \sigma'_1 - \delta \sigma'_2) \quad (4-72)$$

or

$$\delta \varepsilon_a = \frac{2(1 + \nu')}{3E'} \delta q'. \quad (4-73)$$

Equations (4-71) and (4-73) are often written

$$\delta\varepsilon_v = \frac{1}{K'} \delta p', \quad (4-74)$$

$$\delta\varepsilon_s = \frac{1}{3G'} \delta q', \quad (4-75)$$

where  $K' = \frac{1}{3}E'/(1-2\nu')$  is known as the *bulk modulus* and  $G' = \frac{1}{2}E'/(1+\nu')$  is known as the *shear modulus*.

Equations (4-74) and (4-75) demonstrate an important property of an ideal isotropic elastic material. When invariants of strain are correctly associated with invariants of stress, increments of shear strain  $\delta\varepsilon_s$  are dependent only on increments of the corresponding stress invariant  $\delta q'$  and, similarly, increments of volumetric strain  $\delta\varepsilon_v$  are dependent only on increments of the corresponding stress invariant  $\delta p'$ . To emphasize this point, we may write

$$\delta\varepsilon_v = \frac{1}{K'} \delta p' + 0 \cdot \delta q', \quad (4-76)$$

$$\delta\varepsilon_s = 0 \cdot \delta p' + \frac{1}{3G'} \delta q'. \quad (4-77)$$

Thus, volumetric strains  $\varepsilon_v$  are connected with the stress invariant  $p'$  and separated from  $q'$ , while shear strains  $\varepsilon_s$  are connected with the stress invariant  $q'$  and separated from  $p'$ . Although Eqs (4-76) and (4-77) were derived for the special case of  $\sigma'_2 = \sigma'_3$ , it turns out that they are valid for general states of stress for materials which are isotropic and which are linear elastic over the appropriate increments.

#### Example 4.4 Behaviour of an ideal isotropic elastic soil in plane strain

Obtain expressions relating the strain parameters  $\varepsilon_v$  and  $\varepsilon_s$  to the stress parameters  $t'$  and  $s'$  for an ideal isotropic linear elastic soil loaded in plane strain.

For plane strain,  $\varepsilon_3 = 0$ ; hence, from Eq. (4-67),  $\delta\sigma'_3 = \nu' (\delta\sigma'_1 + \delta\sigma'_2)$  and

$$\delta\varepsilon_1 = (1/E') [\delta\sigma'_1(1-\nu'^2) - \delta\sigma'_3(\nu' + \nu'^2)],$$

$$\delta\varepsilon_3 = (1/E') [\delta\sigma'_3(1-\nu'^2) - \delta\sigma'_1(\nu' + \nu'^2)].$$

Therefore, for plane strain loading,

$$\delta\varepsilon_v = (\delta\varepsilon_1 + \delta\varepsilon_3) = \frac{(1+\nu')(1-2\nu')}{E'} (\delta\sigma'_1 + \delta\sigma'_2),$$

or

$$\delta\varepsilon_v = \frac{2(1+\nu')(1-2\nu')}{E'} \delta s'$$

and

$$\delta \varepsilon_\gamma = (\delta \varepsilon_1 - \delta \varepsilon_3) = \frac{(1 + \nu')}{E'} (\delta \sigma'_1 - \delta \sigma'_3),$$

or

$$\delta \varepsilon_\gamma = \frac{2(1 + \nu')}{E'} \delta t'.$$

These may be written

$$\delta \varepsilon_v = \frac{2(1 + \nu')}{3K'} \delta s' + 0. \delta t',$$

$$\delta \varepsilon_v = 0. \delta s' + \frac{1}{G'} \delta t'.$$

## A.I.T. LIBRARY

### 4-12 SUMMARY

1. The history of stressing of a soil element may be recorded by tracing a *stress path* and the history of straining may be traced by a *strain path*.
2. For plane strain conditions, stress and strain paths can conveniently be plotted with axes

$$t' = \frac{1}{2}(\sigma'_1 - \sigma'_3), \quad (4-3)$$

$$s' = \frac{1}{2}(\sigma'_1 + \sigma'_3), \quad (4-4)$$

$$\varepsilon_\gamma = (\varepsilon_1 - \varepsilon_3), \quad (4-33)$$

$$\varepsilon_v = (\varepsilon_1 + \varepsilon_3). \quad (4-34)$$

3. For axial symmetry ( $\sigma'_2 = \sigma'_3$  and  $\varepsilon_2 = \varepsilon_3$ ), the chosen axes are

$$q' = (\sigma'_1 - \sigma'_3), \quad (4-22)$$

$$p' = \frac{1}{3}(\sigma'_1 + 2\sigma'_3), \quad (4-21)$$

$$\varepsilon_a = \frac{2}{3}(\varepsilon_1 - \varepsilon_3), \quad (4-48)$$

$$\varepsilon_v = (\varepsilon_1 + 2\varepsilon_3). \quad (4-47)$$

4. Stress paths may be plotted in terms either of total or of effective stresses; relationships between total and effective stress parameters are

$$t' = t, \quad (4-7)$$

$$s' = s - u, \quad (4-8)$$

$$q' = q, \quad (4-28)$$

$$p' = p - u. \quad (4-27)$$

5. For an ideal isotropic elastic soil,

$$\delta \varepsilon_v = \frac{1}{K} \delta p' + 0 \cdot \delta q', \quad (4-76)$$

$$\delta \varepsilon_s = 0 \cdot \delta p' + \frac{1}{3G'} \delta q'. \quad (4-77)$$

## REFERENCES

- Case, J. and Chilver, A. H. *Strength of Materials and Structures*. Edward Arnold, London, 1971.
- Ford, H. *Advanced Mechanics of Materials*. Longman, London, 1963.

## LABORATORY TESTING OF SOILS

### 5-1 INTRODUCTION

Testing of soil samples in the laboratory plays an important role in soil mechanics research and in civil engineering practice.

Some soil tests are intended only to classify soils into broad groups so that some aspects of a soil's behaviour will be known before more detailed tests are carried out. Particle size analysis tests and Atterberg limits tests are classification tests of this kind and were described in Chapter 1. Some soil tests are performed to examine how easily water can flow through soil; permeability tests will be discussed in Chapter 6 and consolidation tests in Chapter 8.

Other soil tests examine the mechanical behaviour of soils and, in particular, investigate their strengths and deformations during loading. Usually, a small soil sample is placed in a loading machine and the state of stress in the sample is changed; observations are then made of the state of stress, the state of strain, and the pore pressure in the sample at many instants during the loading.

We will make considerable use later of the results of laboratory loading tests in the development of our ideas of soil behaviour. In this Chapter, we will describe briefly some of the different kinds of soil loading apparatus commonly found in commercial and research laboratories and the kinds of tests commonly performed in them. We assume that students will have the opportunity of conducting triaxial, direct shear box, and oedometer tests for themselves, or, at least, will have seen these tests demonstrated.

### 5-2 REQUIREMENTS OF SOIL LOADING TESTS

Figure 5-1 illustrates a set of completely general total stresses on the faces of a cubical element of soil in the ground. Below level ground there will be symmetry about the vertical axis, so  $\sigma_x = \sigma_y$  and  $\tau_{xy} = \tau_{yx} = \tau_{xz} = 0$ , but near building foundations and slopes this will not be the case and there will be a completely general state of stress.

Ideally, we should be able to transfer the element of soil from the ground to an apparatus without disturbance, load or unload the stresses, and

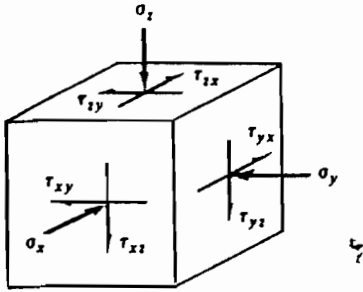


Figure 5-1 Axes of stress in the ground

observe the resulting strains and pore pressures. The apparatus should be able to impose a completely general state of stress in the sample and it should have complete freedom to change the state of stress so that principal planes may rotate during loading.

These are stringent requirements and are very difficult, if not impossible, to satisfy in practice. A serious difficulty arises in accommodating the relatively large deformations that occur in soils as they are loaded; even relatively stiff soils may strain by 5 per cent before failing while, in soft clays, deformations may exceed 50 per cent of the initial sample size. With these very large movements, it is difficult to avoid interference between adjacent loading plates.

### 5-3 BOUNDARY CONDITIONS

A soil loading apparatus will, in general, stress a soil sample on three pairs of opposite faces; the stresses may be applied by rigid platens or flexible membranes but, as we are usually concerned only with compressive stresses, there is no need to attach the loading platens to the soil sample.

A rigid platen is usually plane. Normal and shear forces  $F_a$ ,  $F_{ab}$ , and  $F_{ao}$  are applied to the platen and these forces are transferred into the sample. The conventional assumption is that contact stresses are uniform across the face of the platen and then stresses are calculated from the applied loads and the area of soil in contact with the platen, as indicated in Fig. 5-2(a). Occasionally, however, rigid platens may contain one or more small force transducers, as indicated in Fig. 5-2(b) which can measure any variation of stress across the face of the platen.

If the face of a rigid platen is rough, and sometimes platens are roughened artificially by attaching sand grains or thin vanes to their faces, shear stresses may be transferred from the platen into the soil sample. If, on the other hand, the face of a platen is perfectly smooth and frictionless, there can be no shear stress between soil and platen; in this case normal stresses on the

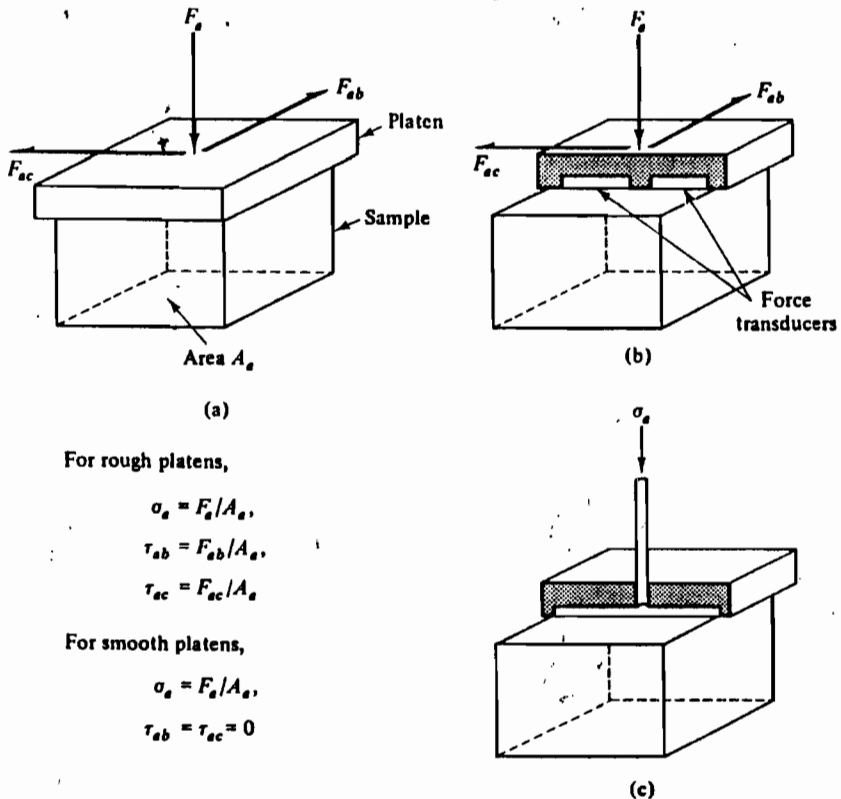


Figure 5-2 Boundary conditions of soil testing machines. (a) Rigid platen. (b) Rigid platen with force transducers. (c) Flexible membrane

platen faces are, by definition, principal stresses and planes parallel to the platen faces are principal planes of stress in the sample.

A flexible membrane will consist of a thin diaphragm, usually rubber, with a fluid pressure acting on it, as indicated in Fig. 5-2(c). If the diaphragm is thin and flexible, no shear stresses will be transmitted into the soil; planes parallel to the faces of the membrane will be principal planes in the sample and the fluid pressure behind the membrane will be a principal stress in the sample. This stress will be approximately uniform across the face of the sample except perhaps near the edges of the membrane where it is attached to a support.

With rigid platens, normal and shear strains in the soil may be found quite simply by measuring the movements of the platens. With flexible membranes, however, direct strain measurement is difficult and there is no guarantee that deformations in the soil will be uniform. If all the platens in a particular apparatus are prevented from rotating, whether they are rigid



or flexible, planes parallel to the platen faces are principal planes of strain in the soil and the normal strains across opposite faces of the sample are principal strains in the soil.

## 5-4 CONTROL OF LOADING

During a test on a soil sample, we may change the state of stress by adding loads or pressures to the sample and we may observe the resulting change in the state of strain; this is known as stress-controlled loading. Alternatively, we may change the state of strain by moving the platens and observe the required change in the state of stress; this is known as strain-controlled loading.

Usually, in laboratory tests on soils, strain-controlled tests involve driving the loading platens at constant velocity, while stress-controlled tests involve adding weights to a loading frame. In some very special tests, the rate of loading is sometimes controlled by feedback from the state of the sample.

## 5-5 CONTROL OF PORE PRESSURE AND DRAINAGE

During loading tests on soils, it is very important that we should be able to control either the drainage of pore water or the pore pressure or both. By controlling both total stresses and pore pressures we control the state of effective stress in the sample and, if we assume that soil grains and water are incompressible, by controlling the volume of water expelled from, or drawn into, the sample, we control the volume of the sample.

In order to control the drainage during a test, the sample must be isolated within a waterproof membrane. In addition, a connection must be made to a pressure transducer to measure the pore pressure, a valve to control the drainage, and a volume gauge to record the volume of water entering or leaving the sample, as illustrated in Fig. 5-3.

It is extremely important to distinguish between a test in which the drainage valve is closed and a test in which it is open.

If the valve is closed, no water can flow from (or into) the sample and the test is known as *undrained*. The mass of the sample will remain constant, but pore pressures will change as the soil responds to changes of stress. If we assume that soil grains and water are incompressible, the sample volume will not change during an undrained test.

If the valve is open and the pore pressure remains constant, water will flow from (or into) the sample as the soil volume responds to changes of effective stress. The test is then known as *drained*. Since pore pressures remain constant, changes in total stress and changes in effective stress are identical.

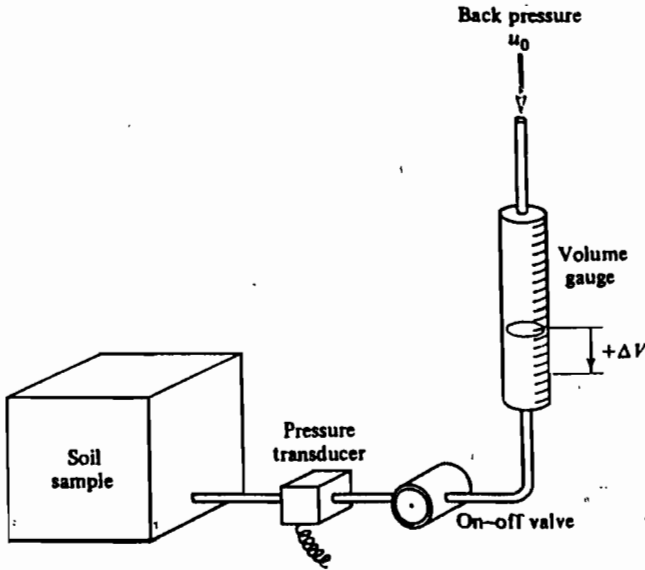


Figure 5-3 Apparatus for control and measurement of volumetric strain and pore pressure

If the volume gauge is open to the atmosphere, pore pressures are zero; often, however, it is convenient to apply a constant back pressure  $u_0$ , as indicated in Fig. 5-3.

Occasionally, special tests are carried out in which the pore pressure is changed independently of the total stresses.

## 5-6 CLASSIFICATION OF SOIL TESTS

Because of the technical difficulties involved in constructing an ideal soil-testing apparatus which is able to impose a completely general state of stress in which principal planes may rotate, the strategy adopted in soil mechanics has been to have several different kinds of apparatus, each of which will load soil samples in a special way. We will describe the more important of these and introduce the conventional terminology for different tests.

We consider first the class of apparatus with smooth, non-rotating rigid platens or flexible membranes in which the sample boundaries are principal planes of stress and of strain. An apparatus of this kind immediately imposes two restrictions on the behaviour of the sample: principal planes of stress and of strain coincide and cannot rotate.

The kinds of test available in this class of apparatus are illustrated in Fig. 5-4. The stresses  $\sigma_a$ ,  $\sigma_b$ , and  $\sigma_c$  are principal stresses, but not necessarily

Special conditions	Name of test	Diagram
$\sigma_a \neq \sigma_b \neq \sigma_c$	True triaxial	
$\sigma_b = \sigma_c = \sigma_r$	Cylindrical compression The 'triaxial' test	
$\epsilon_b = 0$	Plane strain or biaxial	
$\sigma_b = 0$	Plane stress	
$\epsilon_b = \epsilon_c = \epsilon_r = 0$	One-dimensional compression The oedometer test	
$\sigma_b = \sigma_c = \sigma_r = 0$	Uniaxial compression or unconfined compression	
$\sigma_a = \sigma_b = \sigma_c = \sigma$	Isotropic compression	

Figure 5-4 Stress conditions in some common soil tests

in order of magnitude. When the soil sample is cylindrical it is usual to denote the radial stress by  $\sigma_r$  and the axial stress by  $\sigma_a$ . We cannot immediately calculate the magnitude of the tangential stress  $\sigma_\theta$  and it is usual to make the simple assumption that  $\sigma_\theta = \sigma_r$ .

In the true triaxial test, all three principal stresses may differ and each may be varied independently, while in the isotropic compression test all principal stresses are equal; there are various other kinds of test between these extremes. Strictly speaking, the triaxial test in which  $\sigma_b = \sigma_a = \sigma_r = \sigma_\theta$  would be better described as the cylindrical compression test or the axially

symmetric test, but the word 'triaxial' is now firmly established in soil mechanics terminology. A variation of the true triaxial test is the hollow cylinder test, in which the radial stress inside a hollow cylinder may be different from the radial stress outside the cylinder. In general, the state of stress in an element of soil in the wall of a hollow cylinder is  $\sigma_a \neq \sigma_r \neq \sigma_\theta$ , but the magnitudes of  $\sigma_r$  and  $\sigma_\theta$  vary with radius.

The second class of apparatus for soil testing consists of the shear tests illustrated in Fig. 5-5. Here the loading plates are usually rough, and may rotate; consequently, the boundaries of the sample need not be either principal planes of stress or of strain and the principal planes may rotate. Torsion shear samples may be solid or they may be hollow, as shown in Fig. 5-5, and there are two versions of the latter kind. In one version, the sample is like the hollow cylinder but with equal radial stresses inside and outside the cylinder. In the other version, known as the ring shear test, the cross-section of the annulus is approximately square and there are rigid cylindrical platens inside and outside the hollow cylinder so that radial strains are zero. The state of stress in a ring shear sample is like that in a direct shear sample, but, in ring shear, we may apply very large shear deformations to the sample. In direct shear and simple shear tests, strains normal to the diagram are zero and the samples deform in plane strain.

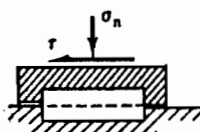
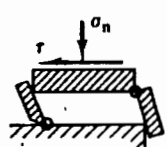
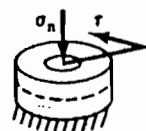
Platens	Name of test	Diagram
Rough: non-rotating	Direct shear The shear box test	
Rough: rotating	Simple shear	
Rough: non-rotating	Torsion The ring shear test	

Figure 5-5 Shear tests for soils

Of the tests illustrated in Figs 5-4 and 5-5, the triaxial test, the oedometer test, and the direct shear test are commonly used in practice to investigate soils for engineering design purposes and apparatus for these tests can be found in most commercial soils laboratories. Of the remainder, true triaxial, plane strain, simple shear, and various kinds of hollow cylinder and torsion tests are usually carried out for research purposes and apparatus for these tests can usually be found only in research laboratories.

### 5-7 THE TRIAXIAL APPARATUS

The triaxial apparatus has been described in detail by Bishop and Henkel (1962, pp. 33-82) in their standard text on triaxial testing of soils.

A conventional triaxial apparatus is illustrated in Fig. 5-6. The soil sample is a cylinder with height usually about twice the diameter; common sizes for triaxial samples are 38 mm and 100 mm diameter. The top and bottom rigid platens are assumed to be smooth and to remain horizontal during a test, so that the top and bottom faces of the sample are principal planes.

The sample is enclosed in a thin rubber sleeve sealed to the top and bottom platens by rubber O-ring seals; the rubber acts both as a flexible membrane and as a seal to separate pore pressures and total stresses. The

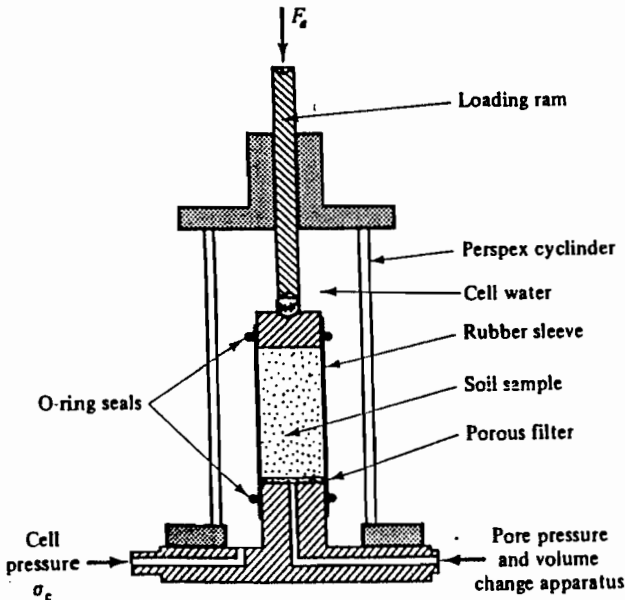


Figure 5-6 The triaxial apparatus

sample is assumed to remain a right cylinder during deformation and, consequently, the vertical sides of the sample are principal planes of stress and of strain.

The sealed sample is placed in a water-filled cell; the cell pressure  $\sigma_c$  supplies a uniform radial total stress  $\sigma_r$  to the vertical sides of the sample and an equal uniform vertical stress to the top rigid platen, as illustrated in Fig. 5-7. A frictionless ram passes through the top of the cell and applies an additional force  $F_a$  to the top platen; the force is measured either by a proving ring outside the cell or by a force transducer inside.

If the cross-sectional area of the sample normal to  $F_a$  is  $A$  then, as indicated in Fig. 5-7, the total axial stress  $\sigma_a$  is given by

$$\begin{aligned}\sigma_a &= \sigma_r + (F_a/A), \\ F_a/A &= \sigma_a - \sigma_r\end{aligned}\quad (5-1)$$

As the sample deforms its dimensions change and so, as a consequence, the cross-sectional area will change as the test progresses. It is assumed that the sample remains a right cylinder and, if the initial cross-sectional area of the unstrained sample was  $A_0$ , its initial volume  $V_0$  and its initial length  $L_0$ , the current area  $A$  in Eq. (5-1) is given by

$$A = A_0 \left[ \frac{1 + (\Delta V/V_0)}{1 + (\Delta L/L_0)} \right] = A_0 \left( \frac{1 - \varepsilon_v}{1 - \varepsilon_a} \right), \quad (5-2)$$

where  $\Delta V$  and  $\Delta L$  are the current changes of the volume and length of the sample, and  $\varepsilon_v$  and  $\varepsilon_a$  are the current volumetric and axial strains.

The force in the loading ram is not equivalent to the axial stress but, instead, it gives rise to a stress equal to  $(\sigma_a - \sigma_r)$  and is known as the deviator stress.

Axial deformations of the sample are measured by observing the movement of the ram using a displacement transducer or a dial gauge. The axial

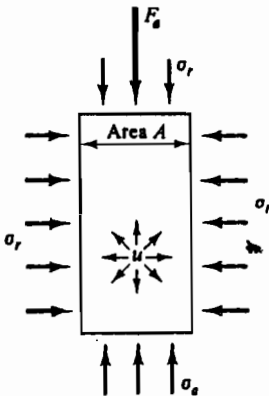


Figure 5-7 Stresses on a triaxial sample

load  $F_a$ , and hence the deviator stress, may be changed either in a strain-controlled manner using a loading frame and motor-driven screw feed or, in a stress-controlled manner, by adding weights to a hanger or pressure to a piston.

A porous filter is placed between the sample and the bottom platen and a drainage connection passes through the base of the cell to pore pressure and volume change measuring equipment similar to that illustrated in Fig. 5-3. It is not usual to measure radial deformations directly, but these may be calculated from the observed volume changes and axial deformations.

The triaxial apparatus may be used to load a sample by changing the total axial stress  $\sigma_a$ , the total radial stress  $\sigma_r$ , or the pore pressure  $u$  either independently or together.

When the loading ram is in compression,  $F_a$  is positive and so  $\sigma_a > \sigma_r$ ; consequently,  $\sigma_a = \sigma_1$  and  $\sigma_r = \sigma_2 = \sigma_3$ . The state of stress is known as triaxial compression. If the loading ram is attached to the top platen, the ram may be put into tension and  $F_a$  would become negative. Then  $\sigma_r > \sigma_a$ ; in this case,  $\sigma_a = \sigma_3$  and  $\sigma_r = \sigma_1 = \sigma_2$  and the state of stress is known as triaxial extension. Provided the magnitude of the tensile force in the ram does not exceed  $A\sigma_r$ , the total axial stress remains compressive. Triaxial extension does not, therefore, necessarily imply that tensile stresses exist in the sample.

If the loading ram is locked so that it does not touch the top platen, the load in the ram is zero,  $\sigma_a = \sigma_r$ , and the state of stress in the sample is isotropic compression, as illustrated in Fig. 5-4. If the cell is emptied,  $\sigma_r = 0$  and the state of stress is uniaxial or unconfined compression. If the apparatus is modified slightly and provision made to measure the radial strain  $\epsilon_r$ , we may conduct a test in which  $\sigma_a$  and  $\sigma_r$  are increased together in such a way that  $\epsilon_r = 0$  and the sample will deform in one-dimensional compression.

We may, therefore, conduct several of the tests illustrated in Fig. 5-4 in a conventional triaxial apparatus. The most common triaxial test is the simple triaxial compression test, in which the cell pressure  $\sigma_o = \sigma_r$  is held constant and the deviator stress  $(\sigma_a - \sigma_r)$  increased as the loading ram force is increased. Triaxial compression tests may be drained or undrained; they may also be stress-controlled or strain-controlled, although strain-controlled tests, in which the ram is pushed into the cell at a constant velocity, are the more common.

#### Example 5-1 Processing data from a drained triaxial test

The first three columns of Table E5-1 give data from a drained triaxial compression test on a sample of soil in which the cell pressure was held constant at  $\sigma_o = 300 \text{ kN m}^{-2}$  and the pore pressure was held constant at  $u = 100 \text{ kN m}^{-2}$ . At the start of the test, the sample was 38 mm in

Table E5-1 Data from a drained triaxial test

Axial force, $F_a$ (N)	Change of length, $\Delta L$ (mm)	Volume of water expelled, $\Delta V_w$ ( $\text{mm}^3 \times 10^3$ )	Volumetric strain, $\epsilon_v$	Axial strain, $\epsilon_a$	Area ( $\text{m}^2 \times 10^{-3}$ )	$q' = (\sigma'_1 - \sigma'_3)$ ( $\text{kN m}^{-2}$ )
0	0	0	0	0	1.134	0
115	-1.95	0.88	0.010	0.025	1.151	100
235	-5.85	3.72	0.042	0.075	1.174	200
325	-11.70	7.07	0.080	0.150	1.227	265
394	-19.11	8.40	0.095	0.245	1.359	290
458	-27.30	8.40	0.095	0.350	1.579	290

diameter and 78 mm long. Plot the test results in the form of  $q' = (\sigma'_1 - \sigma'_3)$  and volumetric strain  $\epsilon_v$  against axial strain  $\epsilon_a$ .

The initial volume  $V_0$  and cross-sectional area  $A_0$  of the sample were

$$A_0 = (\pi/4) \times 38^2 \times 10^{-6} = 1.134 \times 10^{-3} \text{ m}^2,$$

$$V_0 = 1.134 \times 10^{-3} \times 78 \times 10^{-3} = 88.46 \times 10^{-6} \text{ m}^3.$$

The increase in volume  $\Delta V$  of the sample is equal to  $-\Delta V_w$ , where  $\Delta V_w$  is the volume of water expelled. If the sample was initially unstrained with initial volume  $V_0$  and initial length  $L_0$ , the calculated volumetric strain  $\epsilon_v$  and axial strain  $\epsilon_a$  are given by

$$\epsilon_v = -\Delta V/V_0 = \Delta V_w/V_0,$$

$$\epsilon_a = -\Delta L/L_0.$$

At any stage of the test the cross-sectional area of the sample is given by Eq. (5-2),

$$A = A_0[(1 - \epsilon_v)/(1 - \epsilon_a)].$$

For triaxial compression,  $\sigma'_1 = \sigma'_a$  and  $\sigma'_3 = \sigma'_r$ ; hence,  $q' = (\sigma'_1 - \sigma'_3)$  is given by

$$q' = (\sigma'_a - \sigma'_r) = F_a/A.$$

Values of  $q'$ ,  $\epsilon_v$ , and  $\epsilon_a$  are contained in Table E5-1 and plotted in Fig. E5-1. (The data from this test were used for Ex. 4-1, 4-2, and 4-3 and the stress paths for the drained triaxial compression test in this example are shown in Figs E4-1, E4-2(a), and E4-3(a).)



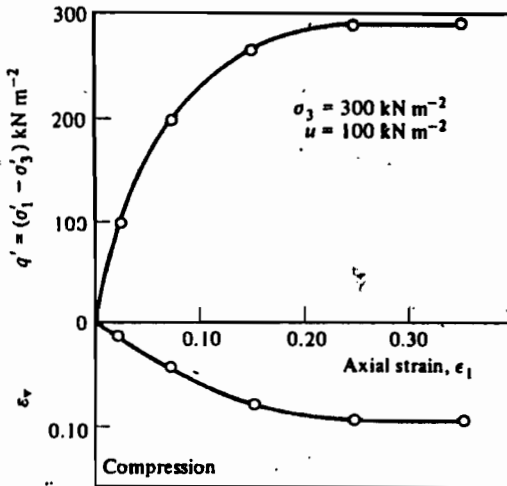


Figure E5-1 Results of drained triaxial test

**Example 5-2 Processing data from an undrained triaxial test**

The first three columns of Table E5-2 give data from an undrained triaxial compression test on a sample of soil in which the cell pressure was held constant at  $\sigma_o = 300 \text{ kN m}^{-2}$ . At the start of the test, the sample was 38 mm in diameter and 78 mm long and the initial pore pressure was  $u_o = 100 \text{ kN m}^{-2}$ . Plot the test results in the form of  $q' = (\sigma'_1 - \sigma'_3)$  and pore pressure  $u$  against axial strain  $\epsilon_a$ .

**Table E5-2 Data from an undrained triaxial test**

Axial force, $F_a$ (N)	Change of length, $\Delta L$ (mm)	Pore pressure, $u$ ( $\text{kN m}^{-2}$ )	Axial strain, $\epsilon_a$	Area ( $\text{m}^2 \times 10^{-3}$ )	$q' = (\sigma'_1 - \sigma'_3)$ ( $\text{kN m}^{-2}$ )
0	0	100	0	1.134	0
58	-1.95	165	0.025	1.163	50
96	-4.29	200	0.055	1.200	80
124	-9.36	224	0.120	1.289	96
136	-14.04	232	0.180	1.383	98
148	-19.50	232	0.250	1.512	98

The calculations proceed as in Ex. 5-1; thus,

$$A_0 = 1.134 \times 10^{-3} \text{ m}^2,$$

$$\epsilon_v = 0 \quad (\text{because the test is undrained}),$$

$$\epsilon_a = -\Delta L/L_0,$$

$$A = A_0(1 - \epsilon_v)^{-1},$$

$$q' = (\sigma'_1 - \sigma'_3) = F_d/A,$$

and the results are given in Table E5-2. Values of  $q'$  and  $u$  are plotted against  $\epsilon_a$  in Fig. E5-2. (The data from this test were used for Ex. 4-1, 4-2, and 4-3 and the stress paths for the undrained triaxial compression test in this example are shown in Figs E4-1, E4-2(b), and E4-3(b).)

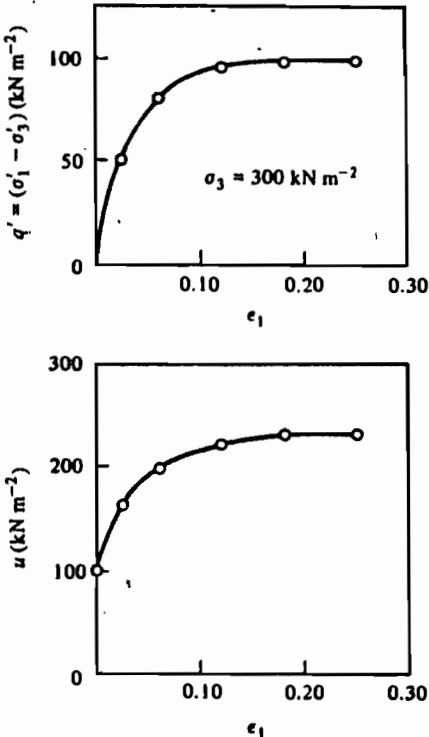


Figure E5-2 Results of undrained triaxial test

### Example 5-3 Failure of triaxial samples

The curves of  $q'$  against  $\epsilon_a$  in Figs E5-1 and E5-2 both become horizontal where  $q'$  reaches a limiting value and the samples fail by continuing to strain without further change of stress, volume, or pore pressure. Plot on the same diagram the Mohr's circles of total and effective stress at failure for both tests.

- (a) In the drained test,  $q'$  at failure is approximately  $(\sigma'_1 - \sigma'_3) = 290 \text{ kN m}^{-2}$  and first occurs after an axial strain of about  $\epsilon_a = 0.25$ . Throughout

the drained test,  $\sigma_3 = \sigma_o = 300 \text{ kN m}^{-2}$  and  $u = 100 \text{ kN m}^{-2}$ . Hence, at failure, the principal stresses are

$$\begin{aligned}\sigma_1 &= 590 \text{ kN m}^{-2}, & \sigma_3 &= 300 \text{ kN m}^{-2}, \\ \sigma'_1 &= 490 \text{ kN m}^{-2}, & \sigma'_3 &= 200 \text{ kN m}^{-2}.\end{aligned}$$

(b) In the undrained test,  $q'$  at failure is approximately  $(\sigma'_1 - \sigma'_3) = 98 \text{ kN m}^{-2}$  and first occurs after an axial strain of about  $\epsilon_a = 0.18$ , where the pore pressure is  $u = 232 \text{ kN m}^{-2}$ . Throughout the undrained test,  $\sigma_3 = \sigma_o = 300 \text{ kN m}^{-2}$ . Hence, at failure, the principal stresses are

$$\begin{aligned}\sigma_1 &= 398 \text{ kN m}^{-2}, & \sigma_3 &= 300 \text{ kN m}^{-2}, \\ \sigma'_1 &= 166 \text{ kN m}^{-2}, & \sigma'_3 &= 68 \text{ kN m}^{-2}.\end{aligned}$$

The Mohr's circles of total and effective stress for both samples at failure are shown in Fig. E5-3.

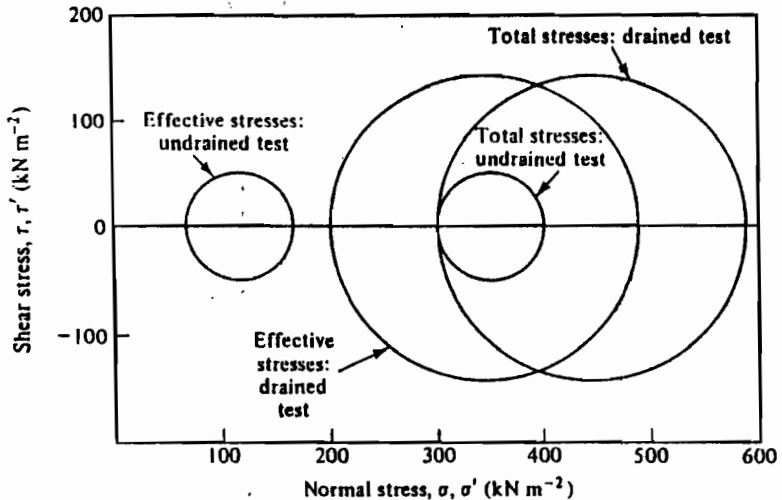


Figure E5-3 Mohr's circles of total and effective stress for drained and undrained triaxial tests at failure

## 5-8 THE OEDOMETER

A section of a standard oedometer is shown in Fig. 5-8. The sample is a disc of soil contained within a rigid circular metal ring and it is loaded from top and bottom by rigid platens. The containing ring effectively prevents any radial strain and so the state of strain in the sample is one-dimensional, with  $\epsilon_r = \epsilon_b = \epsilon_c = 0$ , as indicated in Fig. 5-4. The top and bottom platens and the containing ring do not rotate and the faces of the sample are principal planes of strain; they are assumed to be smooth and so the sample faces are also principal planes of stress.

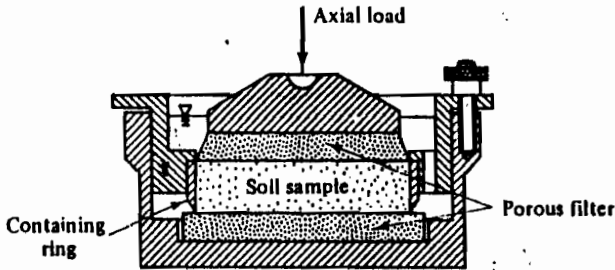


Figure 5-8 The oedometer (after BS 1377 : 1975)

The top and bottom platens consist of porous discs while the containing ring is impermeable and consequently not only strains, but also pore water flows, are one-dimensional. Water pressures in the drainage discs must remain zero, but pore pressures within the body of the sample may change; only very rarely is any attempt made to measure the magnitude of these pore pressures.

During a conventional oedometer test the axial stress is varied in a stress-controlled manner by changing the weights on a hanger supported by the top platen. The magnitude of the axial stress  $\sigma_a$  is simply calculated from the constant area of the sample and the current axial load. The axial strain  $\epsilon_a$  is measured by observing the settlement of the top platen using a dial gauge or displacement transducer.

There are several variations of the standard oedometer apparatus. Normally, no provision is made for measuring the radial stress  $\sigma_r$ , but, in some special oedometers, force transducers or strain gauges are attached to the containing ring to allow measurement of the radial stress. In another variation, due to Rowe, the rigid top platen is replaced by a flexible membrane and provision is made for application of a back pressure to the pore water. This type of oedometer has the capacity for testing large samples and it may also be employed to measure the permeability of a sample under different vertical stresses. Occasionally, in oedometer tests in the standard apparatus, the sample is loaded in a strain-controlled fashion.

## 5-9 THE DIRECT SHEAR BOX

The main purpose of the direct shear box test is to examine the strengths of soil samples; it is unsuitable for measuring soil deformations.

The essential features of the direct shear box apparatus are illustrated in Fig. 5-9. The sample is, typically, 60 mm square in plan and about 25 mm thick, although occasionally larger samples are used in special shear boxes to examine coarse-grained soils.

The sample is contained within a square box split horizontally and is loaded vertically between rigid and rough top and bottom platens. During

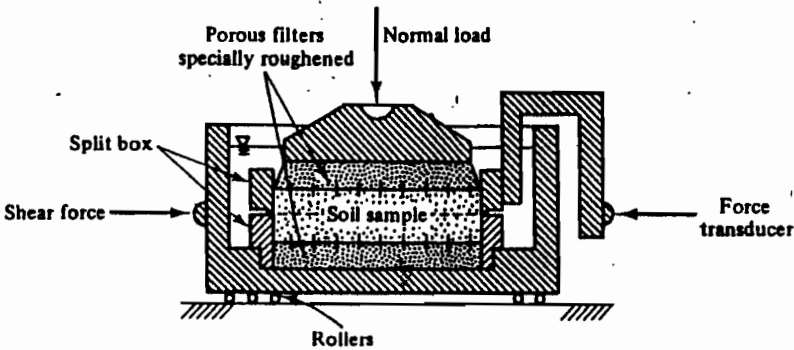


Figure 5-9 The direct shear box

a test, opposing horizontal forces are applied to the two halves of the box which are, therefore, forced to slide apart; the top and bottom platens are artificially roughened and so transfer shear stress into the soil. The stresses imposed on the sample are, approximately, those indicated in Fig. 5-10 and, because of the constraints of the split box, the soil is obliged to shear along the horizontal plane AB.

The total vertical stress  $\sigma_n$  is usually supplied by weights on a hanger and normally remains constant during a test. The shear load is applied by traversing the lower half of the box, which is supported on roller bearings, in a strain-controlled manner. The shear force transferred through the sample to the upper half of the box is measured on a proving ring or force transducer. During a test, measurements are usually made of the relative displacement of the two halves of the box and the vertical displacement of the top platen with respect to the bottom; these measurements are normally observed on dial gauges.

The top and bottom platens are porous and the split box is usually placed in a container and submerged in water; pore water may drain from (or into) the sample at the top and bottom faces but there is no other control of drainage and no provision is made for measurement of pore pressure. Alternatively, water may be omitted and samples tested dry; it is usual to conduct dry tests on samples of sandy soils.

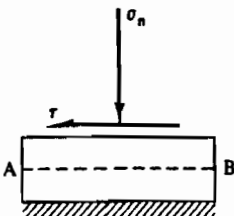


Figure 5-10 Stresses on the boundary of a direct shear sample

The states of stress and strain in direct shear samples cannot be determined completely. The only stresses that are known are the normal and shear stresses ( $\sigma_n, \tau$ ) on the plane AB in Fig. 5-10 and, consequently, it is impossible to construct a unique Mohr's circle of stress and we cannot locate principal planes of stress nor calculate principal stresses. Because the sample is contained in a rigid box, it is obliged to deform in a special way and strains will be non-uniform; we can do no better than calculate the *average* strain in the sample and we cannot determine the strains in elements of the sample which are at failure.

### 5-10 THE SIMPLE SHEAR APPARATUS

The simple shear apparatus is similar to the direct shear box, except that in the simple shear apparatus one pair of platens is allowed to rotate and the sample may deform uniformly, as illustrated in Fig. 5-5.

There are, currently, two basic designs of simple shear apparatus, one developed at Cambridge University and the other at the Norwegian Geotechnical Institute in Oslo. The NGI type is now used in a number of commercial laboratories; details of the machine and the method of testing clay samples are given by Bjerrum and Landva (1966). The Cambridge University type of simple shear apparatus is still mainly used for research and different versions of the apparatus are used for tests on different kinds of soil; some details of this apparatus were given by Røscoc (1970).

The basic design of the NGI simple shear apparatus is illustrated in Fig. 5-11. The sample is a disc 80 mm in diameter by about 10 mm thick and it is contained within a cylindrical rubber membrane; the membrane is

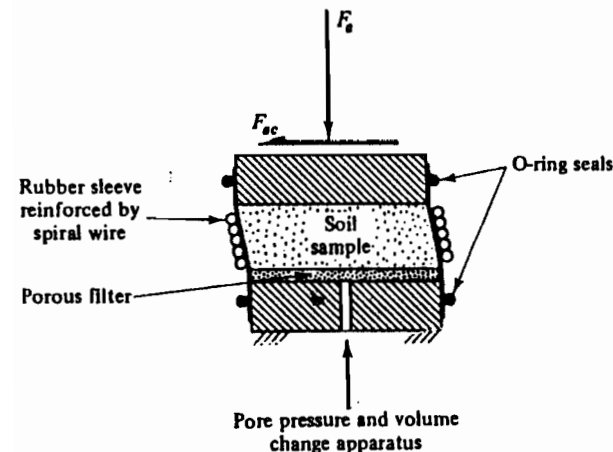


Figure 5-11 NGI simple shear apparatus

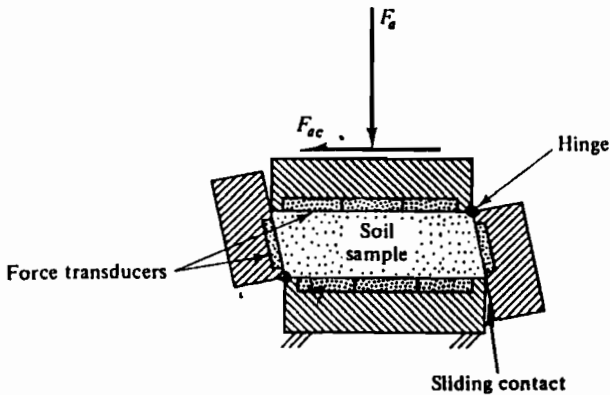


Figure 5-12 Cambridge University simple shear apparatus

reinforced with a spiral winding of thin wire which prevents horizontal direct strain ( $\epsilon_b = \epsilon_o = 0$ ), but which allows rotation of the sides of the sample, as illustrated. The rubber membrane is sealed to the top and bottom platens which consist of rough rigid porous discs.

Normal and shear stresses ( $\sigma_a, \tau_{ac}$ ) are applied across the sample in a manner similar to the application of stress in a direct shear test, and the vertical and angular deformations of the sample are found by observing the relative movements of the top and bottom platens. Drainage of pore water, or the magnitude of the pore pressure, may be controlled in a manner similar to the control of drainage in the triaxial test.

The basic design of the Cambridge simple shear apparatus is illustrated in Fig. 5-12. The sample is a rectangular prism, normally 100 mm square in plan and 20 mm thick. It is contained within a set of interlocking rough and rigid platens as illustrated; the platens are arranged so that horizontal direct strains are prevented ( $\epsilon_b = \epsilon_o = 0$ ), but vertical strains and rotation of the end platens are allowed.

Details of the platens and loading arrangements have varied as the basic design became more sophisticated with the passage of time. Recent models of the apparatus contain an array of force transducers in each platen which measure normal and shear stresses ( $\sigma_a, \sigma_o, \tau_{ac}$ ) as indicated in Fig. 5-12; different designs are available for dry sand and for saturated clay and pore water drainage and pore pressure may be controlled in the latter.

In the NGI apparatus, only normal and shear stresses on horizontal planes are known and, consequently, as was the case with the direct shear test, the state of stress in the sample cannot be determined uniquely. In the Cambridge apparatus, however, when normal and shear stresses on the end faces are measured directly by force transducers, the state of stress in the sample is completely defined; a Mohr's circle of stress can be constructed, principal planes of stress identified and principal stresses calculated.

Horizontal strains are zero ( $\epsilon_h = 0$ ) in any simple shear apparatus, while axial and shear strains are calculated from the observed displacements and rotations of the platens. The state of strain is, therefore, completely defined, and a Mohr's circle of strain may be constructed.

During a simple shear test, principal planes of stress and of strain rotate as the state of stress in the sample changes, but the conditions imposed by the apparatus do not require that the principal planes of stress and of strain coincide.

## 5-11 SUMMARY

1. Loading tests examine the strength and deformation of soil samples as states of stress and of strain are changed.
2. It is difficult to devise an apparatus which is able to load a soil sample in a completely general manner. Different apparatuses exist in which soil samples may be loaded in different ways.
3. The apparatuses most commonly found in practice are the triaxial apparatus, the oedometer, and the direct shear box.
4. Other apparatuses, such as true triaxial and simple shear, are normally used only for research purposes.
5. We distinguish a drained test from an undrained test. During a drained test the pore pressure remains constant, but the volume of the sample may change; during an undrained test the volume of the sample remains constant.

## REFERENCES

- Bishop, A. W. and Henkel, D. J. *The Measurement of Soil Properties in the Triaxial Test*. Edward Arnold, London, 1962.
- Bjerrum, L. and Landva, A. Direct simple shear tests on a Norwegian quick clay. *Geotechnique*, 16, 1-20, 1966.
- British Standards Institution. *Methods of testing soils for civil engineering purposes*. BS 1377 : 1975.
- Roscoe, K. H. The tenth Rankine lecture: The influence of strains in soil mechanics. *Geotechnique*, 20, 129-170, 1970.



**FLOW OF WATER IN SOILS**

**6-1 INTRODUCTION**

It is common experience that water flows downhill; the water flows from a position where its potential is high to a position where its potential is lower. Flow of water from high to low potential occurs also within a porous medium like soil, provided of course that the pores are interconnected, but now the seepage flow is retarded by drag forces acting on the water as it flows past the soil grains. Clearly there will be no seepage if the potential of the pore water in a soil is everywhere the same.

As a practical example of seepage, Fig. 6-1 shows a section of an impermeable wall driven into the bed of a river. If the levels of water either side of the wall are the same, pore pressures at A and at B will be equal and there will be no flow of water below the wall. If, however, the level of water on the right-hand side of the wall is lowered as shown, perhaps by pumping, the pore pressures at A will exceed those at B and water will seep through the soil below the wall. Figure 6-2 illustrates a similar example of seepage through a soil embankment dam founded on impermeable rock. As engineers, we will wish to calculate the leakage below the wall (or through the dam) and to examine the distribution of pore pressure and effective stress throughout the soil.

If the wall (or the dam) is very long, we may neglect any small components of flow normal to the diagram and consider only the flow through a slice

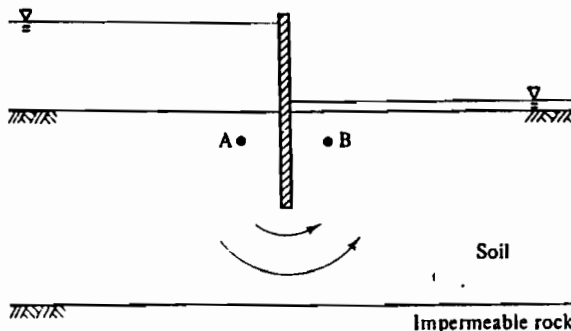


**Figure 6-1** Seepage below an impermeable wall

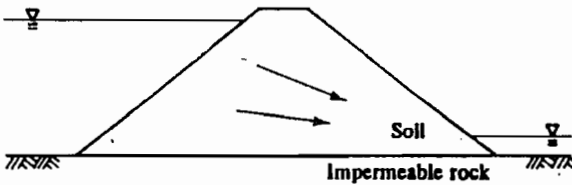


Figure 6-2 Seepage through an embankment dam

of unit thickness. This corresponds to plane or two-dimensional flow and we will consider only this case.

If pore pressures vary with time, as they would if, for example, pumping were halted and the lowered water level in Fig. 6-1 were allowed to rise, the flow will be time-dependent; such non-steady flows are known as *transient seepage*. During transient seepage, pore pressures and effective stresses vary with time and, as a consequence of the principle of effective stress, soil deformations will occur and there will be complex interrelationships between pore pressure, seepage, and deformation. This time-dependent process is known as consolidation and will be considered later.

If pore pressures do not vary with time, the rate of flow will be constant and the flow is known as *steady-state seepage*. During steady-state seepage, pore pressures remain constant and no soil deformations occur.

For the present, we will consider two-dimensional steady-state seepage; the soil may, therefore, be regarded as rigid and stationary with a steady flow of water through the pore spaces.

## 6-2 PORE PRESSURE AND POTENTIAL

The laws governing the flow of water through soils are analogous to those governing the flow of electricity or heat through conducting bodies; all depend on the existence of a potential gradient as the driving force. In seepage, it is the hydraulic potential and, in particular, the hydraulic potential gradient which controls the flow; these terms are usually shortened to potential and hydraulic gradient.

Figure 6-3 shows an open-ended standpipe installed in a body of soil. The end of the tube contains a filter to prevent soil grains entering; this instrument is known generally as a piezometer and is the basic tool for measuring pore pressures in soils. When the system is in equilibrium, the pore pressures either side of the filter must be equal and the pore pressure in the soil is

$$u = \gamma_w h, \quad (6-1)$$

where  $\gamma_w$  is the unit weight of water and  $h$  is the head of water in the standpipe.

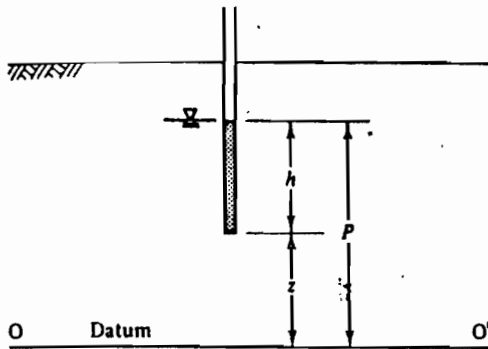


Figure 6-3 Measurement of pore pressure and potential

Inserting imaginary standpipes into a soil body is a convenient method of visualizing the distribution of pore pressures.

Potential, denoted by the letter  $P$ , is defined as

$$P = (u/\gamma_w) + z, \quad (6-2)$$

or

$$P = h + z, \quad (6-3)$$

where  $z$  is the elevation of the standpipe tip above an *arbitrary* datum such as  $OO'$ . Potential has the units of length. Since it is the *potential gradient* which controls seepage, the placing of the arbitrary datum is of no special importance.

### 6-3 SEEPAGE VELOCITY

As water seeps through soil, it must follow the tortuous passages between the soil grains and the velocity of a small element of water will vary as it seeps between the grains. We are not usually concerned with local flow between the grains but, instead, with quantities of water flowing through soil bodies.

If the tortuous paths followed by adjacent elements of water are smoothed, the resulting smooth path is known as a *flowline*. In Fig. 6-4, A and B are two points on a flowline  $\delta s$  apart; water flows from A to B due to an hydraulic gradient. The flowline is surrounded by an imaginary tube of area  $\delta A$  arranged so that, in a time interval  $\delta t$ , equal volumes of water  $\delta Q$  flow into and out from the ends of the tube.

The instantaneous rate of flow is

$$\delta q = \lim_{\delta t \rightarrow 0} \frac{\delta Q}{\delta t} = \frac{dQ}{dt}. \quad (6-4)$$

For steady-state seepage, the limit is unnecessary as the rate of flow remains

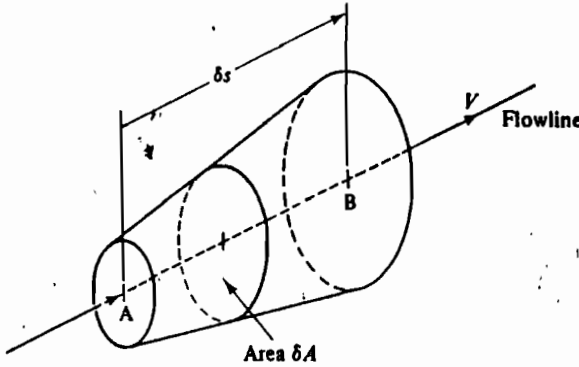


Figure 6-4 Seepage velocity

constant; for transient seepage, however, the instantaneous rate of flow must be found from Eq. (6-4).

The *artificial velocity* is defined as

$$V = \lim_{\delta A \rightarrow 0} \frac{\delta q}{\delta A} = \frac{dq}{dA} \quad (6-5)$$

For steady-state seepage,  $V$  does not vary with time.

The artificial velocity  $V$  is not the velocity of an element of water seeping through the tube in Fig. 6-4; it is, instead, a measure of the total quantity of water which flows through the tube. The water actually follows a tortuous passage through the pore spaces between the soil grains and the pore spaces form only a part of the total cross-section. If each element of water covers a distance  $\delta s$  along its flowline in a time  $\delta t$ , the seepage velocity  $V_s$  is defined by

$$V_s = \lim_{\delta t \rightarrow 0} \frac{\delta s}{\delta t} = \frac{ds}{dt} \quad (6-6)$$

If we observe the velocity of flow by timing the passage of dye or trace elements we will obtain a measure of the velocity of small elements of water, i.e., the seepage velocity.

The water flows only through the area of soil occupied by the pore water and shown as  $\delta A_w$  in Fig. 6-5; the remaining area  $\delta A_s$  is occupied by soil grains. If the voids ratio is  $e$ , then, from the definition of voids ratio and on the average,  $\delta A_w = e \delta A_s$ . The rate of flow through the tube is given by

$$\delta q = V \delta A = V_s \delta A_w, \quad (6-7)$$

therefore,

$$V = V_s e / (1 + e) = V_s (v - 1) / v, \quad (6-8)$$

where  $v$  is the specific volume.

The artificial velocity will always be less than the seepage velocity determined by direct measurement.

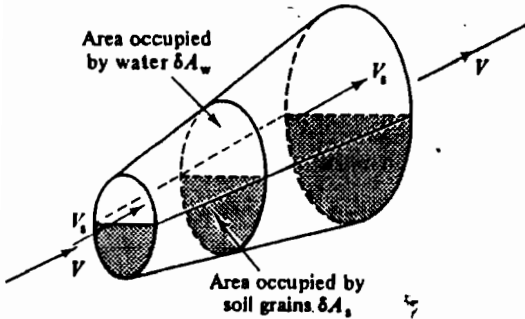


Figure 6-5 Artificial velocity and seepage velocity

### 6-4 HYDRAULIC GRADIENT

In Fig. 6-6, A and B are points on a flowline; because the potential  $P_A$  at A is greater than the potential  $P_B$  at B, water flows from A to B. The points are spaced at a distance  $\delta s$ , measured positively in the direction of flow.

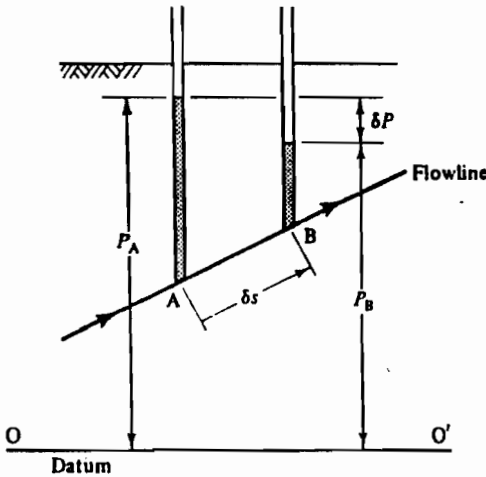


Figure 6-6 Hydraulic gradient

The hydraulic gradient is denoted by the letter  $i$  and is defined by

$$i = - \lim_{\delta s \rightarrow 0} \frac{\delta P}{\delta s} = - \frac{dP}{ds} \tag{6-9}$$

Hydraulic gradient is a vector quantity, it has magnitude and direction but it is dimensionless; the negative sign is introduced so that  $i$  is positive in the direction of flow.

**Example 6-1** Calculation of pore pressure, potential, and hydraulic gradient

Figure E6-1 shows a section along the centre-line of a pipe of square cross-section which contains soil held between two meshes. Water flows from left to right through the soil due to the different levels of water in the two constant head tanks. A pair of standpipes are inserted through the pipe into the soil with their tips at A and at B, 1.0 m apart along the centre-line. The water levels in the standpipes are 2.6 m and 2.4 m above A and B, respectively. Calculate (a) the pore pressures at A and at B, (b) the potentials at A and at B with respect to an arbitrary datum chosen to be at the invert of the pipe, and (c) the hydraulic gradient between A and B.

(a) Pore pressure,  $u = \gamma_w h$  from Eq. (6-1). Hence, at A,

$$u_A = 9.81 \times 2.6,$$

$$u_A = 25.5 \text{ kN m}^{-2}.$$

At B,

$$u_B = 9.81 \times 2.4,$$

$$u_B = 23.5 \text{ kN m}^{-2}.$$

(b) Potential,  $P = (u/\gamma_w) + z = h + z$  from Eq. (6-3). Hence, at A,

$$P_A = (25.5/9.81) + 1.0,$$

$$P_A = 3.6 \text{ m}.$$

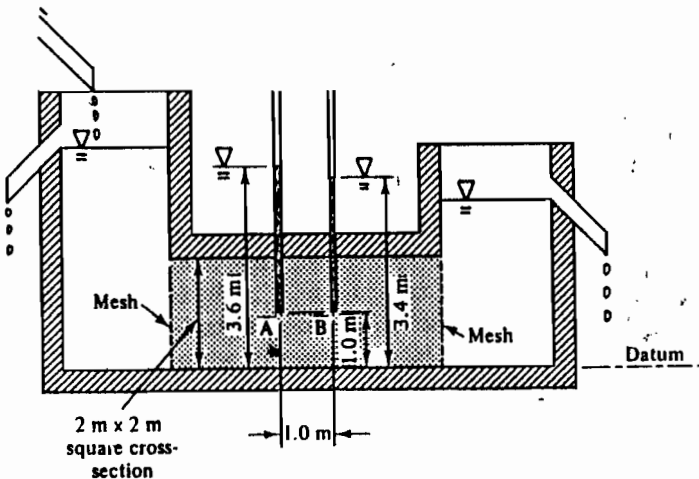


Figure E6-1

At B,

$$P_B = (23.5/9.81) + 1.0,$$

$$P_B = 3.4 \text{ m.}$$

(c) Hydraulic gradient  $i = -dP/ds = -\Delta P/\Delta s$  from Eq. (6-9).

$$\Delta P = P_B - P_A = -0.2 \text{ m,}$$

$$\Delta s = 1.0 \text{ m,}$$

hence,

$$i = 0.2.$$

### Example 6-2 Calculation of seepage velocity and artificial velocity

Figure E6-2 shows a pipe of square cross-section which contains soil and whose dimensions are similar to the pipe described in Ex. 6-1. The water flowing through the soil collects in the graduated vessel at a rate of  $0.24 \text{ m}^3$  per min. The walls of the pipe are transparent and the passage of dye between A' and B', 1.0 m apart, is timed to take 8.3 min. Calculate (a) the seepage velocity and (b) the artificial velocity. Hence, estimate (c) the specific volume of the soil.

(a) Seepage velocity,  $V_s = ds/dt = \Delta s/\Delta t$  from Eq. (6-6). Hence,

$$V_s = 1.0/(8.3 \times 60),$$

$$V_s = 2 \times 10^{-3} \text{ m s}^{-1}.$$

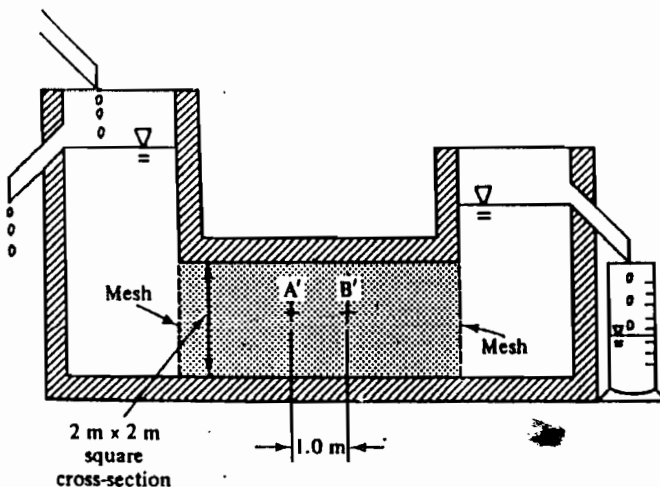


Figure E6-2

(b) Artificial velocity,  $V = \Delta Q / A \Delta t$  from Eqs (6-4) and (6-5). Hence,

$$V = 0.24 / (2^2 \times 60),$$

$$V = 1 \times 10^{-3} \text{ m s}^{-1}.$$

(c) The seepage velocity and the artificial velocity are related to the specific volume  $v$  of the soil by Eq. (6-8):

$$V = V_s[(v-1)/v].$$

Hence,

$$(v-1)/v = V/V_s = \frac{1}{2}.$$

$$v = 2.0.$$

## 6-5 DARCY'S LAW

Darcy's law relates the artificial velocity to the hydraulic gradient by the equation

$$V = ki, \quad (6-10)$$

where the parameter  $k$  is known as the coefficient of permeability;  $k$  is a scalar quantity with the units of velocity.

Darcy's law is valid for the flow of water through porous media like soils provided the flow remains laminar. The value of  $k$  is regarded as a soil constant and has a fixed value for a particular soil in a given state; the value of  $k$  may vary to a minor extent with changes of viscosity of the water (e.g., due to temperature changes), but it is very dependent on the specific volume of the soil.

Typical values of permeability for various soils are contained in Table 6-1. The difference of approximately  $10^6$  in the values of  $k$  for gravels and clays is of great significance and is associated with important differences in the mechanical behaviour of coarse- and fine-grained soils.

**Table 6-1 Typical values of coefficient of permeability for various soils**

Soil type	Coefficient of permeability $k$ ( $\text{m s}^{-1}$ )
Gravel	$> 10^{-2}$
Sand	$10^{-3}$ to $10^{-4}$
Silt	$10^{-5}$ to $10^{-6}$
Clay	$< 10^{-6}$



**Example 6-3** Calculation of the coefficient of permeability

Use the results of Ex. 6-1 and 6-2 to calculate the coefficient of permeability of the soil in the tube.

From Darcy's law, the coefficient of permeability  $k$  is given by Eq. (6-10),  $V = ki$ . From Ex. 6-1, the hydraulic gradient is  $i = 0.2$  and, from Ex. 6-2, the artificial velocity is  $V = 1 \times 10^{-3} \text{ m s}^{-1}$ . Hence, the coefficient of permeability is

$$k = V/i = (1 \times 10^{-3})/0.2,$$

$$k = 5 \times 10^{-3} \text{ m s}^{-1}.$$

**6-6 SEEPAGE FORCES**

As water flows through soil, the potential of the water drops and this drop represents a loss of energy; this energy is lost as drag on the soil grains as water flows through the pore spaces and these drag forces will change the effective stress.

Figure 6-7 shows a section of a small tubular element, of length  $\delta s$  and area  $\delta A$ , which is centred on a flowline AB. The *seepage force*  $\delta F_s$  is due to a potential drop  $\delta P$  and the force acts in the direction of flow; it is given by

$$\delta F_s = -\gamma_w \delta P \delta A \quad (6-11)$$

and, from Eq. (6-9),

$$\delta F_s = \gamma_w i \delta s \delta A,$$

or

$$\delta F_s = \gamma_w i \delta V_0, \quad (6-12)$$

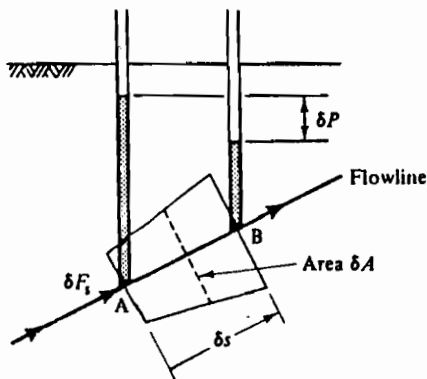


Figure 6-7 Seepage force

where  $i$  is the hydraulic gradient, which is positive in the direction of flow, and  $\delta V_0$  is the volume of the element.

The seepage force, which acts over an area  $\delta A$ , leads to a change in the effective stress of magnitude  $\delta\sigma'_s$  given by

$$\delta\sigma'_s = \gamma_w i \delta s$$

and, in the limit,

$$d\sigma'_s = \gamma_w i ds. \tag{6-13}$$

### 6-7 CRITICAL HYDRAULIC GRADIENT FOR VERTICAL UPWARD FLOW

As the hydraulic gradient increases, seepage forces increase proportionally until the soil grains are disturbed. The hydraulic gradient at which the soil grains are disturbed obviously depends on the direction of flow and on the magnitude of the effective stresses in the soil before any seepage took place. For vertical upward flow, a critical condition known as piping or boiling, which gives rise to a quicksand condition, occurs when the upward seepage forces just balance the submerged weight of the soil grains.

This critical hydraulic gradient for vertical upward flow is best examined by considering the seepage force on an element, volume  $\delta V_0$ , just below the soil surface, as shown in Fig. 6-8. When the hydraulic gradient is critical,  $i = i_c$ , the upward seepage force is equal to the submerged unit weight of the soil grains, or

$$\begin{aligned} \delta F_s &= \gamma_w i_c \delta V_0 = (\gamma - \gamma_w) \delta A \delta s, \\ i_c &= (\gamma/\gamma_w) - 1. \end{aligned} \tag{6-14}$$

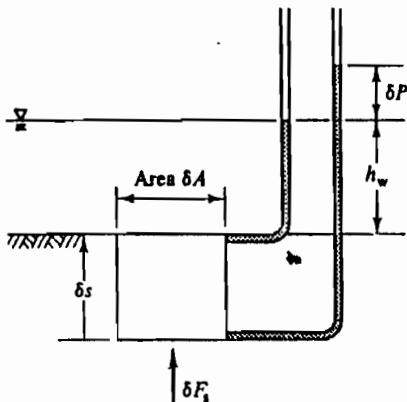


Figure 6-8 Critical hydraulic gradient

For many soils the unit weight is about  $20 \text{ kN m}^{-3}$  and  $i_0$  is approximately unity.

Alternatively, we may examine the vertical effective stress on a horizontal plane at a depth  $\delta s$  below the soil surface. Noting that, since the flow is upward,  $\delta s$  is measured negatively downward, we have, from Fig. 6-8,

$$\sigma_v = -\gamma \delta s + \gamma_w h_w, \quad (6-15)$$

$$u = \gamma_w [\delta P + h_w - \delta s]. \quad (6-16)$$

Therefore,

$$\begin{aligned} \sigma'_v &= -(\gamma - \gamma_w) \delta s - \gamma_w \delta P \\ &= -\gamma_w \delta s \{[(\gamma/\gamma_w) - 1] - i\} \end{aligned} \quad (6-17)$$

$$= -\gamma_w \delta s (i_0 - i), \quad (6-18)$$

where  $i_0$  is the critical hydraulic gradient given by Eq. (6-14).

Consequently, if the hydraulic gradient is critical,  $i = i_0$ , the effective stresses will be zero; under these circumstances the soil will have no strength and even lightly-loaded structures founded at the surface will sink into the quicksand. Clearly, the hydraulic gradient in the region of B in Fig. 6-1 cannot be allowed to approach the critical value without jeopardizing the stability of the wall.

So far, we have considered only vertical upward seepage near a horizontal soil surface and we should also examine the seepage forces, whatever their direction, throughout a soil body, and the overall stability of large blocks of soil. In particular, we must ensure that seepage forces acting on any finite block of soil are less than the forces available to prevent the block being disturbed. Forces preventing movement may be a result of the submerged weight of the soil grains, external forces, and shearing stresses in the soil.

## 6-8 FLOW NET FOR ONE-DIMENSIONAL SEEPAGE

We must now begin to investigate seepage through masses of soil rather than through small elements; it is convenient to start with the simple case of one-dimensional seepage to introduce the concept of flow nets.

Figure 6-9 shows a body of soil of height  $s$  and width  $b$  contained in a parallel-sided container of unit thickness between two gauze meshes. Water is supplied below the soil from a constant head source and overflows from a constant level weir; the rate of flow is measured. An apparatus of this kind is the basis of a constant head permeameter used, in practice, to measure the coefficient of permeability of soil samples.

The permeameter in Fig. 6-9 contains several standpipes; these are spaced at intervals of  $\Delta s$  and the difference of potential between adjacent standpipes is  $\Delta P$ . The total potential drop across the soil is  $(P_2 - P_1)$  and this is

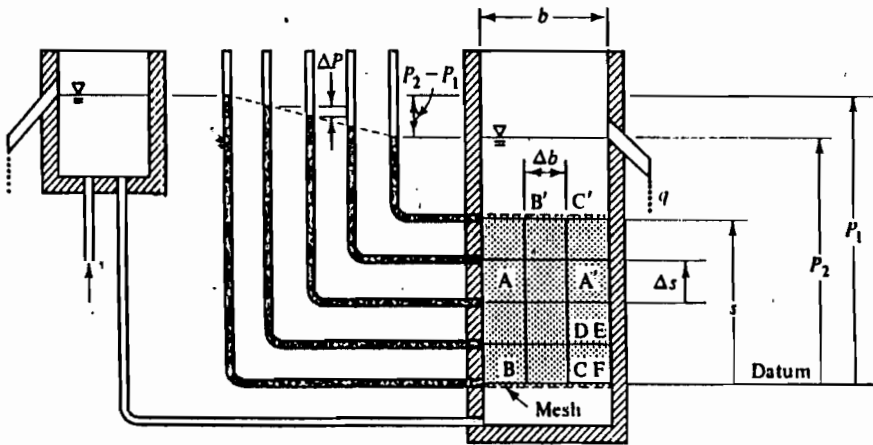


Figure 6-9 One-dimensional seepage

simply the difference in elevation between the constant head supply and the overflow weir.

If the soil is homogeneous, flowlines must be parallel and vertical; lines such as BB' and CC' in Fig. 6-9 are equi-spaced flowlines  $\Delta b$  apart. If the rate of flow between adjacent flowlines is  $\Delta q$  per unit thickness,

$$\Delta q = V \Delta b$$

and

$$q = Vb, \tag{6-19}$$

where  $V$  is the artificial velocity. A standpipe placed anywhere at a given elevation will register the same potential and lines such as AA', joining points of equal potential are known as *equipotentials*; in Fig. 6-9, all equipotentials are straight horizontal lines.

Flowlines such as BB' and equipotentials such as AA' make up what is known as a *flownet*. Two important properties of the flownet in Fig. 6-9 are apparent: first, equipotentials and flowlines intersect orthogonally and, second, if one element of the net such as CDEF is made square by suitable choices of  $\Delta s$  and  $\Delta b$ , all other elements are squares. Later we will find that these are properties of general plane seepage flownets.

The artificial velocity is given by Darcy's law,

$$V = ki = -k(dP/ds) \tag{6-20}$$

and, for one-dimensional flow, as in Fig. 6-9,

$$dP/ds = (P_2 - P_1)/s. \tag{6-21}$$

Hence, the rate of flow through the permeameter is given by

$$q = -k(b/s)(P_2 - P_1). \tag{6-22}$$

If we define  $N_f$  as the number of separate flow channels and  $N_d$  as the number of equipotential drops in a square flownet (in Fig. 6-9,  $N_f = 3$  and  $N_d = 4$ ), then, remembering that all the individual elements of the flownet are square,

$$b/s = N_f/N_d$$

and

$$q = -k(N_f/N_d)(P_2 - P_1), \tag{6-23}$$

where  $(P_2 - P_1)$  is the total change of potential across the permeameter. Later we will show that Eq. (6-23) is valid for any plane seepage flownet properly constructed from squares.

**Example 6-4** Calculation of the rate of flow for one-dimensional seepage

Figure E6-3 shows a section of the square-sectioned pipe described in Ex. 6-1 and 6-2. The coefficient of permeability of the soil contained within the pipe is  $k = 5 \times 10^{-3} \text{ m s}^{-1}$  and other dimensions are shown in Fig. E6-3. Calculate the rate of flow  $q$  through the soil.

The rate of flow through a strip of unit thickness normal to the page is given by Eq. (6-23) as

$$q = -k(N_f/N_d)(P_2 - P_1).$$

Taking an arbitrary datum for potential at the invert of the pipe, the potentials upstream and downstream of the soil are  $P_1 = 4 \text{ m}$  and  $P_2 = 3 \text{ m}$ . A square flownet is sketched in Fig. E6-3 for which  $N_f = 2$  and  $N_d = 5$  (if the squares were made smaller the ratio of  $N_f$  to  $N_d$

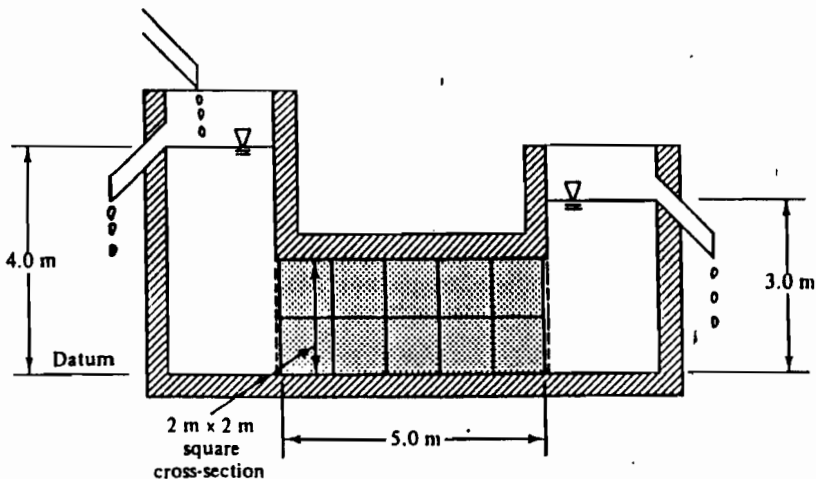


Figure E6-3

would of course remain unchanged). The width of the cross-section of the pipe normal to the page is 2 m and, hence, the rate of flow is

$$q = 2[-5 \times 10^{-3} \times \frac{1}{2}(3-4)],$$

$$q = 4 \times 10^{-3} \text{ m}^3 \text{ s}^{-1} = 0.24 \text{ m}^3 \text{ min}^{-1}.$$

### 6-9 TWO-DIMENSIONAL SEEPAGE

In order to extend the simple one-dimensional flownet to the more general case of two-dimensional seepage, we must appeal to mathematical analysis. Figure 6-10 illustrates the conditions of steady-state, irrotational flow through an element; by irrotational we mean that there is no rotational component of flow completely contained within the element. During steady-state flow neither the effective stresses nor the volume of the element change. From the condition of continuity, the net inflow is zero,

$$\frac{\partial V_x}{\partial x} dx dz + \frac{\partial V_z}{\partial z} dz dx = 0,$$

$$\frac{\partial V_x}{\partial x} + \frac{\partial V_z}{\partial z} = 0. \tag{6-24}$$

The requirement for irrotational flow is given by

$$\frac{\partial V_x}{\partial z} - \frac{\partial V_z}{\partial x} = 0. \tag{6-25}$$

Together, these two partial differential equations define the distribution of artificial velocity throughout the plane region (x, z) in which flow occurs.

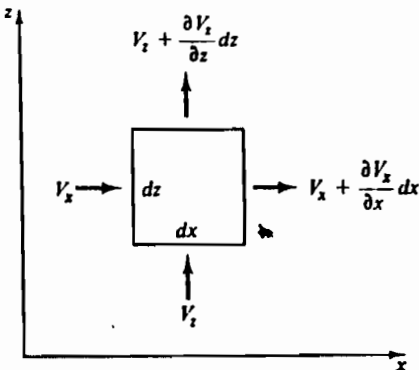


Figure 6-10 General conditions of two-dimensional seepage

Next, we define a potential function  $\Phi(x, z)$  and a flow function  $\Psi(x, z)$  such that

$$V_x = \frac{\partial \Phi}{\partial x}, \quad V_z = \frac{\partial \Phi}{\partial z}, \quad (6-26)$$

$$V_x = \frac{\partial \Psi}{\partial z}, \quad V_z = -\frac{\partial \Psi}{\partial x}. \quad (6-27)$$

From Eqs (6-24) and (6-25) and Eqs (6-26) and (6-27) it follows that

$$\frac{\partial^2 \Phi}{\partial x^2} + \frac{\partial^2 \Phi}{\partial z^2} = 0, \quad (6-28)$$

$$\frac{\partial^2 \Psi}{\partial x^2} + \frac{\partial^2 \Psi}{\partial z^2} = 0. \quad (6-29)$$

These are Laplace equations and they govern the distribution of flow throughout the region  $(x, z)$ . If we can find functions  $\Phi$  and  $\Psi$  which satisfy Eqs (6-28) and (6-29), together with some appropriate boundary conditions, we can calculate the distribution of both artificial velocity and potential throughout the region.

The solutions may be mapped as contours of the potential function  $\Phi(x, z)$  and contours of the flow function  $\Psi(x, z)$ ; along such contours  $d\Phi = 0$  and  $d\Psi = 0$ . From the definition of partial differentiation,

$$d\Phi = \frac{\partial \Phi}{\partial x} dx + \frac{\partial \Phi}{\partial z} dz,$$

$$d\Psi = \frac{\partial \Psi}{\partial x} dx + \frac{\partial \Psi}{\partial z} dz,$$

and, from Eqs (6-26), along  $\Phi = \text{constant}$  contours,

$$d\Phi = V_x dx + V_z dz = 0 \quad (6-30)$$

and the gradient of a contour is

$$\frac{dz}{dx} = -\frac{V_x}{V_z}. \quad (6-31)$$

Similarly, from Eqs (6-27), along  $\Psi = \text{constant}$  contours,

$$d\Psi = -V_z dx + V_x dz = 0 \quad (6-32)$$

and the gradient of a contour is

$$\frac{dz}{dx} = +\frac{V_z}{V_x}. \quad (6-33)$$

Lines of constant  $\Phi$  and lines of constant  $\Psi$  must, therefore, be everywhere orthogonal, since the product of their gradients is  $-1$ . In any problem of

plane irrotational seepage, contours of the potential function  $\Phi(x, z)$  and contours of the flow function  $\Psi(x, z)$  form a network of two families of orthogonal curves; the precise shape of the network is governed by the particular boundary conditions.

**6-10 POTENTIAL FUNCTION  $\Phi(x, z)$**

Darcy's law is valid not only for seepage along a flowline but also for resolved components of velocity and hydraulic gradient; thus, from Eqs (6-9) and (6-10), and assuming the soil to be isotropic,

$$V_x = -k \frac{\partial P}{\partial x}, \quad V_z = -k \frac{\partial P}{\partial z}, \quad (6-34)$$

where  $P = P(x, z)$  is the distribution of potential. Equating Eqs (6-26) and (6-34) gives

$$\Phi = -kP \quad (6-35)$$

and, thus, lines of constant  $\Phi$  (i.e.,  $d\Phi = 0$ ) are equipotentials ( $dP = 0$ ).

**6-11 FLOW FUNCTION  $\Psi(x, z)$**

Figure 6-11 shows the flow through a small triangular element ABC adjacent to a line  $d\Psi = 0$ ; the condition of continuity of flow requires that there is zero net inflow and

$$-V_n ds + V_s dx - V_x dz = 0. \quad (6-36)$$

Since  $d\Psi = 0$  along AB, we have, from Eq. (6-32),

$$V_s dx = V_x dz$$

and, hence,

$$V_n = 0. \quad (6-37)$$

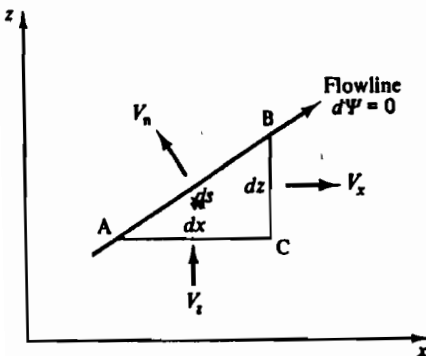


Figure 6-11 Flow through a triangular element to illustrate the meaning of the flow function  $\Psi$



Thus, there is no component of flow across AB and lines of constant  $\Psi$  (i.e.,  $d\Psi = 0$ ) are flowlines.

We have shown already that lines of constant  $\Psi$  and lines of constant  $\Phi$  form an orthogonal network; consequently, throughout a region of plane seepage, flowlines and equipotentials form a similar orthogonal network.

### 6-12 RATE OF FLOW THROUGH A FLOWNET

Figure 6-12 shows two flowlines  $\Psi = \Psi_0$  and  $\Psi = \Psi_0 + \Delta\Psi$  between which the rate of flow is  $dq$ . The rate of flow  $dq$  through the small triangular element is

$$dq = V_x dz - V_z dx \tag{6-38}$$

and, from Eqs (6-27),

$$dq = \frac{\partial\Psi}{\partial z} dz + \frac{\partial\Psi}{\partial x} dx.$$

Hence,

$$dq = d\Psi. \tag{6-39}$$

Integrating Eq. (6-39) between the flowlines,

$$\Delta q = \int_{\Psi_0}^{\Psi_0 + \Delta\Psi} d\Psi = \Delta\Psi. \tag{6-40}$$

Figure 6-13 shows a portion of a flownet consisting of two flowlines and two equipotentials. On average, the distance between the flowlines is  $\Delta b$

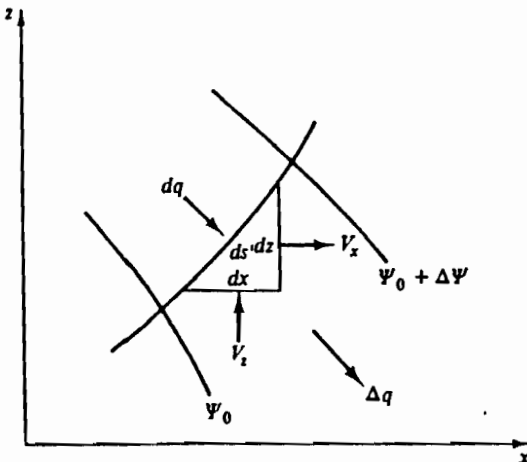


Figure 6-12 Rate of flow between adjacent flowlines

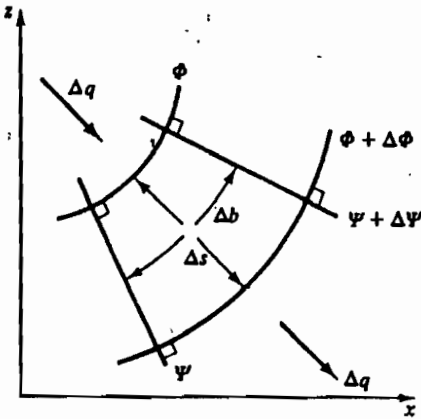


Figure 6-13 Rate of flow through a portion of a flownet

and, on average, the distance between the equipotentials is  $\Delta s$ . The artificial velocity is given by Darcy's law,  $V = ki$ , where

$$V = \Delta q / \Delta b$$

and

$$i = -\Delta P / \Delta s.$$

Hence,

$$\Delta q / \Delta b = -k(\Delta P / \Delta s). \tag{6-41}$$

But, from Eq. (6-35),  $-k\Delta P = \Delta\Phi$  and, therefore,

$$\Delta q = (\Delta b / \Delta s) \Delta\Phi. \tag{6-42}$$

### 6-13 'SQUARE FLOWNETS'

In Eq. 6-42,  $\Delta b$  and  $\Delta s$  simply define the geometry of the flownet and we will choose to construct flownets with  $\Delta b = \Delta s$ , i.e., with each element of the flownet 'square'. Then, from Eqs (6-40) and (6-42),

$$\Delta q = \Delta\psi = \Delta\Phi. \tag{6-43}$$

If the flowlines and equipotentials are curved, a 'square flownet' will consist of elements the mean length and breadth of which are equal and the sides of which intersect orthogonally; we may check whether a flownet is square by attempting to construct circles within the elements of the net, as shown in Fig. 6-14. If we make one element in a flownet square, then all the elements in the flownet must also be square, but they need not all be the same size.

Figure 6-15 shows a 'square flownet' consisting of  $N_f = 2$  flow channels between flowlines each spaced  $\Delta\psi$  apart and  $N_d = 3$  potential drops each of

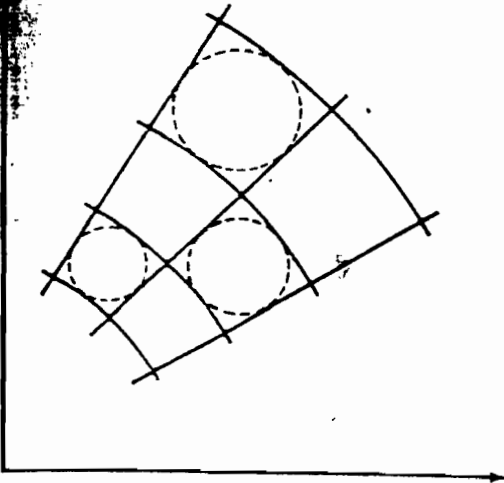


Figure 6-14 A 'square flownet'

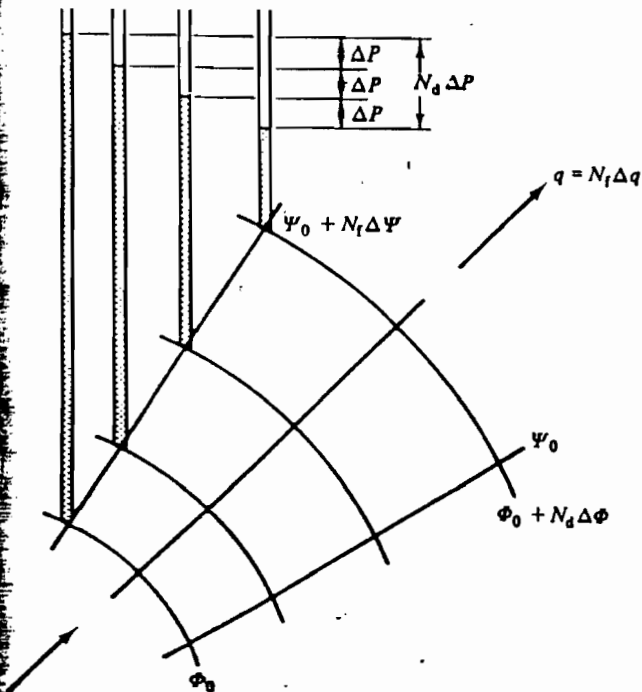


Figure 6-15 Rate of flow through a 'square flownet'

magnitude  $\Delta\Phi$ . The rate of flow through the flownet is the sum of the flows through the individual flow channels and, from Eq. (6-43), is given by

$$q = N_f \Delta q = N_f \Delta \Psi = N_f \Delta \Phi$$

or

$$q = (N_f/N_d) N_d \Delta \Phi. \tag{6-44}$$

However, from Eq. (6-35),

$$N_d \Delta \Phi = -k N_d \Delta P = -k(P_2 - P_1). \tag{6-45}$$

Thus, the rate of flow through the flownet is given by

$$q = -k(N_f/N_d)(P_2 - P_1), \tag{6-46}$$

where  $(P_2 - P_1)$  is the change of potential across the whole flownet. Equation (6-46) is the same as Eq. (6-23), which we derived for the special case of one-dimensional seepage; it may be used to calculate the rate of flow through any 'square flownet' for plane seepage.

### 6-14 BOUNDARY CONDITIONS

Any problem of plane seepage may be solved by constructing a square flownet; the flownet will consist of a network of flowlines ( $d\Psi = 0$ ) and equipotentials ( $d\Phi = 0$ ) intersecting orthogonally. Its precise shape will depend on the geometry of the region of seepage and the boundary conditions.

To illustrate various common boundary conditions we make use of Fig. 6-16, which illustrates a section of a permeable embankment dam resting on an impermeable rock foundation. An orthogonal flownet must be constructed in the region of seepage ABCDE.

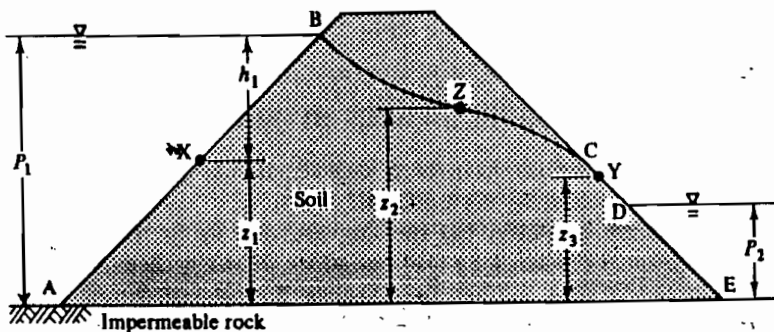


Figure 6-16 Boundary conditions for seepage through an embankment

There are several different kinds of boundary to this region and we consider these in turn:

- (i) A-E. The rock is impermeable, there is no component of seepage velocity normal to AE. The boundary must therefore be a flowline.
- (ii) A-B. We choose foundation level AE as an arbitrary datum for potential. At any point such as X on AB, the potential is given by Eq. (6-2) and is

$$P_x = (u/\gamma_w) + z_1 = h_1 + z_1 = P_1 \quad (6-47)$$

and, thus, AB is an equipotential with  $P = P_1$ . By the same argument, DE is an equipotential with  $P = P_2$ . The total change in potential is  $(P_2 - P_1)$ .

- (iii) C-D. Along CD the pore pressure is zero and, at a point such as Y, the potential is given by  $P_Y = z_3$ . There is a component of flow normal to CD and water flows freely down the surface of the slope; consequently CD is neither a flowline nor an equipotential.
- (iv) B-C. The line BC is not fixed by the geometry of the embankment, but it is defined by two hydraulic conditions: (a) there is no component of flow normal to BC and it must therefore be a flowline and (b) the pore pressure along BC is zero and at a point such as Z the potential is given by  $P_Z = z_2$ . A boundary like BC is known as a *phreatic surface*.

The boundaries AE, AB, DE, and CD are each fixed in space by the geometry of the embankment and for each there is only one hydraulic boundary condition. The precise location of the boundary BC, however, is fixed by the geometry of the flownet and there is only one position of BC for which a properly constructed 'square flownet' is possible; its position must usually be found by trial and error.

The boundary conditions for the plane seepage below an impermeable wall are shown in Fig. 6-17. The boundaries BCD and FG are impermeable and are flowlines; the boundaries AB and DE are equipotentials with potentials  $P_1$  and  $P_2$ , respectively. Unlike the case shown in Fig. 6-16, there is no phreatic surface in Fig. 6-17. The flow is known as *contained*, because the boundaries of the region of flow are fixed. The boundary BC in Fig. 6-16 can be located only after the flownet has been constructed and, in this case, the flow is known as *uncontained*.

## 6-15 CONSTRUCTION OF FLOWNETS BY SKETCHING

Once the boundary conditions have been defined, the flownet may be constructed; this step is often the most difficult.

Several methods are available, but the simplest, and by far the most common, is to sketch the flownet by trial and error. Flownet sketching is principally a question of time and practice. Sketched flownets are shown for

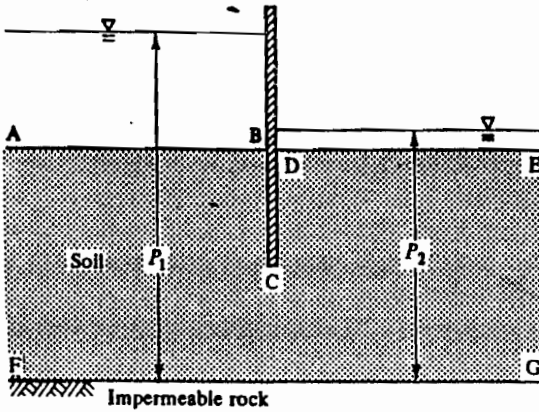


Figure 6-17 Boundary conditions for seepage below an impermeable wall

plane seepage through an embankment (Fig. 6-18) and below an impermeable wall (Fig. 6-19). Close inspection will reveal instances where flowlines and equipotentials are not perfectly orthogonal and where 'squares' are not properly square; both flownets could be improved with further adjustment.

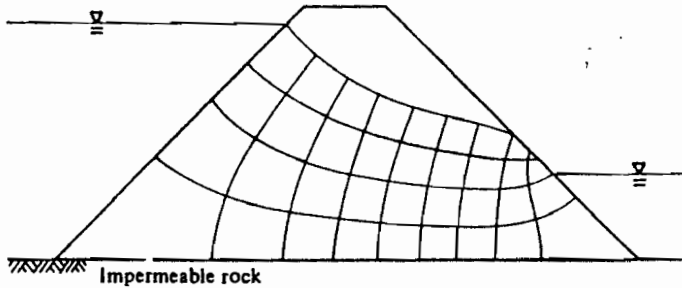


Figure 6-18 Flownet for seepage through an embankment

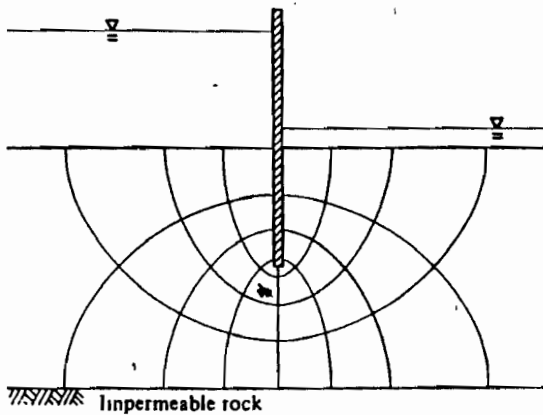


Figure 6-19 Flownet for seepage below an impermeable wall

**Example 6-5 Seepage below an impermeable wall**

Figure E6-4 shows a section through a long impermeable wall driven into the bed of a river; the river bed consists of sand overlying impermeable rock. The water level to the right of the wall is permanently lowered by steady pumping as water flows from left to right through the sand below the wall. The permeability of the sand is  $k = 10^{-4} \text{ m s}^{-1}$  and the dimensions are given in Fig. E6-4. Calculate the rate of flow under the wall and estimate the pore pressure at a point A next to the downstream face of the wall, 1.0 m above the tip.

A 'square flownet' has been sketched and is shown in Fig. E6-5. Choosing the rock-sand interface as an arbitrary datum for potential, the boundary conditions are:

- (i) the upstream river bed is an equipotential with  $P_1 = 7.5 \text{ m}$ ;
- (ii) the downstream river bed is an equipotential with  $P_2 = 5.5 \text{ m}$ ;
- (iii) the impermeable rock and the wall are each flowlines.

For the flownet illustrated in Fig. E6-5,  $N_f = 4$  and  $N_d = 8$ . Hence, the rate of flow  $q$  through a strip of unit thickness normal to the page is

$$q = -k(N_f/N_d)(P_2 - P_1) = -10^{-4} \times \frac{1}{4} \times (5.5 - 7.5),$$

$$q = 10^{-4} \text{ m}^3 \text{ s}^{-1} = 0.36 \text{ m}^3 \text{ h}^{-1}.$$

At the point A, the pore pressure  $u_A$  may be found from the potential  $P_A$ . The point A lies approximately midway between the sixth and seventh equipotentials, counting from zero at the upstream face. Since  $(P_2 - P_1) = -2 \text{ m}$  and  $N_d = 8$ , the potential difference between adjacent equipotentials is  $\Delta P = -0.25 \text{ m}$ . Hence, the potential at A is

$$P_A = 7.5 - (0.25 \times 6\frac{1}{2}) = 5.875 \text{ m}.$$

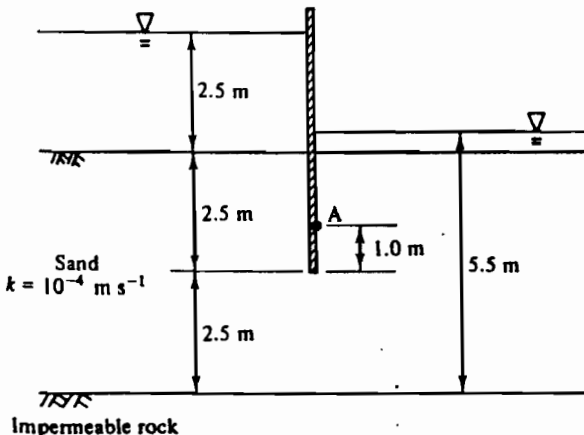


**Figure E6-4** Seepage below an impermeable wall

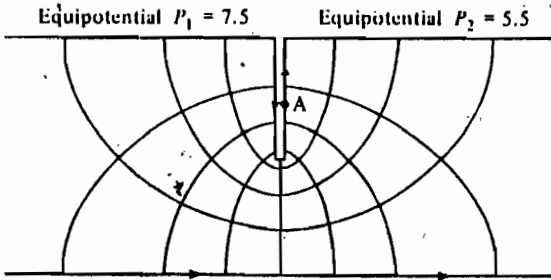


Figure E6-5 A 'square flownet' for seepage below an impermeable wall

The elevation of the point A above the arbitrary datum is  $z_A = 3.5$  m and

$$P_A = (u_A/\gamma_w) + z_A.$$

Hence,

$$u_A = 9.81(5.875 - 3.5),$$

$$u_A = 23.3 \text{ kN m}^{-2}.$$

## 6-16 OTHER METHODS OF SOLUTION

Flownets simply represent solutions of the Laplace equations (6-28) and (6-29) and, for certain simple cases, mathematical solutions may be obtained. An analytical solution for seepage below an impermeable wall in a deep bed of soil is given by Schofield and Wroth (1968, pp. 59-64), but even for this relatively simple case the mathematics is not easy. Alternatively, the Laplace equations may be written in finite difference form, and approximate solutions found by relaxation methods (e.g., Scott, 1963, pp. 134-156) or they may be solved approximately using finite element techniques (e.g., Zienkiewicz, 1971, pp. 295-321).

An alternative method of solution is to construct a model in the laboratory and observe flowlines and equipotentials directly. Flowlines may be drawn by observing the passage of dye and equipotentials found by measuring the distribution of potential using suitable pore pressure probes placed in the soil.

We may note that the coefficient of permeability  $k$  does not appear in Eqs (6-28) and (6-29) and the geometry of a flownet is therefore independent of the value of  $k$ . Only the rate of flow given by Eq. (6-46) is dependent on  $k$  and, consequently, we may use any soil we like in a model intended only to investigate the geometry of a flownet.

Instead of building a physical model of water flowing through soil, we may make use of the analogy between Darcy's law and Ohm's law. Ohm's



law, governing the flow of electricity through conducting bodies, may be written as

$$\left. \begin{aligned} I_x &= -C(\partial E/\partial x), \\ I_z &= -C(\partial E/\partial z), \end{aligned} \right\} \quad (6-48)$$

where  $I_x$  and  $I_z$  are the components of the electric current in the  $x$ - and  $z$ -directions,  $E$  is the electrical potential, and  $C$  is the conductivity of the body. Equations (6-48) are analogous to Eqs (6-34) with equivalence between current and artificial velocity, electrical and hydraulic potential gradients, and conductivity and permeability.<sup>7</sup>

An analogue for two-dimensional seepage may be made from electrically conducting paper and equipotentials found by measuring the distribution of electrical potential. With this method, the effect of varying the geometry of the problem may be investigated rapidly simply by trimming the conducting paper.

### 6-17 SEEPAGE THROUGH ANISOTROPIC, LAYERED, AND NON-UNIFORM SOILS

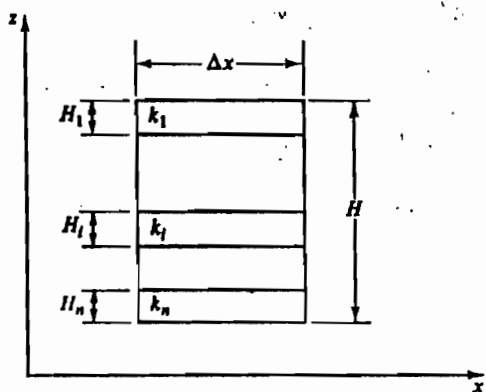
So far we have regarded soil as isotropic and homogeneous, with a single value of the coefficient of permeability. For completeness we must investigate seepage through soils that are anisotropic and which may be layered or otherwise non-uniform.

### 6-18 SEEPAGE THROUGH LAYERED STRATA

Soils are usually deposited in successive horizontal layers and the permeabilities of the layers may differ. It is often convenient to think of a soil stratum as uniform and to calculate equivalent overall permeabilities in the horizontal and vertical directions to account for the variation of permeability of the layers. Figure 6-20(a) shows a soil stratum depth  $H$ , width  $\Delta x$  and with unit thickness normal to the diagram; it consists of  $n$  layers of which a typical layer has thickness  $H_i$  and permeability  $k_i$ . We define axes  $x$  and  $z$  as shown and we will calculate equivalent permeabilities  $k_x$  and  $k_z$  for flow parallel to and normal to the layers. Normally, in nature, soil layers are horizontal and the axes  $x$  and  $z$  will be horizontal and vertical.

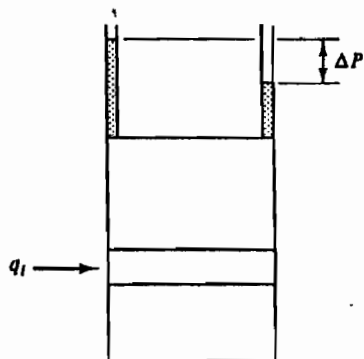
For flow parallel to the layers, as shown in Fig. 6-20(b), flowlines are horizontal and equipotentials are vertical; consequently, the hydraulic gradient is the same for each layer and is

$$i = -\Delta P/\Delta x = \text{constant}. \quad (6-49)$$



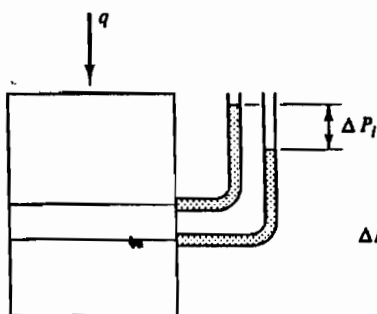
$$H = \sum_{i=1}^n H_i$$

(a)



$$q = \sum_{i=1}^n q_i$$

(b)



$$\Delta P = \sum_{i=1}^n \Delta P_i$$

(c)

Figure 6-20 Flow through layered strata. (a) Layered strata. (b) Horizontal flow. (c) Vertical flow

The rate of flow  $q_i$  through a single layer is given by Darcy's law

$$q_i = k_i H_i i \quad (6-50)$$

and, therefore, the total flow  $q$  is

$$q = i \sum k_i H_i \quad (6-51)$$

The total flow through the stratum can also be expressed in terms of  $k_x$  as

$$q = i k_x H = i k_x \sum H_i \quad (6-52)$$

where  $H$  is the total thickness of the stratum. Then, from Eqs (6-51) and (6-52),

$$k_x = \frac{\sum k_i H_i}{\sum H_i} \quad (6-53)$$

Flow normal to the layers is shown in Fig. 6-20(c). The rate of flow  $q$  through the stratum is equal to the rate of flow through any layer, i.e.,  $q = q_i$ , but the hydraulic gradients differ. For a single layer

$$i_i = -\Delta P_i / H_i \quad (6-54)$$

and for the whole stratum the mean hydraulic gradient is

$$i = -(\sum \Delta P_i) / (\sum H_i) \quad (6-55)$$

From Darcy's law, considering the rate of flow through a single layer,

$$q_i = k_i \Delta x i_i = -k_i \Delta x (\Delta P_i / H_i) \quad (6-56)$$

and through the the whole stratum,

$$q = k_x \Delta x i = -k_x \Delta x (\sum \Delta P_i) / (\sum H_i) \quad (6-57)$$

Rewriting Eq. (6-56) and summing for all layers,

$$\sum \Delta P_i = -(q_i / \Delta x) \sum (H_i / k_i) \quad (6-58)$$

and, rewriting Eq. (6-57),

$$\sum \Delta P_i = -(q / k_x \Delta x) \sum H_i \quad (6-59)$$

Thus, since  $q = q_i$ ,

$$k_x = \frac{\sum H_i}{\sum (H_i / k_i)} \quad (6-60)$$

In general, values of  $k_x$  and  $k_s$  will differ and seepage through a layered soil may be approximated to the seepage through an equivalent homogeneous but anisotropic soil.

#### Example 6-6 Calculation of the permeability of a layered stratum

Figure E6-6 shows part of a layered stratum consisting of silt layers 5 mm thick between clay layers 25 mm thick. The coefficient of

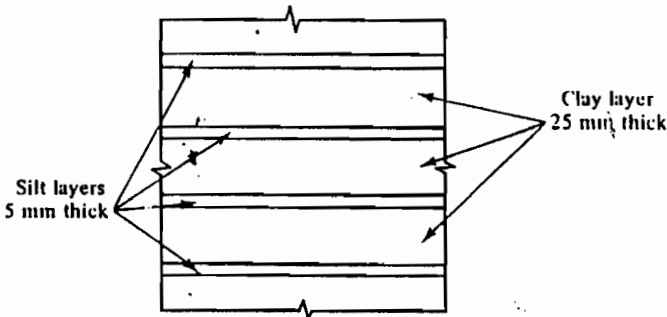


Figure E6-6 Layered stratum

permeability of the silt is  $k_s = 10^{-6} \text{ m s}^{-1}$  and of the clay is  $k_c = 10^{-8} \text{ m s}^{-1}$ . Calculate the equivalent permeability of the stratum for (a) horizontal and (b) vertical flow.

- (a) For horizontal flow, the equivalent coefficient of permeability  $k_h$  is given by Eq. (6-53):

$$k_h = (\sum kH)/(\sum H) = [(5 \times 10^{-6}) + (25 \times 10^{-8})]/30,$$

$$k_h = 1.75 \times 10^{-7} \text{ m s}^{-1}.$$

- (b) For vertical flow, the equivalent coefficient of permeability  $k_v$  is given by Eq. (6-60):

$$k_v = (\sum H)/(\sum H/k) = 30/[(5 \times 10^6) + (25 \times 10^8)],$$

$$k_v = 1.20 \times 10^{-8} \text{ m s}^{-1}.$$

### 6-19 SEEPAGE THROUGH ANISOTROPIC SOILS

For an anisotropic soil with permeabilities  $k_x \neq k_z$ , Eqs (6-34) become

$$V_x = -k_x \frac{\partial P}{\partial x}, \quad V_z = -k_z \frac{\partial P}{\partial z}, \quad (6-61)$$

and, from Eq. (6-24), the distribution of potential is given by

$$k_x \frac{\partial^2 P}{\partial x^2} + k_z \frac{\partial^2 P}{\partial z^2} = 0. \quad (6-62)$$

This is not a Laplace equation and we can no longer obtain solutions to plane seepage problems by drawing 'square flownets'.

We may, however, change the geometry of the problem by defining new axes  $x_1$  and  $z_1$ , where

$$x_1 = \sqrt{\left(\frac{k_z}{k_x}\right)} x, \quad z_1 = z. \quad (6-63)$$

If the soil is more permeable in the  $x$ -direction (i.e.  $k_x > k_z$ ), the transformation has the effect of reducing dimensions in the  $x$ -direction while keeping  $z$ -dimensions unchanged. Making use of Eqs (6-26) and (6-27) in terms of the new axes and defining  $\Phi = -k_x P$ , we obtain

$$\frac{\partial^2 \Phi}{\partial x_1^2} + \frac{\partial^2 \Phi}{\partial z_1^2} = 0, \quad (6-64)$$

$$\frac{\partial^2 \Psi}{\partial x_1^2} + \frac{\partial^2 \Psi}{\partial z_1^2} = 0. \quad (6-65)$$

These are Laplace equations, like Eqs (6-28) and (6-29), and may be solved exactly as before by square flownets. Thus, to analyse a problem of plane seepage through an anisotropic soil, we must first change the geometry of the boundaries, using Eq. (6-63) to transform the scale; we may then proceed to construct a square flownet satisfying the hydraulic boundary conditions, which will remain unchanged. Finally, we may transform the scale back to the original, in which case the real flowlines and equipotentials may not intersect orthogonally.

The rate of flow through the transformed flownet is given by

$$q = -k'(N_y/N_x)(P_2 - P_1), \quad (6-66)$$

where  $k'$  is the equivalent coefficient of permeability of the transformed section. Figure 6-21(a) shows the flow through a rectangular element of a real flownet and Fig. 6-21(b) shows the flow through the same element with scales transformed according to Eq. (6-63). The potential drop across the element is  $\Delta P$  in each case. The equivalent permeability  $k'$  is defined so that the rate of flow  $\Delta q$  is the same through each element. Hence,

$$\Delta q = -k_x \Delta P \frac{\Delta b}{\Delta s} = -k' \Delta P \frac{\Delta b}{\Delta s \sqrt{(k_x/k_z)}}, \quad (6-67)$$

and, therefore,

$$k' = \sqrt{(k_x k_z)}. \quad (6-68)$$

## 6-20 SEEPAGE ACROSS A BOUNDARY BETWEEN TWO SOILS

Figure 6-22 illustrates the conditions of seepage across a boundary between two soils which are homogeneous and isotropic, but which have different permeabilities. The flownet to the left of the boundary in soil 1 has elements which are square with sides  $\Delta a$ , while, because of the different permeability of soil 2 to the right of the boundary, the elements of the flownet in soil 2 are rectangular with sides  $\Delta s$  and  $\Delta b$ . However, as can be seen in Fig. 6-22, flowlines and equipotentials are continuous across the boundary though their slopes change. The rate of flow between adjacent flowlines must be the

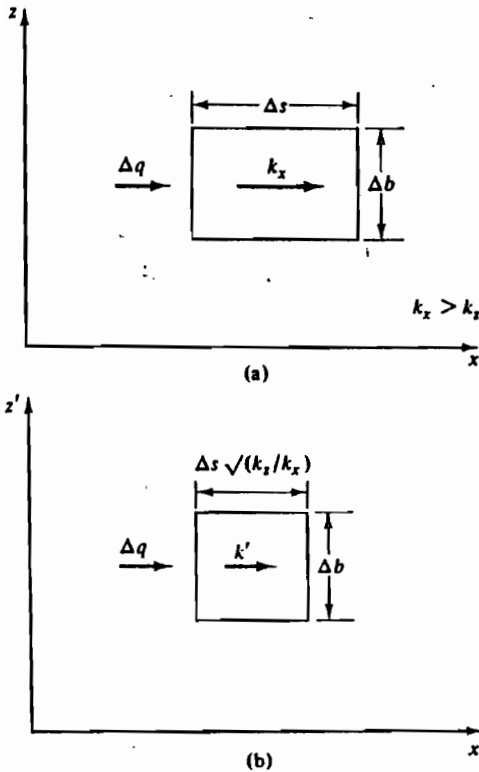


Figure 6-21 Flow through a single element of a real and a transformed flownet

same everywhere and the change of potential between adjacent equipotentials must also be the same everywhere. The rate of flow between a pair of adjacent flowlines is given by Eq. (6-42):

$$\Delta q = (\Delta a / \Delta a) \Delta \Phi_1 = (\Delta b / \Delta s) \Delta \Phi_2, \tag{6-69}$$

where the subscripts 1 and 2 refer to conditions in the soils 1 and 2. From Eq. (6-35),

$$\Delta \Phi_1 = -k_1 \Delta P_1, \quad \Delta \Phi_2 = -k_2 \Delta P_2, \tag{6-70}$$

and, because equipotentials are continuous across the boundary,  $\Delta P_1 = \Delta P_2$ . Thus, from Eqs (6-69) and (6-70),

$$\Delta b / \Delta s = k_1 / k_2. \tag{6-71}$$

From the geometry of Fig. 6-22,

$$AB = \Delta a / \cos \alpha_1 = \Delta b / \cos \alpha_2 \tag{6-72}$$

and

$$CD = \Delta a / \sin \alpha_1 = \Delta s / \sin \alpha_2. \tag{6-73}$$

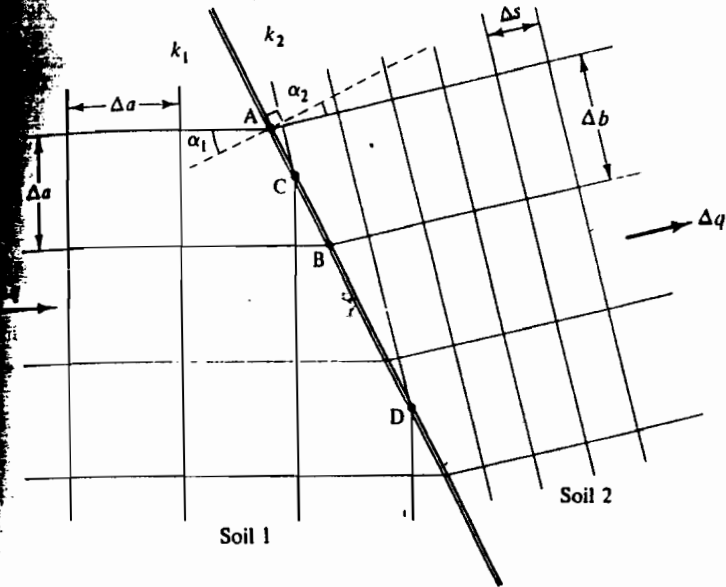


Figure 6-22 Flow across the boundary between soils with different permeabilities

Hence, from Eqs (6-72) and (6-73),

$$\Delta b / \Delta s = \tan \alpha_1 / \tan \alpha_2 \quad (6-74)$$

and, from Eq. (6-71),

$$k_1 / k_2 = \tan \alpha_1 / \tan \alpha_2 \quad (6-75)$$

Equation (6-75) defines the deflection of the flowlines as they cross the boundary and Eq. (6-71) defines the dimensions of the flownet to one side of the boundary when the flownet on the other side is square.

## 6-21 SUMMARY

### 1. Some useful definitions:

pore pressure  $u = \gamma_w h;$  (6-1)

potential  $P = h + z;$  (6-3)

artificial velocity  $V = dq/dA;$  (6-5)

hydraulic gradient  $i = -dP/ds.$  (6-9)

### 2. The steady-state flow of water through soil is governed by Darcy's law,

$$V = ki, \quad (6-10)$$

where  $k$  is the coefficient of permeability.

3. Seepage of pore water produces seepage stresses in the soil; the change  $d\sigma'_s$  of effective stress due to seepage forces in a length  $ds$  along a flowline is

$$d\sigma'_s = \gamma_w i ds. \quad (6-13)$$

The critical hydraulic gradient for piping is  $i_c = [(\gamma/\gamma_w) - 1] \approx 1.0$ .

4. Steady-state seepage through a region of soil is governed by Laplace equation and solutions may be obtained by mapping an orthogonal net of flowlines ( $d\Psi = 0$ ) and equipotentials ( $d\Phi = 0$ ). If the flownet is 'square',

$$\Delta q = \Delta\Psi = \Delta\Phi \quad (6-43)$$

and the total flow  $q$  through the whole net is

$$q = -k(N_f/N_d)(P_2 - P_1). \quad (6-46)$$

5. Seepage through layered and anisotropic soils may be tackled by calculating equivalent permeabilities and using a scale transformation.

## REFERENCES

- Schofield, A. N. and Wroth, C. P. *Critical State Soil Mechanics*. McGraw-Hill Book Co., London, 1968.
- Scott, R. F. *Principles of Soil Mechanics*. Addison-Wesley, Reading, Mass., 1963.
- Zienkiewicz, O. C. *The Finite Element Method in Engineering Science*. McGraw-Hill Book Co., London, 1971.



## 7-1 INTRODUCTION

The principle of effective stress states, among other things, that volume changes in soils are due exclusively to changes in effective stress; this means that if the volume of a soil changes the effective stress must also change.

Since soil grains and water are assumed to be incompressible, the volume of a saturated soil can only change as water is squeezed from (or drawn into) the pore space. As water flows from the innermost pores of a mass of soil towards its boundaries the flow will be governed by Darcy's law but, since the rate of flow must be finite, the soil volume will change with time. Consequently, the effective stress must change with time and, in general, so will the hydraulic gradient and the rate of flow. The variation of soil volume with time will be governed by complex interactions between effective and total stress, pore pressure, seepage, and compressibility.

This time-dependent process of volume change in soil as water is squeezed from the pores is known as *consolidation*. The relationship between the volume of the soil and the effective stress, which is a relationship independent of time, is known as *compression*.

## 7-2 COMPRESSION AND CONSOLIDATION – A SIMPLE MODEL

The distinction between compression and consolidation is best illustrated by the simple model shown in Fig. 7-1.

A water-filled cylinder has a close-fitting, light, and frictionless piston. The piston is connected to the base of the cylinder by a spring and it contains a drainage lead and a valve. The volume of water passing out through the valve is  $\Delta V_w$  and a gauge measures the settlement  $\Delta \rho$  of the piston.

The resistance to flow of water due to the valve represents the resistance to flow of water past the soil grains and so the degree of opening of the valve models the permeability of a soil. The stiffness of the spring represents soil compressibility; the spring characteristics correspond to those of the soil skeleton which may or may not be linear and reversible. The piston has unit area, so that a force  $\sigma$  applied to the piston causes an equivalent total stress  $\sigma$ ;

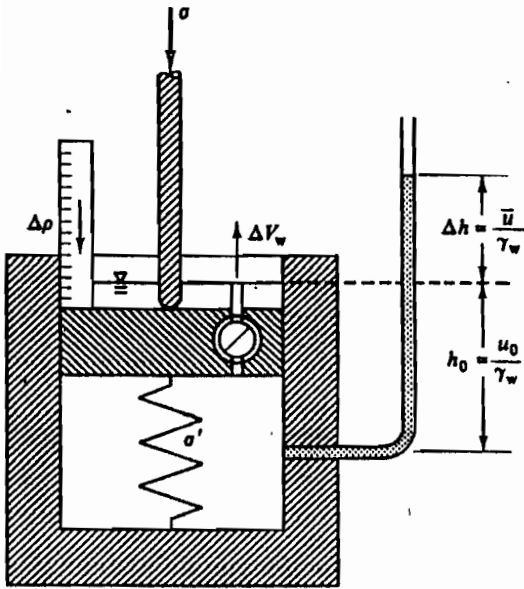


Figure 7-1 Model for soil compression and consolidation

if the pressure of water in the cylinder is  $u$ , then, for equilibrium, the force in the spring must equal  $(\sigma - u)$ , which is equivalent to an effective stress  $\sigma'$ . If the spring compresses and the piston settles by  $\Delta\rho$ , the volume within the cylinder changes by  $\Delta V$ , but, because  $\Delta V$  is defined as positive for an increase in volume,  $\Delta V$  is negative and equal in magnitude to the volume  $\Delta V_w$  of water squeezed out. Since the area of the piston is unity, settlements and volume changes are numerically equal and

$$\Delta V = -\Delta V_w = -\Delta\rho. \tag{7-1}$$

A standpipe of negligible volume is connected to the cylinder as shown and the level of water in the standpipe ( $h_0 + \Delta h$ ) measures the pore pressure ( $u_0 + \bar{u}$ ) at the mid-height of the cylinder. If the valve is open, the system is in equilibrium and the pore pressure is  $u_0$ ; this is known as the equilibrium or steady-state pore pressure and will not change with time. If the system is disturbed so that the level of water in the standpipe is  $\Delta h$  above (or below) its equilibrium position, there will be an excess pore pressure  $\bar{u} = \gamma_w \Delta h$ . If there is an excess pore pressure and the valve is open, water will flow from the cylinder due to the potential difference across the piston and the excess pore pressure will diminish. The excess pore pressure  $\bar{u}$  will, therefore, change with time. After an infinite time there will be no excess pore pressure left, the system will once again be in equilibrium, the final pore pressure will equal the steady-state pore pressure, and the final excess pore pressure will be zero.

Figure 7-2 shows the results of applying an increment of load to the piston; the graphs illustrate the variation of total and effective stress and volume with time for various stages in the behaviour of the model.

**Stage I**

The model is in equilibrium with the valve open: i.e.,

$$\begin{aligned} \text{Total stress} &= \sigma_0, \\ \text{Pore pressure} &= u_0, \\ \text{Effective stress} &= \sigma'_0 = \sigma_0 - u_0, \\ \text{Volume} &= V_0, \\ \text{Settlement} &= \rho_0 = 0. \end{aligned}$$

**Stage II**

The drainage valve is closed and the total stress raised by  $\Delta\sigma$ ; this corresponds to sudden loading of a soil mass before any water can drain from the pores. Since the valve is closed,  $\Delta V_w = 0$  and  $\Delta V = \Delta\rho = 0$ . The piston has not moved, the spring has not compressed, and, therefore,  $\Delta\sigma' = 0$ . The effective stress equation then gives

$$\bar{u} = \Delta\sigma. \tag{7-2}$$

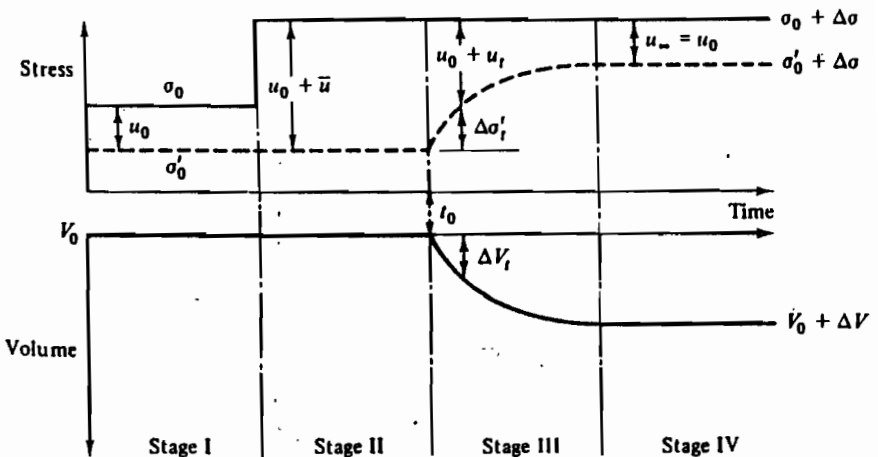


Figure 7-2 Behaviour of the soil compression and consolidation model

After this (undrained) loading, the conditions are:

$$\begin{aligned}
 \text{Total stress} &= \sigma_0 + \Delta\sigma, \\
 \text{Pore pressure} &= u_0 + \bar{u} = u_0 + \Delta\sigma, \\
 \text{Effective stress} &= \sigma' = \sigma'_0, \\
 \text{Volume} &= V_0, \\
 \text{Settlement} &= \rho_0 = 0.
 \end{aligned}$$

The model satisfies the principle of effective stress for soil because there has been no volume change and no change of effective stress. There is, however, an excess pore pressure in the cylinder so causing a hydraulic gradient across the piston.

### Stage III

At some instant  $t_0$ , the drainage valve is opened, water begins to flow from the cylinder, and the piston sinks. The rate of flow depends in part on the opening of the valve and this may be adjusted to represent different soil permeabilities. After a time  $t$ , the settlement is  $\Delta\rho_t$  and the volume within the cylinder is  $V_0 + \Delta V_t$  (where  $\Delta V_t$  is negative). As the piston sinks, the spring compresses; after a time  $t$ , the effective stress has increased to  $\sigma'_0 + \Delta\sigma'_t$  and the pore pressure has reduced to  $u_0 + \bar{u}_t$ . As the pore pressure drops, so the hydraulic gradient and the rate of flow of water through the valve diminish; consequently, the rate of settlement slows as time passes. At some time  $t$  the conditions are:

$$\begin{aligned}
 \text{Total stress} &= \sigma_0 + \Delta\sigma, \\
 \text{Pore pressure} &= u_0 + \bar{u}_t, \\
 \text{Effective stress} &= \sigma'_0 + \Delta\sigma'_t, \\
 \text{Volume} &= V_0 + \Delta V_t, \\
 \text{Settlement} &= \Delta\rho_t.
 \end{aligned}$$

### Stage IV

After a very long time; the hydraulic gradient and the flow of water through the valve will be negligible and the model is once again in equilibrium with zero excess pore pressure: i.e.,

$$\begin{aligned}
 \text{Total stress} &= \sigma_0 + \Delta\sigma, \\
 \text{Pore pressure} &= u_0, \\
 \text{Effective stress} &= \sigma'_0 + \Delta\sigma, \\
 \text{Volume} &= V_0 + \Delta V, \\
 \text{Settlement} &= \Delta\rho_\infty.
 \end{aligned}$$

The behaviour of the model after unloading the total stress will be similar, except that the pore pressure will fall and the volume within the container will increase as water is drawn into the model and the piston rises.

If we apply many increments of total stress, both loading and unloading, allowing the excess pore pressures to dissipate completely before the next increment is applied, we may plot the volume against the effective stress for all points where equilibrium is reached and the excess pore pressure is zero. Such a plot would appear like Fig. 7-3 and, for the model, this represents the spring compression. We have shown the model compression in Fig. 7-3 as non-linear and not fully reversible because the compression of real soil is neither linear nor fully reversible.

In certain important respects our simple model does not properly represent the consolidation of real soil, but it does distinguish between time-dependent consolidation and equilibrium states of compression. For the remainder of this Chapter we will consider only the equilibrium states of compression and we will examine the relationships between volume and effective stress in soils.

### 7-3 ISOTROPIC COMPRESSION TEST

We will begin by looking at the behaviour of a clay soil during an isotropic compression test. The test may be carried out either in the triaxial apparatus with the axial loading ram locked clear of the sample top cap or in a special apparatus. The state of stress in isotropic compression lies on the space diagonal of Fig. 4-1 and, consequently, there are no shear stresses; the boundary conditions are illustrated in Fig. 7-4, where  $\sigma_c$  is the cell pressure in the triaxial apparatus. Figure 7-4 also illustrates the drainage and pore pressure measurement arrangements required. In terms of the relevant invariants the state of stress in isotropic compression is

$$\begin{aligned} q &= q' = 0, \\ p &= \sigma_c, \\ p' &= \sigma_c - u. \end{aligned}$$

The soil grains and pore water are assumed to be incompressible, and a reduction in sample volume from  $V$  to  $V + \Delta V$ , where  $\Delta V$  is negative, causes an increase  $\Delta V_w$  in the volume of water in the burette; the (compressive) volumetric strains given by Eq. (4-49) are

$$\Delta \varepsilon_v = -\frac{\Delta V}{V} = \frac{\Delta V_w}{V}. \quad (7-3)$$

As an example, consider a test where a sample is placed in the apparatus and the cell pressure set to  $\sigma_c$  with the drainage valve open. It is left until the

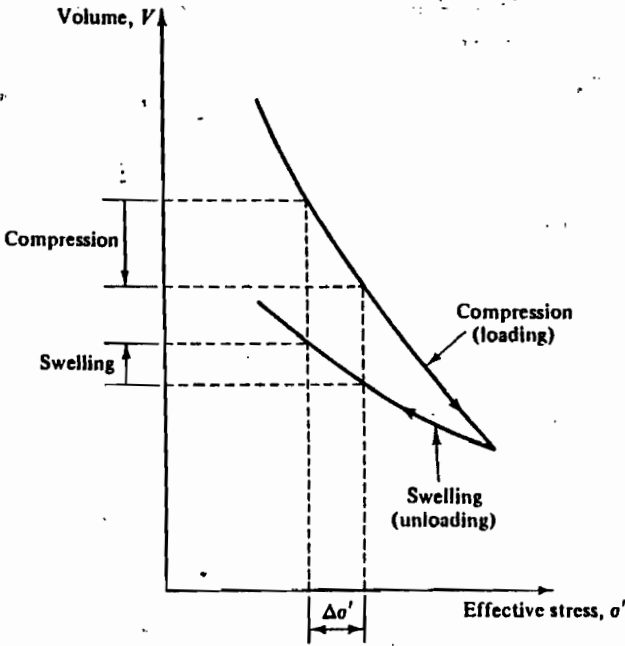


Figure 7-3 Compression and swelling of the model during loading and unloading

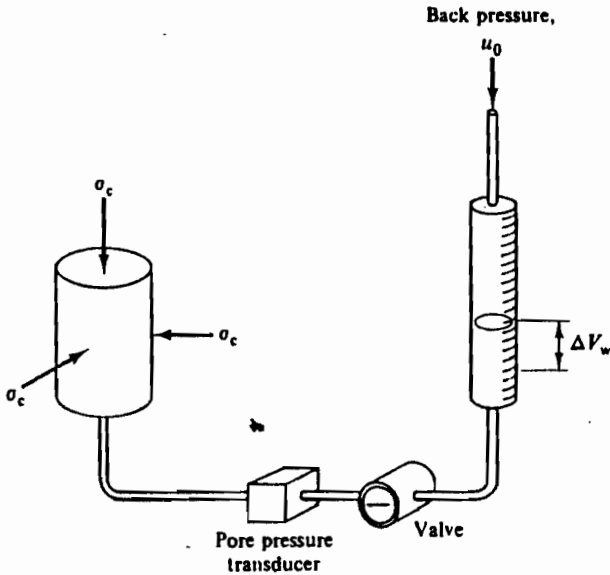


Figure 7-4 Loading and drainage arrangements for isotropic compression

level of water in the burette is steady and the sample is in equilibrium with  $u = 0$  and  $p = p' = \sigma_c$ ; this corresponds to Stage I of the simple model. The valve is closed, the cell pressure raised by  $\Delta\sigma_c$ , and the resulting rise  $\Delta u$  in pore pressure measured; this corresponds to Stage II. The valve is then opened, the pore pressure at the drainage connection is immediately reduced to zero, but pore pressures within the soil do not immediately change. Hydraulic gradients due to excess pore pressures cause water to flow from the sample and the volume  $\Delta V_w$  of water expelled into the burette is measured at convenient intervals. This flow of water from the sample is caused by the consolidation process and corresponds to Stage III of the simple model. The sample is left until the level of water in the burette is steady and the soil is once again in equilibrium with  $u = 0$  and  $p' = (\sigma_c + \Delta\sigma_c)$ .

#### 7-4 BACK PRESSURE

The test could be carried out with a minor variation; instead of allowing the burette to be open to the atmosphere we could apply a constant back pressure  $u_0$ . This would not affect our observations of changes of effective stress and volume in the slightest; it would only mean that the equilibrium effective stresses before loading and at the end of consolidation would be given by

$$p' = p - u_0. \quad (7-4)$$

The technique of applying a constant back pressure to the pore water is commonly used in soil testing. The purpose of a back pressure is to saturate the sample by dissolving any air or gas present in the pore water. Provided that the results are expressed in terms of effective stress, the magnitude of the back pressure will have no influence on the test.

#### 7-5 SECONDARY COMPRESSION - CREEP

The change of sample volume  $\Delta V$  may be found from the change of volume of water in the burette and, if we plot  $\Delta V$  against time, we will obtain a curve like that shown in Fig. 7-5.

At small times the hydraulic gradients within the sample, and hence the rates of flow, are relatively large and the slope of the curve is relatively steep; as time passes hydraulic gradients diminish and the curve flattens. After a very long time, the hydraulic gradients should approach zero, there should be no more flow of water from the sample, and volume changes should cease.

At first sight the curve appears to have a horizontal asymptote and the sample appears to reach a constant volume at some point such as E in Fig. 7-5. This will coincide with zero excess pore pressure and constant effective stress and the principle of effective stress would lead us to expect no further volume changes. However, if we make further observations, we

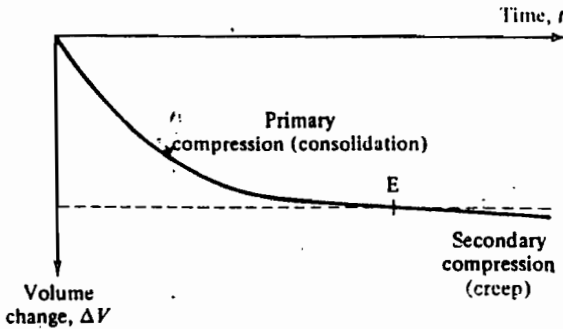


Figure 7-5 Typical time dependent compression of soil

will find that additional small volume changes occur slowly as time passes; these are due to soil creep and the process is often known as *secondary compression*.

It is unfortunate that all real soils seem to exhibit some degree of creep but, luckily, in many cases, creep deformations are small compared to those due to changes of effective stress. For our broad view of soil behaviour we will neglect creep, but we will have to recognize that small time-dependent deformations that are not due exclusively to changes of effective stress do occur in soils.

## 7-6 ISOTROPIC COMPRESSION OF CLAY

It is convenient to record the results of an isotropic compression test by plotting specific volume  $v$  (defined by Eq. (1-4)) against  $p'$  at points such as E in Fig. 7-5 for each loading or unloading increment. The points plotted will represent equilibrium states of volume and effective stress and so creep will be neglected.

The results of an isotropic compression test on a sample of kaolin clay are shown in Fig. 7-6; the test involved loading by increasing  $p'$  in increments along A → B, unloading to D and reloading along D → B → C. If we inspect results from tests on other clay soils, we find that the isotropic compression curves all show the same features.

## 7-7 AN IDEALIZATION OF ISOTROPIC COMPRESSION OF CLAY

Figure 7-7 shows the test results of Fig. 7-6 replotted as  $v$  against  $\ln p'$ , where  $\ln p'$  is the natural logarithm of  $p'$  (i.e.,  $\log_e p'$ ). If the small loop in the unloading and reloading cycle B → D → B is neglected, then, without serious error, Fig. 7-7 may be idealized to two straight lines, as shown in Fig. 7-8.



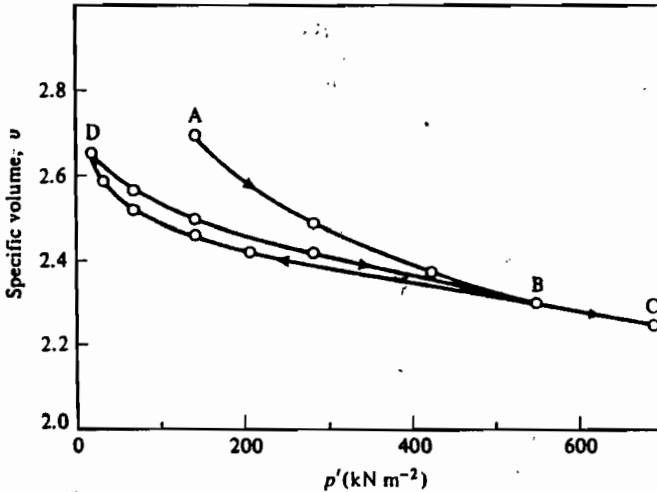


Figure 7-6 Isotropic compression of kaolin clay (after Amerasinghe, 1973)

The results of isotropic compression tests on most clay soils can usually be idealized to straight lines of the form shown in Fig. 7-8. Of course, the slopes of the lines and their positions will be different for different soils.

Figure 7-8 is known as the isotropic compression diagram or the  $v : \ln p'$  plot, and represents the behaviour of a clay soil during isotropic compression.

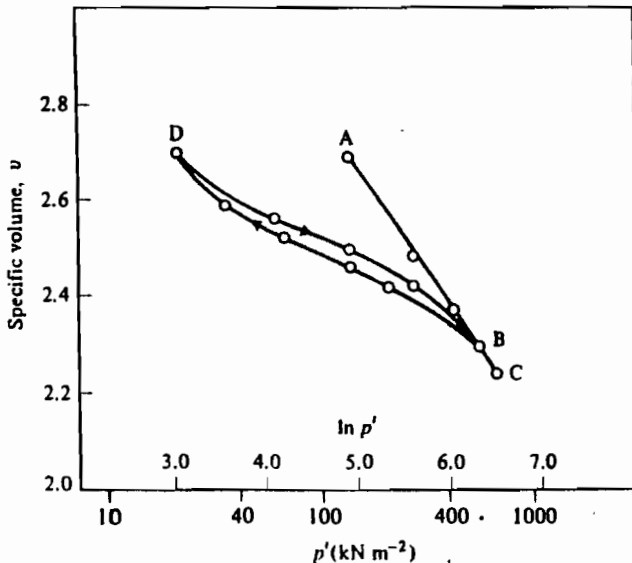


Figure 7-7 Isotropic compression of kaolin clay (data from Fig. 7-6)

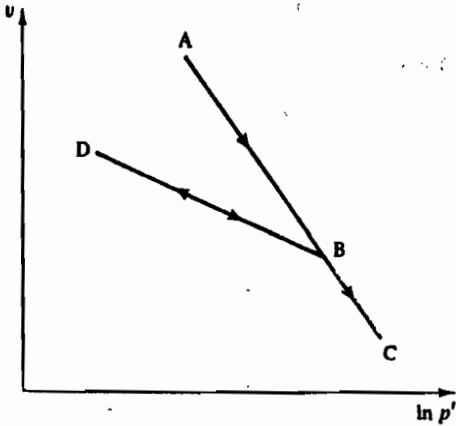


Figure 7-8 An idealization for the isotropic compression of clay

If isotropic compression tests are conducted in which a clay is repeatedly loaded and unloaded, it is found that the results can be represented by a single line AC together with a family of unloading-reloading lines, of which  $D_1B_1$  and  $D_2B_2$  in Fig. 7-9 would be typical members. If soil has once been loaded to  $B_1$  and then unloaded, its state will be on  $B_1D_1$  but, if it is reloaded beyond  $B_1$ , it will lie on AC provided it is not unloaded again.

### 7-8 OVERCONSOLIDATION

Figure 7-10 is an isotropic compression diagram for clay soil; it is essentially the same as Fig. 7-8.

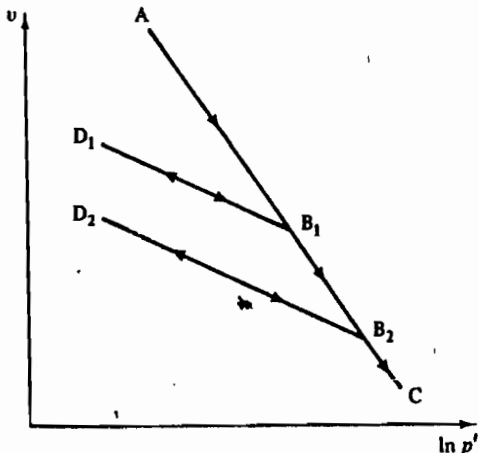


Figure 7-9 The effect of repeated loading and unloading on the isotropic compression of clay

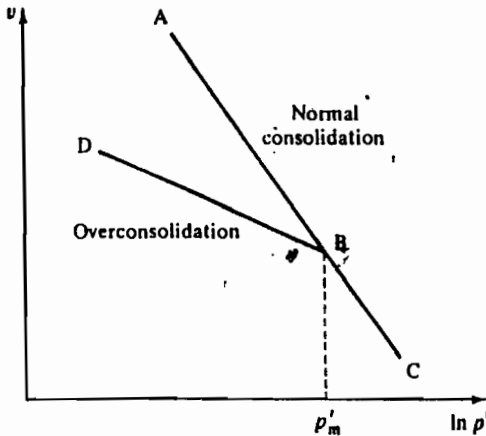


Figure 7-10 Overconsolidation

A soil which is in equilibrium with zero excess pore pressure and whose state lies somewhere on AC is known as *normally consolidated*,† and AC is known as the normal or virgin consolidation line. If the soil is in equilibrium with zero excess pore pressure and its state lies on a line such as BD, it is known as *overconsolidated* and lines such as BD are known as swelling lines. The position of a swelling line may be defined by the maximum previous stress  $p'_m$  corresponding to the point B.

For convenience we define the overconsolidation ratio

$$R_p = \frac{p'_m}{p'}, \quad (7-5)$$

where the subscript p is a reminder that  $R_p$  is a ratio of mean normal stresses. The value of  $R_p$  cannot be less than 1.0 and, if  $R_p = 1.0$ , the soil is normally consolidated and its state lies on AC. Hence, a soil is normally consolidated if its present state of stress has never been exceeded.

## 7-9 POSSIBLE STATES OF ISOTROPIC COMPRESSION

The normal consolidation line AC (Fig. 7-10) has a special significance. A sample of soil loaded isotropically from A will follow AC; its state may be moved to the left of AC by unloading along a swelling line such as BD, but it is not possible to move the state of the soil to the right of AC.

† Although this Chapter is concerned with compression rather than consolidation, the terms normally consolidated and overconsolidated are firmly established and are used to describe, respectively, the states of soils compressed along AC or swelled along BD.

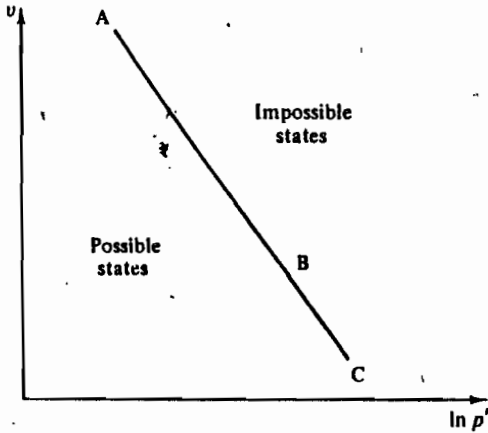


Figure 7-11 A state boundary for isotropic compression

The line AC represents a boundary between possible states to the left and impossible states to the right, as indicated in Fig. 7-11.

### 7-10 MATHEMATICAL REPRESENTATION OF ISOTROPIC COMPRESSION

Figure 7-12 is an isotropic compression diagram for a clay soil; it is essentially the same as Fig. 7-8.

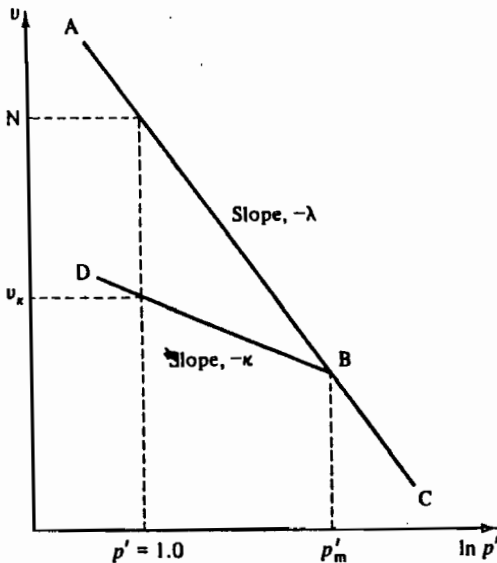


Figure 7-12 Isotropic compression of clay

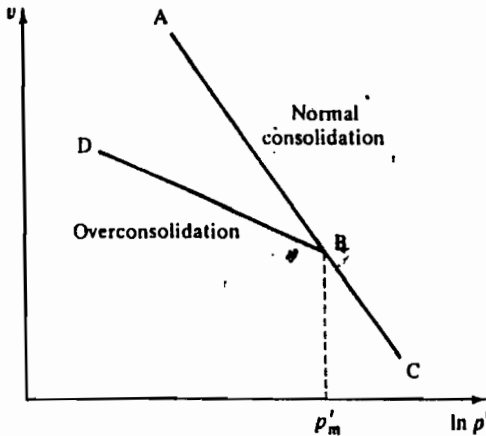


Figure 7-10 Overconsolidation

A soil which is in equilibrium with zero excess pore pressure and whose state lies somewhere on AC is known as *normally consolidated*,† and AC is known as the normal or virgin consolidation line. If the soil is in equilibrium with zero excess pore pressure and its state lies on a line such as BD, it is known as *overconsolidated* and lines such as BD are known as swelling lines. The position of a swelling line may be defined by the maximum previous stress  $p'_m$  corresponding to the point B.

For convenience we define the overconsolidation ratio

$$R_p = \frac{p'_m}{p'}, \quad (7-5)$$

where the subscript p is a reminder that  $R_p$  is a ratio of mean normal stresses. The value of  $R_p$  cannot be less than 1.0 and, if  $R_p = 1.0$ , the soil is normally consolidated and its state lies on AC. Hence, a soil is normally consolidated if its present state of stress has never been exceeded.

## 7-9 POSSIBLE STATES OF ISOTROPIC COMPRESSION

The normal consolidation line AC (Fig. 7-10) has a special significance. A sample of soil loaded isotropically from A will follow AC; its state may be moved to the left of AC by unloading along a swelling line such as BD, but it is not possible to move the state of the soil to the right of AC.

† Although this Chapter is concerned with compression rather than consolidation, the terms normally consolidated and overconsolidated are firmly established and are used to describe, respectively, the states of soils compressed along AC or swelled along BD.

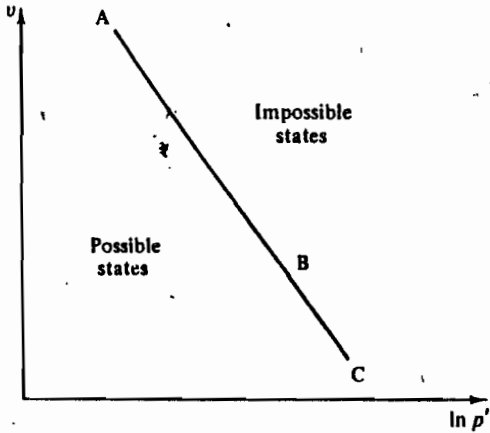


Figure 7-11 A state boundary for isotropic compression

The line AC represents a boundary between possible states to the left and impossible states to the right, as indicated in Fig. 7-11.

### 7-10 MATHEMATICAL REPRESENTATION OF ISOTROPIC COMPRESSION

Figure 7-12 is an isotropic compression diagram for a clay soil; it is essentially the same as Fig. 7-8.

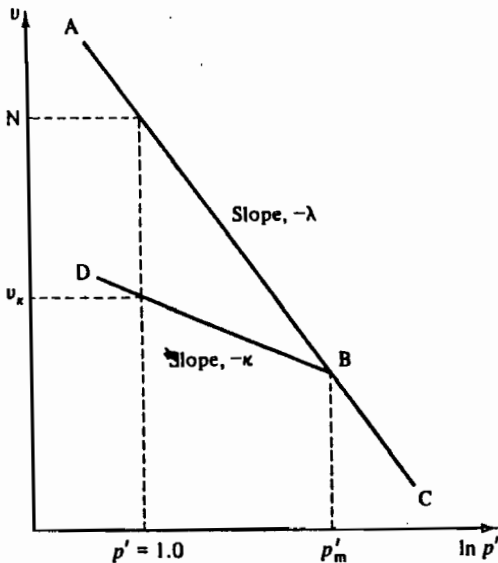


Figure 7-12 Isotropic compression of clay

We define parameters  $\lambda$  (small lambda) and  $\kappa$  (small kappa) for the (negative) slopes of the normal consolidation line and a typical swelling line, respectively. Hence,

$$\text{along AC, } -\lambda = \frac{dv}{d(\ln p')} = \frac{p' dv}{dp'}, \quad (7-6)$$

$$\text{and along BD, } -\kappa = \frac{dv}{d(\ln p')} = \frac{p' dv}{dp'}. \quad (7-7)$$

Often, the normal consolidation line is known as the  $\lambda$ -line and a swelling line as a  $\kappa$ -line.

Two further parameters are required to define the positions of the  $\lambda$ - and  $\kappa$ -lines. For the  $\lambda$ -line we define  $N$  (capital nu) as the specific volume of a normally consolidated soil at  $p' = 1.0 \text{ kN m}^{-2}$ .† Thus, the equation of the  $\lambda$ -line is

$$v = N - \lambda \ln p'. \quad (7-8)$$

The position of a  $\kappa$ -line is not unique, but depends on  $p'_m$ , the maximum previous stress. For the  $\kappa$ -line, we define  $v_\kappa$  as the specific volume of an overconsolidated soil at  $p' = 1.0 \text{ kN m}^{-2}$ ,† and the equation of a  $\kappa$ -line is

$$v = v_\kappa - \kappa \ln p'. \quad (7-9)$$

$\lambda$ ,  $N$ , and  $\kappa$  are regarded as soil constants; their values will depend on the particular soil and must be found by experiment.

#### Example 7-1 Calculation of $\lambda$ , $\kappa$ , and $N$ from isotropic compression test results

The first two columns of Table E7-1 contain data from an isotropic compression test on a sample of soil conducted in a triaxial cell. At the end of the test, when the cell pressure  $\sigma_o = 60 \text{ kN m}^{-2}$ , the volume of the sample was  $V = 67.7 \text{ cm}^3$ , and its water content was  $w = 0.409$ . The

Table E7-1 Isotropic compression test results

Cell pressure, $\sigma_c$ (kN m <sup>-2</sup> )	Volume of water expelled, $\Delta V_w$ (cm <sup>3</sup> )	Volume of sample, $V$ (cm <sup>3</sup> )	Specific volume, $v$	$\ln p'$
20	0	88.5	2.72	3.00
60	7.2	81.3	2.50	4.09
200	15.0	73.5	2.26	5.30
1000	25.4	63.1	1.94	6.91
200	22.8	65.7	2.02	5.30
60	20.8	67.7	2.08	4.09

† Although  $N$  and  $v_\kappa$  are themselves dimensionless, their values will depend on the units chosen for  $p'$ .

relative density of the soil grains is  $G_s = 2.65$ . Calculate values for  $\lambda$ ,  $\kappa$ , and  $N$  for the soil.

The current volume  $V$  of the sample may be found from the final volume and the change of volume  $\Delta V = -\Delta V_w$ , where  $\Delta V_w$  is the volume of water expelled. By definition, the specific volume  $v = V/V_s$ , where  $V_s$  is the volume occupied by the soil grains and, since soil grains are incompressible,  $V_s = \text{constant}$ .

Hence, at any stage of the test,  $v/V = \text{constant}$ .

At the end of the test, from Eq. (1-5),  $v = 1 + wG_s$ . Hence,

$$v = 1 + (0.409 \times 2.65) = 2.08,$$

$$V = 67.7 \text{ cm}^3,$$

and, therefore,

$$v/V = \text{constant} = 0.031 \text{ cm}^{-3}.$$

Hence, the specific volume at each stage of the test may be calculated directly from the current volume. The values of  $v$  are contained in Table E7-1.

For isotropic compression, where  $u = 0$ , at the end of each loading stage  $\sigma_o = p = p'$ . The test results are shown as specific volume  $v$  plotted against  $\ln p'$  in Fig. E7-1. The equations of the compression and swelling lines are, respectively, Eqs (7-8) and (7-9):

$$v = N - \lambda \ln p',$$

$$v = v_\kappa - \kappa \ln p'.$$

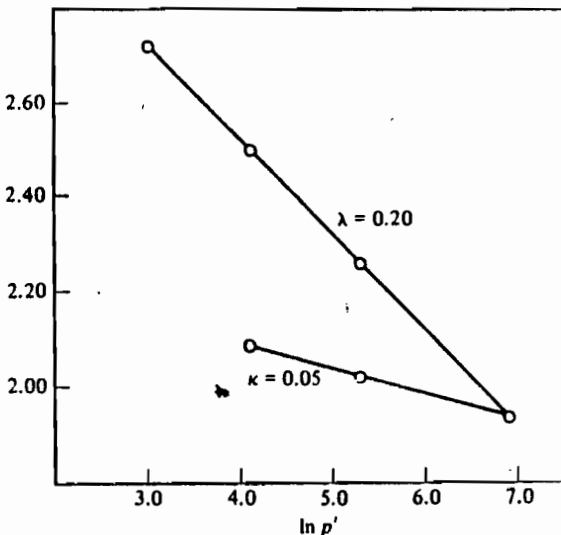


Figure E7-1 Isotropic compression test results



Scaling the slopes from Fig. E7-1,

$$\lambda = 0.20 \quad \text{and} \quad \kappa = 0.05$$

and inserting, for example,  $v = 2.72$  and  $\ln p' = 3.0$  into Eq. (7-8),

$$N = 3.32.$$

### 7-11 ISOTROPIC COMPRESSION OF SAND

The compression of a sand soil is slightly different to that of a clay soil. The state of an isotropically normally consolidated clay must lie on a  $\lambda$ -line such as ABC in Fig. 7-12 and its specific volume is uniquely determined by the current state of stress. In contrast, the specific volume of a sand during first loading is not uniquely determined by the current state of stress.

If sand is tipped rapidly into a container, the grains will pack together relatively loosely and the specific volume will be relatively large. If the container is then vibrated, the grains will pack together more closely and the specific volume will reduce. In both cases the state of stress will be approximately the same; typically, the value of  $p'$  will be  $1 \text{ kN m}^{-2}$  at a depth of about 100 mm below the surface of the sand.

Figure 7.13 shows the results of isotropic compression tests on initially dense and initially loose samples of a sand. The state of the initially loose

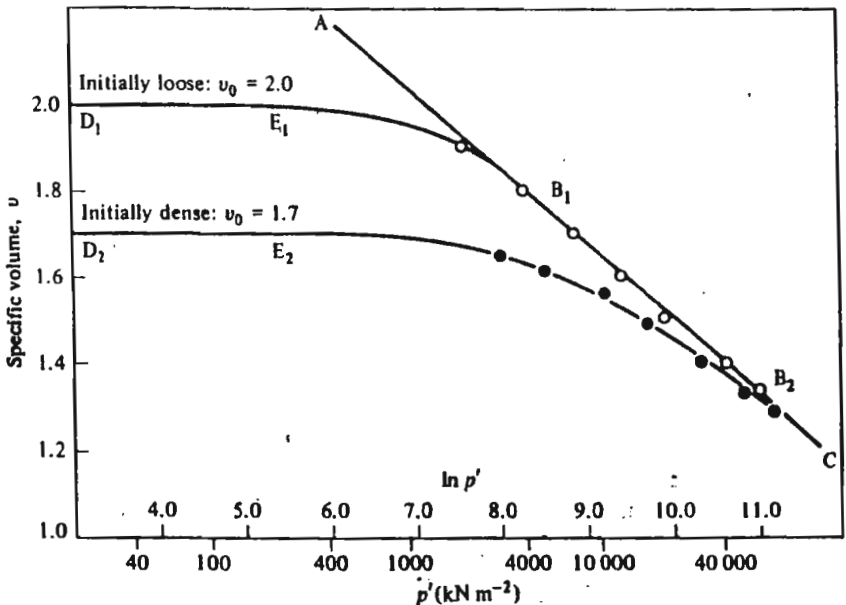


Figure 7-13 Isotropic compression of Chattahoochee River sand (after Vesic and Clough, 1968)

sample followed the line  $D_1E_1B_1$  and the state of the initially dense sample followed the line  $D_2E_2B_2$ .

Both samples were prepared at the very low stresses corresponding to the self weight of the sand and, consequently, the true initial states must lie to the left of  $D_1$  and  $D_2$ ; the points  $D_1$  and  $D_2$  are the states of the samples in the testing apparatus when small stresses are applied to the boundaries.

The paths  $D_1E_1B_1$  and  $D_2E_2B_2$  are similar in shape and their positions depend only on the initial specific volumes of the samples; there would be a whole family of paths, intermediate between the two shown, each path corresponding to a sample with a different initial specific volume. The paths are noticeably curved and approach a common envelope AC at relatively large stresses.

Similar tests on other sand soils will produce a pattern of behaviour similar to that shown in Fig. 7-13; the positions of the lines will depend principally on the grading of the soil and the shape of the grains.

At first sight, sand and clay soils appear to behave differently during isotropic compression loading. However, for values of  $p'$  not exceeding about  $700 \text{ kN m}^{-2}$ , paths like DEB are approximately linear and almost parallel with the  $\ln p'$  axis, and Fig. 7-13 may then be idealized to Fig. 7-14. Although the idealization in Fig. 7-14 is really valid only in the range DE and along part of AC, it is often a useful simplification and, for mathematical analysis, it is convenient to project DE to meet AC at points such as B.

Figure 7-14 is the same as the isotropic compression diagram for clay in Fig. 7-12, but now  $\kappa$  is almost equal to zero. Direct measurement of  $\lambda$  (and  $N$ ) for sand is difficult because it requires tests at high stresses, but experimental

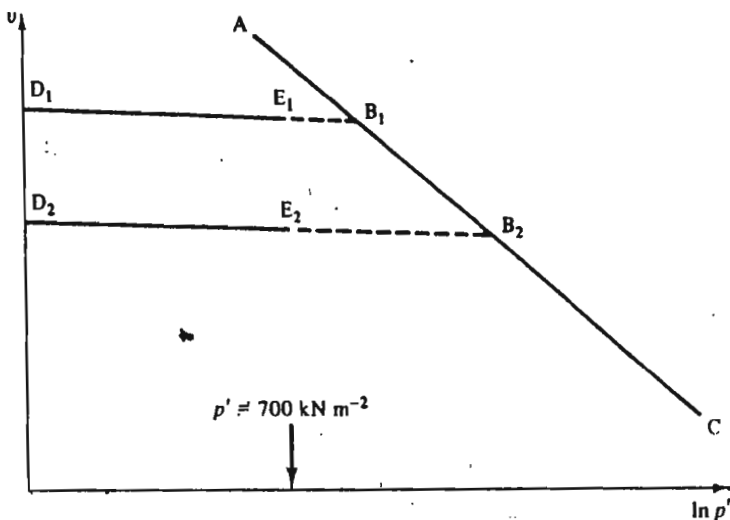


Figure 7-14 An idealization for isotropic compression of sand

determination of the value of  $\kappa$  over the range of stresses of interest in civil engineering is fairly straightforward.

If we accept Fig. 7-14 as a reasonable representation of the isotropic compression of sand, there are obvious similarities between the behaviour of sands and of clays. We should note, however, that at modest stresses sands behave as though they were overconsolidated, irrespective of their stress history, and, since  $\kappa \approx 0$ , they are nearly rigid during isotropic compression. At large stresses, sands approach the  $\lambda$ -line (AC) and behave as though they were normally consolidated.

## 7-12 ONE-DIMENSIONAL COMPRESSION - THE OEDOMETER TEST

Although, in principle, isotropic compression is a very simple kind of loading, in practice isotropic compression tests are rather difficult to carry out satisfactorily. A more convenient test, and one which is common both in soil mechanics research and in engineering practice is the one-dimensional compression test carried out in the oedometer described in Chapter 5.

The boundary conditions for one-dimensional compression are indicated in Fig. 7-15; two principal strains are zero and horizontal pore water flow is prevented so that both deformations and drainage are one-dimensional.

One-dimensional compression has an important practical aspect. As sediments are deposited to form soils, they are compressed by the weight of successive layers of sediment. Because of symmetry there will be no horizontal strain in any element in the ground and, in the absence of other disturbances, the state of stress will correspond to the state of stress in one-dimensional compression.

For one-dimensional compression, it is convenient to relabel the stresses as  $\sigma'_v$  and  $\sigma'_h$ , where the subscripts denote vertical and horizontal directions, respectively. During one-dimensional compression,  $\sigma'_h$  will vary with  $\sigma'_v$  and will adjust itself to maintain  $\epsilon_h = 0$ . The relationship between  $\sigma'_v$  and  $\sigma'_h$  is usually written

$$\sigma'_h = K_0 \sigma'_v, \quad (7-10)$$

where  $K_0$  is known as the coefficient of earth pressure at rest; the value of  $K_0$  is not constant even for a particular soil, but varies with overconsolidation ratio. The value of  $K_0$  should, therefore, be found by experiment. Nevertheless, there are various empirical expressions for estimating the value of  $K_0$  for normally consolidated soils. The most common of these is attributed to Jaky and is

$$K_0 = 1 - \sin \phi', \quad (7-11)$$

where  $\phi'$  is known as the angle of internal friction with respect to effective stresses, a soil parameter discussed in detail in Chapter 14.

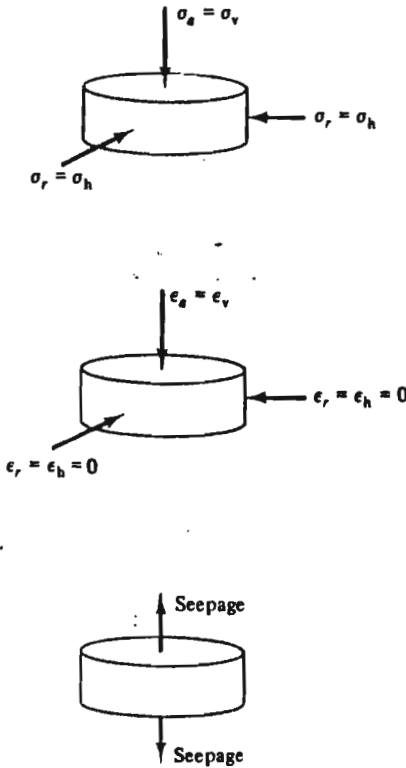


Figure 7-15 Boundary conditions for one-dimensional compression

Assuming that  $\sigma'_v$  and  $\sigma'_h$  are principal stresses, the stress invariants  $q'$  and  $p'$  corresponding to one-dimensional compression are

$$p' = \frac{1}{3}\sigma'_v(1 + 2K_0), \quad (7-12)$$

$$q' = \sigma'_v(1 - K_0). \quad (7-13)$$

The conduct of an oedometer test is much the same as the conduct of an isotropic compression test in the triaxial apparatus. The vertical total stress is raised or lowered in increments and the sample allowed to reach a new equilibrium with zero excess pore pressure after each increment. Pore pressures or horizontal stresses are not usually measured, although some special oedometers exist in which horizontal stresses are measured by force transducers or by strain gauges bonded to the containing ring.

Deformations of the sample are found by observing the settlement  $\Delta p$  of the top loading platen with respect to the bottom. Conventionally, settlements are reckoned positive downwards. Since horizontal strains are

zero, volumetric strains and vertical strains must be equal and, for one-dimensional compression,

$$\Delta \epsilon_v = -\Delta V/V = -\Delta H/H \quad (7-14)$$

and

$$\Delta p = -\Delta H. \quad (7-15)$$

For each increment of load the settlement-time relationship will have a form similar to that shown in Fig. 7-5; when the sample has reached a point such as E it may be regarded as being in equilibrium and a new increment of load added or subtracted. As for isotropic compression, we will neglect creep deformations.

For one-dimensional compression, we define an overconsolidation ratio  $R_0$  as

$$R_0 = \sigma'_{vm}/\sigma'_v, \quad (7-16)$$

where  $\sigma'_{vm}$  is the maximum previous value of  $\sigma'_v$ . Since  $K_0$  will vary during overconsolidation,  $R_0$  will not, in general, equal  $R_p$ , the overconsolidation ratio in terms of  $p'$ .

### 7-13 VARIATION OF $K_0$ IN OEDOMETER TESTS

Figure 7-16 shows the results of an oedometer test on a sample of kaolin clay in which both  $\sigma'_v$  and  $\sigma'_h$  were measured. The sample was loaded one-dimensionally along A → B and unloaded to D. The values of  $K_0 = \sigma'_h/\sigma'_v$  from Fig. 7-16(a) have been plotted against  $\sigma'_v$  and overconsolidation ratio  $R_0$  in Fig. 7-16(b) and (c). Along AB in Fig. 7-16(a), the sample is one-dimensionally normally consolidated and  $K_0$  has a constant value; for normally consolidated clays  $K_0$  is typically near 0.7. Along B → D the sample is one-dimensionally overconsolidated and  $K_0$  varies; for large values of overconsolidation ratio,  $K_0$  may exceed 1.0 as  $\sigma'_h$  becomes larger than  $\sigma'_v$ .

### 7-14 ONE-DIMENSIONAL COMPRESSION OF CLAY

Figure 7-17 shows the results of a one-dimensional compression test on a sample of kaolin clay plotted as specific volume against vertical effective stress for equilibrium states. Figure 7-18 shows the same results replotted as  $v$  against  $\ln \sigma'_v$ . The sample was loaded along A → B, unloaded to D, and reloaded along D → C.

We may idealize the one-dimensional compression behaviour of kaolin clay to the straight lines shown in Fig. 7.19. Data from one-dimensional compression tests on other clay soils may usually be idealized to similar straight lines; the slopes and positions of the lines depend on the particular soil.

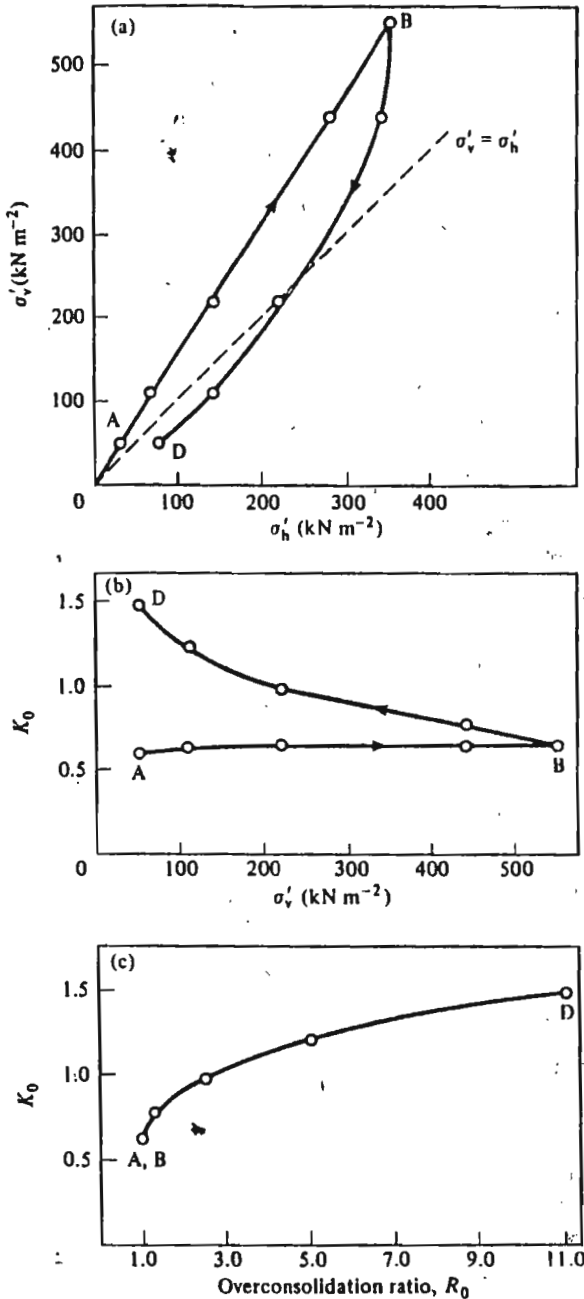


Figure 7-16 Axial and radial stresses during one-dimensional compression of kaolin clay (after Nadarajah, 1973)

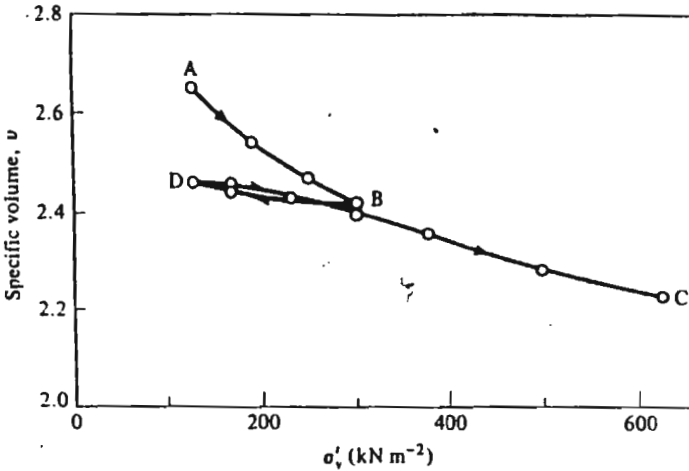


Figure 7-17 One-dimensional compression of kaolin clay (after Nadarajah, 1973)

**7-15 ONE-DIMENSIONAL AND ISOTROPIC COMPRESSION OF CLAY**

If the values of  $\sigma'_v$ ,  $\sigma'_h$ , and  $v$  are known throughout a one-dimensional compression test, the results may be shown on a  $v : \ln p'$  plot together with the appropriate  $\lambda$ -line for isotropic compression, as shown in Fig. 7-20.

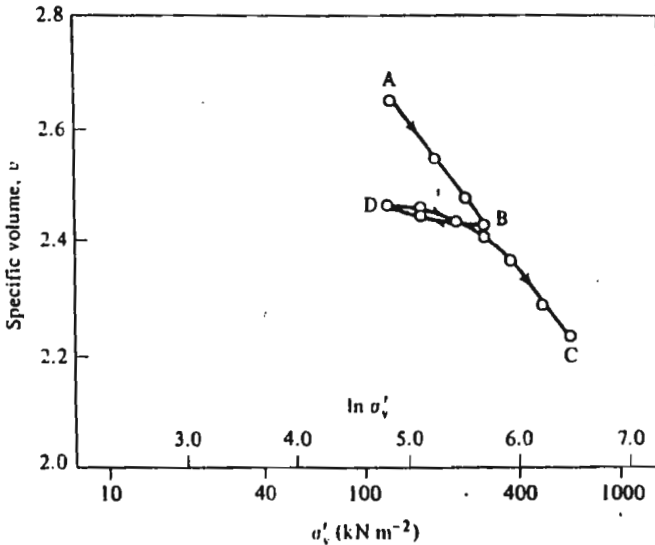


Figure 7-18 One-dimensional compression of kaolin clay

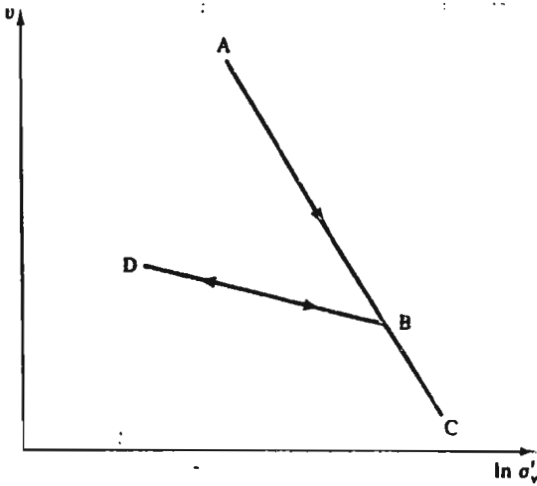


Figure 7-19 An idealization for one-dimensional compression of clay

It turns out that the normal consolidation line for one-dimensional compression has a slope close to  $-\lambda$  and the swelling line has a slope close to  $-\kappa$ . It is a good approximation to assume that both normal consolidation lines are parallel with slopes  $-\lambda$ , and all swelling lines are parallel with slopes  $-\kappa$ . In order to locate the  $\lambda$ -line for one-dimensional compression,

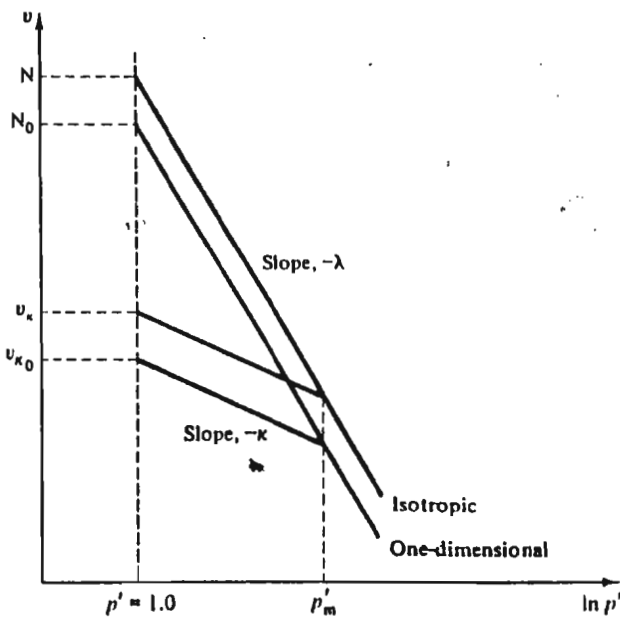


Figure 7-20 Isotropic and one-dimensional compression of soil



We define  $N_0$  as the specific volume of one-dimensionally normally consolidated soil at  $p' = 1.0 \text{ kN m}^{-2}$ ; the equation of the one-dimensional normal consolidation line is then

$$v = N_0 - \lambda \ln p' \quad (7-17)$$

As was the case for isotropic compression, the position of the overconsolidation line for one-dimensional compression is not unique but depends on the maximum previous stress. In order to locate a  $\kappa$ -line for one-dimensional compression, we define  $v_{\kappa_0}$  as the specific volume of a one-dimensionally overconsolidated soil at  $p' = 1.0 \text{ kN m}^{-2}$ , and the equation of a  $\kappa$ -line for one-dimensional compression is

$$v = v_{\kappa_0} - \kappa \ln p' \quad (7-18)$$

Neither  $v_{\kappa}$  nor  $v_{\kappa_0}$  are soil constants, both depend on the value of  $p'_m$ , the maximum previous stress, as indicated in Fig. 7.20.

Although  $q'/p' = 0$  for isotropic compression, the value of  $q'/p'$  for one-dimensional compression is non-zero and may be found from Eqs (7-12) and (7-13) as

$$\frac{q'}{p'} = \frac{3(1 - K_0)}{(1 + 2K_0)} \quad (7-19)$$

During normal consolidation,  $K_0$  has a constant value and, consequently,  $q'/p' = \text{constant}$  along either  $\lambda$ -line in Fig. 7.20. We might guess that there will be a family of  $\lambda$ -lines each corresponding to a particular value of  $q'/p'$ ; this point will be discussed further in Chapter 14.

#### Example 7-2 Calculation of $K_0$ , $\lambda$ , and $N_0$ from oedometer test results

Table E7-2 contains data from an oedometer test on a sample of soil in which the horizontal total stress  $\sigma_h$ , the vertical total stress  $\sigma_v$ , and the settlement  $\rho$  of the top platen were measured. At the start of the test, when  $\sigma_v = 30 \text{ kN m}^{-2}$  and the pore pressure was  $u = 0$ , the specific volume of the sample was  $v = 2.67$  and its thickness was  $z = 20 \text{ mm}$ . Calculate the values of  $K_0$ ,  $\lambda$ , and  $N_0$  for the soil.

Table E7-2 Oedometer test results

Vertical stress, $\sigma_v$ ( $\text{kN m}^{-2}$ )	Horizontal stress, $\sigma_h$ ( $\text{kN m}^{-2}$ )	$K_0$	Settlement $\rho$ (mm)	Change of sample			
				thick-ness, $\Delta z$ (mm)	Specific volume, $v$	$p'$ ( $\text{kN m}^{-2}$ )	$\ln p'$
30	15	0.5	0	0	2.67	20	3.00
90	45	0.5	1.65	-1.65	2.45	60	4.09
300	150	0.5	3.70	-3.70	2.21	200	5.30
1500	750	0.5	5.85	-5.85	1.89	1000	6.91

When the sample is in equilibrium,  $u = 0$ , total and effective stresses are equal, hence

$$K_0 = \sigma'_h / \sigma'_v = \sigma_h / \sigma_v,$$

and, from the data,

$$K_0 = 0.5$$

and, at any stage of the test  $p' = \frac{1}{3}(\sigma'_v + 2\sigma'_h) = \frac{2}{3}\sigma'_v$ . For one-dimensional compression,  $\Delta v/v = \Delta z/z$ , where  $\Delta z$  is the increase in the thickness  $z$  of the sample. At the start of the test  $v = 2.67$  and  $z = 20$  mm. Hence, throughout the test,

$$\Delta v / \Delta z = 0.134 \text{ mm}^{-1}.$$

Therefore, the specific volume at each stage of the test may be calculated from the change of sample thickness. The values of  $v$  are contained in Table E7-2.

The test results are shown as specific volume  $v$  plotted against  $\ln p'$  in Fig. E7-2. The equation of the one-dimensional compression line is Eq. (7-17)

$$v = N_0 - \lambda \ln p'.$$

Scaling the slope from Fig. E7-2,

$$\lambda = 0.20$$

and inserting, for example,  $v = 2.67$  and  $\ln p' = 3.0$ ,

$$N_0 = 3.27.$$

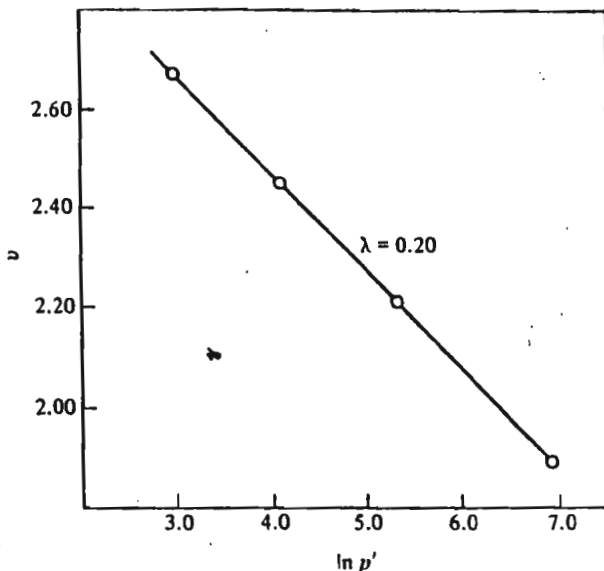


Figure E7-2 Oedometer test results

### 7-16 COEFFICIENT OF VOLUME COMPRESSIBILITY $m_v$

For many calculations involving the settlements of structures and for a derivation of the basic equation for one-dimensional consolidation given in Chapter 8, it is convenient to define a parameter  $m_v$ , the coefficient of volume compressibility for one-dimensional compression, as

$$\delta \varepsilon_v = m_v \delta \sigma'_v \quad (7-20)$$

where  $\delta \varepsilon_v$  is an increment of volumetric strain caused by a change of vertical effective stress  $\delta \sigma'_v$  during one-dimensional compression. Alternatively, we may make use of Eq. (5-54) and define  $m_v$  in terms of specific volume as

$$\delta v/v = -m_v \delta \sigma'_v \quad (7-21)$$

For one-dimensional normal consolidation,  $K_0$  has a constant value and so

$$\delta \sigma'_v / \sigma'_v = \delta p' / p' \quad (7-22)$$

Hence, from Eqs (7-21) and (7-22) together with Eq. (7-6),

$$m_v = \lambda / v \sigma'_v \quad (7-23)$$

Clearly, if  $\lambda$  is a constant,  $m_v$  cannot be a soil constant also; consequently, Eqs (7-20) and (7-21) are valid only for the relatively small increments of stress for which the normal consolidation line ABC in Fig. 7-6 may be assumed to be linear.

### 7-17 COMPRESSION INDEX $C_C$ AND SWELLING INDEX $C_S$

In current geotechnical engineering practice, the results of one-dimensional compression tests are usually plotted as voids ratio  $e$  against  $\log_{10} \sigma'_v$ , where  $\sigma'_v$  is the vertical effective stress. The slope  $C_C$  of the normal consolidation line is known as the compression index and the slope  $C_S$  of a swelling line is known as the swelling index, where

$$-C_C = \frac{de}{d(\log_{10} \sigma'_v)} \quad \text{for normal consolidation,} \quad (7-24)$$

$$-C_S = \frac{de}{d(\log_{10} \sigma'_v)} \quad \text{for overconsolidation.} \quad (7-25)$$

Now  $\log_{10} \sigma'_v = 0.434 \ln \sigma'_v$  and  $de = dv$ . Hence,

$$-C_C = \frac{dv}{0.434 d(\ln \sigma'_v)}, \quad (7-26)$$

and, therefore,

$$-0.434 C_C = \frac{dv}{d(\ln \sigma'_v)} = \frac{\sigma'_v dv}{d\sigma'_v} \quad (7-27)$$

For one-dimensional consolidation,  $K_0$  has a constant value and, hence, from Eqs (7-22) and (7-27) together with eq. (7-6),

$$C_G = 2.303\lambda. \quad (7-28)$$

For one-dimensional swelling,  $K_0$  does not have a constant value and so there is no simple relationship between  $\kappa$  and  $C_G$ ; however, it is usual to assume an approximately constant value for  $K_0$ , in which case, reasoning similar to that above leads to

$$C_G \approx 2.303\kappa. \quad (7-29)$$

## 7-18 SUMMARY

1. For both isotropic compression ( $q'/p' = 0$ ) and one-dimensional compression ( $q'/p' > 0$ ) the observed relationships between specific volume and mean normal stress for soil can be represented by straight lines on a  $v : \ln p'$  diagram.

2. For isotropic compression of

(i) normally consolidated clay,

$$v = N - \lambda \ln p'; \quad (7-8)$$

(ii) overconsolidated clay,

$$v = v_{\kappa} - \kappa \ln p'. \quad (7-9)$$

3. For isotropic compression of sand

(i) at very large stresses,

$$v = N - \lambda \ln p';$$

(ii) at normal engineering stresses,

$$v = v_{\kappa} - \kappa \ln p'.$$

But  $\kappa$  is small.

4. For one-dimensional compression of

(i) normally consolidated clay,

$$v = N_0 - \lambda \ln p'; \quad (7-17)$$

(ii) overconsolidated clay,

$$v = v_{\kappa_0} - \kappa \ln p'. \quad (7-18)$$

5.  $N$ ,  $\lambda$ , and  $\kappa$  are soil constants whose values must be found by experiment for each soil.

6. For one-dimensional compression,

$$K_0 = \sigma'_h / \sigma'_v, \quad (7-10)$$

$$\eta_{1v} = \lambda / v \sigma'_v, \quad (7-23)$$

$$C_O = 2.303\lambda. \quad (7-28)$$

## REFERENCES

- Amerasinghe, S. F. The stress-strain behaviour of clay at low stress levels and high overconsolidation ratio. PhD Thesis, Cambridge University, 1973.
- Ndarajah, V. Stress-strain properties of lightly overconsolidated clays. PhD Thesis, Cambridge University, 1973.
- Vesic, A. S. and Clough, G. W. Behaviour of granular materials under high stresses. *Proc. Am. Soc. Civil Engrs*, 94: SM3, 661-688, 1968.

## ONE-DIMENSIONAL CONSOLIDATION

### 8-1 INTRODUCTION

The time-dependent process as water is squeezed from a soil is known as consolidation. The interactions between pore pressure, stress, and compression in the simple model of Fig. 7-1 are illustrated in Fig. 7-2, where the curved paths during Stage III represent the consolidation process. Similar time-dependent behaviour occurs for soil.

Our objective in this Chapter is to devise an analysis for the consolidation process so that we may estimate the variation of pore pressure, stress, and volume with time for any given situation. It turns out that it is not difficult to devise a basic differential consolidation equation, but analytical solutions have only been found for cases with relatively simple boundary conditions. The simplest solution of practical importance is that for one-dimensional consolidation and we will consider only this special case.

### 8-2 THEORY OF ONE-DIMENSIONAL CONSOLIDATION

The following theory of one-dimensional consolidation is attributed to Terzaghi; the necessary assumptions are that:

1. the soil is saturated and homogeneous;
2. the principle of effective stress is valid;
3. Darcy's law is valid;
4. the pore water and soil grains are incompressible;
5. all displacements of the soil and flow of the pore water are one-dimensional;
6. the coefficients of permeability,  $k$ , and compressibility,  $m_v$ , remain constant.

Consider the element of soil in Fig. 8-1. It has a cross-sectional area  $A$  and thickness  $\delta z$ ; in a small time interval  $\delta t$  the thickness increases by  $\delta l$ . The flow of water through the element is one-dimensional and vertical and the rates of flow in through the top and out through the bottom are  $q$  and  $q + \delta q$ , respectively. The pore pressure at the top face is  $(u_0 + \bar{u})$  and at the bottom face is  $(u_0 + \bar{u} + \delta \bar{u})$ , where  $u_0$  is a steady-state pore pressure and  $\bar{u}$  is an excess pore pressure. It will later be assumed that the total vertical

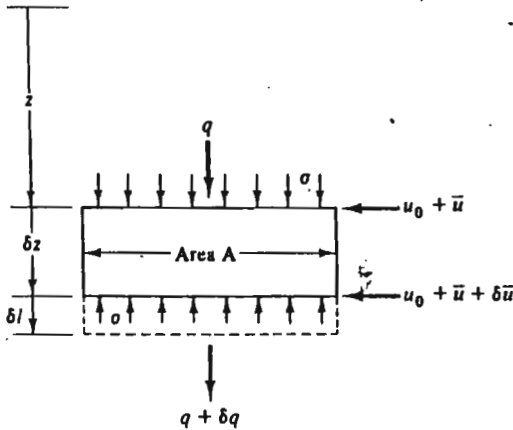


Figure 8-1 Conditions in an element in a one-dimensionally consolidating soil stress remains constant over the time interval, but the effective vertical stress changes by  $\delta\sigma'$ .

The coefficient of volume compressibility  $m_v$  was defined in Chapter 7 as

$$\delta\varepsilon_v = m_v \delta\sigma' \tag{8-1}$$

Thus, the increase  $\delta l$  of thickness of the element due to a small increment of effective stress  $\delta\sigma'$  for one dimensional compression is given by

$$\delta l = -m_v \delta\sigma' \delta z \tag{8-2}$$

and, since we assume that  $m_v$  remains constant, the present theory of consolidation will be valid only for relatively small increments of stress.

As soil grains and pore water are assumed to be incompressible, the condition of continuity is

$$A \delta l = -\delta q \delta t \tag{8-3}$$

and, from Eqs (8-2) and (8-3),

$$\frac{\delta q}{\delta z} = A m_v \frac{\delta\sigma'}{\delta t} \tag{8-4}$$

At the limit, noting that  $q$  and  $\sigma'$  are both functions of  $z$  and  $t$ ,

$$\frac{\partial q}{\partial z} = A m_v \frac{\partial \sigma'}{\partial t} \tag{8-5}$$

The rate of flow across the element is given by Darcy's law as

$$q = Aki, \tag{8-6}$$

where the hydraulic gradient  $i$  is

$$i = -\frac{1}{\gamma_w} \frac{\delta \bar{u}}{\delta z} \tag{8-7}$$

Hence,

$$\frac{\delta q}{\delta z} = -\frac{Ak}{\gamma_w} \frac{\delta}{\delta z} \left( \frac{\delta \bar{u}}{\delta z} \right) \quad (8-8)$$

and, at the limit,

$$\frac{\partial q}{\partial z} = -\frac{Ak}{\gamma_w} \frac{\partial^2 \bar{u}}{\partial z^2} \quad (8-9)$$

Then, from Eqs (8-5) and (8-9),

$$\frac{k}{m_v \gamma_w} \frac{\partial^2 \bar{u}}{\partial z^2} = -\frac{\partial \sigma'}{\partial t} \quad (8-10)$$

The effective stress is given by

$$\sigma' = \sigma - (u_0 + \bar{u}) \quad (8-11)$$

Hence, noting that  $u_0$  remains constant,

$$\frac{\partial \sigma'}{\partial t} = \frac{\partial \sigma}{\partial t} - \frac{\partial \bar{u}}{\partial t} \quad (8-12)$$

We now consider the simple and common case when the total stress remains constant with time. Then  $\partial \sigma / \partial t = 0$  and Eq. (8-10) becomes

$$c_v \frac{\partial^2 \bar{u}}{\partial z^2} = \frac{\partial \bar{u}}{\partial t} \quad (8-13)$$

where

$$c_v = \frac{k}{m_v \gamma_w} \quad (8-14)$$

$c_v$  is known as the coefficient of consolidation. Eq. (8-13) is the basic differential equation for one-dimensional consolidation. If we can obtain a solution of the form  $\bar{u} = \bar{u}(z, t)$  for Eq. (8-13) which satisfies the appropriate boundary conditions, we will then know the variation with time of the excess pore pressure and the effective stress at any point within a one-dimensionally consolidating soil layer.

### 8-3 ISOCHRONES

It is often convenient to illustrate the solution of Eq. (8-13) graphically by plotting the variation of excess pore pressure with position at given times. We will then obtain a family of curves called *isochrones* (from the Greek and meaning equal time).

A simple way to visualize an isochrone is to imagine a set of standpipes inserted into the consolidating soil. Figure 8-2 shows such a set of standpipes in a stratum of uniform clay above an impermeable rock: a total stress  $\Delta \sigma$  was applied suddenly to the clay surface at a time  $t = 0$  and was held constant



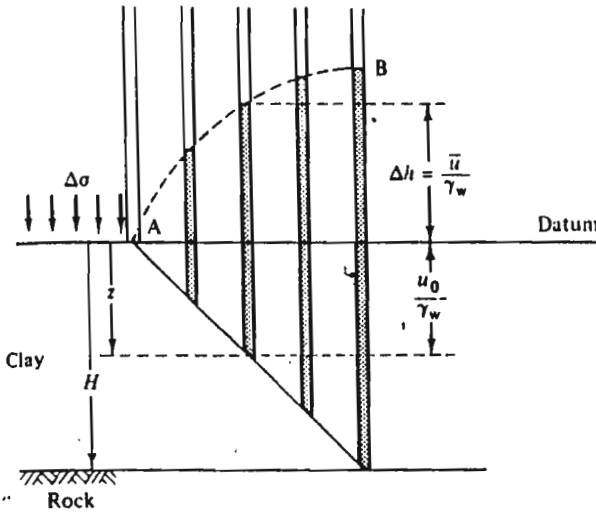


Figure 8-2 Standpipe levels in a bed of one-dimensionally consolidating clay

thereafter. We assume that  $\Delta\sigma$  is applied over a sufficiently large area so that the clay consolidates one-dimensionally.

Before the increment of total stress was applied to the clay surface the levels of water in all the standpipes were at ground level and the steady-state pore pressure  $u_0$  at any depth  $z$  was  $u_0 = \gamma_w z$ . At any instant of time, the excess pore pressure  $\bar{u}$  is given by  $\bar{u} = \gamma_w \Delta h$ , where  $\Delta h$  is the level of water in each standpipe above the datum at ground level. Thus, the curve AB in Fig. 8-2 which joins the water levels in the standpipes will give the shape of the isochrone at that instant of time. However, the height  $\Delta h$  of the curve above the datum at ground level will have to be multiplied by  $\gamma_w$  to give the correct magnitude of the excess pore pressure represented by the isochrone.

Isochrones are normally shown with the datum line drawn vertically and the excess pore pressure plotted to the right, as illustrated in Fig. 8-3. It is convenient to denote the value of the excess pore pressure at a depth  $z$  and at a time  $t$  by  $\bar{u}(z, t)$ ; thus, for example, the excess pore pressure at the base of the clay layer at a depth  $H$  at  $t = 0$  is written  $\bar{u}(H, 0)$ .

Isochrones must satisfy the boundary conditions of the particular problem considered. For the clay layer in Fig. 8-2 at  $t = 0$ , no water has been squeezed from the clay and so there has been no volume change and no change of effective stress. After a very long time, the clay will reach a new steady-state equilibrium with no flow of pore water and no excess pore pressures anywhere. The boundary conditions are

$$\left. \begin{aligned} t = 0, \quad \bar{u}(z, 0) &= \Delta\sigma; \\ t = \infty, \quad \bar{u}(z, \infty) &= 0. \end{aligned} \right\} \quad (8-15)$$

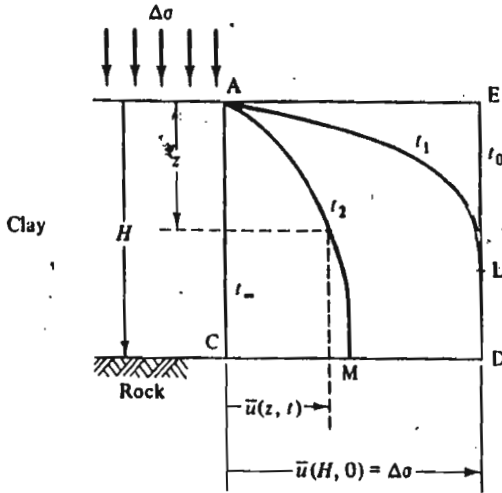


Figure 8-3 Isochrones in a bed of one-dimensionally consolidating clay

The isochrones shown in Fig. 8-3 satisfy these boundary conditions.

The slope of an isochrone is related to the instantaneous hydraulic gradient and, hence, to the instantaneous rate of flow. We define  $s(z, t)$  as the slope of an isochrone for time  $t$  at depth  $z$ , where

$$s(z, t) = \partial \bar{u} / \partial z. \tag{8-16}$$

Thus  $s(z, t) = 0$  when the isochrone is vertical in Fig. 8-3. The slope of the isochrone is related to the instantaneous hydraulic gradient by

$$s(z, t) = -\gamma_w i(z, t) \tag{8-17}$$

and, from Darcy's law, the instantaneous artificial velocity at a time  $t$  and depth  $z$  is given by

$$V(z, t) = -(k/\gamma_w) s(z, t). \tag{8-18}$$

With the axes for  $z$  and  $\bar{u}$  shown in Fig. 8-3, the isochrones have positive slopes everywhere and, hence, the seepage of pore water is everywhere upwards as the clay compresses.

At the base of the clay layer in Fig. 8-3 the rock is impermeable and  $V(H, t) = 0$ ; consequently  $s(H, t) = 0$  and an isochrone such as that at time  $t_2$  intersects the rock surface orthogonally at M. An isochrone such as that at time  $t_1$  intersects the line ED at a point such as L. Below L there has been no consolidation and no change in volume; consequently there is no flow of pore water below L and the isochrone  $t_1$  is vertical at L.

Since soil grains and water are assumed to be incompressible, the upward artificial velocity at any depth must exactly balance the downward rate of settlement at that level. Hence,

$$\partial \rho / \partial t = -V(z, t) = (k/\gamma_w) s(z, t), \tag{8-19}$$

where  $\rho = \rho(z, t)$  is the settlement, with respect to the rock surface, of the layer at depth  $z$  after a time  $t$ .

#### 8-4 BOUNDARY CONDITIONS FOR ONE-DIMENSIONAL CONSOLIDATION

The one-dimensional consolidation equation, Eq. (8-13), is a differential equation and its solution requires certain boundary conditions to be specified; these are concerned with the particular drainage and pore pressure conditions at the top and bottom surfaces of the consolidating layer. The boundary conditions for the layer in Fig. 8-2 are

$$\begin{aligned} t = 0, \quad 0 \leq z \leq H, \quad \bar{u} &= \Delta\sigma; \\ 0 < t \leq \infty, \quad z = 0, \quad \bar{u} &= 0; \\ 0 \leq t \leq \infty, \quad z = H, \quad \partial\bar{u}/\partial z &= 0; \\ t = \infty, \quad 0 \leq z \leq H, \quad \bar{u} &= 0. \end{aligned}$$

For different conditions of drainage at the top and bottom surfaces, the boundary conditions will obviously be different.

We will find that it is convenient to obtain solutions for the consolidation equation in terms of the time factor  $T_v$  and the average degree of consolidation  $U_t$ .

#### 8-5 TIME FACTOR $T_v$

Figure 8-4(a) shows a layer of consolidating soil overlying impermeable rock; pore water can only seep upwards and the flow is known as one-way. For this situation we define the time factor  $T_v$  as

$$T_v = c_v t / H^2, \quad (8-20)$$

where  $H$  is the depth of the consolidating layer. If the layer overlies a very permeable deposit, water may seep upwards and downwards as shown in Fig. 8-4(b). This two-way drainage case contains two halves each identical to the one-way drainage case. We may, therefore, adopt the one-way drainage solution if we define the depth of the two-way draining layer as  $2H$ .

We may avoid any ambiguity by redefining  $H$  as the maximum drainage path; thus  $H$  in Eq. (8-12) is the longest direct path taken by any element of water as it is squeezed from the soil.

#### 8-6 AVERAGE DEGREE OF CONSOLIDATION $U_t$

The average degree of consolidation  $U_t$ , which has taken place at a time  $t$ , is defined as

$$U_t = \Delta\rho_t / \Delta\rho_\infty, \quad (8-21)$$

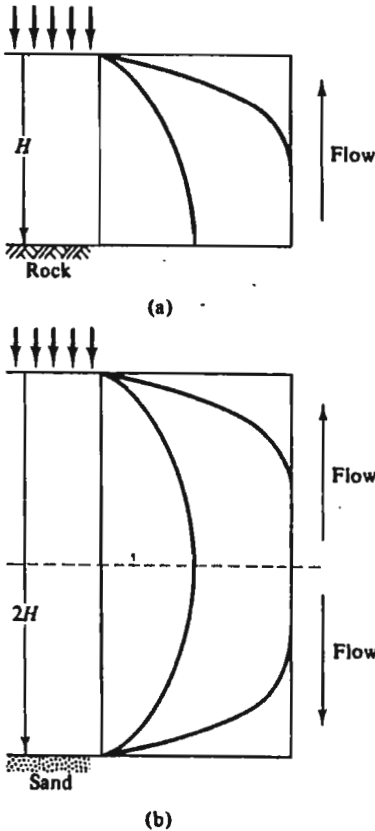


Figure 8-4 One-way and two-way drainage for one-dimensional consolidation. (a) One-way drainage. (b) Two-way drainage

where  $\Delta \rho_t$  is the overall settlement of the surface of the clay layer in Fig. 8-2 with respect to the rock at a time  $t$  and  $\Delta \rho_\infty$  is the final overall settlement when excess pore pressures are everywhere zero. The limits of the degree of consolidation are

$$\left. \begin{aligned} t = 0, \quad U_0 = 0; \\ t = \infty, \quad U_\infty = 1.0. \end{aligned} \right\} \quad (8-22)$$

We should note that at a time  $t$  the excess pore pressure  $\bar{u}(z, t)$  varies throughout the layer, as shown by the isochrones in Fig. 8-3, and the local degree of consolidation is, therefore, not constant throughout the layer. We may define a local degree of consolidation  $U_f(z)$  at a depth  $z$  and a time  $t$  as

$$U_f(z) = 1 - \{\bar{u}(z, t) / \bar{u}(z, 0)\} \quad (8-23)$$

and the limits of  $U_f(z)$  are given by Eqs (8-22).

### 8-7 APPROXIMATE SOLUTION FOR ONE-DIMENSIONAL CONSOLIDATION BY PARABOLIC ISOCHRONES

The solution of the one-dimensional consolidation equation, Eq. 8-13, together with the boundary conditions discussed in Sec. 8-4, will emerge as a family of isochrones like those illustrated in Fig. 8-3. We may obtain an approximate, but nevertheless reasonably accurate, solution by assuming that the isochrones may be approximated by parabolas.

We must distinguish between two stages of consolidation. In Fig. 8-5 there is an isochrone for a critical time  $t_c$  which passes through the point D for which

$$\bar{u}(H, t_c) = \Delta\sigma,$$

and we must consider solutions for  $t = t_1 \leq t_c$  separately from those for  $t = t_m \geq t_c$ . The ideas behind each analysis will remain the same but the algebra differs slightly.

(i)  $t = t_1 \leq t_c$

A parabolic isochrone for  $t_1 \leq t_c$  is shown in Fig. 8-6; its slope is vertical at L and no consolidation has occurred below a depth  $z = l$ . Summing the settlements of all elementary layers and using Eq. (8-1), the surface settlement is given by

$$\Delta\rho_t = \int_0^l m_v \Delta\sigma' dz \quad (8-24)$$

$$\begin{aligned} &= m_v \times (\text{Area AEL}) \\ &= \frac{1}{3} m_v \Delta\sigma l. \end{aligned} \quad (8-25)$$

Since  $m_v$  and  $\Delta\sigma$  are assumed to remain constant during consolidation, Eq. (8-19) may be differentiated with respect to time to give the rate of surface settlement as

$$\frac{d\rho_t}{dt} = \frac{1}{3} m_v \Delta\sigma \frac{dl}{dt}. \quad (8-26)$$

The rate of surface settlement is also given by Eq. (8-19) with  $z = 0$ . Hence,

$$\frac{d\rho_t}{dt} = \frac{k}{\gamma_w} s_t, \quad (8-27)$$

where  $s_t = s(0, t)$  is the slope of the isochrone for time  $t$  at the soil surface. From the geometry of a parabola,  $s_t = 2\Delta\sigma/l$  and so

$$\frac{d\rho_t}{dt} = \frac{2k\Delta\sigma}{\gamma_w l}. \quad (8-28)$$

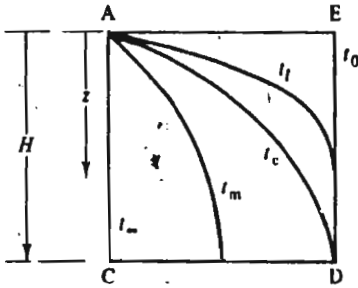


Figure 8-5 Parabolic isochrones

Hence, equating the rate of surface settlement from Eqs (8-26) and (8-28),

$$l \frac{dl}{dt} = 6 \frac{k}{m_v \gamma_w} \tag{8-29}$$

and integrating with the boundary condition  $l = 0$  at  $t = 0$

$$l = \sqrt{(12c_v t)}, \tag{8-30}$$

where  $c_v$  is the coefficient of consolidation defined by Eq. (8-14). Equation (8-30) represents the rate at which the point L in Fig. 8-6 progresses down ED; no effects of consolidation will be noticed at depths  $z$  greater than  $l$ .

The surface settlement  $\Delta \rho_t$  after some time  $t \leq t_c$  is given by substituting for  $l$  into Eq. 8-25. Hence,

$$\Delta \rho_t = \frac{1}{3} m_v \Delta \sigma \sqrt{(12c_v t)}$$

or

$$\Delta \rho_t = m_v \Delta \sigma H \frac{2}{\sqrt{3}} \sqrt{T_v}, \tag{8-31}$$

where  $T_v$  is the time factor given by Eq. (8-20). The final surface settlement

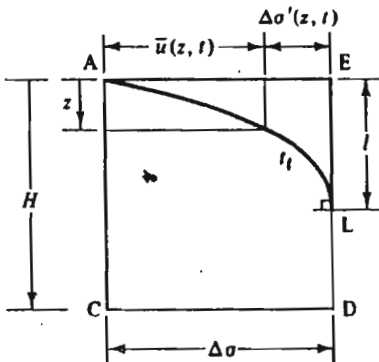


Figure 8-6 Parabolic isochrones for  $t < t_c$

will occur when the excess pore pressure is everywhere zero and  $\Delta\sigma' = \Delta\sigma$ . The final surface settlement  $\Delta\rho_\infty$  is, therefore, given by

$$\Delta\rho_\infty = m_v \Delta\sigma H \tag{8-32}$$

and the average degree of consolidation defined by Eq. (8-21) is simply

$$U_t = \frac{2}{\sqrt{3}} \sqrt{T_v} \tag{8-33}$$

Equation (8-33) is the approximate solution for one-dimensional consolidation assuming parabolic isochrones. The solution is valid until the point L in Fig. 8-6 reaches D when  $t = t_c$ ; at this instant  $l = H$  and

$$T_v = \frac{1}{18}, \quad U_t = 0.33. \tag{8-34}$$

For  $t \geq t_c$ , the isochrone no longer touches ED and a new analysis must be performed.

(ii)  $t = t_m \geq t_c$

A parabolic isochrone for  $t_m \geq t_c$  is shown in Fig. 8-7; the isochrone intersects the base of the layer orthogonally at M with  $\bar{u} = m\Delta\sigma$ . Making use of the geometry of a parabola and proceeding as before, the surface settlement after a time  $t_m$  is given by

$$\Delta\rho_t = m_v \Delta\sigma H (1 - \frac{2}{3}m) \tag{8-35}$$

The rate of surface settlement may be obtained from Eq. (8-35) as

$$\frac{d\rho_t}{dt} = -\frac{2}{3}m_v \Delta\sigma H \frac{dm}{dt} \tag{8-36}$$

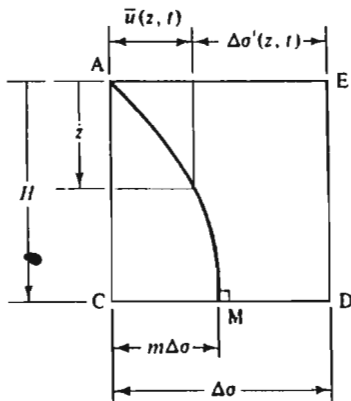


Figure 8-7 Parabolic isochrones for  $t > t_c$

and from the slope of the isochrone at the surface as

$$\frac{d\rho_t}{dt} = \frac{2mk \Delta\sigma}{\gamma_w H} \quad (8-37)$$

Hence,

$$\frac{1}{m} \frac{dm}{dt} = -\frac{3c_v}{H^2}, \quad (8-38)$$

where  $c_v$  is the coefficient of consolidation.

Equation (8-38) must be integrated between the limits  $t = t_0$  and  $t = \infty$ . At the critical time  $t_0$  corresponding to  $T_v = \frac{1}{4}$  the isochrone passes through the point D in Fig. 8-5 and  $m = 1$ . Integration of Eq. (8-38) between these limits gives  $m$  as a function of time as

$$m = \exp\left(\frac{1}{4} - 3T_v\right). \quad (8-39)$$

The surface settlement after a time  $t \geq t_0$  is obtained by substituting for  $m$  into Eq. (8-35) to give

$$\Delta\rho_t = m_v \Delta\sigma H \left[1 - \frac{3}{4} \exp\left(\frac{1}{4} - 3T_v\right)\right]. \quad (8-40)$$

The final surface settlement  $\Delta\rho_\infty$  is given by Eq. (8-32), and so the average degree of consolidation is given by

$$U_t = 1 - \frac{3}{4} \exp\left(\frac{1}{4} - 3T_v\right). \quad (8-41)$$

Equations (8-33) and (8-41) together describe the one-dimensional consolidation of the soil stratum, for they relate the average degree of consolidation  $U_t$  to the time factor  $T_v$ . They are, however, valid only for the initial and final excess pore pressures represented by the isochrones  $t_0$  and  $t_\infty$  in Fig. 8-5. The time factor defined by Eq. (8-20) is dimensionless and contains time, the maximum drainage path, the soil compressibility, and the soil permeability. Consequently, the solutions are valid for all soils and all layer thicknesses. The theoretical relationship between  $U_t$  and  $\sqrt{T_v}$  for parabolic isochrones assumed above is shown in Fig. 8-8; it is conventional to plot  $U_t$  positively downwards to represent settlement. The portions OD and DE are given by

$$U_t = \frac{2}{\sqrt{3}} \sqrt{T_v}, \quad (8-33)$$

$$U_t = 1 - \frac{3}{4} \exp\left(\frac{1}{4} - 3T_v\right), \quad (8-41)$$

and the two parts meet at D, where

$$\sqrt{T_v} = \frac{1}{\sqrt{12}}, \quad U_t = 0.33. \quad (8-42)$$

We may note that DE becomes asymptotic to  $U_t = 1$  for large values of  $T_v$ .



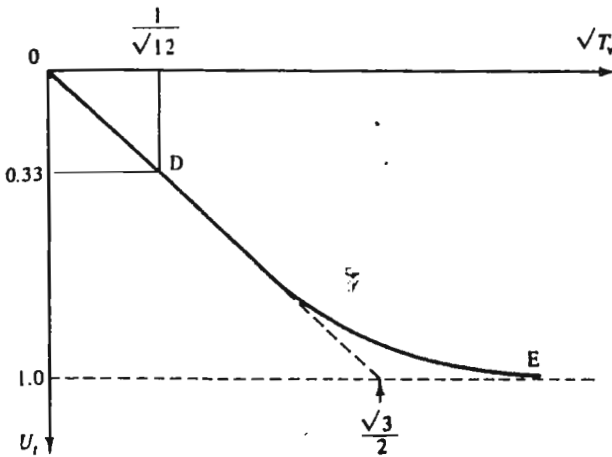


Figure 8-8 Solution for one-dimensional consolidation with parabolic isochrones

**Example 8-1** Calculation of the rate of foundation settlement by the approximate solution

Figure E8-1 shows a foundation on a thin bed of sand which rests on the surface of a clay stratum 8 m thick which overlies a layer of highly permeable sand. The foundation is so wide that consolidation of the clay may be assumed to be one-dimensional and, immediately after construction, excess pore pressures in the clay are everywhere equal to the foundation pressure. The coefficient of consolidation of the clay is  $c_v = 2 \text{ m}^2$  per year. Calculate the time after construction at which the settlement reaches (a) 30 per cent and (b) 90 per cent of its final value.

The drainage is two-way, up to the surface and down to the lower sand layer, and, hence,  $H = 4 \text{ m}$ . Thus,

$$t = T_v H^2 / c_v = (T_v \times 4^2) / 2 = 8T_v.$$

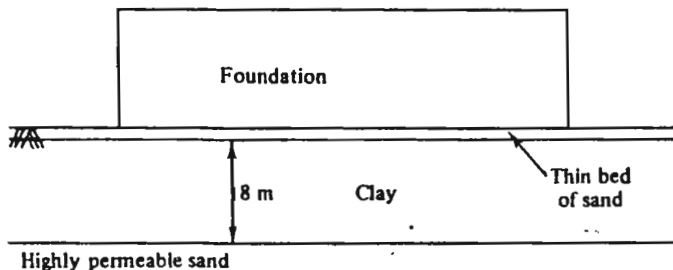


Figure E8-1

(a) For  $U_t < 0.33$ ,

$$U_t = \frac{2}{\sqrt{3}} \sqrt{T_v}$$

Hence, for  $U_t = 0.3$ ,

$$T_v = \frac{3}{4} U_t^2 = \frac{3}{4} \times 0.3^2 = 0.068$$

and

$$t = 0.068 \times 8.$$

Therefore,

$$t = 0.54 \text{ years.}$$

(b) For  $U_t > 0.33$ ,

$$U_t = 1 - \frac{2}{\sqrt{3}} \exp\left(\frac{1}{3} - 3T_v\right).$$

Hence, for  $U_t = 0.9$ ,

$$\begin{aligned} T_v &= \frac{1}{3} \left\{ \frac{1}{3} - \ln \left\{ \frac{2}{\sqrt{3}} (1 - U_t) \right\} \right\} \\ &= \frac{1}{3} \left\{ \frac{1}{3} - \ln \left\{ \frac{2}{\sqrt{3}} \times (1 - 0.9) \right\} \right\} \\ &= 0.716 \end{aligned}$$

and

$$t = 0.716 \times 8.$$

Therefore,

$$t = 5.73 \text{ years.}$$

The settlements will, therefore, be 30 per cent complete after approximately 6 months and 90 per cent complete after nearly 6 years.

## 8-8 THE EXACT SOLUTION FOR ONE-DIMENSIONAL CONSOLIDATION

The one-dimensional consolidation equation,

$$c_v \frac{\partial^2 \bar{u}}{\partial z^2} = \frac{\partial \bar{u}}{\partial t}, \quad (8-13)$$

may be solved analytically for appropriate boundary conditions. The method of solution, by separation of variables, is described in detail by Taylor (1948, pp. 229-234) and we will do no more here than quote the result.

The solution emerges as a Fourier series and for  $\Delta\sigma = \text{constant}$  and for our particular boundary conditions

$$\bar{u}(z, t) = \sum_{m=0}^{\infty} \frac{2\Delta\sigma}{M} \sin MZ \exp(-M^2 T_v), \quad (8-43)$$

where  $M = \frac{1}{2}\pi(2m+1)$ ,  $Z = z/H$ ,  $T_v = c_v t/H^2$ .

Equation (8-43) provides an expression for the excess pore pressure  $\bar{u}(z, t)$  and so, using Eq. (8-23), the local degree of consolidation at depth  $z$  and time  $t$  is given by

$$U(z) = 1 - \sum_{m=0}^{\infty} \frac{2}{M} \sin MZ \exp(-M^2 T_v) \quad (8-44)$$

Equation (8-44) is plotted for different values of  $T_v$  in Fig. 8-9.

The average degree of consolidation of the whole stratum, defined by Eq. (8-21), may be obtained by integrating Eq. (8-44) as

$$U_t = 1 - \sum_{m=0}^{\infty} \frac{2}{M^2} \exp(-M^2 T_v) \quad (8-45)$$

Equation (8-45) relates the average degree of consolidation of a one-dimensionally consolidating stratum to the time factor and it is analogous to Eqs (8-33) and (8-41), which were derived for the same case by assuming that the isochrones could be approximated by parabolas.

Equation (8-45) is shown plotted as  $U_t$  against  $\sqrt{T_v}$  in Fig. 8-10, and the line ODE from Fig. 8-8 (obtained assuming parabolic isochrones) has been included for comparison. For values of  $U_t$  not greater than 0.6, Eq. (8-45) may be approximated to

$$U_t = \frac{2}{\sqrt{\pi}} \sqrt{T_v} \quad (8-46)$$

which may be compared with the parabolic isochrone solution for  $U_t < 0.33$ ,

$$U_t = \frac{2}{\sqrt{3}} \sqrt{T_v} \quad (8-33)$$

Thus, the difference between the approximate and the exact solutions for one-dimensional consolidation is extremely small.

It should be noted that both the solutions quoted above (the exact and the approximate) apply only to the case where the initial excess pore pressure

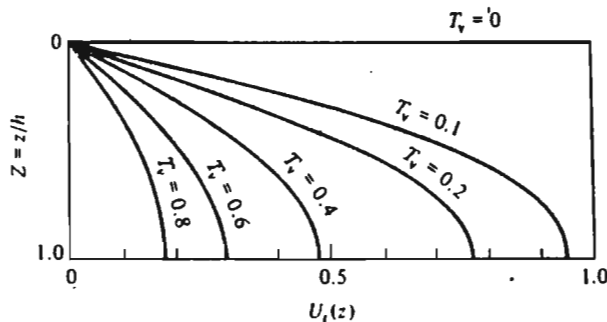


Figure 8-9 Isochrones for one-dimensional consolidation from the exact solution

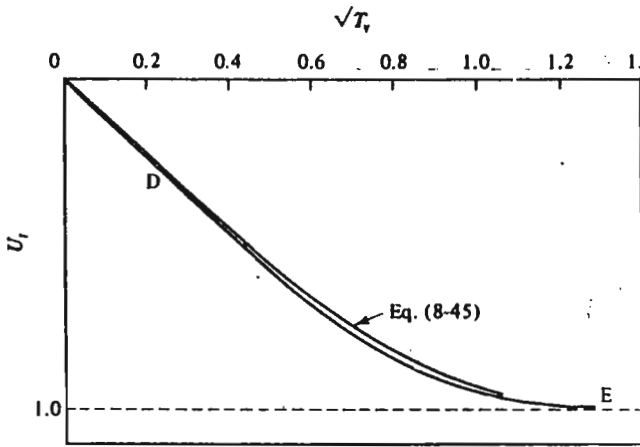


Figure 8-10 Comparison of the exact solution and the parabolic isochrone solution for one-dimensional consolidation

is constant throughout the layer and where the final excess pore pressure is everywhere zero. The exact analysis may be extended relatively easily to allow for different initial excess pore pressures, e.g., Taylor (1948, pp. 236-237). Relationships between average degree of consolidation and time factor  $T_v$  for three cases of initial excess pore pressure distribution (including the case when the initial excess pore pressure is constant throughout the layer) are listed in Table 8-1.

Table 8-1 Exact solutions for one-dimensional consolidation with one-way drainage for various distributions of initial excess pore pressure

 Impermeable $\bar{u}(z, 0)$ $U_i$	 Case 1	 Case 2 $T_v$	 Case 3
0.1	0.008	0.047	0.003
0.2	0.031	0.100	0.009
0.3	0.071	0.158	0.024
0.4	0.126	0.221	0.048
0.5	0.196	0.294	0.092
0.6	0.287	0.383	0.160
0.7	0.403	0.500	0.271
0.8	0.567	0.665	0.440
0.9	0.848	0.940	0.720

**Example 8-2** Calculation of the rate of foundation settlement by the exact solution

Repeat Ex. 8-1 using the exact solution for one-dimensional consolidation given in Table 8-1.

Drainage is two way and, as before,  $t = 8T_v$ . Immediately after construction, excess pore pressures are everywhere equal to the foundation pressure and Case 1 of Table 8-1 applies.

(a) For  $U_t = 0.3$  and Case 1 from Table 8-1,

$$T_v = 0.071.$$

Hence,

$$t = 0.071 \times 8,$$

$$t = 0.57 \text{ years.}$$

(b) For  $U_t = 0.9$  and Case 1 from Table 8-1,

$$T_v = 0.848.$$

Hence,

$$t = 0.848 \times 8,$$

$$t = 6.78 \text{ years.}$$

The results do not differ substantially from those found in Ex. 8-1 using the approximate solution.

## 8-9 DETERMINATION OF $c_v$ FROM AN OEDOMETER TEST

The results of a single stage of consolidation of a sample in an oedometer test may be used to estimate a value for the coefficient of consolidation of a soil. Since the time factor  $T_v$  is a function of  $c_v$ , we cannot immediately plot experimental results as  $U_t$  against  $T_v$ . However, if the test is continued until consolidation is complete, we may find the final settlement and, hence, the degree of consolidation at any time and so plot  $U_t$  against time  $t$ .

If the experimental  $U_t$  against  $t$  curve can be fitted to a theoretical  $U_t$  against  $T_v$  curve, a relationship between  $t$  and  $T_v$  may be obtained and so  $c_v$  found from Eq. (8-20). Two alternative curve fitting approximations are available.

**A  $\sqrt{(\text{time})}$  method** This method makes use of the observation that settlement against  $\sqrt{(\text{time})}$  curves have an initial portion which may be approximated by a straight line and this straight line can be fitted to Eq. (8-46).

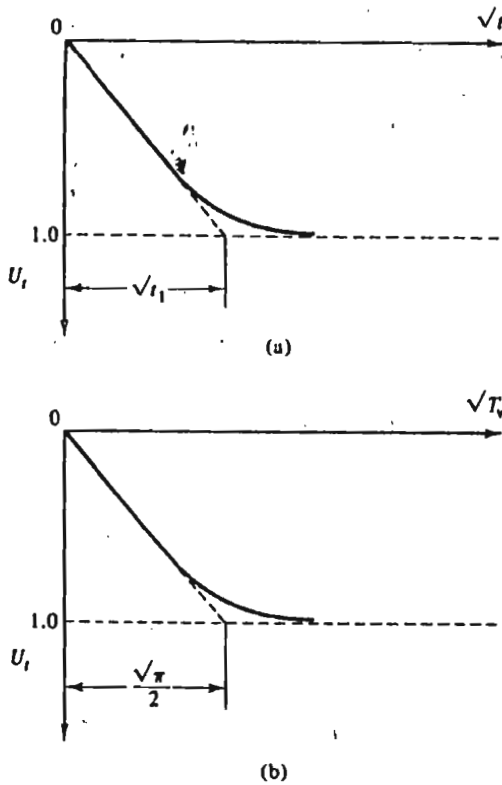


Figure 8-11 Calculation of  $T_v$  from oedometer test results by a  $\sqrt{(\text{time})}$  curve-fitting method

Figure 8-11(a) shows the results of a single stage of consolidation of a sample of clay in an oedometer test plotted as  $U_i$  against  $\sqrt{t}$ . The slope of the initially linear part of the curve is given by  $\sqrt{t_1}$  as shown on Fig. 8-11(a). Figure 8-11(b) shows the theoretical consolidation curve given by Eq. (8-45); the slope of the initially linear portion may be found from Eq. (8-46) and is given by  $\sqrt{(\pi)/2}$  as shown on Fig. 8-11(b).

The two curves fit when

$$T_v = c_v t / H^2. \quad (8-20)$$

Therefore,

$$\pi/4 = c_v t_1 / H^2, \quad (8-47)$$

where  $H$  is the maximum drainage path in the test sample. In practice there is no need to draw Fig. 8-11(b); we simply plot the test results as  $U_i$  against  $\sqrt{t}$  as shown in Fig. 8-11(a), construct  $t_1$  and calculate  $c_v$  from

$$c_v = \pi H^2 / 4 t_1. \quad (8-48)$$

**A log<sub>10</sub> (time) method** As an alternative, it is sometimes more convenient to fit the experimental and theoretical consolidation curves at  $U_t = 0.5$ , that is, when half of the consolidation is complete.

The value of  $T_v$  for  $U_t = 0.5$  may be found from Eq. (8-45) and is  $T_v = 0.196$ . To estimate a value for  $t_{50}$ , the time for  $U_t = 0.5$  during a single stage of consolidation in an oedometer test, it is convenient to plot  $U_t$  against  $\log t$ . Figure 8-12 shows the results of the oedometer test on a sample of clay already shown in Fig. 8-11(a). The value for  $t_{50}$  may be read directly from the experimental consolidation curve.

The theoretical and experimental curves fit when

$$T_v = c_v t / H^2, \tag{8-20}$$

$$0.196 = c_v t_{50} / H^2, \tag{8-49}$$

where  $H$  is the maximum drainage path in the oedometer sample. From Eq. (8-49) and the experimental value for  $t_{50}$ , the coefficient of consolidation may be calculated from

$$c_v = 0.196(H^2/t_{50}). \tag{8-50}$$

We must note that  $U_t$  cannot be calculated until the final settlement  $\Delta\rho_\infty$  has been found. Ideally, settlement time curves would approach horizontal asymptotes as illustrated in Figs 8-11 and 8-12 and it would not be difficult to estimate a value for  $\Delta\rho_\infty$ . For most experimental settlement : time curves, however, these horizontal asymptotes are not clearly defined and, moreover, there is often an initial settlement which is observed immediately after the loading increment has been applied. For most practical cases it is necessary to estimate a value for  $\Delta\rho_\infty$  by means of special constructions. A construction for estimating  $\Delta\rho_\infty$  from a plot of  $\Delta\rho_t$  against  $\sqrt{t}$  was proposed by Taylor and a construction for estimating  $\Delta\rho_\infty$  from a

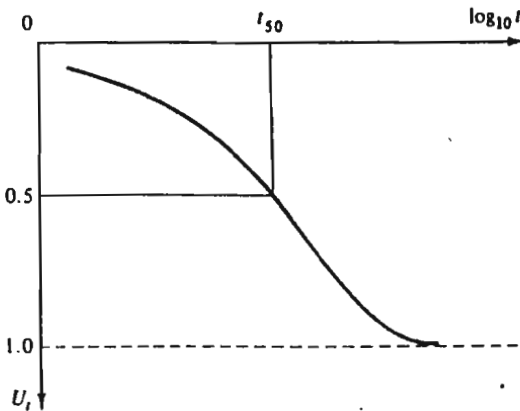


Figure 8-12 Calculation of  $T_v$  from oedometer test results by the log<sub>10</sub>(time) curve-fitting method

plot of  $\Delta\rho_t$  against  $\log_{10} t$  was proposed by Casagrande; both constructions are described by Taylor (1948, pp. 238–242).

### Example 8-3 Calculation of $c_v$ from oedometer test results

The first two columns of Table E8-1 contain data from a single increment of an oedometer test on a sample of clay. At a time  $t = 0$ , when the

**Table E8-1 Oedometer test results**

Time (min)	Settlement, $\Delta\rho_t$ (mm)	$U_t$	$\sqrt{t}$ ( $\text{min}^{1/2}$ )	$\log_{10} t$ ( $t$ in min)
0	0	0	0	—
0.25	0.206	0.107	0.50	-0.602
1.0	0.414	0.216	1.00	0
2.25	0.624	0.325	1.50	0.352
4	0.829	0.432	2	0.602
9	1.233	0.642	3	0.954
16	1.497	0.780	4	1.204
25	1.685	0.878	5	1.398
36	1.807	0.941	6	1.556
49	1.872	0.975	7	1.690
24 h	1.920	1.000	—	—

sample thickness was 20 mm, the total vertical stress was suddenly raised and the settlement of the top loading platen observed after various intervals of time; after a period of 24 h there was no further settlement. The sample was allowed to drain to both the top and bottom faces. Calculate the values of  $c_v$  for the soil for the loading increment.

For two-way drainage, the drainage path may be taken as  $H = 10$  mm for the increment. The average degree of consolidation  $U_t$  at any time may be found by dividing the settlement at that time  $\Delta\rho_t$  by the settlement at  $t = 24$  h, which may be taken as the final settlement  $\Delta\rho_\infty$ , and values are given in Table E8-1.

- (a)  $\sqrt{t}$ (time) method. Figure E8-2 shows  $U_t$  plotted against  $\sqrt{t}$ . From the figure,  $\sqrt{t_1} = 4.6$  and, hence,  $t_1 = 21.2$  min. The coefficient of consolidation  $c_v$  is given by

$$c_v \approx \pi H^2 / 4t_1 = \pi(10 \times 10^{-3})^2 / (4 \times 21.2 \times 60),$$

$$c_v = 6.2 \times 10^{-8} \text{ m}^2 \text{ s}^{-1}$$

or

$$c_v = 6.2 \times 10^{-8} \times 60^2 \times 24 \times 365 \text{ m}^2 \text{ per year,}$$

$$c_v = 1.9 \text{ m}^2 \text{ per year.}$$



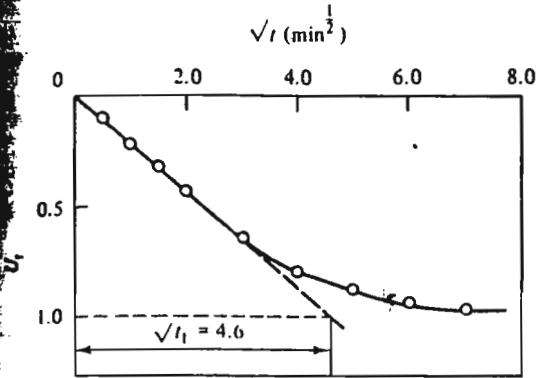


Figure E8-2 Calculation of  $c_v$  by  $\sqrt{t}$  method

- (b)  $\log_{10}(\text{time})$  method: Figure E8-3 shows  $U_t$  plotted against  $\log_{10} t$ . From the figure,  $\log_{10} t_{50} = 0.70$  and, hence,  $t_{50} = 5.01$  min. The coefficient of consolidation  $c_v$  is given by

$$c_v = 0.196H^2/t_{50} = 0.196 \times (10 \times 10^{-3})^2 / 5.01 \times 60,$$

$$c_v = 6.5 \times 10^{-8} \text{ m}^2 \text{ s}^{-1}.$$

or

$$c_v = 6.5 \times 10^{-8} \times 60^2 \times 24 \times 365 \text{ m}^2 \text{ per year},$$

$$c_v = 2.1 \text{ m}^2 \text{ per year}.$$

The values of the coefficient of consolidation  $c_v$  calculated by the two curve-fitting methods do not differ appreciably and, on average,  $c_v$  may be taken as  $6.35 \times 10^{-8} \text{ m}^2 \text{ s}^{-1}$  or  $2.0 \text{ m}^2$  per year.

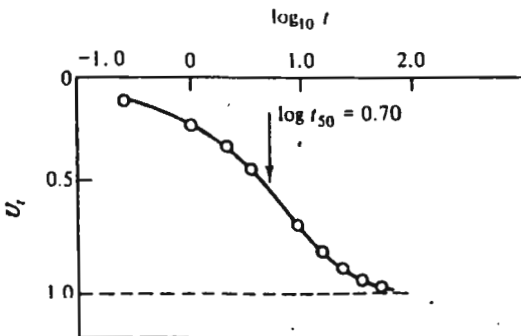


Figure E8-3 Calculation of  $c_v$  by  $\log_{10} t$  method

**Example 8-4** Calculation of  $\lambda$ ,  $N_0$ ,  $m_v$ , and  $k$  from oedometer test results

For the increment of the oedometer test described in Ex. 8-3, the total vertical stress was raised from  $\sigma_v = 90 \text{ kN m}^{-2}$  to  $\sigma_v = 300 \text{ kN m}^{-2}$ . The coefficient of earth pressure at rest is  $K_0 = 0.5$  and, at the start of the increment, the specific volume  $v = 2.45$ . Calculate values of  $\lambda$  and  $N_0$  and values of  $m_v$  and  $k$  for the increment of loading.

For one-dimensional compression,

$$v = N_0 - \lambda \ln p' \quad \text{and so} \quad \Delta v = -\lambda \Delta(\ln p').$$

Since there is no lateral strain during one-dimensional compression,  $\Delta v/v = \Delta z/z$ , where  $\Delta z$  is the change of thickness  $z$  of the sample. Hence,

$$\Delta v = v \Delta z/z = -\lambda \Delta(\ln p')$$

or

$$\lambda = -\frac{v \Delta z}{z \Delta(\ln p')}.$$

When the sample is in equilibrium,  $u = 0$  and  $\sigma'_h = K_0 \sigma'_v$  hence  $p' = \frac{1}{2} \sigma_v$ . At the beginning of the increment  $p' = 60 \text{ kN m}^{-2}$  and at the end of consolidation  $p' = 200 \text{ kN m}^{-2}$ . Thus,

$$\Delta p' = (200 - 60) \text{ kN m}^{-2}$$

or

$$\begin{aligned} \Delta(\ln p') &= \ln(200) - \ln(60) \\ &= 5.30 - 4.09 \\ &= 1.21. \end{aligned}$$

From the test results,  $z = 20 \text{ mm}$ ,  $\Delta z = -1.92 \text{ mm}$ , and  $v = 2.45$ . Hence,

$$\begin{aligned} \lambda &= (2.45 \times 1.92)/(20 \times 1.21), \\ \lambda &= 0.20. \end{aligned}$$

From  $v = N_0 - \lambda \ln p'$  and inserting  $v = 2.45$  and  $p' = 60 \text{ kN m}^{-2}$ ,

$$\begin{aligned} N_0 &= 2.45 + 0.20 \ln(60), \\ N_0 &= 3.27. \end{aligned}$$

The coefficient of compressibility  $m_v$  is given by

$$m_v = -\frac{\Delta z}{z \Delta \sigma'_v}.$$

From the test results,  $\Delta \sigma'_v = 300 - 90 = 210 \text{ kN m}^{-2}$ ,  $z = 20 \text{ mm}$ , and  $\Delta z = -1.92 \text{ mm}$ . Hence,

$$\begin{aligned} m_v &= 1.92/(20 \times 210), \\ m_v &= 4.6 \times 10^{-4} \text{ m}^2 \text{ kN}^{-1}. \end{aligned}$$

The coefficient of permeability  $k$  is given by  $k = c_v m_v \gamma_w$ , where the coefficient of consolidation is  $c_v = 6.35 \times 10^{-8} \text{ m}^2 \text{ s}^{-1}$ , from Ex. 8-3. Hence,

$$k = 6.35 \times 10^{-8} \times 4.6 \times 10^{-4} \times 9.81,$$

$$k = 2.9 \times 10^{-10} \text{ m s}^{-1}.$$

## 8-10 SUMMARY

1. One-dimensional consolidation is governed by

$$c_v \frac{\partial^2 \bar{u}}{\partial z^2} = \frac{\partial \bar{u}}{\partial t}, \quad (8-13)$$

where the coefficient of consolidation  $c_v = k/(m_v \gamma_w)$ .

2. Solutions of the one-dimensional consolidation equation may be represented graphically by isochrones; an isochrone represents the magnitude of the excess pore pressures at a particular time throughout the consolidating soil.
3. The time factor  $T_v$  and degree of consolidation  $U_i$  are defined as

$$T_v = c_v t / H^2 \quad \text{and} \quad U_i = \Delta \rho_i / \Delta \rho_\infty,$$

where  $\Delta \rho$  is the surface settlement and  $H$  is the maximum direct drainage path.

4. Relationships between  $U_i$  and  $T_v$  may be found analytically or by assuming that isochrones may be approximated by parabolas.
5. Values for  $c_v$  may be found from the results of oedometer tests by various curve-fitting methods.

## REFERENCE

Taylor, D. W. *Fundamentals of Soil Mechanics*. Wiley, New York, 1948.

**SHEAR TESTING**

**9-1 INTRODUCTION**

We discussed in Chapter 7 how soils behave when they are subjected to changes in mean normal effective stress. Of course, in many situations, elements of soil may also be subjected to changing shear stresses and we need, therefore, to study the response of soils to combinations of shear and normal stresses.

**9-2 SHEAR TESTING APPARATUS**

Various kinds of apparatus for testing soil were described in Chapter 5. The key requirement for a shear testing apparatus is that soil specimens can be subjected to known and controllable combinations of shear and normal stress while any strains and distortions are observed. ✓

The simplest and earliest shear testing apparatus is the direct shear box described in Chapter 5, but there are several difficulties with this apparatus. First, we do not know the complete stress state in the soil contained within the apparatus. Even if we suppose that both the effective normal stress  $\sigma'$  on the failure plane is uniform, and hence equal to  $F_N/A$  in Fig. 9-1, and the shear stress  $\tau$  is uniform and equal to  $F_S/A$ , we are only able to plot a single

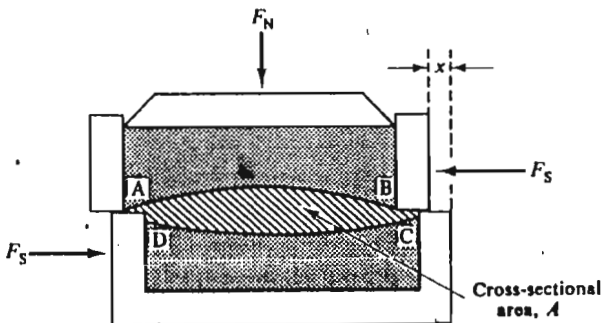


Figure 9-1 Forces applied to a specimen in the shear box

point R in a Mohr stress diagram (Fig. 9-2). We can now draw an infinity of Mohr's stress circles through R, of which only three are shown. We are, therefore, unable to determine the principal stresses  $\sigma'_1, \sigma'_3$  and cannot, without additional assumptions, discover what combinations of  $\sigma'_1$  and  $\sigma'_3$  cause failure.

Second, we only observe the boundary displacements of the soil specimen, we do not observe strains. Such a distinction would be unimportant if the soil sample deformed uniformly, for we could then just obtain the vertical strain as the ratio between the vertical compression of the sample and the vertical height of the sample. In practice, the sample only deforms in some region such as ABCD, as shown in Fig. 9-1. As we do not know the dimensions of the zone ABCD, we are unable to determine the strains in the deforming region of soil.

The shear box can, therefore, be seen to be unsatisfactory as a test apparatus if we wish to investigate the interrelation between strains and stresses. The apparatus is better suited to the determination of stresses which cause failure on a particular plane of the soil, and it is well suited to find the strength of pre-existing failure surfaces in a soil specimen.

Many of the difficulties associated with the standard shear box have been overcome by the development of the simple shear apparatus, but this apparatus is a sophisticated device currently mainly used for research.

The shear testing device most commonly used both for design and research is the triaxial apparatus which was described in some detail in Sec. 5-7.

The stresses on the boundaries of a cylindrical sample in the triaxial apparatus are illustrated in Fig. 9-3. If the top and bottom rigid platens are smooth, the axial, radial, and tangential stresses in the sample are principal

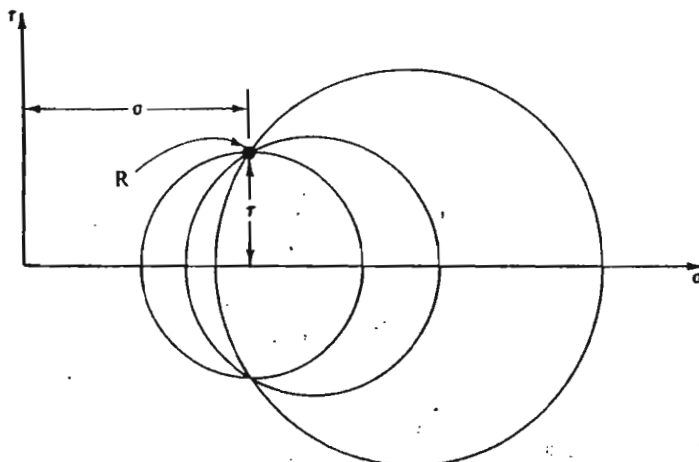


Figure 9-2 Possible Mohr's circles of stress for a sample in the shear box

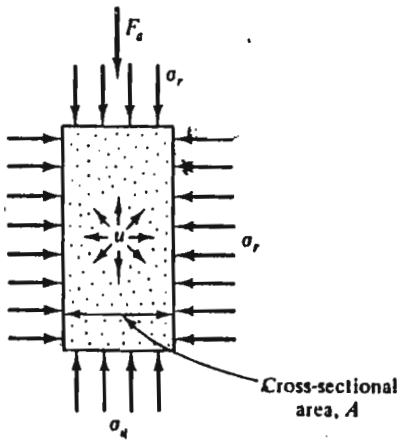


Figure 9-3 State of stress in a triaxial sample

stresses; it is usual to assume that the latter two are equal, i.e.,  $\sigma_\theta = \sigma_r$ . If the top and bottom platens do not rotate, the axial, tangential, and radial strains are principal strains and, again, it is usual to assume that  $\epsilon_\theta = \epsilon_r$ . If the cell pressure is  $\sigma_o$  and the force in the loading ram is  $F_a$ , the principal stresses in the sample are, from Eq. (5-1),

$$\sigma_r = \sigma_\theta = \sigma_o, \quad (9-1)$$

$$\sigma_a = \sigma_o + (F_a/A). \quad (9-2)$$

The radial strain is not usually measured directly; instead, it is usual to observe the volume change by means of a burette (as illustrated in Fig. 5-3) and to calculate the radial strain from

$$\epsilon_v = \epsilon_a + 2\epsilon_r, \quad (9-3)$$

where  $\epsilon_v$  and  $\epsilon_a$  are the volumetric and the axial strains, respectively. The pore pressure  $u$  will either be zero, as in a conventional drained test, or it will be measured by a pressure transducer; in either case  $u$  will be known and the effective principal stresses may be found from

$$\sigma'_a = \sigma_a - u, \quad (9-4)$$

$$\sigma'_r = \sigma_r - u. \quad (9-5)$$

When the loading ram is in compression, i.e.,  $F_a$  is positive,  $\sigma_a > \sigma_r$  and, consequently,  $\sigma_a = \sigma_1$  and  $\sigma_r = \sigma_2 = \sigma_3$ . The state of stress is known as triaxial compression. If the loading ram is attached to the top platen, the ram may be put into tension,  $F_a$  then becomes negative and  $\sigma_a < \sigma_r$ . In this case,  $\sigma_a = \sigma_3$ ,  $\sigma_r = \sigma_1 = \sigma_2$ , and the state of stress is known as triaxial extension.

Following the arguments of Chapter 4, it would be convenient to plot the results of triaxial tests in terms of the parameters

$$q' = (\sigma'_1 - \sigma'_3), \quad (4-22)$$

$$p' = \frac{1}{3}(\sigma'_1 + 2\sigma'_3), \quad (4-21)$$

$$\epsilon_a = \frac{2}{3}(\epsilon_1 - \epsilon_3), \quad (4-48)$$

$$\epsilon_v = (\epsilon_1 + 2\epsilon_3). \quad (4-47)$$

However, if this were done, we would not be able to distinguish properly between triaxial compression and extension since, in both cases,  $q'$  must be positive because  $\sigma'_1 > \sigma'_3$  by definition.

We may avoid this difficulty by redefining the parameters of stress and of strain as

$$q' = (\sigma'_a - \sigma'_r), \quad (9-6)$$

$$p' = \frac{1}{3}(\sigma'_a + 2\sigma'_r), \quad (9-7)$$

$$\epsilon_a = \frac{2}{3}(\epsilon_a - \epsilon_r), \quad (9-8)$$

$$\epsilon_v = (\epsilon_a + 2\epsilon_r). \quad (9-9)$$

In this case,  $q'$  is positive for triaxial compression when  $\sigma'_a > \sigma'_r$ , but  $q'$  is negative for triaxial extension when  $\sigma'_a < \sigma'_r$ . It would seem logical to report test results by plotting  $q'$  against  $\epsilon_a$ , but, since much published data are plotted in terms of the axial strain  $\epsilon_a$ , this variable will sometimes be used in place of  $\epsilon_a$ . Further, the use of volumetric strain  $\epsilon_v$  for interpretation of the test data is sometimes misleading. This point may be illustrated by considering a family of simple shear tests reported by Roscoe, Schofield, and Wroth (1958) on samples of randomly-packed steel balls. The change of volume of the sample in the simple shear apparatus was measured as the sample was sheared under constant vertical load. The progress of the test was indicated by the relative horizontal displacement  $x$  of the top and bottom of the apparatus. The specific volume of each sample at every stage of each test was computed and so a family of curves was obtained as shown in Fig. 9-4; samples with high specific volume compressed during shear while samples with a low specific volume dilated (expanded) during shear. The striking feature of Fig. 9-4 is that all samples reached the same specific volume (approximately 1.64) after large shear displacements.

An alternative way of plotting the data of Fig. 9-4 is shown in Fig. 9-5, where the ordinate is volumetric strain  $\epsilon_v$  (instead of the specific volume  $v$ ). Although some sort of pattern of behaviour emerges from the five separate tests, it is not evident from Fig. 9-5 alone that all samples reach the same specific volume after large shear displacements; the essential unifying feature is lost simply because we chose to plot volumetric strain and not specific volume.

It may reasonably be argued that specific volume is a more appropriate parameter than volumetric strain, if we wish to correlate the behaviour of

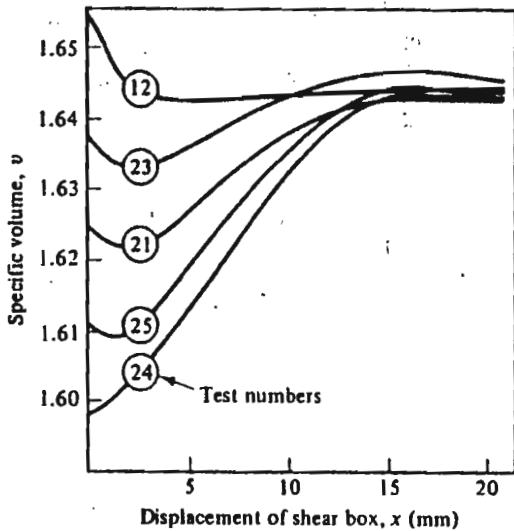


Figure 9-4 Relationship between specific volume  $v$  and relative shear displacement  $x$  of simple shear apparatus during shear tests on randomly packed steel balls (after Roscoe, Schofield, and Wroth, 1958)

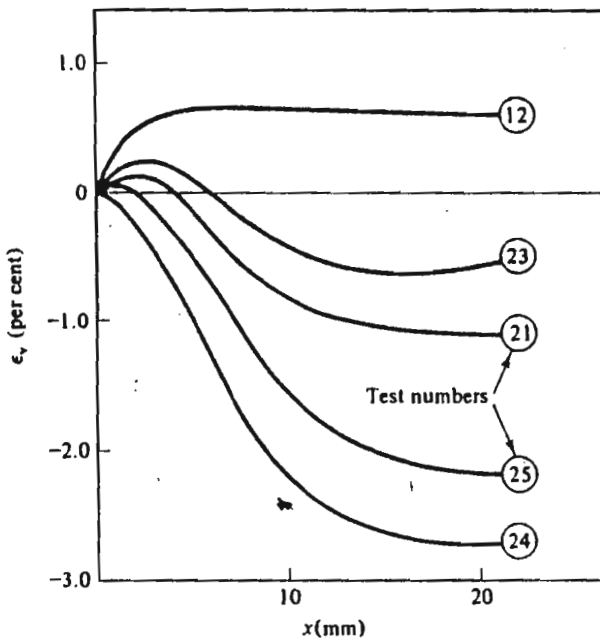


Figure 9-5 Relationship between volumetric strain  $\epsilon_v$  and relative shear displacement  $x$  of simple shear apparatus during shear tests on randomly packed steel balls (data from Roscoe, Schofield, and Wroth, 1958)



samples with widely different initial conditions. The essential point is that the volumetric strain  $\epsilon_v$  is computed not only from the volume changes that occur, but also from the initial volume of the sample. However, the initial volume of a sample is significant *for that sample alone*. Thus, in order to compare directly the behaviour of two or more samples it is essential to take account of their specific volumes.

The behaviour of a sample during a loading test may be recorded in a number of ways. For example, the results of standard triaxial compression tests are usually shown as the deviator stress  $q = q' = (\sigma_a - \sigma_r)$  plotted against axial strain  $\epsilon_a$  and as volume strain  $\epsilon_v$  or pore pressure  $u$  also plotted against axial strain. Alternatively, we could record the loading of a soil sample by plotting its stress path using appropriate axes, as described in Chapter 4, and by plotting the specific volume against the stress invariant  $p'$ , as we did for the isotropic and one-dimensional compression tests described in Chapter 7.

For our examination of the behaviour of soils in laboratory tests in the next few chapters we will describe the current *state* of the sample by the stress invariants  $q'$  and  $p'$  together with the specific volume  $v$ . Thus, we may record the history of loading of a sample by plotting its stress path with axes  $q'$  and  $p'$  where, for triaxial tests,

$$q' = (\sigma'_a - \sigma'_r) \quad (9-6)$$

and

$$p' = \frac{1}{3}(\sigma'_a + 2\sigma'_r), \quad (9-7)$$

and by plotting the specific volume  $v$  against  $p'$ . Later, in Chapter 10, we will discover how we may represent the state of a sample by plotting a single point in a space defined by axes  $q'$ ,  $p'$ , and  $v$ .

### 9-3 SIMPLE TESTS IN THE TRIAXIAL APPARATUS

The triaxial apparatus is extremely versatile and, by simultaneously changing the cell pressure and ram load, a wide variety of tests may be performed in the apparatus. The simplest test that can be performed on a sample is that of isotropic compression, as described in Chapter 7, in which the ram load is zero and the cell pressure is changed. ✓

The next simplest test to perform would be a test in which the cell pressure was held constant but the sample was compressed axially by a steadily increasing ram load. We might choose to allow the sample to drain freely to a burette, and so perform a standard drained test.

#### (i) Standard Drained Compression Tests

We will now examine the stress path followed by the sample during the test. Suppose that the sample is initially consolidated to  $p' = a$  and that

$u = 0$ , i.e., the cell pressure is  $a$  and the pore pressure is zero. The state of the sample would be represented by point A in Fig. 9-6(a), and, because  $u$  is zero, point A represents both total and effective stresses.

As the stresses on the sample increase, both  $q'$  and  $p'$  increase; we can relate changes  $\delta q'$ ,  $\delta p'$  in  $q'$  and  $p'$  to the change  $\delta\sigma_a$  in  $\sigma_a$  and  $\delta\sigma_r$  in  $\sigma_r$  as

$$\delta p' = \delta p = \frac{1}{3}(\delta\sigma_a + 2\delta\sigma_r), \tag{9-10}$$

$$\delta q' = \delta q = (\delta\sigma_a - \delta\sigma_r). \tag{9-11}$$

For a standard drained compression test, we hold the cell pressure constant (i.e.,  $\Delta\sigma_r = 0$ ) and so

$$\delta p' = \delta p = \delta\sigma_a/3, \tag{9-12}$$

$$\delta q' = \delta q = \delta\sigma_a, \tag{9-13}$$

and the slope of the total stress path is

$$dq/dp = 3. \tag{9-14}$$

A typical stress point at a late stage of the test is indicated as B on Fig. 9-6(a). We may also investigate the path followed in  $v : p'$  space (Fig. 9-6(b)). Unfortunately, we cannot specify the direction of the path A'B' unless we know the changes of specific volume which occur during the test, and this

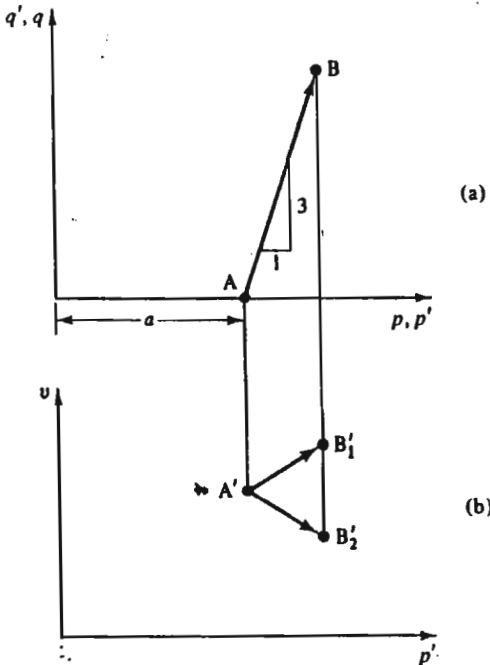


Figure 9-6 Test paths for a drained compression test in the triaxial apparatus

change of specific volume may be positive (e.g., path  $A'B'_1$ ) or it may be negative (e.g., path  $A'B'_2$ ). All we can say with certainty is that  $p'$  increases, and points  $B'_1, B'_2$  must lie somewhere on the projection at constant  $p'$  from the point B in  $q' : p'$  space.

The stress path is completely fixed in  $q' : p'$  space for a drained compression test. Samples must follow a line of slope 3 from the initial state A. The only question that remains is how far the samples progress up the stress path before failure intervenes. In contrast, the path is not fixed in  $v : p'$  space and depends on the magnitude (and sign) of the volume change that occurs.

(ii) Standard Undrained Tests

In a standard undrained compression test, we hold the cell pressure constant, increase the axial stress on the specimen, but do not allow any drainage to take place from the specimen. In consequence, the pore water pressure changes as the test proceeds and the sample responds to the changes of total stress at constant volume.

We should note that the *total* stress path applied to the sample is identical to that applied in a standard drained test, as indicated in Fig. 9-7. We note, as before, that  $\Delta\sigma_a$  is positive but that  $\Delta\sigma_r = 0$ . If we know how  $u$  varies as  $q'$  increases, the effective stress path can be sketched in Fig. 9-7, for we know

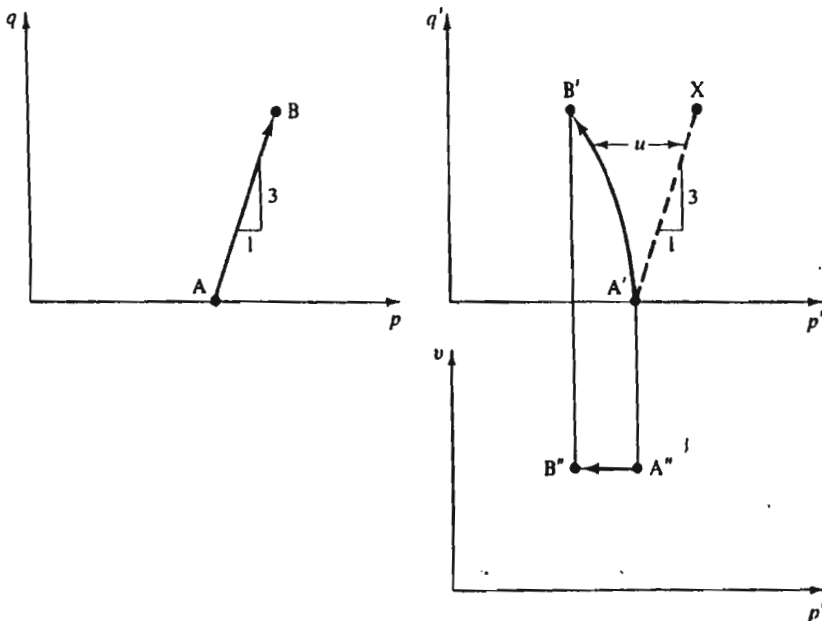


Figure 9-7 Test paths for an undrained compression test in the triaxial apparatus

that a positive pore water pressure  $u$  has the effect of shifting the effective stress point to the left by a distance equal to  $u$  from the total stress point (for  $p' = p - u$ ). By sketching in a line  $A'X$  of slope 3 through  $A'$  in effective stress space, we can mark the effective stress point  $B'$  for any known  $q'$  as being  $u$  to the left of  $A'X$ . We may then construct the stress path  $A'B'$  by considering different stages of the test.

The test path in  $v : p'$  space is straightforward, for, by definition, the specific volume  $v$  is constant in an undrained test. The test path is then simply a line at constant  $v$  from  $A''$  to  $B''$ , remembering again that points  $A''$ ,  $B''$  must project vertically down from points  $A'$ ,  $B'$  in  $q' : p'$  space.

### (iii) Other Tests

There are an enormous variety of other tests that may be performed in the triaxial apparatus. One such test might be a drained extension test, where  $\sigma_a$  was reduced, the cell pressure  $\sigma_r$  and pore pressure  $u$  being held constant, and so  $\sigma'_a < \sigma'_r$  at failure. The relevant drained stress path in  $q' : p'$  space is indicated in Fig. 9-8; for triaxial extension,  $q'$  becomes negative since  $\sigma'_a < \sigma'_r$  and the stress path is directed downwards with slope  $dq'/dp' = 3$ .

A second unusual test might be a drained test, where  $q'$  was increased and  $p'$  held constant; this could be achieved by reducing the cell pressure  $\sigma'_r$  at one half the rate the axial stress  $\sigma'_a$  was increased (i.e.,  $\Delta\sigma_r = -\Delta\sigma_a/2$ ,  $p' = \text{constant}$ ).

## 9-4 TYPICAL TEST RESULTS

We will now discuss the results of four typical tests on a particular soil so that we may have a framework against which we may discuss the shear behaviour of soil in more detail in the next Chapter.

We take test data from the classic series of tests performed on remoulded Weald clay at Imperial College, London, in the 1950s. These data are well known and will form the framework for much of our discussion of the shear

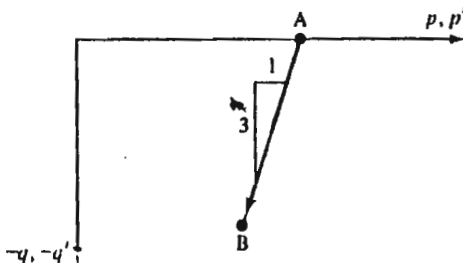


Figure 9-8 Test paths for a drained extension test in the triaxial apparatus

behaviour of soils, though confirmation of patterns of behaviour will be sought by recourse to published test data on other materials.

Two of the four tests we will discuss were drained and two were undrained, while two of the tests were performed on normally consolidated samples and two on overconsolidated samples. All samples were isotropically compressed after preparation by remoulding and were then either tested at once or allowed to swell isotropically before being tested.

### (i) Normally Consolidated Samples

The two samples we shall consider were isotropically compressed to  $207 \text{ kN m}^{-2}$  at which point their specific volumes were 1.632 ( $w = 23$  per cent). Sample A was then subjected to a standard drained compression test and the observed relationships between  $q'$  and  $\epsilon_a$  and  $\epsilon_v$  and  $\epsilon_a$  are shown in Fig. 9-9. The axial strain is over 20 per cent at failure, and there is a relatively large (4 per cent) compression of the sample. We can represent the test path in  $q' : p'$  and  $v : p'$  space as in Fig. 9-10. The  $q' : p'$  path is straight and of slope 3, while the compression of the sample implies that  $v$  decreases substantially as  $p'$  increases.

The second sample B was subjected to a standard undrained test after consolidation to  $207 \text{ kN m}^{-2}$ . The relationships between  $q'$  and  $\epsilon_a$  and the

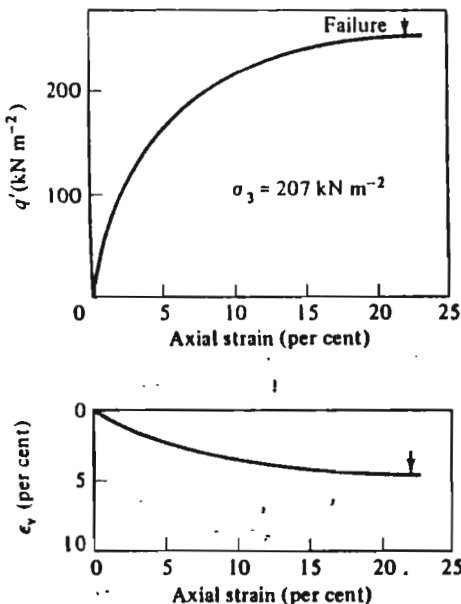


Figure 9-9 Test data from a drained compression test on a normally consolidated sample of Weald clay (Sample A) (after Bishop and Henkel, 1962, p. 128)

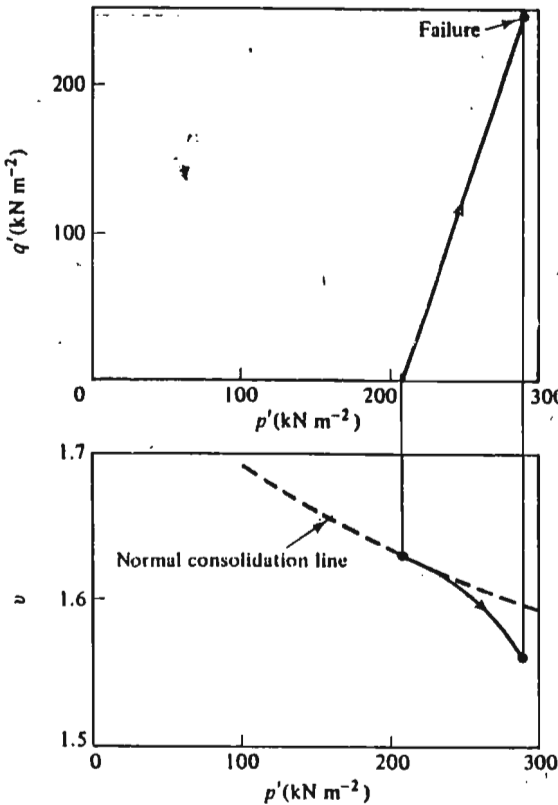


Figure 9-10 Test paths in  $q' : p'$  and  $v : p'$  spaces for the drained test on sample A (see Fig. 9-9)

change  $\Delta u$  in pore water pressure and  $\varepsilon_v$  are shown in Fig. 9-11. Again, there are large strains to failure (greater than 15 per cent) but now, because the reduction in volume that occurs in the drained test is no longer permitted, a relatively large positive pore water pressure is generated. This positive pore water pressure reduces the effective stress  $p'$  in the sample and so in some way compensates for the reduction in volume that would have occurred had volume change been allowed. The deviator stress at failure is  $119 \text{ kN m}^{-2}$  and so is about one half of that observed in the drained test on an identical specimen. The stress path is shown in  $q' : p'$  and  $v : p'$  space in Fig. 9-12.

## (ii) Overconsolidated Samples

The two overconsolidated samples we shall discuss were initially isotropically compressed to  $827 \text{ kN m}^{-2}$  and then allowed to swell to a pressure of  $34.5 \text{ kN m}^{-2}$ . The overconsolidation ratio  $R_p$  was, therefore, 24. The

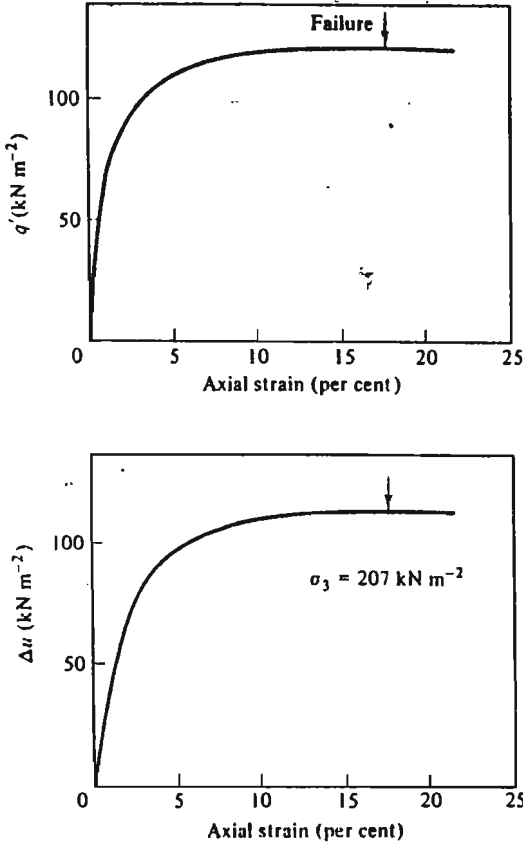


Figure 9-11 Test data from an undrained compression test on a normally consolidated sample of Weald clay (Sample B) (after Bishop and Henkel, 1962, p. 115)

water content of the samples was 22.7 per cent and so was almost identical to that of the normally consolidated samples (23 per cent). The difference between the two pairs of samples was, then, simply the difference in stress history.

One of the overconsolidated samples (Sample C) was subjected to a standard drained compression test. The relationships between  $q'$  and  $\epsilon_a$  and  $\epsilon_v$  and  $\epsilon_a$  are shown in Fig. 9-13. It is immediately obvious that sample C behaves very differently from the normally consolidated sample A (see Fig. 9-9). The  $q' : \epsilon_a$  curve for test C shows a clear peak which occurs at the smaller strain of  $\epsilon_a = 8$  per cent. However, the most striking difference between the two  $q' : \epsilon_a$  curves is that the maximum value of  $q'$  for the test on the overconsolidated sample (C) is  $56 \text{ kN m}^{-2}$ , while it is  $247 \text{ kN m}^{-2}$  for the test on the normally consolidated sample (A).

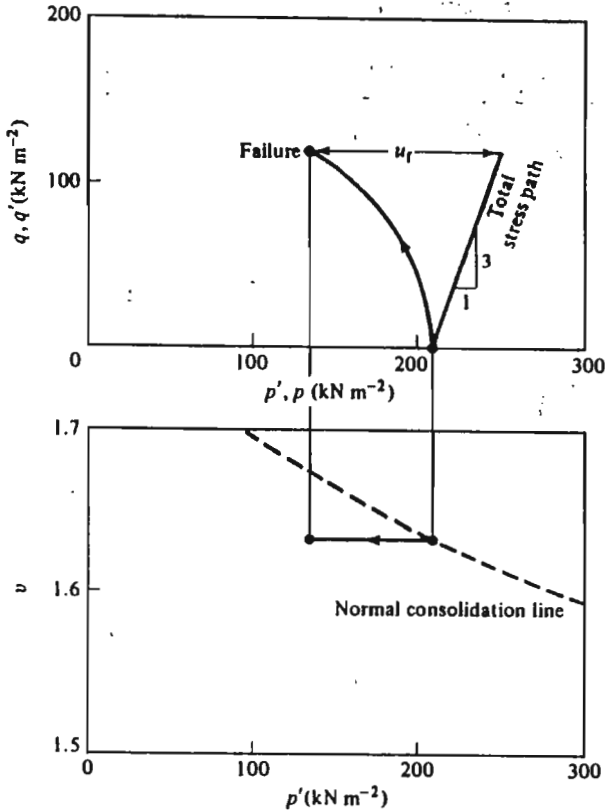


Figure 9-12 Test paths in  $q' : p'$  and  $v : p'$  spaces for the undrained test on sample B (see Fig. 9-11)

The volumetric strain curve is also distinctly different from that observed for the normally consolidated sample. The overconsolidated sample (C) contracts initially but then dilates strongly, so that by the end of the test, the sample has expanded by nearly 3 per cent.

One consequence of the shape of the  $q' : \epsilon_a$  curve is that we might expect that the deformation of the specimen will become non-uniform after failure at point F, Fig. 9-13. Elements of soil which have strained more than  $(\epsilon_a)_F$  will be weaker than elements of soil which have strained less than  $(\epsilon_a)_F$  and so deformation will be concentrated in those elements of soil which have already failed. We must, therefore, be suspicious of results obtained using boundary measurements of force and displacement to compute the stresses and strains in the most deforming region of the samples.

The stress paths in  $q' : p'$  and  $v : p'$  spaces are shown in Fig. 9-14. As before, the stress path is straight in  $q' : p'$  space and of slope 3, but now the



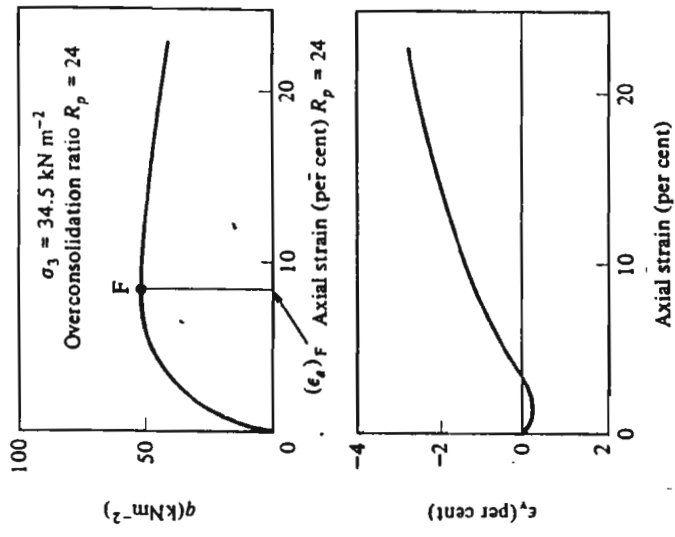


Figure 9-13 Test data from a drained compression test on an overconsolidated sample of Weald clay (Sample C) (after Bishop and Henkel, 1962, p. 128)

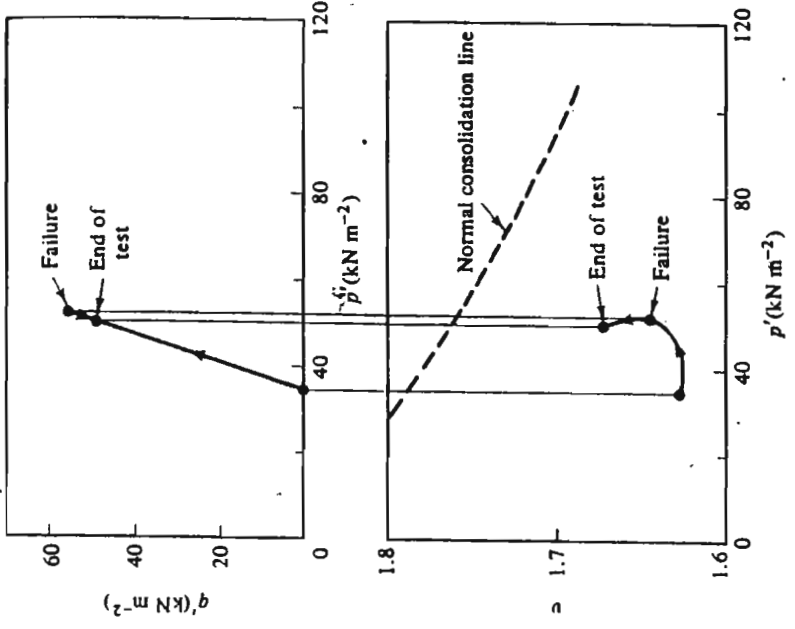


Figure 9-14 Test paths in  $q' : p'$  and  $v' : p'$  spaces for the drained test on Sample C (see Fig. 9-13)

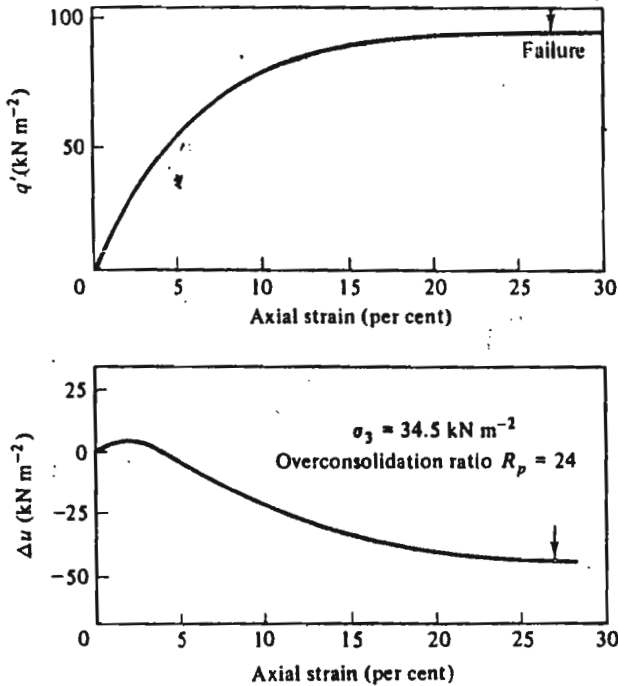


Figure 9-15 Test data from an undrained compression test on a sample of Weald clay (Sample D) (after Bishop and Henkel, 1962, p. 116)

sample follows a path which rises to a maximum value of  $q'$ , and then returns to a lower value of  $q'$  at the end of the test. We must, therefore, be careful to distinguish the failure point from the point corresponding to the end of the test.

The second overconsolidated sample (Sample D) was subjected to a standard undrained test. Observed relationships between  $q'$  and  $\epsilon_a$  and the change  $\Delta u$  in pore water pressure and  $\epsilon_a$  are shown in Fig. 9-15. The shape of the  $q' : \epsilon_a$  curve is similar to that observed for the normally consolidated sample (B), with large strains being required to fail the specimen, and the failure value of  $q'$  ( $95 \text{ kN m}^{-2}$ ) is comparable with the value ( $119 \text{ kN m}^{-2}$ ) observed for Sample B. The shape of the  $\Delta u : \epsilon_a$  curve is very similar to the shape of the  $\epsilon_v : \epsilon_a$  curve observed for the drained test on the overconsolidated sample (C), again suggesting that the change in pore water pressure in an undrained test is a different manifestation of the same physical phenomenon which gives rise to volume changes in a drained test.

The stress paths are plotted in  $q' : p'$  and  $v : p'$  spaces in Fig. 9-16. As before, it is easiest to construct the effective stress path in  $q' : p'$  space by offsetting the path by  $u$  to the left of the total stress path, which rises at slope 3 from the point representing the initial state of the sample. At failure, the

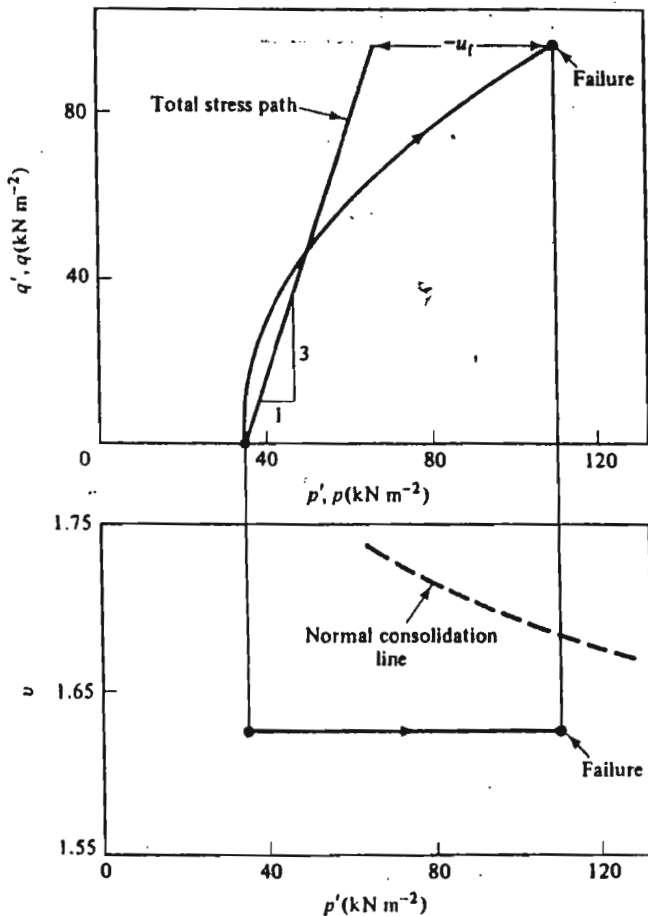


Figure 9-16 Test paths in  $q' : p'$  and  $v : p'$  spaces for the undrained test on Sample D (see Fig. 9-15)

effective stress path is to the right of the total stress path as the pore water pressure is then negative.

The stress path is easy to plot in  $v : p'$  space, for, again,  $v$  remains constant in an undrained test, and the  $p'$  values may be obtained by projection from the  $q' : p'$  diagram.

### 9-5 PATTERNS OF BEHAVIOUR; SUMMARY OF MAIN POINTS

We have now considered four typical triaxial compression tests on samples of clay all isotropically compressed to (nearly) the same specific volume.

It is striking that we have observed that one sample contracts during shear, one expands, one sample causes the pore water pressure to rise during shear, and one causes it to reduce. The maximum values of  $q'$  range from 56 to 247 kN m<sup>-2</sup>, though we note that the two undrained specimens had nearly the same strength at failure. One sample exhibited a strength which reached a peak, and then reduced as straining continued, the rest had  $q' : \epsilon_a$  curves with flat maxima. Thus, even for these simple, standard tests, we have a wide range of stress paths in  $q' : p'$  and  $v : p'$  space; no doubt an even wider variety would be observed had we chosen to consider more complex testing procedures.

The differences in behaviour that are observed may seem bewildering in their variety. It is the objective of the next two chapters to suggest how all the test data we have considered may be combined into a neat and coherent whole.

## REFERENCES

- Bishop, A. W. and Henkel, D. J. *The Triaxial Test*. Edward Arnold, London, 1962.  
 Roscoe, K. H., Schofield, A. N., and Wroth, C. P. On the yielding of soils. *Geotechnique*, 8, 22-53, 1958.

THE CRITICAL STATE LINE AND THE  
ROSCOE SURFACE

10-1 INTRODUCTION

The objective of this chapter is to find a way of unifying the observed shearing behaviour of clay into a coherent whole. It is convenient at first only to discuss normally consolidated specimens, but the same ideas will be discussed for overconsolidated specimens in Chapter 11.

10-2 FAMILIES OF UNDRAINED TESTS

We considered a single undrained triaxial compression test on a normally consolidated specimen of clay in Chapter 9 (Figs 9-11 and 9-12). We can now consider the results of undrained triaxial tests on a family of isotropically

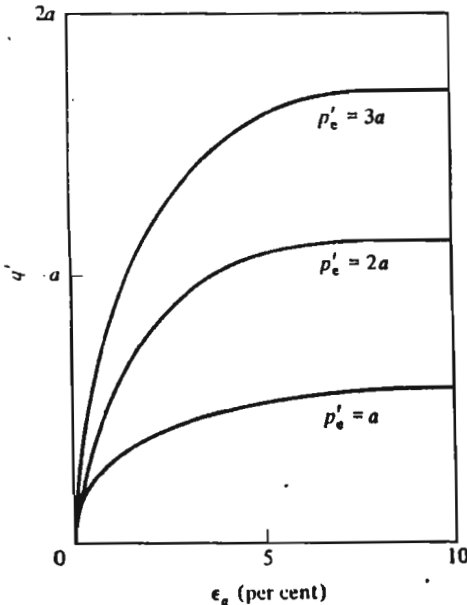


Figure 10-1 Relationship between deviator stress  $q'$  and axial strain  $\epsilon_a$  in undrained triaxial tests on samples normally consolidated to  $p'_c = a, 2a, 3a$

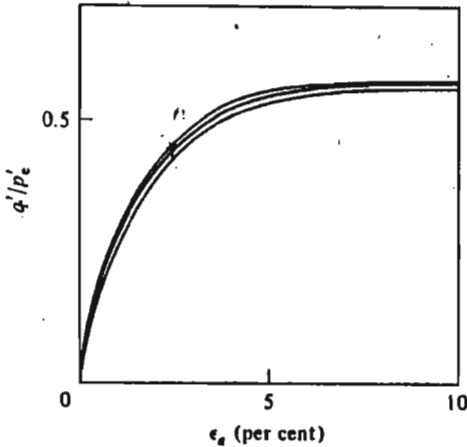


Figure 10-2 Relationship between normalized deviator stress  $q'/p'_0$  and axial strain  $\epsilon_a$  for the tests shown in Fig. 10-1

compressed specimens, each specimen being compressed to a different initial value of  $p'$  (equal to  $a$ ,  $2a$ , and  $3a$ , respectively) and denoted by  $p'_0$ . It is found that the stress-strain curves are of the form illustrated in Fig. 10-1. The specimens which were compressed to higher values of  $p'$  sustain higher values of  $q'$  at failure, but the *shape* of the  $q' : \epsilon_a$  curves are similar for all tests. Thus, it is possible to normalize the curves by plotting  $q'/p'_0$  against  $\epsilon_a$ , as shown in Fig. 10-2. The stress paths followed by a family of such tests may be represented in  $q' : p'$  space as indicated in Fig. 10-3(a). We find that the shapes of the different stress paths are similar, suggesting that all curves could be collapsed into one by plotting  $q'/p'_0$  against  $p'/p'_0$ . We will not pursue this point at this stage, but we will concentrate instead on the conditions at failure. The paths followed by the tests are illustrated in  $v : p'$  space in Fig. 10-3(b). Samples start out from the normal consolidation line  $A_1 A_2 A_3$  and travel to the left until failure occurs at points  $B_1, B_2, B_3$ .

The failure points  $B_1-B_3$  define a straight line in the  $q' : p'$  space of Fig. 10-3(a) and a smooth curve, apparently of similar shape to the normal consolidation line, in the  $v : p'$  space of Fig. 10-3(b).

### 10-3 FAMILIES OF DRAINED TESTS

We will now consider drained triaxial compression tests on a family of samples of clay isotropically normally consolidated to different initial values  $p'_0$  of the mean normal stress. The observed relationships between  $q'$  and  $\epsilon_a$  and  $\epsilon_v$  and  $\epsilon_a$  are found to be as sketched in Fig. 10-4, with the  $\epsilon_v : \epsilon_a$  curves being similar for all tests. Again, the  $q' : \epsilon_a$  curves are all of the same shape, and samples which have been compressed to higher stresses

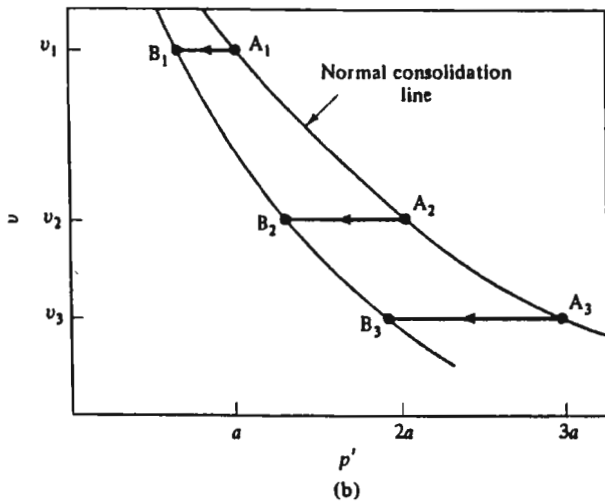
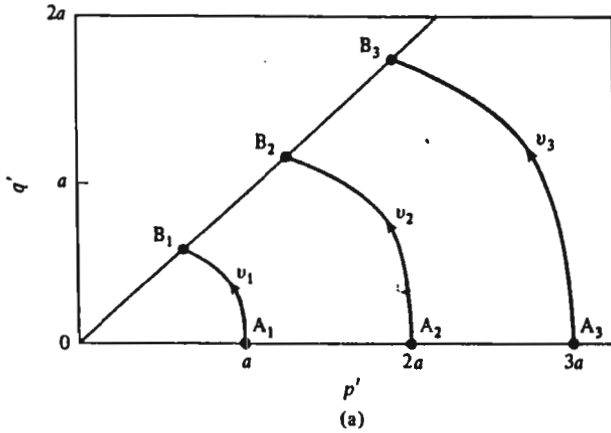


Figure 10-3 Stress paths in (a)  $q' : p'$  and (b)  $v : p'$  space for undrained tests on normally consolidated samples

exhibit higher values of  $q'$  at failure. The curves of Fig. 10-4 may be normalized by plotting  $q'/p'_0$  against  $\epsilon_a$ , as shown in Fig. 10-5; it is found that data obtained in tests at different pressures all fall close to a single curve.

Stress paths for such a series of tests are shown in  $q' : p'$  and  $v : p'$  spaces in Fig. 10-6. As expected, all the test paths are straight in  $q' : p'$  space and rise at slope 3 from the initial value  $p'_0$  of the mean normal effective stress for each sample. The samples fail (i.e., there is no further change in stress, or volume, as large shear distortions occur) at values of  $q'$  and  $p'$  which define

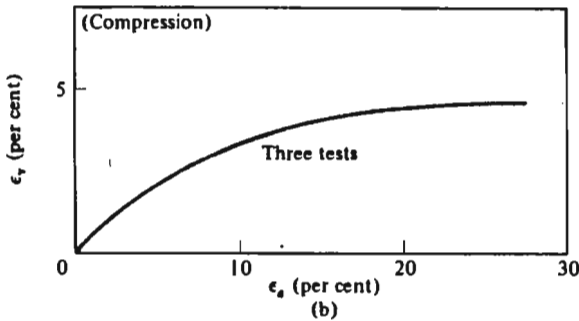
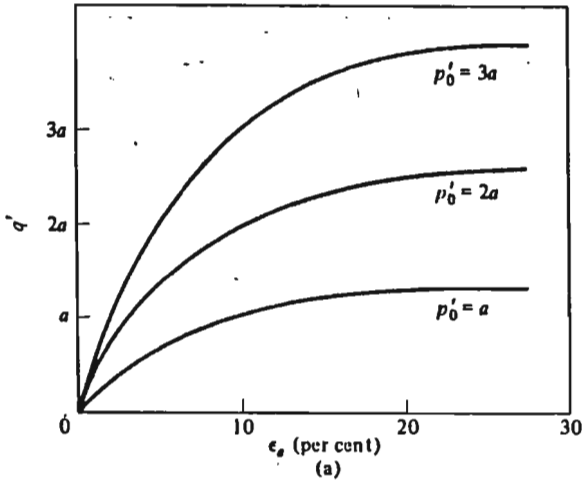


Figure 10-4 Relationship between (a) deviator stress  $q'$  and axial strain  $\epsilon_a$  and (b) volumetric strain  $\epsilon_v$  and axial strain  $\epsilon_a$  in drained triaxial tests on samples isotropically normally consolidated to  $p'_0 = a, 2a, 3a$

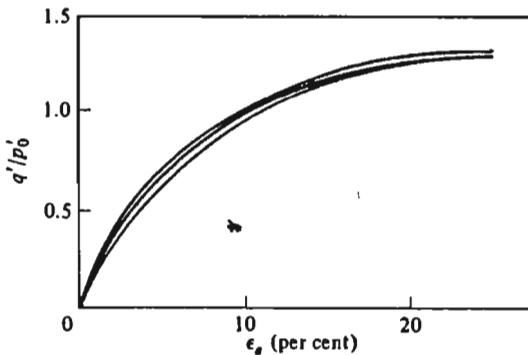


Figure 10-5 Relationship between normalized deviator stress  $q'/p'_0$  and axial strain  $\epsilon_a$  for tests shown in Fig. 10-4



a straight line in  $q' : p'$  space. The test paths are curved in  $v : p'$  space, with each sample compressing as  $p'$  increases. The failure points  $B_1-B_3$  define a smooth curve which appears to be of similar shape to the normal consolidation line.

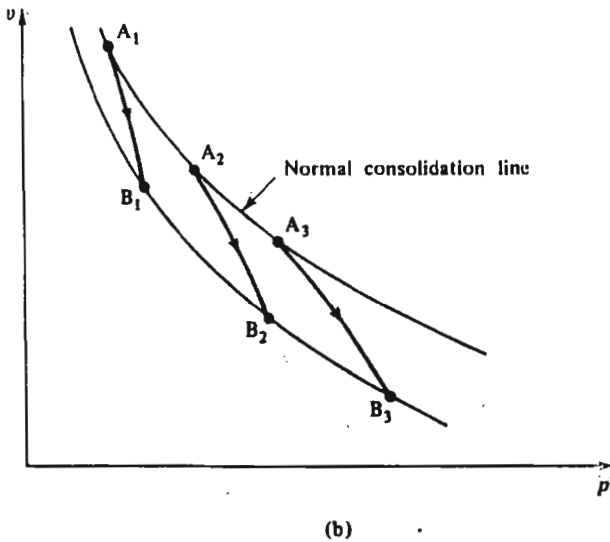
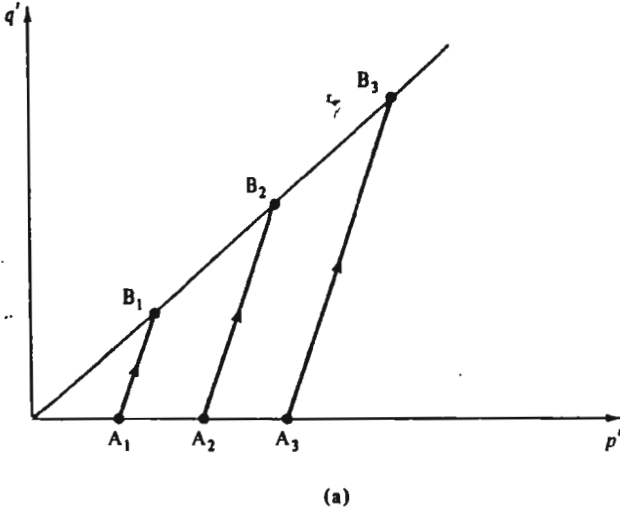


Figure 10-6 Stress paths in (a)  $q' : p'$  and (b)  $v : p'$  space for drained triaxial tests on normally consolidated samples

## 10-4 THE CRITICAL STATE LINE

We have now considered separately the failure of clay samples which were initially isotropically compressed and then loaded in drained and undrained triaxial compression tests. It is striking that the lines of failure points in Figs 10-3 and 10-6 appear to be similar for the two families of tests and it is instructive to compare these directly. Figure 10-7 shows the failure states of drained and undrained triaxial compression tests on isotropically compressed samples of Weald clay, as reported by Parry (1960). Plotted together,

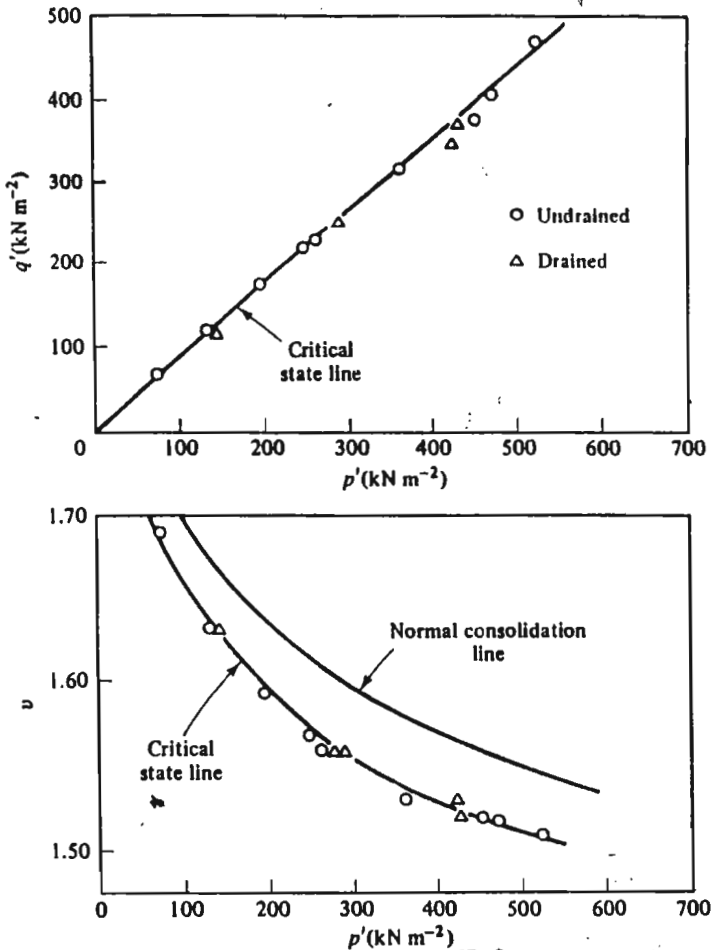


Figure 10-7 Failure points for drained and undrained tests on normally consolidated specimens of Weald clay (data from Parry, 1960)

the data points define a single straight line through the origin in  $q' : p'$  space and a single curved line in  $v : p'$  space whose shape is similar to the normal consolidation line.

This single and unique line of failure points of both drained and undrained tests is defined as the *critical state line*. Its crucial property is that failure of initially isotropically compressed samples will occur once the stress states of the samples reach the line, irrespective of the test path followed by the samples on their way to the critical state line. Failure will be manifested as a state at which large shear distortions occur with no change in stress, or in specific volume.

The projection of the critical state line onto the  $q' : p'$  plane in Fig. 10-7 may be described by

$$q' = Mp', \quad (10-1)$$

where  $M$  (capital mu) is its gradient. The projection of the critical state line onto the  $v : p'$  plane in Fig. 10-7 is curved. However, if the same data are replotted with axes  $v : \ln p'$ , the points fall close to a straight line, as shown in Fig. 10-8. It is highly convenient that the gradient of this line turns out to be the same as the gradient of the corresponding normal consolidation line discussed in Chapter 7. The critical state line may be described by

$$v = \Gamma - \lambda \ln p' \quad (10-2)$$

and Eq. 10-2 may be compared with Eq. 7-7 for the normal consolidation line. In Eq. 10-2,  $\Gamma$  (capital gamma) is defined as the value of  $v$  corresponding to  $p' = 1.0 \text{ kN m}^{-2}$  on the critical state line†; thus  $\Gamma$  locates the critical state line in the  $v : \ln p'$  plane in the same way that  $N$  located the normal compression line. Equations (10-1) and (10-2) together define the position of the critical state line in  $q' : p' : v$  space;  $M$  and  $\Gamma$ , like  $N$ ,  $\lambda$ , and  $\kappa$  are regarded as soil constants. Typical values of these for various clay soils are contained in Table 10-1.

**Table 10-1 Values of soil constants for various clays**  
(after Schofield and Wroth, 1968, p. 157)

	London clay	Weald clay	Kaolin
$\lambda$	0.161	0.093	0.26
$\kappa$	0.062	0.035	0.05
$\Gamma$	2.759	2.060	3.767
$M$	0.888	0.95	1.02

Note: the value of  $\Gamma$  is that for  $p' = 1.0 \text{ kN m}^{-2}$ .

† We should note that although  $\Gamma$ , like  $N$ , is itself dimensionless, its value will depend on the units chosen for the measurement of  $p' = 1.0$ ; the values contained in Table 10.1 are for  $p' = 1.0 \text{ kN m}^{-2}$ .

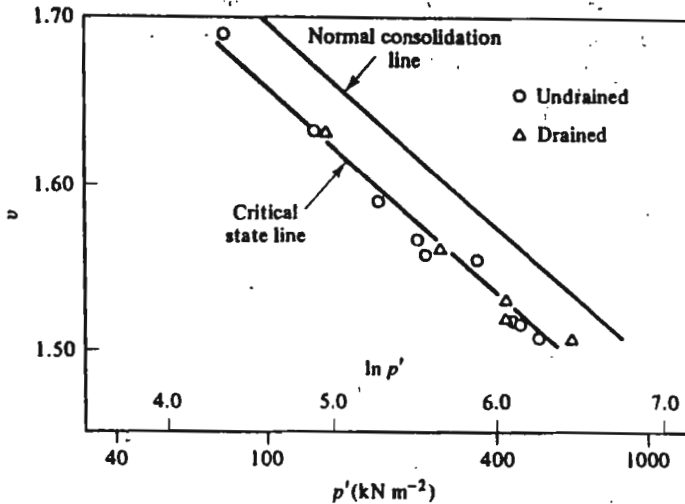


Figure 10-8 The critical state line in  $v : \ln p'$  space (data from Parry, 1960)

The position of the critical state of a soil sample is a function of  $q'$ ,  $p'$ , and  $v$ , and so it is often helpful to think of the critical state line in a three-dimensional  $q' : p' : v$  space, as sketched in Fig. 10-9. The normal isotropic consolidation line is shown in the  $q' = 0$  plane, i.e., on the 'floor' of the  $q' : p' : v$  space. The critical state line rises (i.e.,  $q'$  increases) as  $p'$  increases and  $v$  decreases. The projections of points ABC on the critical state line are shown as points  $A_1$ ,  $B_1$ , and  $C_1$  in the plane containing the  $q'$  and  $p'$  axes and as points  $A_2$ ,  $B_2$ , and  $C_2$  on the  $q' = 0$  plane.

### 10-5 'DRAINED' AND 'UNDRAINED' PLANES

The test paths followed in standard triaxial tests may also be represented in  $q' : p' : v$  space. It is easiest to consider undrained tests first. A typical sample might be isotropically compressed to point A (Fig. 10-10) and then subjected to a standard undrained triaxial compression test until it fails at a point B on the critical state line. The test path can be projected into  $q' : p'$  space and is shown as path  $A_1 B_1$ . The test is undrained, and so, by definition, the specific volume  $v$  is constant. The specific volume at point B must, therefore, be the same as that at point A, and indeed  $v$  must remain constant for the whole test path from A to B. The test path must therefore remain in the shaded constant  $v$  plane ACDE (Fig. 10-10) which is parallel to the plane containing the  $q', p'$  axes. We may loosely think of plane ACDE as the 'undrained plane' through A.

The point B represents the intersection of the undrained plane ACDE and the critical state line. Thus, if the initial conditions of the sample are

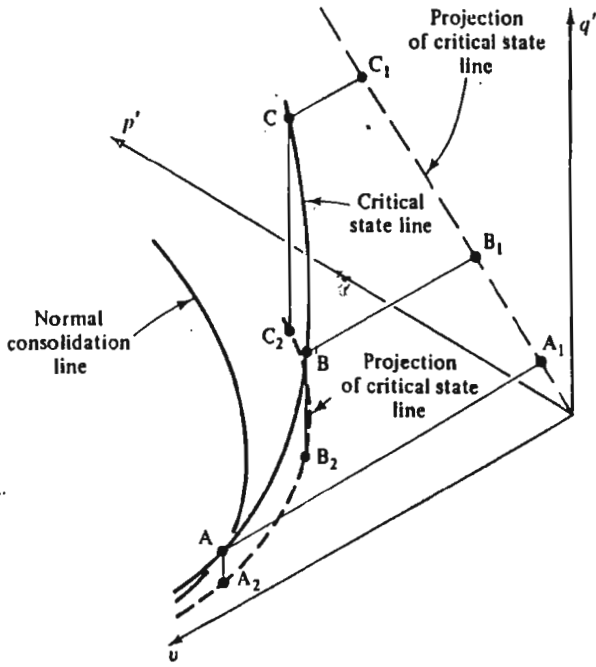


Figure 10-9 The critical state line in  $q' : p' : v$  space

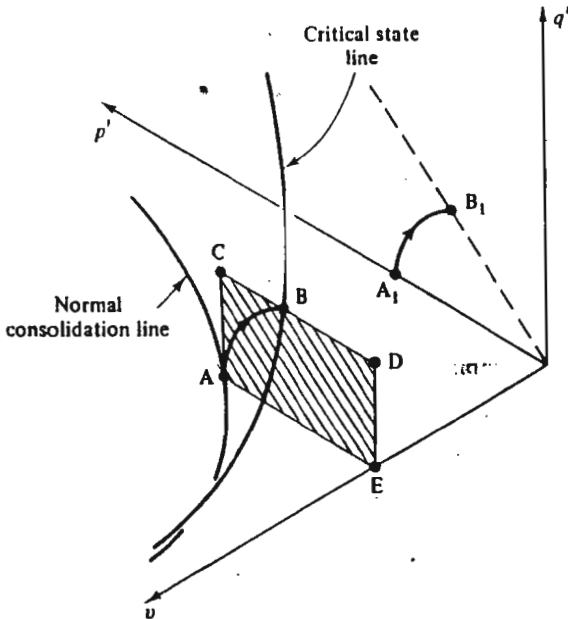


Figure 10-10 The path followed by an undrained test in  $q' : p' : v$  space

fixed at point A, and we know the test is to be undrained, we need only to construct the undrained plane through A in order to fix the failure conditions for the sample as the intersection of the critical state line and the undrained plane (i.e., point B). In other words, the initial state of the sample and the test conditions completely determine the precise point on the critical state line at which the sample will fail.

This argument may be expressed mathematically. Suppose that a sample is isotropically compressed to a mean normal effective stress of  $p'_0$  and a specific volume of  $v_0$  and we wish to find the values of the stresses  $q'_t$  and  $p'_t$  and specific volume  $v_t$  of the sample at failure in a standard undrained triaxial compression test. We first note that

$$v_0 = v_t. \quad (10-4)$$

We may then determine  $p'_t$  from Eq. (10-2) as

$$p'_t = \exp[(\Gamma - v_0)/\lambda] \quad (10-5)$$

and the value of  $q'_t$  follows, using Eq. (10-1), as

$$q'_t = M \exp[(\Gamma - v_0)/\lambda]. \quad (10-6)$$

#### Example 10-1 Calculation of the failure conditions in an undrained test

The values of the soil constants for a clay are  $N = 3.25$ ,  $\lambda = 0.20$ ,  $\Gamma = 3.16$ , and  $M = 0.94$ . A sample of the clay is isotropically normally consolidated to  $p' = 400 \text{ kN m}^{-2}$  and is then subjected to a standard undrained triaxial compression test. Calculate the values of  $q'$ ,  $p'$ , and  $v$  at failure.

For normal consolidation, from Eq. (7-7),

$$v_0 = N - \lambda \ln p'_0 = 3.25 - 0.20 \ln(400),$$

$$v_0 = 2.0517.$$

For an undrained test,  $\Delta v = 0$ . Hence,  $v_t = v_0$  and, at failure,

$$v_t = 2.0517.$$

At failure, from Eq. (10-6),

$$q'_t = M \exp[(\Gamma - v_0)/\lambda] = 0.94 \exp[(3.16 - 2.0517)/0.2],$$

$$q'_t = 240 \text{ kN m}^{-2}.$$

and, from Eq. (10-1),

$$p'_t = q'_t/M = 240/0.94,$$

$$p'_t = 255 \text{ kN m}^{-2}.$$

The test path for a standard drained triaxial compression test ( $\Delta\sigma_v = 0$ ) rises at a slope of 3 in  $q' : p'$  space from the initial value  $p'_0$  of mean normal effective stress at  $q' = 0$ . The sample may compress (or dilate) and so the specific volume changes. The plane in which drained tests lie must therefore be parallel to the  $v$ -axis and must have a projection in  $q' : p'$  space which is a straight line of slope 3; the 'drained plane'  $ACB_1A_1$ , is shown shaded in Fig. 10-11. The initial state of the sample on the normal consolidation line is shown as point A and the test path ends at failure on the critical state line at B. The projection of the test path is shown as  $A_1B_1$  on the  $q' : p'$  plane. The exact shape of the test path within the drained plane  $ACB_1A_1$  will depend on the experimental relationship between volume change and increase of  $q'$  as the test proceeds. However, *whatever* that relationship, the path AB must remain within the plane  $ACB_1A_1$ .

If the initial conditions of the sample are specified as those at A, and it is known that the test is to be a standard drained triaxial compression test, the point at which the specimen fails is fixed unambiguously as the intersection of the drained plane and the critical state line (i.e., point B). Location of point B then becomes an exercise in simple geometry. Again, we can proceed mathematically. Suppose that the sample is initially compressed to

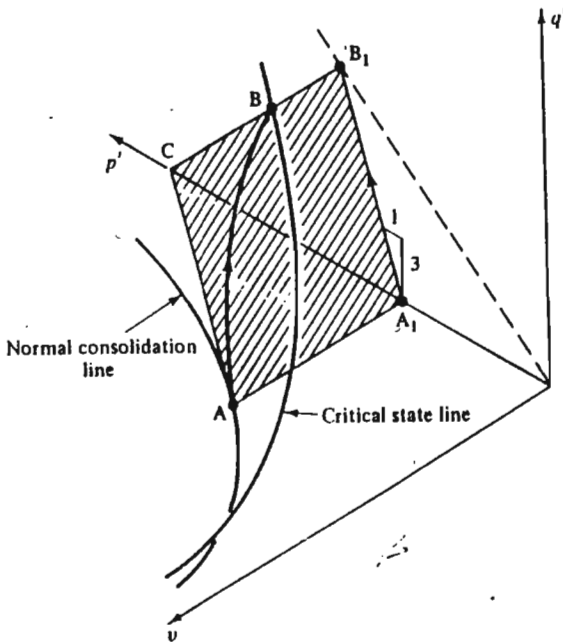


Figure 10-11 The path followed by a drained test in  $q' : p' : v$  space

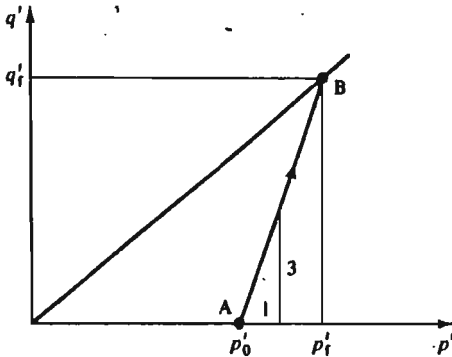


Figure 10-12 The path followed by a drained test in  $q' : p'$  space

a mean normal effective stress of  $p'_0$  and specific volume of  $v_0$  and we wish to find the stresses  $q'_t, p'_t$ , and the specific volume  $v_t$  at failure. From the geometry of Fig. 10-12 we may write

$$q'_t = 3(p'_t - p'_0), \quad (10-7)$$

while we have

$$q'_t = Mp'_t. \quad (10-8)$$

Combination of Eqs (10-7) and (10-8), eliminating  $p'_t$ , gives

$$q'_t = 3Mp'_0/(3 - M). \quad (10-9)$$

Using Eq. (10-8), we find

$$p'_t = 3p'_0/(3 - M) \quad (10-10)$$

and, hence, we may obtain the specific volume  $v_t$  from Eq. (10-2) as

$$v_t = \Gamma - \lambda \ln [3p'_0/(3 - M)]. \quad (10-11)$$

### Example 10-2 Calculation of the failure conditions in a drained test

The values of the soil constants for a clay are  $N = 3.25$ ,  $\lambda = 0.20$ ,  $\Gamma = 3.16$ , and  $M = 0.94$ . A sample of the clay is isotropically normally consolidated to  $400 \text{ kN m}^{-2}$ , where  $v_0 = 2.052$ , and is then subjected to a standard drained compression test. Calculate the values of  $q'$ ,  $p'$ ,  $v$ , and  $\epsilon_v$  at failure.

At failure, from Eq. (10-9),

$$\begin{aligned} q'_t &= 3Mp'_0/(3 - M) = 3 \times 0.94 \times 400/(3 - 0.94), \\ q'_t &= 548 \text{ kN m}^{-2} \end{aligned}$$



and, from Eq. (10-1),

$$p'_t = q'_t/M = 548/0.94,$$

$$p'_t = 583 \text{ kN m}^{-2}.$$

From Eq. (10-2),

$$v_t = \Gamma - \lambda \ln p'_t = 3.16 - 0.20 \ln(583),$$

$$v_t = 1.886.$$

The volumetric strain  $\varepsilon_v$  during the test is

$$\varepsilon_v = -\Delta v/v_0 = -(1.886 - 2.052)/2.052,$$

$$\varepsilon_v = 8.09 \text{ per cent.}$$

We have now demonstrated that given (i) the initial conditions of a sample, (ii) the position of the critical state line (i.e., the values of the constants  $M$ ,  $\Gamma$ , and  $\lambda$ ), and (iii) the conditions of the triaxial test (drained or undrained), the failure state of the sample is uniquely determined. Of course, the reasoning could be extended to cover a whole range of tests (e.g., extension tests,  $p'$  constant tests). Indeed, if we know the position of the critical state line, we only need to know the value of one variable ( $p'$ ,  $q'$ , or  $v$ ) at failure in order to fix the values of the other two.

It is clear, therefore, that a knowledge of the position of the critical state line for a particular soil allows us to predict with confidence the stresses and specific volumes at failure of normally consolidated samples subjected to a variety of stress paths.

## 10-6 THE ROSCÖE SURFACE

We have established that for a particular value of  $p'_0$ , we may construct the relevant undrained or drained plane over which the test path moves as the sample progresses to failure. Of course, there will be different drained or undrained planes for each different value of  $p'_0$ . Undrained planes are shown for four different values of  $p'_0$  in Fig. 10-13 and drained planes are shown for two values of  $p'_0$  in Fig. 10-14. In each case, the relevant test path from the normal consolidation line to the critical state line is also shown. Both the undrained tests and the drained tests seem to define a curved three-dimensional surface linking the normal consolidation line to the critical state line. The undrained test paths are especially helpful in defining the surface, for each test path traces out a section of the surface at constant  $v$ . The drained tests follow paths which cut across the undrained paths, for the samples compress as the test proceeds, see Fig. 10-15.

It is tempting to ask if the families of undrained and drained tests on normally consolidated samples define the same three-dimensional surface in

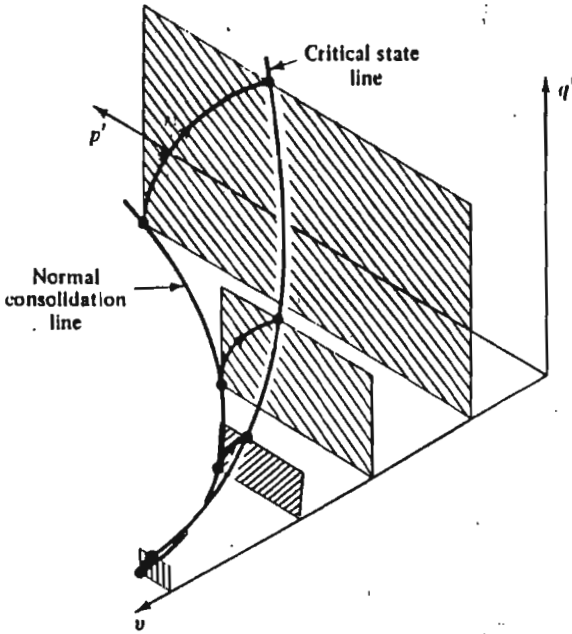


Figure 10-13 Four undrained planes in  $q' : p' : v$  space

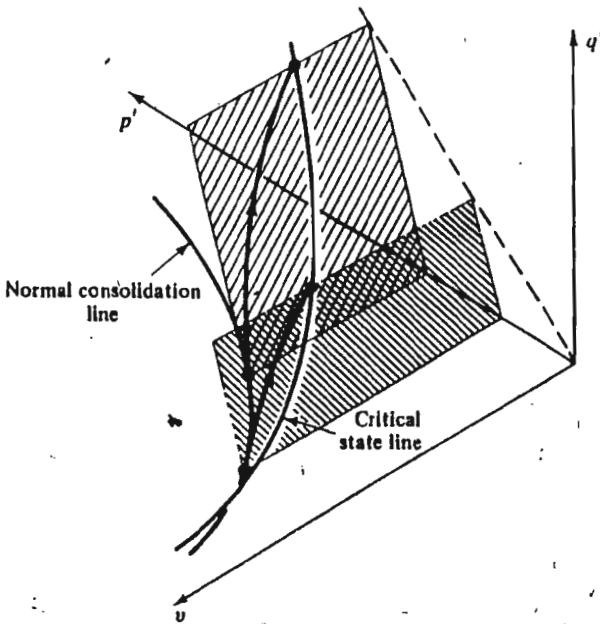


Figure 10-14 Two drained planes in  $q' : p' : v$  space

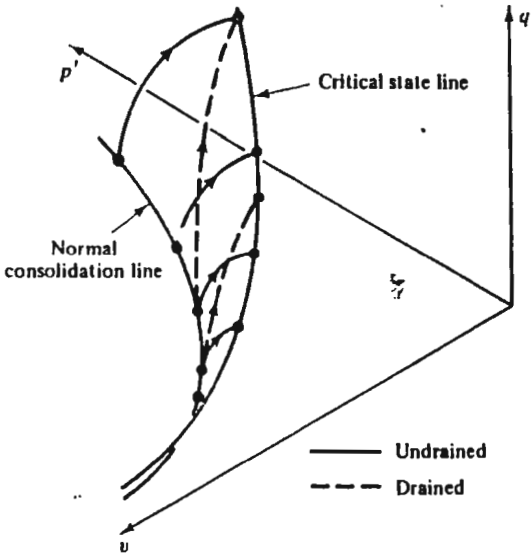


Figure 10-15 Families of drained and undrained tests in  $q' : p' : v$  space

$q' : p' : v$  space. Clearly, it is reasonable that they should, for both drained and undrained tests start from the normal consolidation line and finish at the critical state line. One way of checking whether the surface is unique is to investigate whether samples in the course of drained or undrained tests have the same specific volumes when they are subjected to the same effective stresses. Thus, in Fig. 10-16, we should investigate whether the normally consolidated sample tested drained with an effective stress path ABC has the

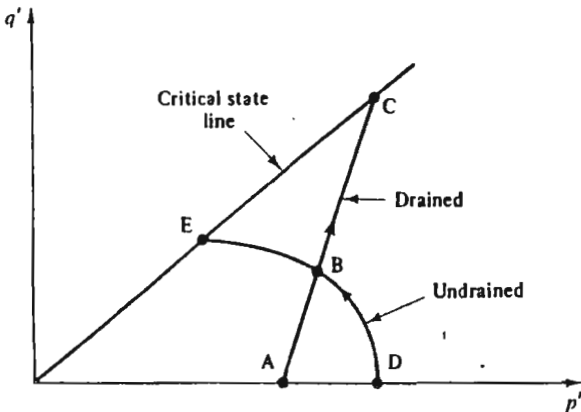


Figure 10-16 Drained and undrained paths in  $q' : p'$  space

same specific volume at B as the normally consolidated sample tested undrained along the effective stress path DBE. If the two specific volumes were the same, we would have encouragement that the surfaces followed by drained and undrained tests were the same, but we would then want to check this finding for a large number of other tests.

A more systematic procedure would be to perform a series of drained tests on normally consolidated samples and, from the specific volumes measured at different stage of the tests, construct a series of contours of constant  $v$  in  $q' : p'$  space, as sketched in Fig. 10-17. The undrained test paths in  $q' : p'$  space are themselves contours of constant  $v$ , see Fig. 10-3 for example. The check as to whether there was a single surface in  $q' : p' : v$  space for both drained and undrained tests would then be whether the two sets of contours (one from drained tests, one from undrained) were of the same shape and were consistent with one another, as shown in Fig. 10-18.

Henkel (1960), following the approach of Rendulic (1936), plotted contours of constant water content in a plane with  $\sigma'_n, \sqrt{2}\sigma'_r$ -axes for both drained and undrained tests, see Fig. 10-19. Of course, this comparison is exactly equivalent to the comparison of Fig. 10-18. It is clear that the contours obtained from drained and undrained tests are entirely consistent with each other and are of the same shape.

We may, therefore, conclude that the curved surface traced out in  $q' : p' : v$  space by families of drained and undrained tests is identical for both families of tests. We may go further and hypothesize that the same surface is followed by all isotropically normally consolidated samples which are loaded by axial compression in the triaxial apparatus. We shall call this surface the *Roscoe surface*.

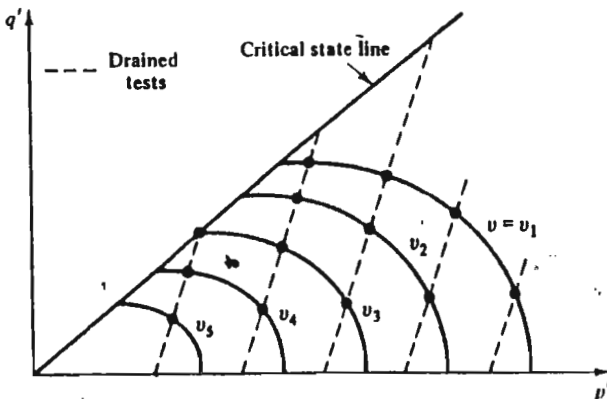


Figure 10-17 Contours of constant  $v$  from drained tests

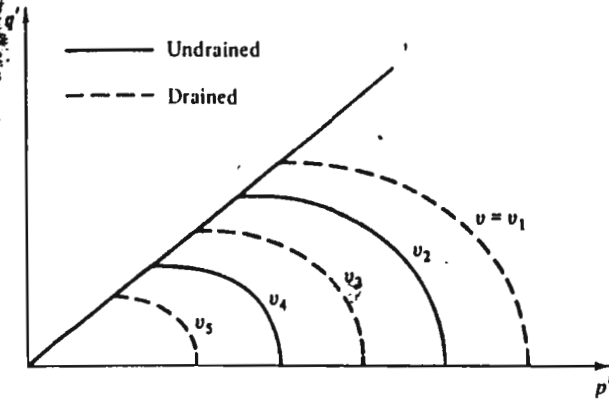


Figure 10-18 Contours of constant  $v$  from drained and undrained tests

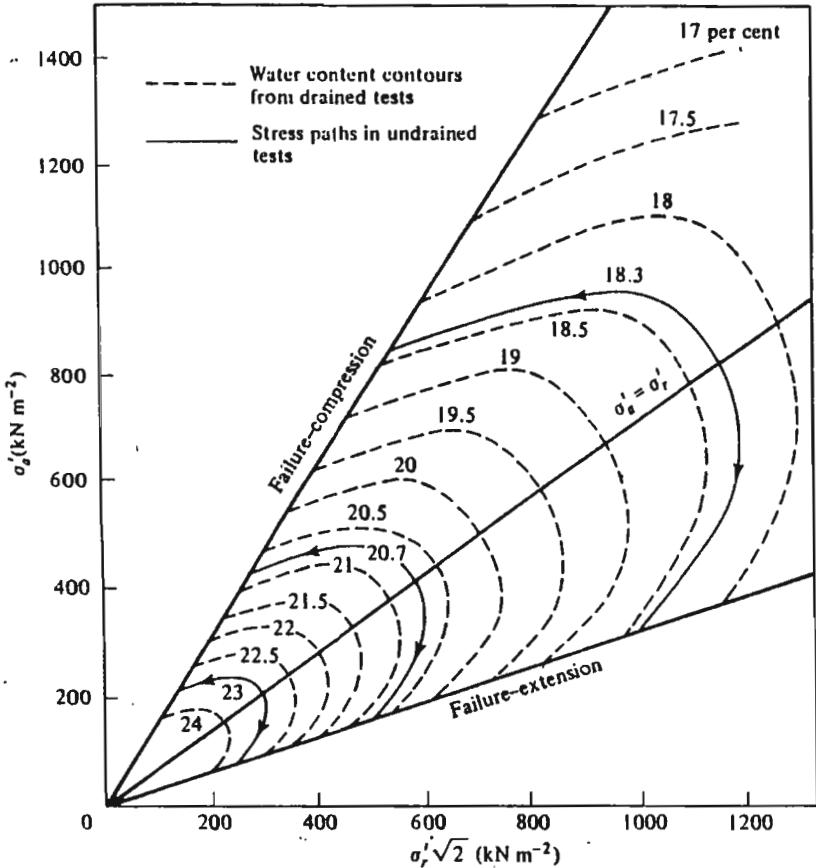


Figure 10-19 Contours of constant water content for drained and undrained tests on Weald clay (after Henkel, 1960)

## 10-7 THE SHAPE OF THE ROSCOE SURFACE

The method of investigating the uniqueness of the Roscoe surface by comparing contours of constant  $v$  for drained and undrained tests is satisfactory as far as it goes, but still no direct comparison can be made of paths followed by drained and undrained tests. The difficulty is that  $v$  changes in the drained test, and so the test path moves through a succession of constant  $v$  sections of the Roscoe surface, each section being of different size. One way round this difficulty is to scale the stresses so as to account for the changes in specific volume that occur during the test. The point can be best appreciated by considering again the undrained test paths shown in Fig. 10-3. We note that all paths are the same *shape* in  $q' : p'$  space, but of different *size*, because the initial isotropic stress  $p'_0$ , and, hence, initial specific volume, is different for each test. Thus, if the stresses were scaled by division by  $p'_0$ , all test paths would reduce to the single curve of Fig. 10-20. We have, therefore, scaled the test paths obtained from tests at different specific volumes so that they may be directly compared. The factor  $p'_0$  which was used is simply the isotropic stress at the start of the test.

The specific volume changes in drained tests, and so the test path will move through an infinity of constant  $v$  sections of the Roscoe surface, each of different size. We expect, though, that the *shape* of each constant  $v$  section will be the same for different values of  $v$ ; each section could, therefore, be scaled down to the same form as that of Fig. 10-20 by dividing the stresses  $q'$  and  $p'$  by the value  $p'_0$  of the mean normal effective stress on the normal consolidation line at that specific volume. The parameter  $p'_0$ , the *equivalent pressure*, at any specific volume is, thus, obtained from the equation for the normal consolidation line (Eq. (7-7)) using the current value of  $v$  for the specimen, *whatever* the current stresses, as

$$p'_0 = \exp [(N-v)/\lambda]. \quad (10-12)$$

The procedure is illustrated in Fig. 10-21. Suppose that a sample at A has stresses  $q'_A, p'_A$  and specific volume  $v_A$ . The relevant value of  $p'_0$  for the sample is obtained by tracing a line at constant  $v$  (i.e.,  $v = v_A$ ) from A to the normal consolidation line, and then reading off the corresponding value of mean normal stress to give  $p'_0$ . We should note that, for undrained tests,  $p'_0$  is constant throughout the test.

The effect of the scaling of the stress axes can be illustrated with the aid of Fig. 10-22. A drained test path  $A_1 D_2 B_3$  is shown cutting three constant  $v$  sections of the Roscoe surface at specific volumes of  $v_1, v_2$ , and  $v_3$ . At the beginning of the test, point  $A_1$ , the equivalent pressure  $p'_0$  is identical with the value of mean normal effective stress  $p'_{A_1}$  experienced by the sample. The parameter  $p'/p'_0$  is, therefore, exactly unity, while  $q'/p'_0$  is zero. The corresponding point  $A_1$  may, therefore, be plotted in the scaled axes of Fig. 10-23. When the sample has been sheared and compressed to point  $D_2$

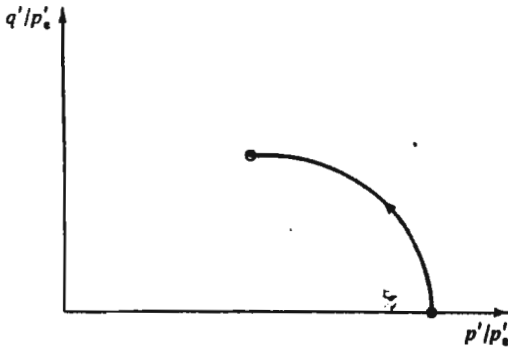


Figure 10-20 Path in  $q'/p'_0 : p'/p'_0$  space for undrained tests

in Fig. 10-22, the size of the constant  $v$  section of the Roscoe surface through point  $D_2$  (i.e.,  $A_2 D_2 B_2 C_2$ ) will be larger than the constant  $v$  section through  $A_1$  (i.e.,  $A_1 B_1 C_1$ ). The value of  $p'_0$  corresponding to the state  $D_2$  will be given by the value of mean normal stress at  $A_2$ , the point on the normal consolidation line with the same specific volume as at point  $D_2$ . Thus, although the value of  $p'$  will be larger at  $D_2$  than at  $A_1$ , the value of  $p'_0$  corresponding to  $D_2$  will also be larger than that corresponding to  $A_1$ , and so the value of  $p'/p'_0$  at  $D_2$  will be less than unity. The corresponding point in  $q'/p'_0 : p'/p'_0$  space is shown as  $D_2$  in Fig. 10-23.

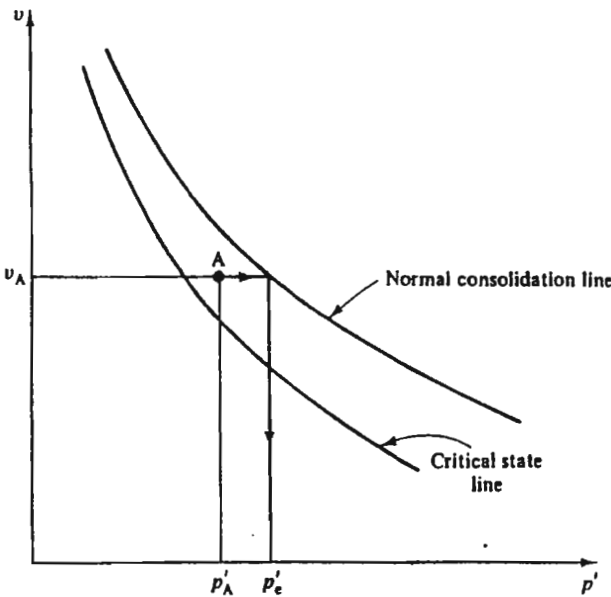


Figure 10-21 Method of obtaining the equivalent pressure  $p'_0$

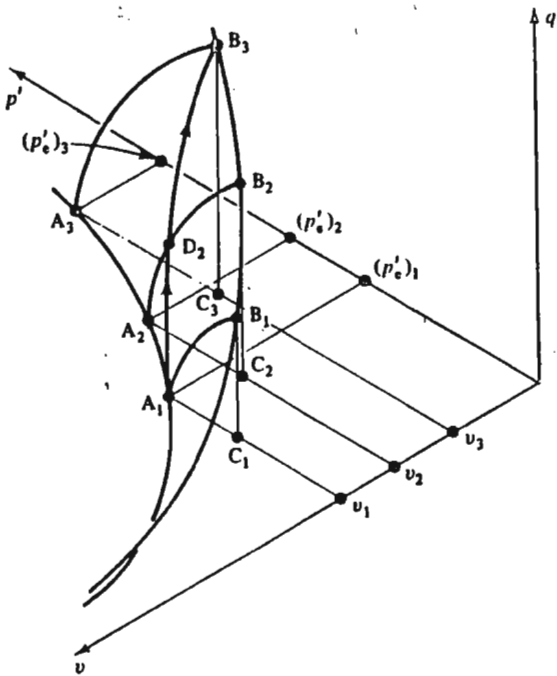


Figure 10-22 The path for a drained test in  $q' : p' : v$  space

A similar argument applies when the sample has reached the critical state line at  $B_3$ . The constant  $v$  section of the Roscoe surface is then larger than the sections at  $A_1$  and  $D_2$  because the sample has compressed and  $v$  reduced. The corresponding value of  $p'_0$  is then the mean normal effective stress at  $A_3$ . The point  $B_3$  may, therefore, be plotted in Fig. 10-23.

The whole test path for the drained test may, therefore, be represented by the line  $A_1 D_2 B_3$ , which has the same shape as the undrained path shown in Fig. 10-20. It should be noted that the same drained stress path  $A_1 D_2 B_3$

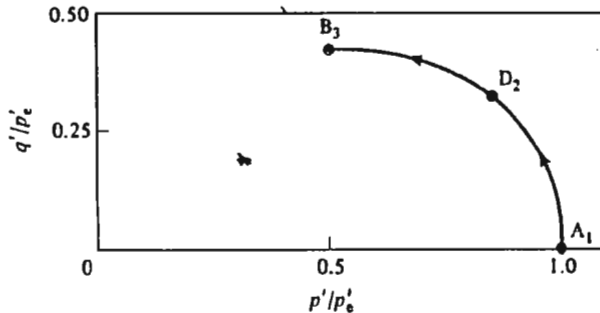


Figure 10-23 The path in  $q'/p'_e : p'/p'_e$  space for a drained test



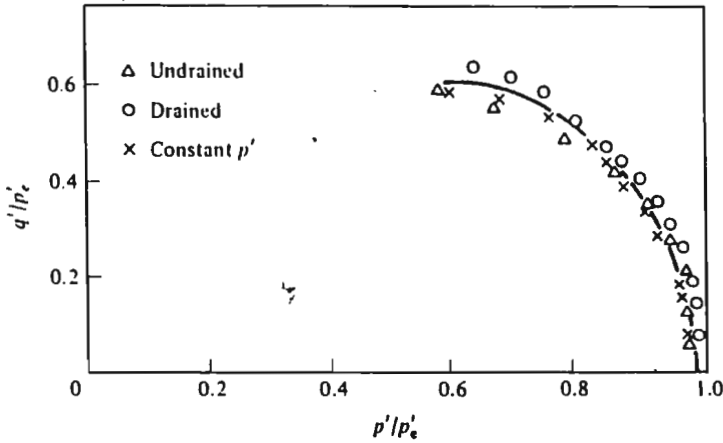


Figure 10-24 Test paths in  $q'/p'_0 : p'/p'_0$  space for a drained test, an undrained test, and a test at constant  $p'$  on samples of normally consolidated kaolin clay (after Balasubramaniam, 1969)

is a straight line of slope 3 when plotted in  $q' : p'$  space; the curvature in  $q'/p'_0 : p'/p'_0$  space is due to the increase of  $p'_0$  as the sample compresses.

A precise check may now be made as to whether the Roscoe surface is the same for drained and undrained tests by plotting data from those tests on a single diagram, as shown in Fig. 10-24. The data shown were obtained by Balasubramaniam (1969) from tests on remoulded kaolin. The agreement between the drained and undrained tests (and the test at constant  $p'$ ) is sufficiently good for us to make the assumption that the Roscoe surface is unique for all compression tests, irrespective of the applied loading paths.

**Example 10-3** Calculation of the normalized stress path in  $q'/p'_0 : p'/p'_0$  space for a drained test

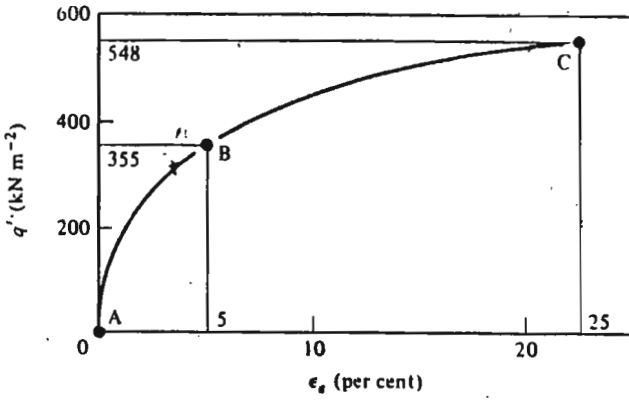
A drained triaxial compression test is performed on a sample of clay which is isotropically normally consolidated to  $p'_0 = 400 \text{ kN m}^{-2}$ ,  $v_0 = 2.052$ . Readings are taken of  $q'$ ,  $\varepsilon_v$  at values of  $\varepsilon_a$  equal to 0, 5, and 25 per cent (failure). The values of the soil constants for the clay are  $N = 3.25$  and  $\lambda = 0.2$ . Plot the normalized stress path in  $q'/p'_0 : p'/p'_0$  space.

The observed test data are plotted in Fig. E10-1(a) and (b) and values given in Table E10-1.

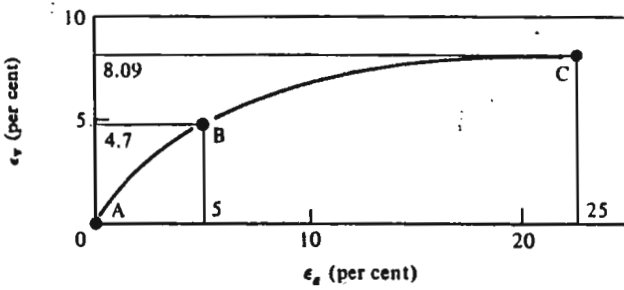
Calculated values were determined from the equations

$$v = v_0(1 - \varepsilon_v),$$

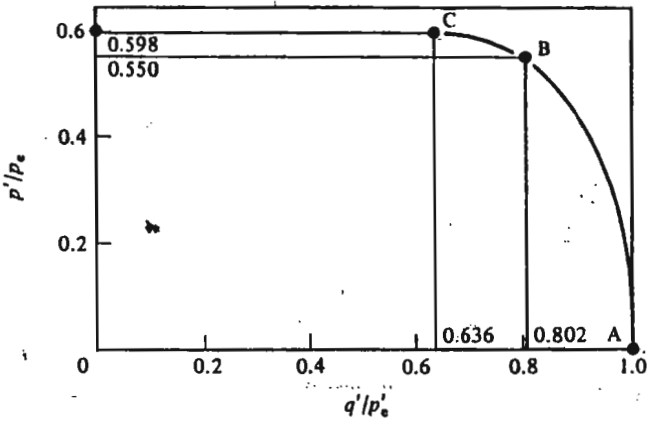
$$p'_0 = \exp[(N - v)/\lambda] \quad (\text{from Eq. (10-12)}).$$



(a)



(b)



(c)

Figure E10-1

Table E10-1

	Reference letter		
	A	B	C
<b>Observed</b>			
$\varepsilon_a$ (per cent)	0	5	25
$q'$ (kN m <sup>-2</sup> )	0	355	548
$\varepsilon_v$ (per cent)	0	4.70	8.09
<b>Calculated</b>			
$p'$ (kN m <sup>-2</sup> )	400	518	583
$v$	2.052	1.956	1.886
$p'_0$ (kN m <sup>-2</sup> )	400	646	916
$q'/p'_0$	0	0.550	0.598
$p'/p'_0$	1.0	0.802	0.636

For a drained triaxial compression test  $\Delta u = 0$ ,  $q'_0 = 0$ , and  $dq'/dp' = 3$  and, hence,

$$p' = p'_0 + q'/3.$$

The calculated values are plotted in Fig. E10-1(c).

## 10-8 THE ROSCOE SURFACE AS A STATE BOUNDARY SURFACE

So far in this chapter we have considered isotropically normally consolidated samples. It is now helpful to discuss the behaviour of lightly overconsolidated samples. Let us consider undrained tests on a family of samples which have been isotropically compressed and unloaded to different overconsolidation ratios, as indicated in Fig. 10-25. Sample 1 is normally consolidated to specific volume  $v_1$  and mean normal effective stress of  $p'_1$ , while samples 2, 3, and 4 have each been isotropically normally consolidated to specific volumes less than  $v_1$  and then been allowed to swell until their specific volumes are  $v_1$ , but their mean normal effective stresses are less than  $p'_1$ . Samples 2, 3, and 4 are, therefore, overconsolidated. Each sample is subjected to a standard undrained triaxial compression test and the test paths plotted in  $q' : p'$  space. Alternatively, if the initial specific volumes of the samples are slightly different, the stress paths can be more properly compared in  $q'/p'_0 : p'/p'_0$  space. Typical test data obtained by Loudon (1967) are shown in Fig. 10-26. We note first that the starting point for each test path is below the Roscoe surface, for the Roscoe surface coincides with the test path for the normally consolidated sample. The test paths must, therefore, deviate from the Roscoe surface, though it is clear that the lightly overconsolidated samples fail at the same point as the normally consolidated sample, i.e., at the critical state line. The test paths for the overconsolidated

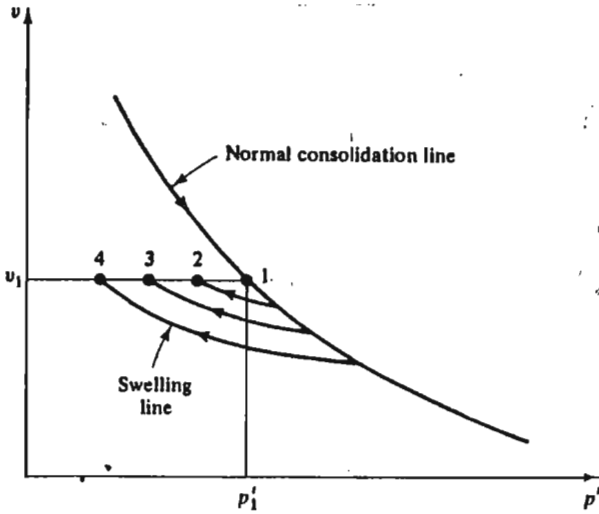


Figure 10-25 Consolidation and swelling of lightly overconsolidated samples

samples rise almost vertically towards the Roscoe surface and then move along close to the Roscoe surface towards the critical state. We can see, therefore, that the Roscoe surface forms a boundary beyond which the test paths do not go. There is an analogy with the normal consolidation line; at a particular stress level, samples cannot exist at a higher specific volume than that on the normal consolidation line at that stress. Thus, in Fig. 10-27, samples cannot exist above and to the right of the normal consolidation

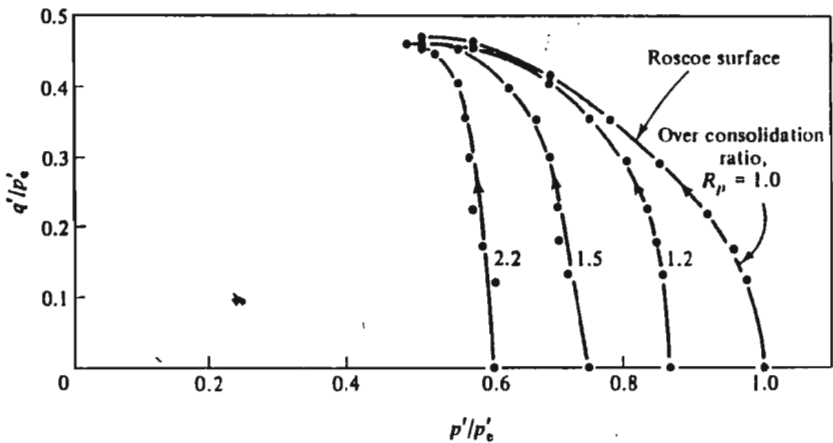


Figure 10-26 Paths in  $q'/p'_0 : p'/p'_0$  space for undrained tests on lightly overconsolidated samples of kaolin clay (after Loudon, 1967)

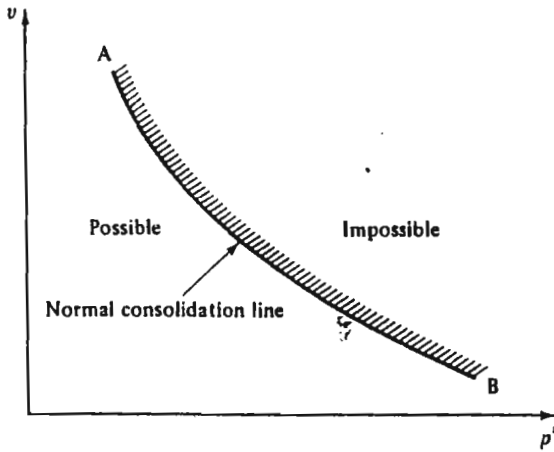


Figure 10-27 The normal consolidation line as a state boundary surface

line AB. In fact, the analogy between the Roscoe surface and the normal consolidation line is more than that; the normal consolidation line is that part of the Roscoe surface lying in the  $q' = 0$  plane.

We may, therefore, think of the Roscoe surface as a surface which separates states which samples can achieve from states which samples can never achieve, Fig. 10-28. The Roscoe surface is, therefore, a *state boundary surface*.

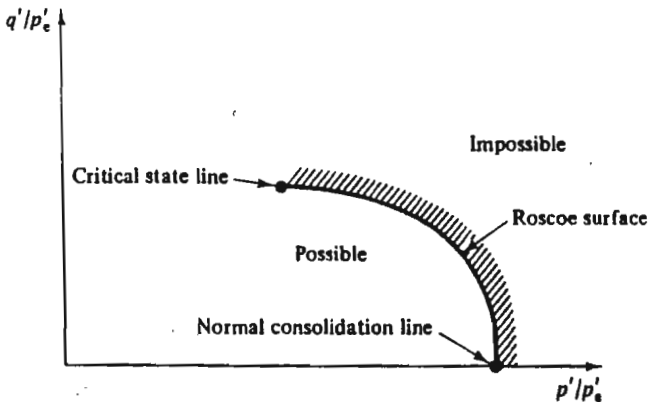


Figure 10-28 The Roscoe surface as a state boundary surface

## 10-9 SUMMARY

1. There exists a critical state line in  $q' : p' : v$  space on which all test paths from triaxial compression tests on isotropically normally consolidated samples terminate.

2. The test paths for both drained and undrained tests follow the same curved surface (the Roscoe surface) which links the normal consolidation line with the critical state line in  $q' : p' : v$  space. The intersection of the test plane for any test with the Roscoe surface fixes the complete test path in  $q' : p' : v$  space for that test.
3. The geometry of the Roscoe surface is such that all constant  $v$  sections of the surface have the same *shape* but are of different *size*. The sections may be scaled to a single normalized curve if the stresses are divided by the equivalent pressure  $p'_o$ .
4. The Roscoe surface is a state boundary surface.

## REFERENCES

- Balasubramaniam, A. S. Some factors influencing the stress-strain behaviour of clay. PhD Thesis, University of Cambridge, 1969.
- Henkel, D. J. The shear strength of saturated remoulded clay. In *Proceedings of Research Conference on Shear Strength of Cohesive Soils* at Boulder, Colorado, pp. 533-540, 1960.
- Loudon, P. A. Some deformation characteristics of kaolin. PhD Thesis, University of Cambridge, 1967.
- Patry, R. H. G. Triaxial compression and extension tests on remoulded saturated clay. *Geotechnique*, 10, 166-180, 1960.
- Rendulić, L. Pore-index and pore water pressure. *Bauingenieur*, 17, 559, 1936.
- Schofield, A. N. and Wroth, C. P. *Critical State Soil Mechanics*. McGraw-Hill Book Co., London, 1968.

**THE BEHAVIOUR OF OVERCONSOLIDATED  
SAMPLES: THE HVORSLEV SURFACE**

**11-1 INTRODUCTION**

We found in Chapter 10 that, for normally consolidated specimens, there exists a critical state line at which specimens fail, and a state boundary surface, the Roscoe surface, which limits the state of specimens in  $q' : p' : v$  space as they move from the normal consolidation line to the critical state line. We must now ask ourselves whether the same concepts, perhaps with modification, apply for overconsolidated specimens.

**11-2 DRAINED TESTS**

We will consider the behaviour of specimens which have been isotropically consolidated to some mean normal effective stress  $p'_{max}$  and then allowed to swell isotropically to some lower mean normal stress  $p'_0$ , as indicated in Fig. 11-1. The overconsolidation ratio  $R_p$  is defined as  $p'_{max}/p'_0$ , and so

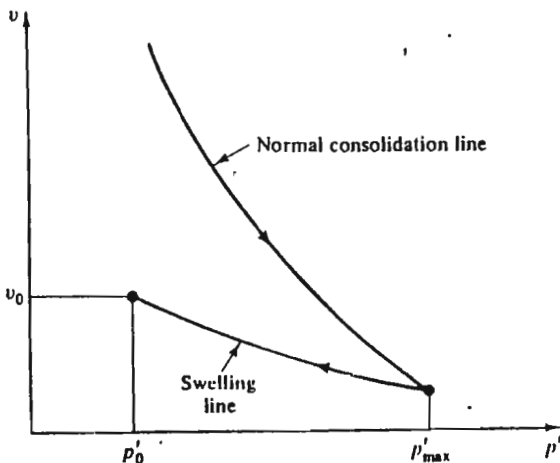
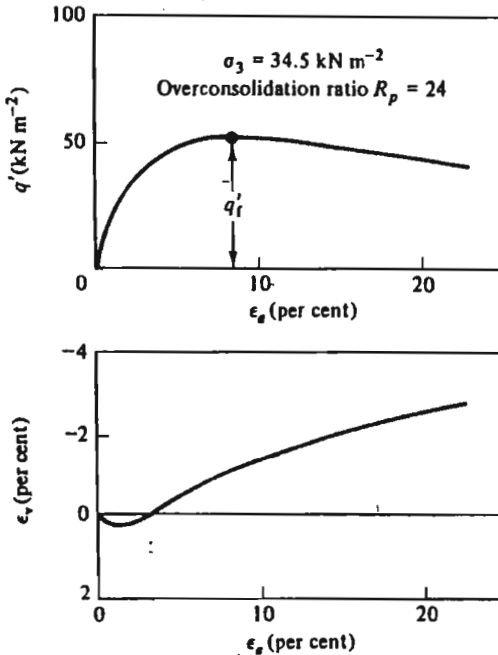


Figure 11-1 Compression and swelling lines



A.I.T. LIBRARY

Figure 11-2 Test data from a drained test on an overconsolidated sample of Weald clay (after Bishop and Henkel, 1962, p. 128)

normally consolidated samples have  $R_p = 1$  while  $R_p$  is large for heavily overconsolidated samples.

A typical drained test on a heavily overconsolidated sample ( $R_p = 24$ ) of Weald clay was discussed in Sec. 9-4 and  $q' : \epsilon_a$  and  $\epsilon_v : \epsilon_a$  curves are reproduced in Fig. 11-2. A significant feature of the  $q' : \epsilon_a$  curve is that the sample exhibits a peak strength, denoted by  $q'_f$ , after which the value of  $q'$  falls as  $\epsilon_a$  increases. The value of  $q'$  seems to be decreasing towards a steady value at the end of the test, but, as discussed in Sec. 9-4, we must be suspicious about the accuracy of the data of both stress and strain at large shear strains. We note also that the sample initially decreases in volume, before it expands substantially as the test proceeds. There is a hint that the rate of volume expansion is decreasing towards the end of the test, but again we cannot rely on the data at this stage of the test.

We can now plot the stress path for the test in  $q' : p'$  space as shown in Fig. 11-3. The test path moves above the projection of the critical state line to the failure point before moving back along the same path towards the projection of the critical state line. The state boundary surface for overconsolidated specimens must therefore have a projection in  $q' : p'$  space that lies above the projection of the critical state line.



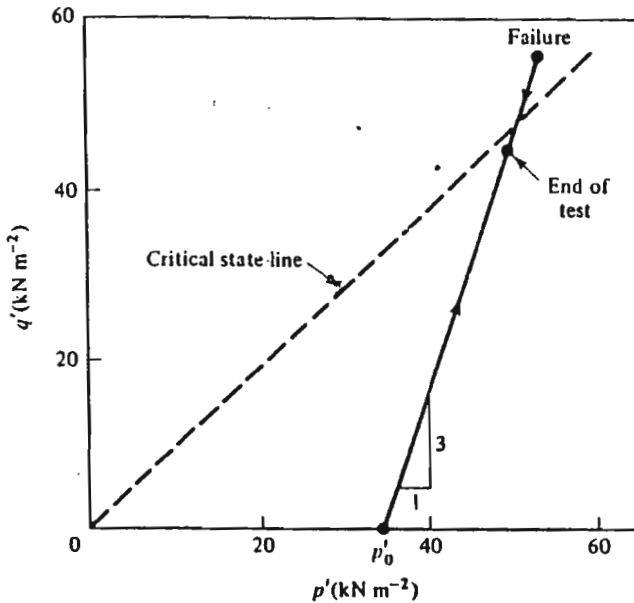


Figure 11-3 Test path followed in the drained test of Fig. 11-2

We could consider a family of drained tests to obtain more information about the shape of the state boundary surface. However, the difficulty with such a family of tests, and indeed with drained tests in general, is that the specific volume of the specimens is changing throughout the tests. The projections of the test paths, or the failure point, into  $q' : p'$  space then refer to different constant  $v$  sections of the state boundary surface. By analogy with the Roscoe surface, we expect that each constant  $v$  section of the state boundary surface is of different size, though we hope of the same shape. The most convenient way of investigating the shape of the state boundary surface is, therefore, to scale the stresses to allow for changes in specific volume that occur during the tests.

### 11-3 THE HVORSLEV SURFACE

In order to scale the stresses, we argue as before that the size of each constant  $v$  section of the state boundary surface will be different for each value of  $v$ , and will be in proportion to the equivalent stress  $p'_0$ . The value of  $p'_0$  for any specific volume is simply the stress on the normal consolidation line at that specific volume. We can allow for differences in specific volume by plotting stress paths in  $q'/p'_0 : p'/p'_0$  space; drained and undrained tests may then be compared directly.

This method of scaling was adopted by Hvorslev, who was concerned with the correlation of failure strengths of specimens tested in the shear box.

We can consider the failure states of specimens in the triaxial apparatus and plot the data on normalized stress axes, as shown in Fig. 11-4. The data were obtained from a series of compression tests on overconsolidated Weald clay and are taken from Parry (1960). It is clear that the data of both drained and undrained tests lie on a single line in  $q'/p'_e : p'/p'_e$  space. The line is limited on its right-hand end by the point representing the critical state line at the top edge of the Roscoe state boundary surface. By the following argument, the line of failure points is also limited on its left-hand end. The maximum value of  $q'/p'$  would be when  $\sigma'_1$  was large and  $\sigma'_3$  was small. If the soil could not withstand tensile *effective* stresses, the highest value of  $q'/p'$  that could be observed would correspond to  $\sigma'_3 = 0$ . Then, for a triaxial compression test,

$$q' = \sigma'_1, \quad (11-1)$$

$$p' = \frac{1}{3}\sigma'_1, \quad (11-2)$$

and

$$q'/p' = 3. \quad (11-3)$$

The locus of failure points can then be idealized as line AB in Fig. 11-5. The locus is limited on its left-hand side by the line OA which has slope 3, corresponding to tensile failure, and on its right-hand side by the critical

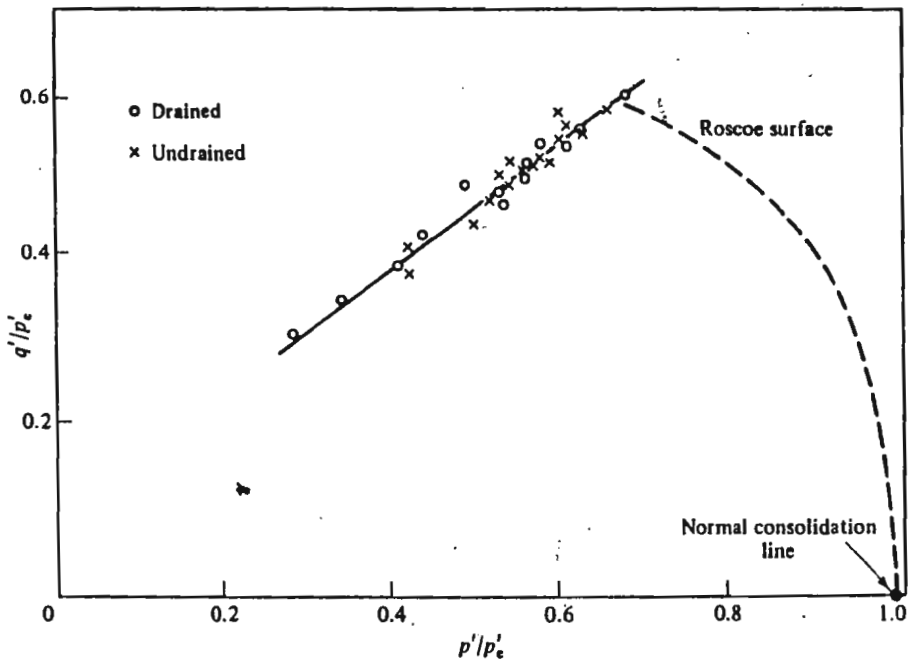


Figure 11-4 Failure states of drained and undrained tests on overconsolidated samples of Weald clay (data from Parry, 1960)

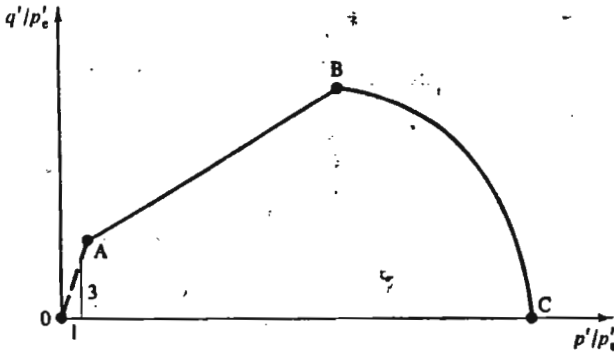


Figure 11-5 The complete state boundary surface in  $q'/p'_0 : p'/p'_0$  space

state line (point B) and the Roscoe surface (BC). Of course, if the soil could sustain tensile effective stresses, the line corresponding to tensile failure would lie to the left of OA, and might be curved. This latter possibility is relevant for many cohesive powders whose handling is important in the chemical engineering industry.

We shall call the locus AB of failure points in Fig. 11-5 the *Hvorslev surface*. The significant feature of the surface with which Hvorslev was particularly concerned is that the shear strength of a specimen at failure is a function both of the mean normal stress  $p'$ , and of the specific volume  $v$  of the specimen at failure. The specific volume appears in Fig. 11-5 through its influence on the equivalent stress  $p'_0$ , which depends directly on specific volume. The point can be illustrated if we idealize the Hvorslev surface as a straight line whose equation is

$$q'/p'_0 = g + h(p'/p'_0), \quad (11-4)$$

where  $g$  and  $h$  are soil constants as shown in Fig. 11-6. Equation 11-4 may be rewritten as

$$q' = gp'_0 + hp' \quad (11-5)$$

and, using Eq. (10-12),

$$p'_0 = \exp[(N-v)/\lambda]. \quad (11-6)$$

We may substitute to get

$$q' = g \exp[(N-v)/\lambda] + hp'. \quad (11-7)$$

The Hvorslev surface intersects the critical state line given by Eqs (10-1) and (10-2) at  $q'_t$ ,  $p'_t$  and  $v_t$  where

$$q'_t = Mp'_t; v_t = \Gamma - \lambda \ln p'_t \quad (11-8)$$

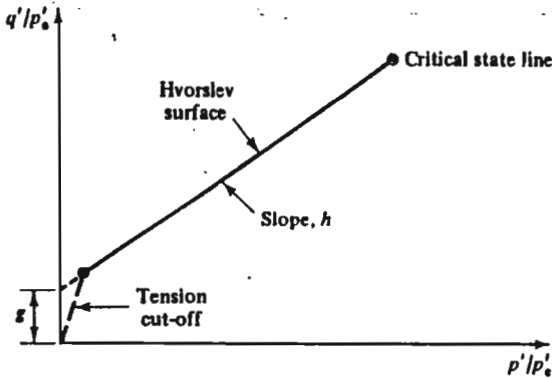


Figure 11-6 The Hvorslev surface

and hence, from Eq. (11-7)

$$(M-h)p'_t = g \exp \left[ \left( \frac{N-\Gamma}{\lambda} \right) + \ln p'_t \right] \quad (11-9)$$

$$g = (M-h) \exp \left( \frac{\Gamma-N}{\lambda} \right). \quad (11-10)$$

Thus the equation of the Hvorslev surface is

$$q' = (M-h) \exp \left( \frac{\Gamma-v}{\lambda} \right) + hp'. \quad (11-11)$$

Equation (11-11) states explicitly that the deviator stress at failure of an overconsolidated specimen is made up of two components. The first component ( $hp'$ ) is proportional to mean normal effective stress, and so may be thought of as being frictional by nature, while the second component ( $[(M-h) \exp \{(\Gamma-v)/\lambda\}]$ ) depends only on the current specific volume, and the value of certain soil constants. The form of the exponential term is such that the second component of strength increases as the specific volume of the specimen decreases. Thus if two specimens were brought to failure in drained tests at the same value of  $p'$  but at different specific volumes  $v_1$  and  $v_2$ , where  $v_1 > v_2$ , the failure of the specimens would occur at different values of  $q'$ , as shown in Fig. 11-7. The lines  $A_1B_1$  and  $A_2B_2$  are sections of the Hvorslev surface corresponding to the two specific volumes  $v_1$  and  $v_2$ .

We might expect that samples at failure have progressed outwards as far as they can in  $q' : p' : v$  space. Therefore, we will now adopt as a working hypothesis the idea that the Hvorslev surface is the state boundary surface for heavily overconsolidated samples in the same way that the Roscoe surface is a state boundary surface for normally and lightly overconsolidated samples. We note that the Hvorslev and Roscoe state boundary surfaces intersect and that the line of intersection is the critical state line.

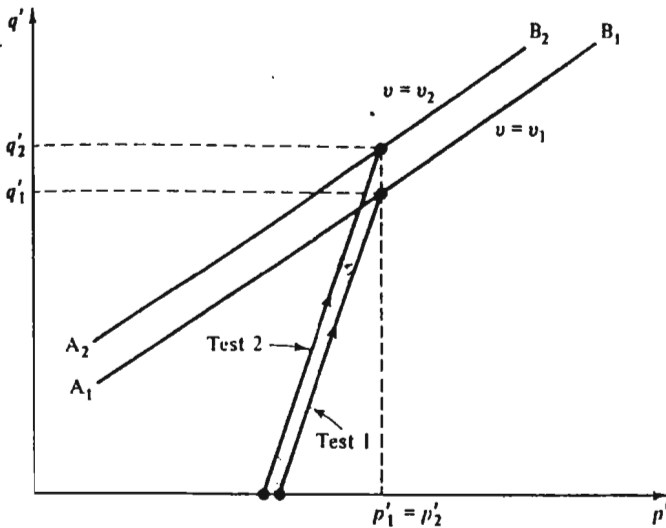


Figure 11-7 Failure states of drained specimens at different specific volumes

**Example 11-1** Calculation of the values of the deviator stress at failure for samples which fail on the Hvorslev surface

Three samples A, B, and C are brought to failure on the Hvorslev surface at the following combinations of  $v$  and  $p'$ : Sample A,  $v = 1.90$ ,  $p' = 200 \text{ kN m}^{-2}$ ; Sample B,  $v = 1.90$ ,  $p' = 500 \text{ kN m}^{-2}$ ; Sample C,  $v = 2.05$ ,  $p' = 200 \text{ kN m}^{-2}$ . The clay has  $N = 3.25$ ,  $\lambda = 0.2$ ,  $\Gamma = 3.16$ ,  $M = 0.94$ , and  $h = 0.675$ . Calculate the values of  $q'$  at failure of each sample.

For states on the Hvorslev surface, the deviator stress is given by Eq. (11-11):

$$q' = (M - h) \exp[(\Gamma - v)/\lambda] + hp'$$

Calculated values are given in Table E11-1.

**Table E11-1**

	A	Sample B	C
$v$	1.90	1.90	2.05
$p'$ ( $\text{kN m}^{-2}$ )	200	500	200
$q'$ ( $\text{kN m}^{-2}$ )	279	482	203

## 11-4 THE CRITICAL STATE LINE

We must now consider what feature for overconsolidated specimens corresponds to the critical state line which is observed for normally consolidated specimens. Our first task is to consider what happens during a drained test on an overconsolidated specimen. We know that the deviator stress first increases to a peak and then reduces from its peak value (see Fig. 11-2) and that the sample continues to dilate until the end of the test. The sample has, therefore, not reached a steady-state condition at the end of the test at which the stresses are constant and there is no change in volume as the sample shears.

We must, therefore, distinguish carefully two particular states attained by the overconsolidated specimens. The first state is the *failure state*, at which the deviator stress reaches a maximum. This state is clearly of interest if we wish to know how much load an element of soil can sustain, and is the state most often sought for in tests whose results are to be used in engineering practice. The second state can be called the *ultimate state*, and it is that state at which large shear strains can occur with no change in stresses or in volume. An ultimate state may or may not be achieved at the end of a test, and indeed it appears from the data shown previously that overconsolidated specimens often do not reach a well-defined ultimate state.

One real difficulty in discussion of the behaviour of overconsolidated specimens is that the test data become unreliable at large strains. Consider the situation when a drained triaxial test is conducted on overconsolidated clay which has a stress-strain relationship as illustrated in Fig. 11-8. For the initial part of the curve, up to point F, the sample gets stronger as it deforms. Thus, any small inhomogeneities of strain will be reduced as the sample is loaded, for the more strained elements of soil will be stronger than those which have strained less.

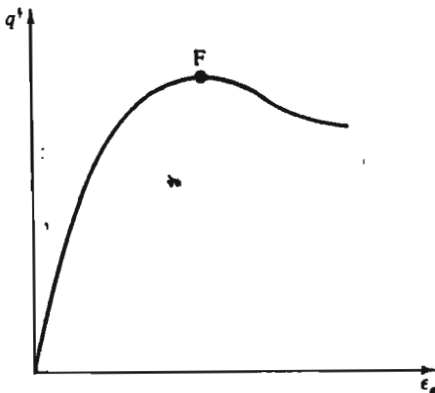


Figure 11-8 Stress-strain curve for a drained test on overconsolidated clay

In contrast, after F, the sample becomes weaker as it strains further. Thus, any inhomogeneities of strain will become intensified, because further strain will be concentrated in the weaker regions of the specimen, i.e., those regions which have already suffered more strain than the average. We expect, therefore, to observe the formation of thin zones of concentrated deformation within the specimen after failure, and we must be suspicious of the accuracy of stresses and strains calculated from boundary measurements on the assumption that conditions within the sample are uniform.

It follows that it is difficult to establish, with confidence, where the points corresponding to end points of tests should be plotted in  $q' : p' : v$  space. We have even more difficulty in fixing the positions of the ultimate points the samples would have reached had the tests been continued to large shear strains. Of course, it is the ultimate states of overconsolidated samples that are of interest if we wish to establish some feature comparable to the critical state line.

One way of proceeding is to ask in which direction the samples were moving in  $q' : p' : v$  space at failure. This was the approach adopted by Parry (1958). For drained tests, Parry examined the rate (and sign) of the volume change at failure and, as shown in Fig. 11-9, plotted that against the ratio  $p'_u/p'_t$ , where  $p'_u$  is the mean normal stress of the point on the critical state line at the same specific volume as that of the sample and  $p'_t$  is the mean effective normal stress at failure. The rate of volume change is expressed as a ratio of the increment of volumetric strain  $\delta\varepsilon_v$  to the increment of shear strain  $\delta\varepsilon_s$ . There is a clear linear relationship between  $\delta\varepsilon_v/\delta\varepsilon_s$  and  $p'_u/p'_t$  on the semilogarithmic plot of Fig. 11-9. The line representing the trend of the data indicates that samples which fail at the critical state ( $p'_t = p'_u$ , point U in Figs 11-9 and 11-10) have zero rate of volume change at failure, and that samples which fail with  $p'_t < p'_u$  (i.e., samples which were initially heavily overconsolidated) are expanding at failure. Thus, a sample which fails at point A on the  $v : \ln p'$  plot of Fig. 11-10 is expanding and so moving towards the critical state line at a higher specific volume. Similarly, a sample which fails at point B with  $p'_t > p'_u$  was observed to be contracting at failure, and so moving down from B towards the critical state line at a lower specific volume. It is significant that the rate of movement towards the critical state line at failure increases as the distance between the failure state of the sample and the critical state line increases.

Parry reported a similar set of data for undrained tests. Obviously, in undrained tests, the volume of the sample is constant and so, instead of  $\delta\varepsilon_v/\delta\varepsilon_s$ , he examined the rate of pore pressure change at failure. He plotted  $((\delta u/p'_t)/\delta\varepsilon_s)$  against  $p'_u/p'_t$  (Fig. 11-11). The change of pore pressure is expressed as  $\delta u/p'_t$  so that samples which fail at different mean normal effective stresses may be compared directly. The pattern of Fig. 11-11 is clear, and exactly analogous to that of Fig. 11-9. The rate of pore water pressure change at failure is largest for samples which fail furthest away

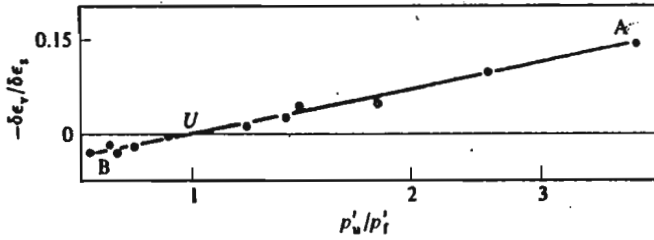


Figure 11-9 Rates of volume change at failure in drained tests (after Parry, 1958)

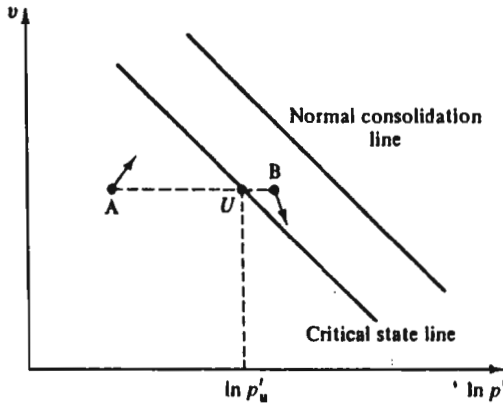
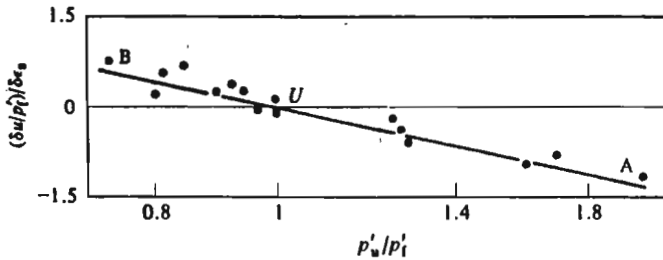

 Figure 11-10 Failure states of specimens in  $v : \ln p'$  space


Figure 11-11 Rates of pore pressure change in undrained tests (after Parry, 1958)

from the critical state line, and the sign of the pore pressure change is such as to move the specimen towards the critical state line (Fig. 11-12). Sample A has  $p'_t < p'_u$ , and so, from Fig. 11-11,  $\delta u/\delta e_s$  is negative; the sample is, therefore, moving to the right from A. The sample which fails at point B has  $\delta u/\delta e_s$  positive and so it is moving to the left in Fig. 11-12.

We may, therefore, conclude that at failure both drained and undrained samples are moving towards the critical state line at rates which are related to the distance of samples from the critical state line. It should be noted that



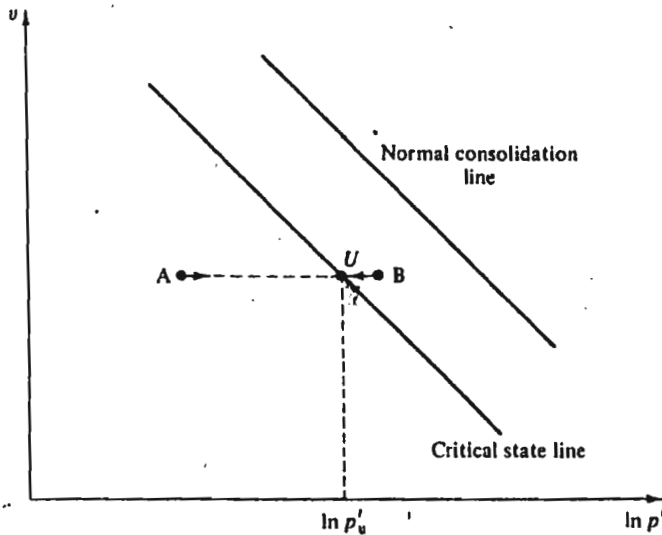


Figure 11-12 Failure states of undrained specimens in  $v : \ln p'$  space

this conclusion applies for both overconsolidated and normally consolidated samples, even though the position of the critical state line was established from the data of normally consolidated samples alone.

As discussed previously in this section, we have to be suspicious of data obtained after failure of the samples, and, thus, it is not worthwhile examining the test data to see if samples approach a critical state condition after failure.

We shall, therefore, adopt the following working hypothesis suggested by the data of Figs 11-9 and 11-11: with continuing shear, individual elements of clay each proceed towards the critical state line after failure of the sample as a whole and eventually reach ultimate states on the critical state line.

One implication of this hypothesis is that 'ultimate states' of samples under test must refer to the condition at which the complete sample has reached the critical state line: the term 'ultimate' can, therefore, only apply to the state of a sample as a whole if the strains remain essentially homogeneous throughout the sample. If a sample divides into distinct blocks which slide past each other across very thin zones, there will be very large strains taking place in the soil within these regions and clay particles may become aligned in preferred directions. In this case, the strength of the soil may reduce below its critical state strength towards its residual strength as discussed in Sec. 15-5. The term ultimate state must be thought of as the final state which would be reached by *homogeneous* shearing of an element or sample of clay in which the arrangement of the particles remained essentially random.

### 11-5 THE COMPLETE STATE BOUNDARY SURFACE

We can now discuss the complete state boundary surface and the position of the critical state line on it. We know that the curved Roscoe surface joins the normal consolidation line to the critical state line and that the Hvorslev surface extends up to the critical state line from the other side. The most precise representation of the complete state boundary surface is to plot the surface in  $q'/p'_e : p'/p'_e$  space, as shown in Fig. 11-13. Any constant  $v$  section of the state boundary surface will then have the shape shown in Fig. 11-13, though the size of the section will be such that the point A always lies on the normal consolidation line. The shape of the complete state boundary surface can be represented more graphically in  $q' : p' : v$  space, as shown in Fig. 11-14; allowing for the change of view, the shape of any constant  $v$  section of the surface can be seen to be the same as that shown in Fig. 11-13. The critical state line forms a ridge separating the Roscoe and Hvorslev surfaces, and its height and gradient increase as the mean normal effective pressure increases.

We can now find the intersection of different test planes with the state boundary surface. An undrained plane is, of course, identical to a constant  $v$  section of the surface and has the shape illustrated in Fig. 11-13. We note that the critical state is the state at which the maximum value of  $q'$  can be sustained by a sample if it is tested undrained. We would expect, therefore, if conditions within a sample were uniform, that undrained tests on heavily overconsolidated samples would follow paths which rose almost vertically up to the state boundary surface, in the same way as observed for lightly overconsolidated samples. The paths would then be expected to traverse the

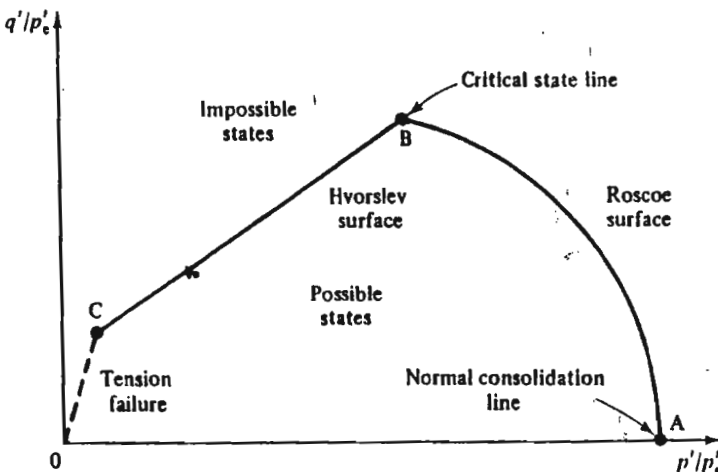


Figure 11-13 The complete state boundary surface in  $q'/p'_e : p'/p'_e$  space

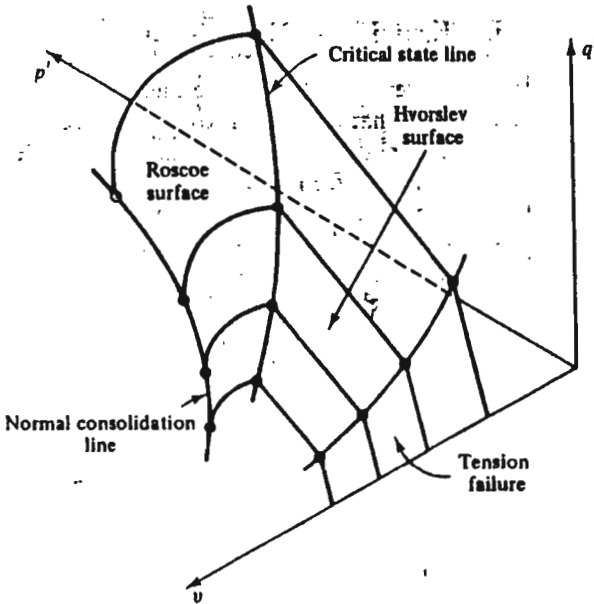


Figure 11-14 The complete state boundary surface in  $q' : p' : v$  space

surface until failure occurred at the critical state line. Of course, the experimental difficulty arises that the conditions within the sample may not be uniform, even in undrained tests. There is the possibility that failure of a triaxial sample occurs prematurely, probably soon after the sample reaches the Hvorslev surface, even though the undrained paths followed by uniform elements of clay would be those shown in Fig. 11-15.

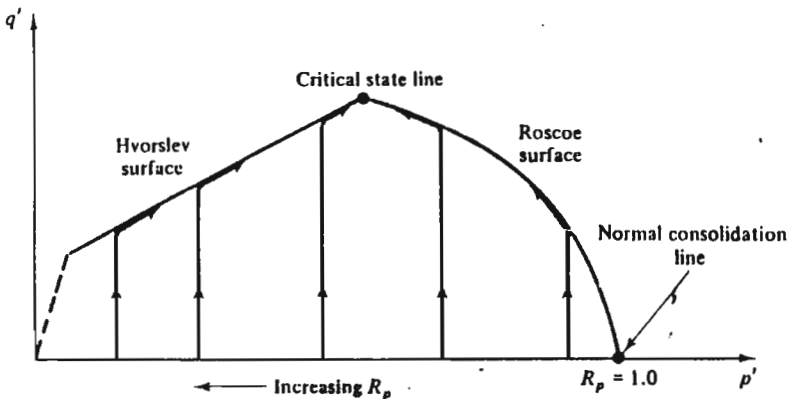


Figure 11-15 Expected undrained test paths for samples at different overconsolidation ratios

Data from a family of undrained tests on kaolin conducted by Loudon (1967) are illustrated in Fig. 11-16; the general pattern of behaviour is what we expect, except that the sharp corners of the paths in Fig. 11-15 have been rounded off.

A drained plane, for which  $dq'/dp' = 3$ , is illustrated in  $q' : p' : v$  space in Fig. 11-17, and its intersection with the state boundary surface is indicated. The intersection can be viewed much better either in  $q' : p'$  space (Fig. 11-18) or on the drained plane itself (Fig. 11-19). Figure 11-18 shows the successive constant  $v$  sections of the state boundary surface that are cut by the drained plane. As  $v$  decreases, the size of the constant  $v$  section increases, while the relative position of the point of intersection of the constant  $v$  section and the drained plane moves from the normal consolidation line (A), round the Roscoe surface (B), through the critical state line (C), onto the Hvorslev surface (D), and away from the critical state line (E).

Figure 11-19 shows a normal view of the drained plane itself. The Roscoe surface now appears less sharply curved, while the Hvorslev surface rises as  $v$  decreases. The vertical axis of Fig. 11-19 measures the distance  $a$  of a point up the drained plane above the intersection of the drained plane and the floor ( $q' = 0$ ) of Fig. 11-17. We see from Fig. 11-20 that  $a = [\sqrt{(10)/3}]q'$ . The line OA forming the horizontal axis of Fig. 11-19 is shown on a view of the floor of  $q' : p' : v$  space in Fig. 11-21. Figure 11-21 also shows a series of swelling lines for samples which have been isotropically consolidated to different maximum pressures and then allowed to swell isotropically until they are all at the same mean normal effective stress  $p'_0$ . The sample at O

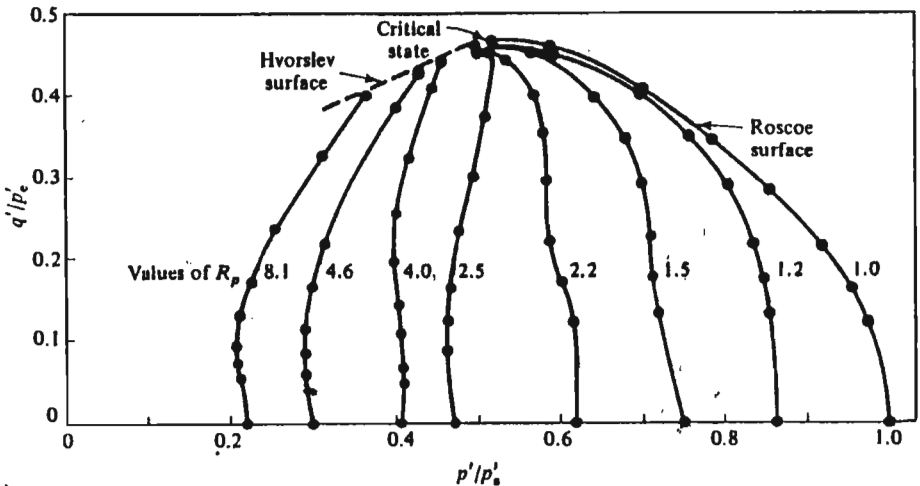


Figure 11-16 Normalized stress paths for undrained tests on overconsolidated samples of kaolin clay (after Loudon, 1967)

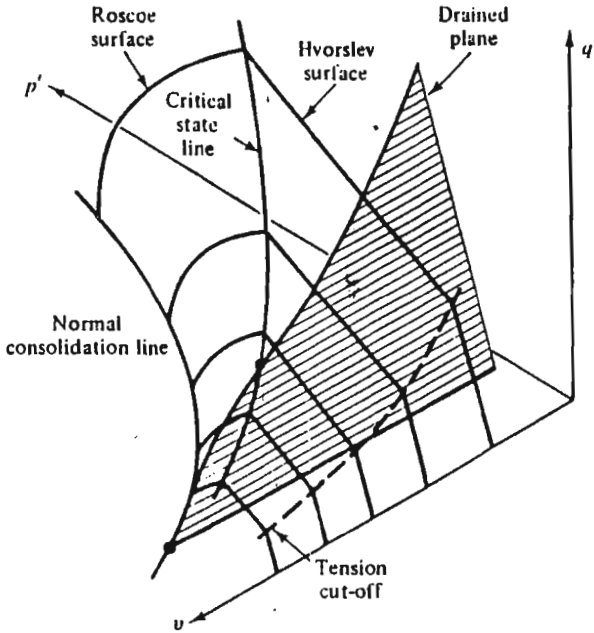


Figure 11-17 A drained plane in  $q' : p' : v$  space

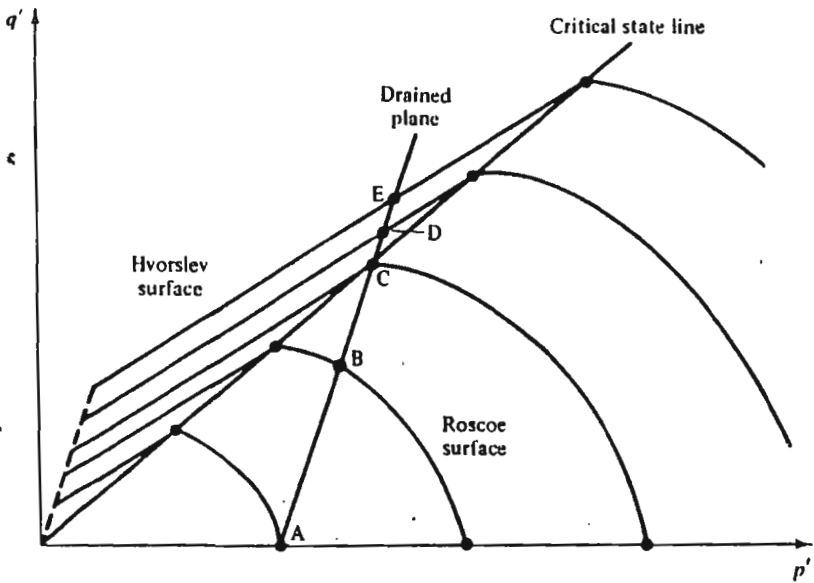


Figure 11-18 A drained plane in  $q' : p'$  space

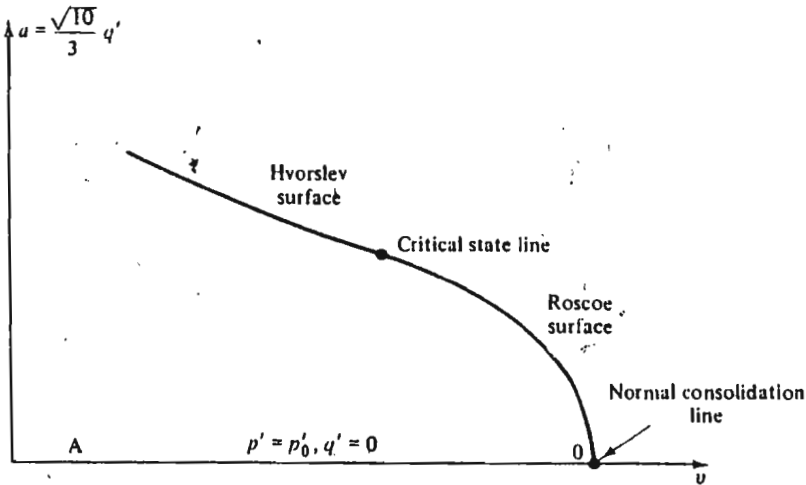


Figure 11-19 The intersection of the state boundary surface and the drained plane

is normally consolidated (i.e.,  $R_p = 1$ ) and samples have higher overconsolidation ratios the closer they are to A.

The expected pattern of behaviour for drained tests on samples at different overconsolidation ratios is shown in the drained plane in Fig. 11-22. Initially, samples will deform so that  $v$  decreases slightly as  $q'$  and  $p'$  increase and then samples will reach the state boundary surface, and traverse across it towards the critical state line. A significant feature of Fig. 11-22 is that the critical state line is not the point on the state boundary surface which has the highest value of  $q'$ . All samples on the Hvorslev surface to the left of the critical state line in Fig. 11-22 can sustain higher values of  $q'$  than that at

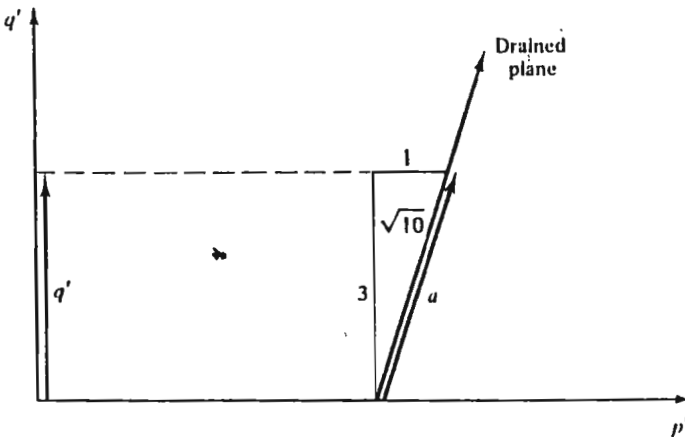


Figure 11-20 Geometry of the drained plane

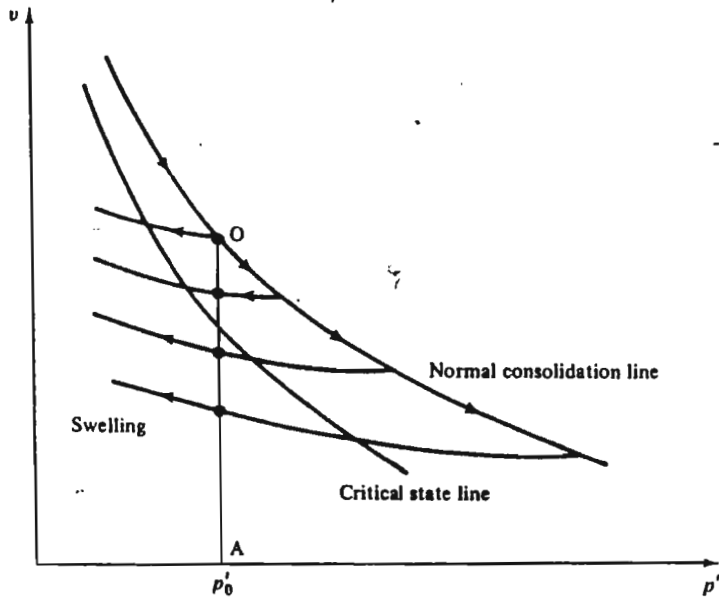


Figure 11-21 The line OA of Fig. 11-19 in  $v : p'$  space

the critical state line. A drained test on an overconsolidated specimen will, therefore, give a maximum value of  $q'$  (i.e., failure) at a stage in the test just before the sample moves down the Hvorslev surface towards the critical state line. The consequence, for any real specimen, is that after failure the

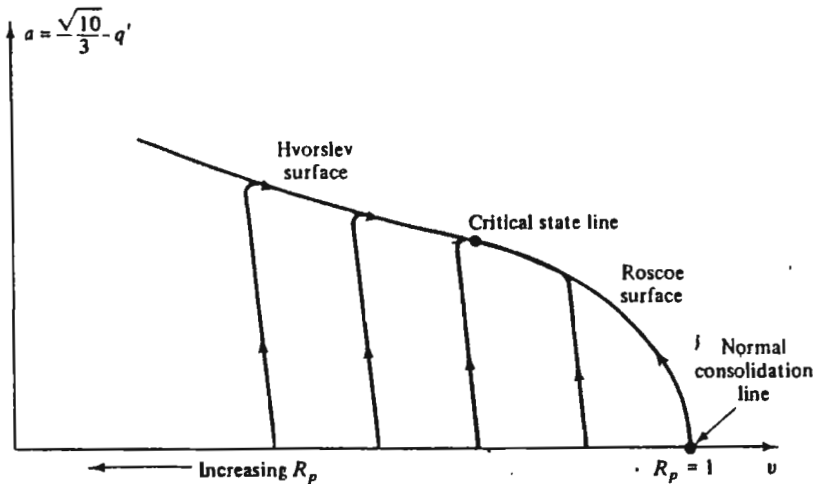


Figure 11-22 Paths followed by drained tests on samples at different overconsolidation ratios

deformation becomes non-uniform and only elements of clay in the thin slip bands move down the Hvorslev surface; the remainder of the sample does not soften significantly.

Samples which are to the left in Fig. 11-22 (i.e., they have higher overconsolidation ratios) will fail further away from the critical state line. Thus, the failure states for specimens all consolidated to the same maximum stress  $p'_{max}$  and then allowed to swell to different overconsolidation ratios will follow the pattern shown in Fig. 11-23. The locus of failure states of the

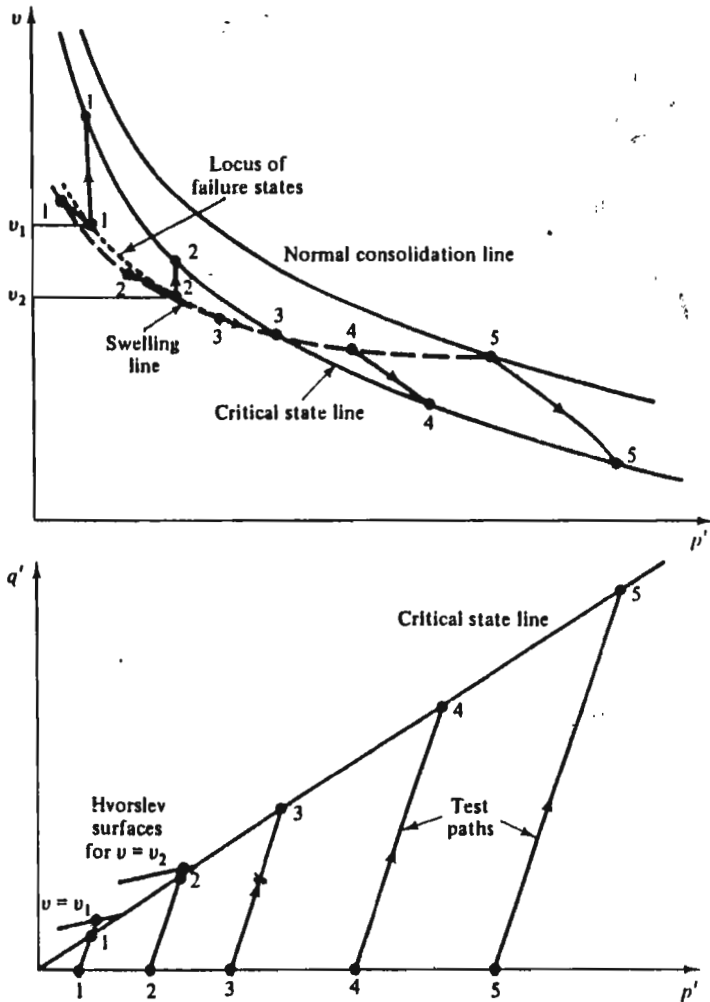


Figure 11-23 Failure states of drained tests on samples at different overconsolidation ratios



overconsolidated specimens will lie to the left of the critical state line in  $v : p'$  space, with the deviation from the critical state line increasing as  $R_p$  increases. Indeed, arguments discussed in Chapter 13 concerning the distinction between 'elastic' and 'plastic' behaviour of clay, suggest that the failure states of overconsolidated samples will lie along the swelling line in  $v : p'$  space.

The  $q' : p'$  plot of Fig. 11-23 shows the test paths for drained tests on samples at different values of  $R_p$ ; each sample fails when it reaches the appropriate constant  $v$  section of the Hvorslev surface. We note from Fig. 11-23 that the lightly overconsolidated samples (3, 4) fail on the critical state line.

## 11-6 VOLUME CHANGES AND PORE WATER PRESSURE CHANGES

We have now discussed the shape of the state boundary surface and the position of the critical state line; these ideas have allowed us to fix the pattern of test paths in  $v : p'$  and  $q' : p'$  space. The implications for changes in volume and pore water pressure will now be discussed.

We will first consider undrained tests. Test paths for a typical pair of tests, one on a normally consolidated specimen and the other on an overconsolidated specimen, are illustrated in Fig. 11-24. The normally consolidated specimen A must fail without change in specific volume at C on the critical state line. We may project down to  $q' : p'$  space to obtain the corresponding failure point C. We can also draw the total stress path applied to the specimen in  $q : p$  space (assuming that  $u = 0$  at the beginning of the test), noting as before that the path is of slope 3. The pore water pressure  $u_A$  at failure of specimen A is then given as the difference between  $p$  and  $p'$  at failure; the value of  $u_A$  may be scaled from the diagram as indicated.

In the same way, the overconsolidated specimen B is loaded along a total stress path of slope 3; but, if the initial specific volumes of samples A and B are the same and if the specimen deforms uniformly, the specimen again fails at the critical state at point C. The pore water pressure at failure of specimen B is then just the horizontal offset  $-u_B$  from C to the total stress path for specimen B.

The normally consolidated specimen A fails with a large positive pore water pressure, while the overconsolidated specimen B fails with a negative pore water pressure. The value (and sign) of the pore pressures are fixed by the geometry of Fig. 11-24; Examination of Fig. 11-24 indicates that the pore water pressures at failure are considerably affected by the initial overconsolidation ratios of the specimens.

A prediction of the pore water pressure at failure is clearly of considerable significance if stability calculations are to be made; the topic will therefore be further discussed in Chapter 14.

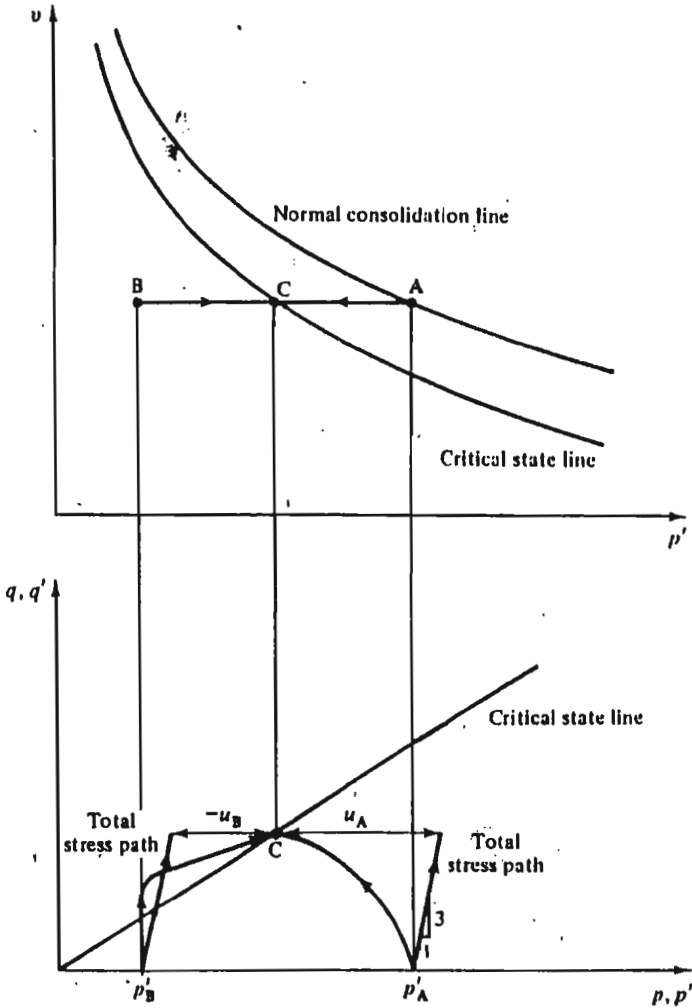


Figure 11-24 Test paths for undrained tests on normally consolidated and overconsolidated samples of clay

**Example 11-2** Calculation of the pore pressure at failure in undrained tests on heavily overconsolidated and normally consolidated samples

A sample of clay (Sample A) is isotropically normally consolidated to  $p'_0 = p_0 = 400 \text{ kN m}^{-2}$  and  $v_0 = 2.052$ . A second sample (Sample B) is isotropically consolidated to  $863 \text{ kN m}^{-2}$  and allowed to swell to  $p'_1 = p_1 = 40 \text{ kN m}^{-2}$  when  $v_0 = 2.052$ . Both samples are then subjected

to standard undrained compression tests. The values of the soil constants for the clay are  $\Gamma = 3.16$ ,  $\lambda = 0.2$ , and  $M = 0.94$ . Find the pore pressure at failure of each sample.

For an undrained test,  $\Delta v = 0$  and, hence,  $v_t = v_0$ ; the approximate effective stress paths are shown in Fig. E11.1. The value of  $p'_t$  at failure

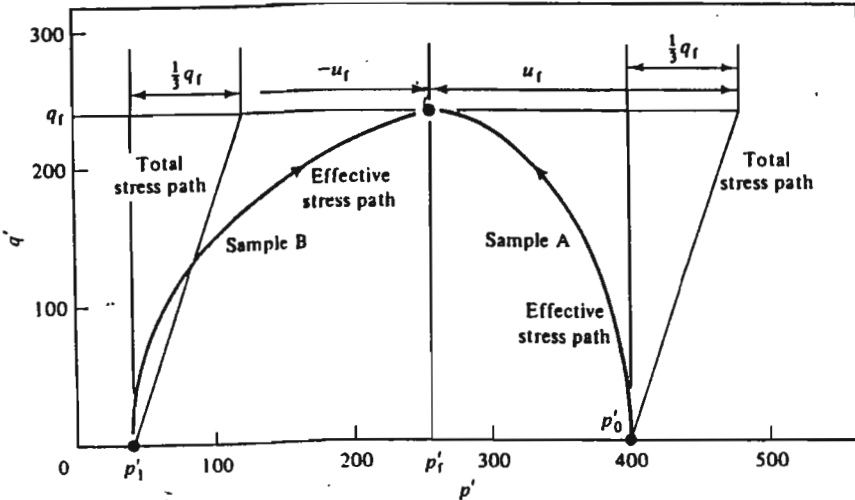


Figure E11-1

of both samples at the critical state may be obtained from the equation for the critical state line (Eq. (10-2)):

$$v_t = \Gamma - \lambda \ln p'_t = v_0,$$

or

$$p'_t = \exp[(\Gamma - v_0)/\lambda] = \exp[(3.16 - 2.052)/0.2],$$

$$p'_t = 255 \text{ kN m}^{-2}.$$

At failure, from Eq. (10-1),

$$q'_t = Mp'_t = 0.94 \times 255,$$

$$q'_t = 239 \text{ kN m}^{-2}.$$

The value of pore pressure at failure  $u_t$  for Sample A is then, from Fig. E11-1,

$$(u_t)_A = (p'_0 - p'_t) + \frac{1}{3}q'_t = 400 - 255 + \frac{1}{3} \times 239,$$

$$(u_t)_A = 225 \text{ kN m}^{-2}.$$

The value of  $u_t$  for Sample B, similarly, is

$$-(u_t)_B = (p'_t - p'_1) - \frac{1}{3}q'_t = 255 - 40 - \frac{1}{3} \times 239,$$

$$(u_t)_B = -135 \text{ kN m}^{-2}.$$

A similar argument allows volume changes to be estimated for drained tests. Consider a normally consolidated specimen D and an overconsolidated specimen E which are tested under drained conditions (Fig. 11-25). The total (and effective) stress paths in  $q' : p'$  and  $q : p$  space are again of slope 3; and the intersections of these paths with the projection of the critical state line in  $q' : p'$  space (points F, G) fix the ultimate points for the tests. Once points F and G are fixed in  $q' : p'$  space, we may project up to  $v : p'$  space to obtain the relevant specific volumes. We can see that the specific volume at point F

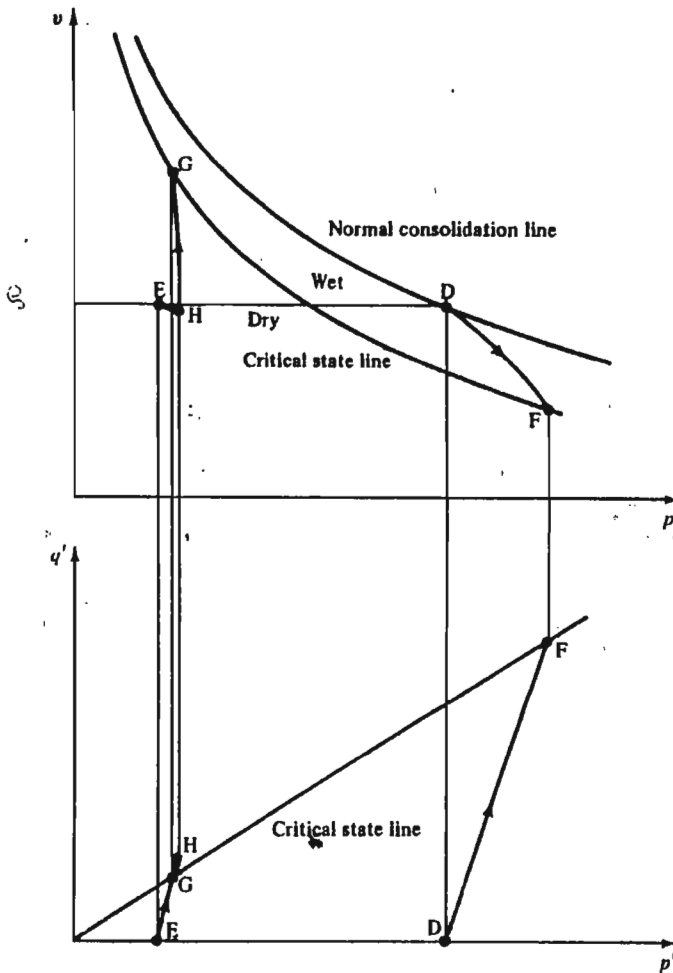


Figure 11-25 Test paths for drained tests on normally consolidated and overconsolidated samples of clay

is substantially lower than that at point D, i.e., the normally consolidated sample must compress during shear.

Similarly, the specific volume at G is substantially higher than that at E; clearly, the overconsolidated sample E must expand during shear. We should note that the sample will fail at point H on the Hvorslev surface before it reaches the critical state line at G. The specific volume at H cannot be specified from the geometry of Fig. 11-25 alone, but, as a consequence of the arguments in Chapter 13, concerning the distinction between elastic and plastic behaviour of soils, we would expect that the sample would ideally compress slightly from E to H due to the increase of  $p'$  and, hence, the specific volume at H might be slightly lower than that at E.

We should note the contrast in behaviour between overconsolidated samples, which expand (and soften) during shear, and that of normally consolidated samples, which compress (and harden) during shear. We can associate the expansion of overconsolidated specimens during drained tests with the generation of negative pore water pressure during undrained tests, and, for normally consolidated specimens, compression during drained tests can be associated with positive pore water pressures during undrained tests. Each phenomenon is a consequence of the combination of the geometry of the state boundary surface, the initial state of the specimens, and the applied total stress path.

It is convenient to distinguish between samples which lie above and to the right of the critical state line in  $v : p'$  space and those which lie below and to the left. The first group of samples will be termed wet of critical, for each sample has a moisture content higher than that of a sample on the critical state line at the same value of  $p'$ , and the second group as dry of critical, see Fig. 11-25. This classification is useful in that it groups together samples with similar pore pressure and volume change behaviour, and will be discussed in detail in Chapter 15.

**Example 11-3** Calculation of the ultimate conditions for drained tests on normally consolidated and heavily overconsolidated samples

A sample of clay (Sample A) is isotropically normally consolidated to  $p'_0 = p_0 = 400 \text{ kN m}^{-2}$  and  $v_0 = 2.052$  and a second sample (Sample B) is isotropically consolidated to  $863 \text{ kN m}^{-2}$  and allowed to swell to  $p'_1 = p_1 = 40 \text{ kN m}^{-2}$ , when the specific volume is  $v_0 = 2.052$ . Both samples are then subjected to standard drained triaxial compression tests. The clay has  $\Gamma = 3.16$ ,  $\lambda = 0.2$ , and  $M = 0.94$ . Find values for  $p'$ ,  $v$ , and  $\epsilon_v$ , when the two samples reach their ultimate states on the critical state line.

Using Eq. (10-10), the value  $p'_u$  of  $p'$  at the *ultimate* condition is given by

$$p'_u = 3p'_0 / (3 - M).$$

For Sample A,

$$(p'_u)_A = 3 \times 400 / (3 - 0.94),$$

$$(p'_u)_A = 583 \text{ kN m}^{-2}.$$

For Sample B,

$$(p'_u)_B = 3 \times 40 / (3 - 0.94),$$

$$(p'_u)_B = 58 \text{ kN m}^{-2}.$$

The value  $v_u$  of  $v$  at the ultimate condition is

$$v_u = \Gamma - \lambda \ln p'_u.$$

For Sample A,

$$(v_u)_A = 3.16 - 0.2 \ln (583),$$

$$(v_u)_A = 1.886.$$

For Sample B,

$$(v_u)_B = 3.16 - 0.2 \ln (58),$$

$$(v_u)_B = 2.347.$$

The volumetric strain  $\varepsilon_v$  during the test is

$$\varepsilon_v = -\Delta v/v.$$

For Sample A,

$$(\varepsilon_v)_A = -(1.886 - 2.052) / 2.052,$$

$$(\varepsilon_v)_A = 8.09 \text{ per cent (compression)}.$$

For Sample B,

$$(\varepsilon_v)_B = -(2.347 - 2.052) / 2.052,$$

$$(\varepsilon_v)_B = -14.4 \text{ per cent (expansion)}.$$

## 11-7 SUMMARY

1. A state boundary surface, the Hvorslev surface, limits the states of overconsolidated specimens in  $q' : p' : v$  space.
2. We have accepted as a working hypothesis that ultimate states of individual elements of overconsolidated clay lie on the same critical state line as was defined by ultimate states of tests on normally consolidated samples.
3. The complete state boundary surface, consisting of the Roscoe and Hvorslev surfaces, which meet at the critical state line, serves for drained and undrained tests on normally consolidated and overconsolidated samples and, hence, unifies a wide range of behaviour.

4. Predictions may be made of the ultimate pore pressure in an undrained test or the ultimate volume change in a drained test once the initial conditions of the test are specified.

## REFERENCES

- Bishop, A. W. and Henkel, D. J. *The Triaxial Test*. Edward Arnold, London, 1962.
- Loudon, P. A. Some deformation characteristics of kaolin. PhD Thesis, University of Cambridge, 1967.
- Parry, R. H. G. Discussion. *Geotechnique*, 8, 183-186, 1958.
- Parry, R. H. G. Triaxial compression and extension tests on remoulded saturated clay. *Geotechnique*, 10, 166-180, 1960.

## THE BEHAVIOUR OF SANDS

### 12-1 INTRODUCTION

In the last two chapters we have discussed the shear behaviour of normally consolidated and overconsolidated clay in some detail and we found a common framework for understanding our observations. We will now discuss the shear behaviour of sand. We shall find that the behaviour of sand can be fitted into the same framework that serves for clay and so it may be argued that this same framework will be relevant for a wide range of soils.

It is convenient, first, to consider typical triaxial data obtained from standard drained and undrained compression tests performed by Eldin (1951) on loose and dense samples of Brasted sand. Data from drained tests are shown in Fig. 12-1 and from undrained tests in Fig. 12-2.

A cursory glance at Figs 12-1 and 12-2 will indicate the large differences in behaviour between the four samples. The drained test on the loose specimen (Fig. 12-1(b)) gives a  $q' : \epsilon_a$  curve which reaches a flat maximum after about 20 per cent axial strain, while the sample compresses substantially as the test proceeds. At the end of the test, the sample appears to have reached an ultimate state, for there are negligible changes in stresses or in volume for continuing shear distortion.

In contrast, the dense sample (Fig. 12-1(a)) exhibits a marked peak in its  $q' : \epsilon_a$  curve, and, thereafter,  $q'$  decreases and is still decreasing at the end of the test. The sample contracts slightly initially, but then expands strongly until the end of the test. It is clear that no ultimate point has been reached at the end of the test, for the sample is still expanding and  $q'$  is decreasing. It is worth noting, however, that the value of  $q'$  at the end of the test on the dense specimen seems to be decreasing towards the value (about  $500 \text{ kN m}^{-2}$ ) observed at the ultimate point of the test on the loose specimen (Fig. 12-1(b)).

The shapes of the  $q' : \epsilon_a$  curves for the undrained tests (Fig. 12-2), one on a medium dense specimen ( $\nu = 1.75$ ) consolidated to  $p' = 73 \text{ kN m}^{-2}$  and one on a loose specimen ( $\nu = 1.84$ ), also consolidated to  $73 \text{ kN m}^{-2}$ , are similar, though the values of  $q'$  at failure ( $1270$  and  $121 \text{ kN m}^{-2}$ , respectively) are very different. The pore water pressure changes at failure in the two tests are strikingly different; the loose specimen has a positive pore water pressure at failure, while the pore water pressure is large and negative for the medium



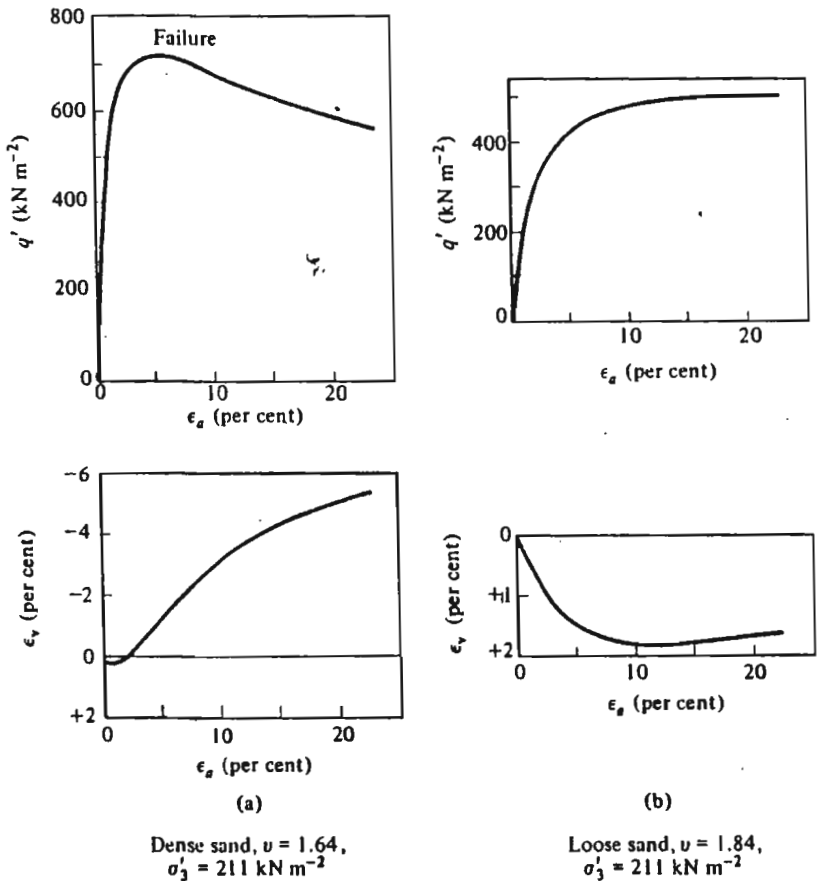
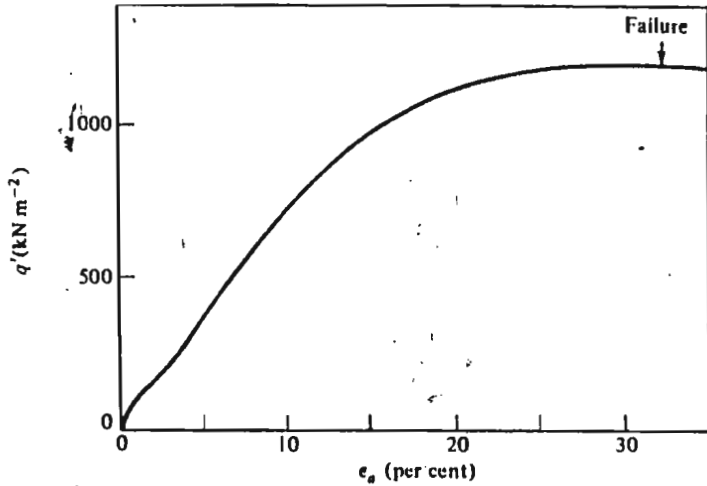


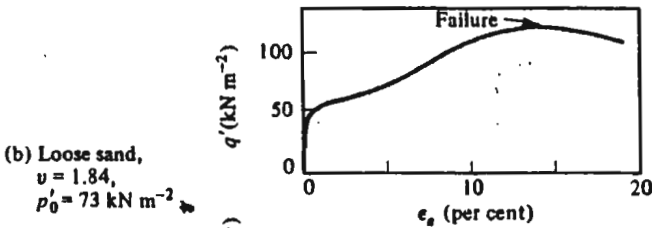
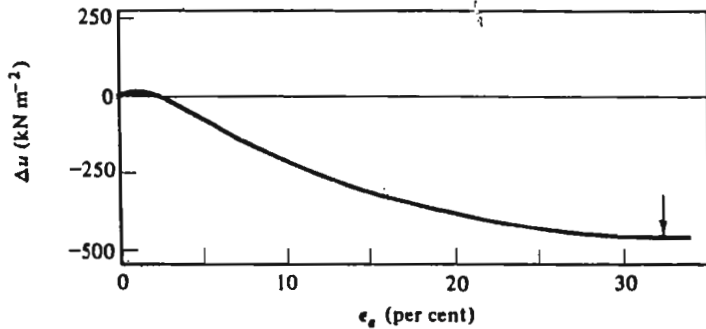
Figure 12-1 The results of drained triaxial tests on (a) a dense sample and (b) a loose sample of Brasted sand (after Bishop and Henkel, 1962, p. 123)

dense specimen. The difference in pore water pressures at failure is the major cause of the large difference in the observed shear strength of the two specimens, for the effective radial stress at failure in the dense specimen ( $\sigma'_r = 550 \text{ kN m}^{-2}$ ) is substantially larger than that for the loose specimen ( $\sigma'_r = 62 \text{ kN m}^{-2}$ ); the ratios of  $\sigma'_d/\sigma'_r$  (3.3 and 3.0, respectively) are, however, almost the same for the two cases.

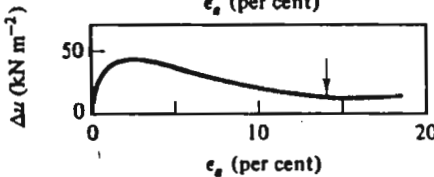
For both dense and loose samples, we note the similarity between the  $\epsilon_v : \epsilon_a$  curves from the drained tests and the  $\Delta u : \epsilon_a$  curves from the undrained tests. The loose sample contracts in the drained test and generates positive pore water pressures in the undrained test, while the dense specimen expands and generates negative pore water pressures. This pattern of behaviour is similar to that observed for clay, for heavily overconsolidated specimens of clay expand during shear and generate negative pore water pressures,



(a) Medium dense sand,  
 $v = 1.75$ ,  
 $p'_0 = 73 \text{ kN m}^{-2}$



(b) Loose sand,  
 $v = 1.84$ ,  
 $p'_0 = 73 \text{ kN m}^{-2}$



Figures 12-2 Data from undrained triaxial tests on (a) medium dense and (b) loose samples of Brasted sand (after Bishop and Henkel, 1962, p. 110)

while normally consolidated specimens of clay contract during shear and generate positive pore water pressures.

We can immediately see a similarity between the behaviour of loose sand and that of normally consolidated clay, and between that of dense sand and that of overconsolidated clay. The purpose of this Chapter is to pursue that analogy further and to consider new features of soil behaviour which are particularly relevant for sand.

## 12-2 THE CRITICAL STATE LINE FOR SAND

We saw in Chapters 10 and 11 how there were significant differences in behaviour between normally consolidated and overconsolidated clays. First of all, therefore, we must enquire about the initial states of sand samples when they are at different specific volumes and stresses, for we expect that the initial states of samples will have an important influence on their subsequent behaviour.

One of the most obvious features about sand, as discussed in Chapter 7, is that samples may be set up at different specific volumes at zero stress. If a sand sample is vibrated, it can become extremely dense (say,  $v = 1.50$ ) and firm to the touch. Conversely, if a sample is set up by slumping the sand rapidly into a container from a small height, the specific volume can be high (e.g.,  $v = 2.0$ ) and the sample will feel soft and compressible.

If the two samples are now compressed one-dimensionally, the loose sample will deform more than the dense sample, but the deformations of each will remain relatively small, as discussed in Chapter 7. Typical compression curves for loose and dense specimens of quartz sand are sketched in Fig. 12-3, which is taken from Fig. 7-13. It is clear that, for the stress levels usually adopted for laboratory testing and common in engineering construction (say  $< 700 \text{ kN m}^{-2}$ ), both loose and dense samples of this sand may be regarded as heavily overconsolidated, for they are to the left of the estimated normal consolidation line AB shown in Fig. 12-3. However, the geometry of Fig. 12-3 is such that the loose specimen is nearer the normal consolidation line (i.e., it is less overconsolidated) than the dense specimen, and, depending on the specific volume and stress level, the loose specimen may even lie on the right (wet) side of the critical state line, which we may expect in the approximate position CD.

Because sand samples normally exist on the left (dry) side of the critical state line, there are considerable experimental difficulties, as there are for overconsolidated clay, in achieving uniform stress and strain conditions in triaxial specimens at the large deformations that are required to take the states of the specimens to the critical state line. The most convincing experimental demonstration of the existence of the critical state line for sands is, therefore, provided by data from the (plane strain) simple shear apparatus.

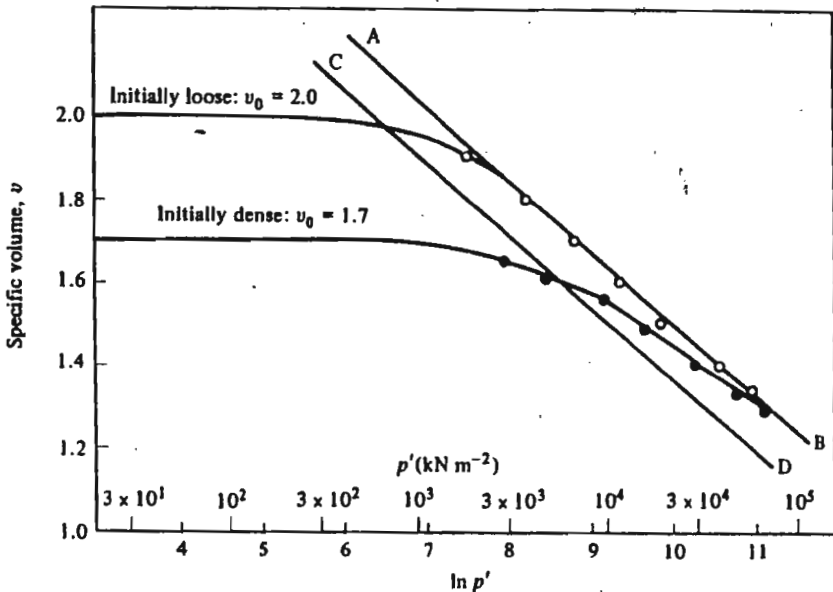


Figure 12-3 Isotropic compression of Chattahoochee River sand (after Vesic and Clough, 1968)

Comparable data for randomly packed steel balls have already been shown in Fig. 9-5. Data from ultimate points of tests on samples of Leighton Buzzard sand initially set up at different specific volumes are shown in Fig. 12-4 where, for plane strain, the appropriate stress parameters are  $t'$  and  $s'$ . The actual specific volumes of elements of sand within the specimens have been checked by careful radiographic techniques, while the boundary stresses on the sample have been measured with special stress transducers (Stroud, 1971); the data can therefore be considered to be of high reliability. The data of Fig. 12-4 define the locus of ultimate points, the critical state line, convincingly for this sand.

We will now adopt the existence of the critical state line for sands as a basis for our subsequent discussion of the behaviour of sands. We should note (i) that the line is relatively flat in  $v : \ln p'$  space (i.e.,  $\lambda$  is small, for sand is relatively incompressible) and (ii) that, at stress levels common in laboratory testing, samples on the critical state line will be extremely loose, often looser than the loosest state that can be set up by pouring sand in the laboratory. The very loose critical states for sands can often only be reached by dilation during shear.

We expect, therefore, that the shear behaviour of the sand samples, especially those that are dense, will be similar to the behaviour of heavily overconsolidated clay specimens. Thus, an undrained test on a dense sample of sand should give the test path O'A shown in Fig. 12-5. We expect that the

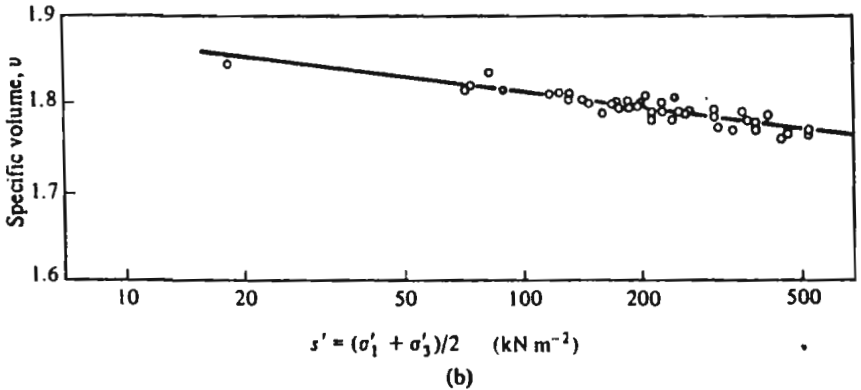
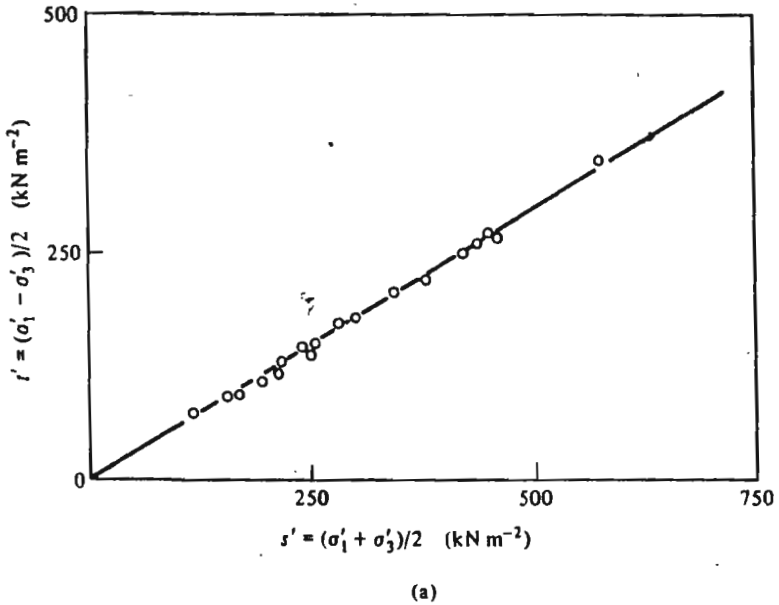


Figure 12-4 The position of the critical state line in  $t' : s'$  and  $v : \ln s'$  space for Leighton Buzzard sand tested in the simple shear apparatus (data from Stroud, 1971, and Cole, 1967)

test path will be limited by a state boundary surface similar to the Hvorslev surface and that the Roscoe surface will not be relevant for this heavily overconsolidated specimen. The position of the critical state line is such that we expect a very large negative pore water pressure to be generated.

The position of the loose specimen of sand as regards the critical state line is less clear cut, and would in any case depend on the initial consolidation stress for the sample. However, we expect a test path of the form OB sketched in Fig. 12-5.

The data from the two undrained tests given in Fig. 12-2 are in no way inconsistent with the ideas discussed above, which arise from our understanding of the behaviour of clay. We should note that the size of the constant  $v$  section of the state boundary surface is larger for the denser specimen and smaller for the looser specimen. We expect, therefore, that, at the ultimate points on the critical state line, the value of  $q'$  is larger for the dense specimen than for the looser specimen.

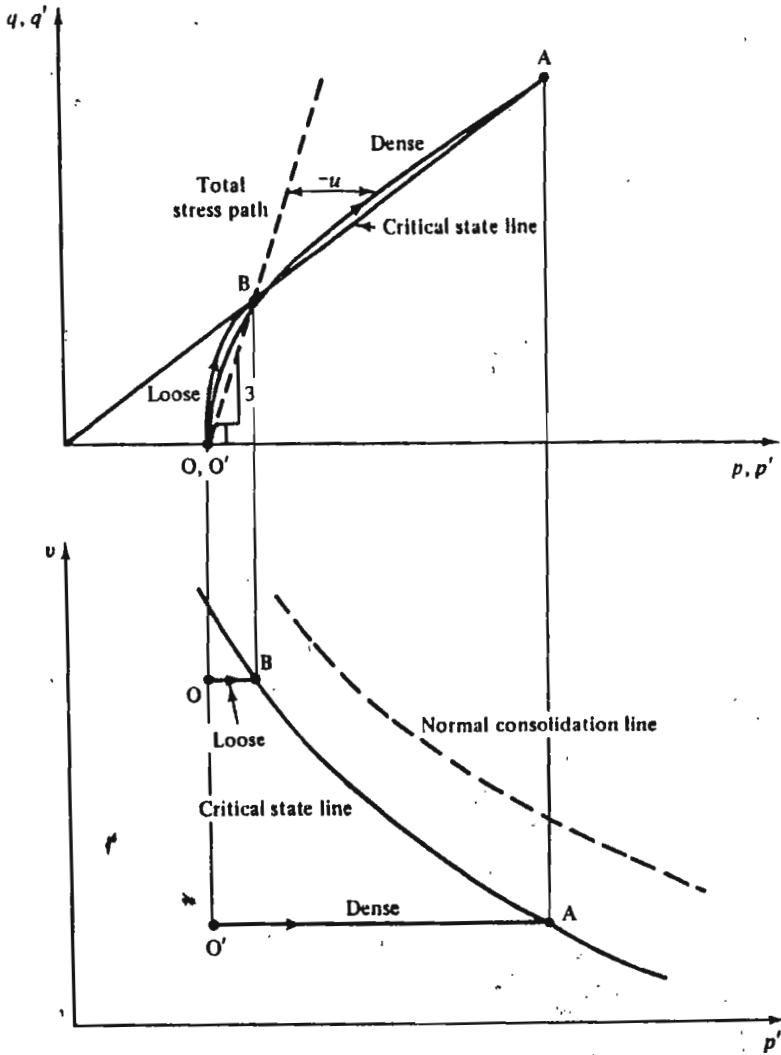


Figure 12-5 Test paths in  $q' : p'$  and  $v : p'$  space for undrained tests on dense and loose specimens of sand

We may now consider a drained test on a heavily overconsolidated specimen (i.e., a dense specimen) of sand; we expect the test paths sketched in Fig. 12-6. The peak point B in  $q' : p'$  space will lie close to the constant  $v$  section of the Hvorslev surface through B in  $v : p'$  space. Initially, the sample will compress slightly between A and B and will then expand markedly as the test proceeds and the sample moves up towards the critical state line. Both features are clearly evident in the data of Fig. 12-1(a).

The behaviour of a sand specimen which is less overconsolidated can be illustrated either by considering a drained test on a loose specimen, or, more convincingly, by a drained test conducted on a dense specimen which has

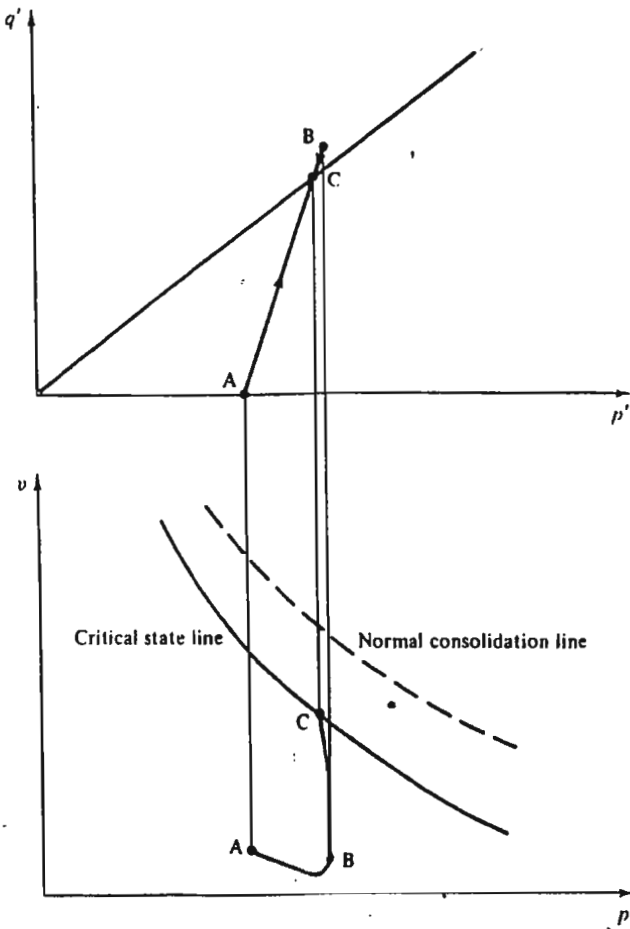


Figure 12-6 Test paths in  $q' : p'$  and  $v : p'$  space for a drained test on a dense sample of sand

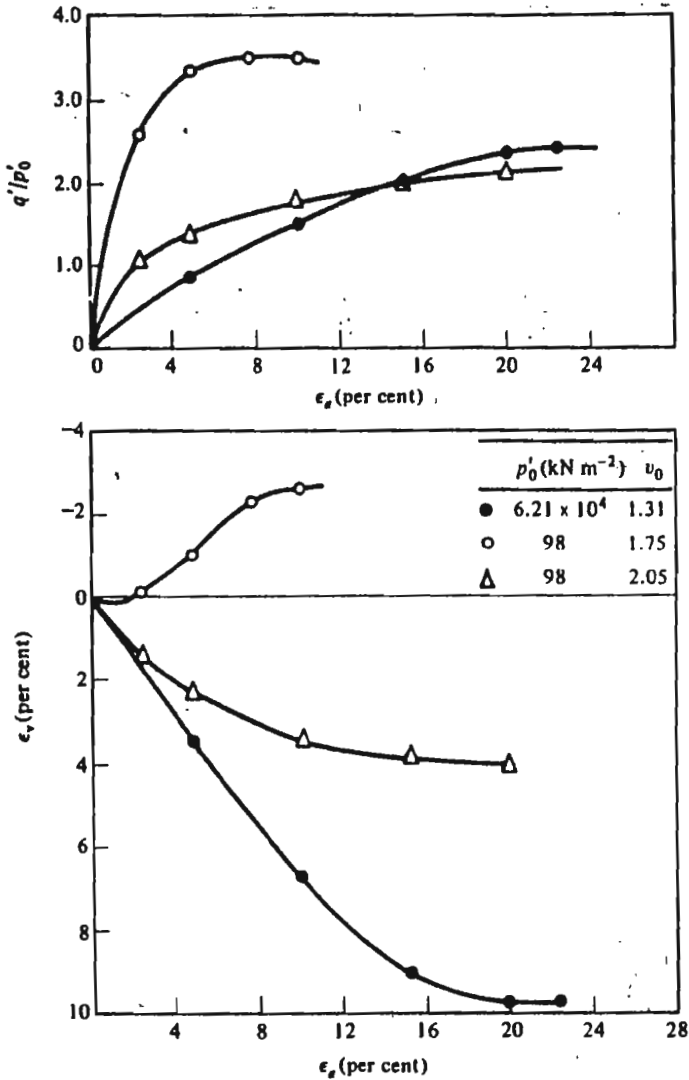


Figure 12-7 Data from drained triaxial tests on Chattahoochee River sand (after Vesic and Clough, 1968)

been consolidated to very high stresses, and so is on, or close to, the normal consolidation line. Data from three drained tests reported by Vesic and Clough (1968) are replotted in Fig. 12-7. One of the dense specimens has a specific volume of 1.75 (relative density, 80 per cent) after consolidation to 98 kN m<sup>-2</sup>; it gives a peaked stress-strain curve with failure at about 8 per cent axial strain, but with considerable expansion throughout the test. This



behaviour is entirely consistent with that shown in Fig. 12-1. The second dense specimen has a specific volume of 1.31 after consolidation to  $62\,100\text{ kN m}^{-2}$ . This specimen contracts substantially during shear, and the deviator stress reaches a flat maximum, but only after a strain of greater than 20 per cent. The behaviour of this specimen is comparable with the behaviour of a normally consolidated specimen of clay. The third specimen is loose, for it has  $v = 2.05$  (relative density, 20 per cent) when it is consolidated to  $98\text{ kN m}^{-2}$ , and shows behaviour intermediate between that of the two dense specimens at the different cell pressures. The three tests clearly confirm that the dense specimen is heavily overconsolidated at  $p' = 98\text{ kN m}^{-2}$ , the loose specimen is lightly overconsolidated at  $98\text{ kN m}^{-2}$  and the dense specimen is normally consolidated at  $62\,100\text{ kN m}^{-2}$ .

### 12-3 NORMALIZED PLOTS

We have discussed the paths followed by drained and undrained tests on loose and dense sand in  $q' : p' : v'$  space. We ought now to represent the same test paths in normalized plots so that different tests may easily be compared. As before, the equivalent stress  $p'_e$  is used to non-dimensionalize  $q'$  and  $p'$ , for we argue that each constant  $v$  section of the state boundary surface is of the same shape, but that the size of each section depends on the value of the specific volume. Test paths for drained and undrained tests on loose and dense samples of sand are sketched in Fig. 12-8. Only the drained test on the dense specimen goes through a maximum value of  $q'/p'$  before descending towards the critical state; the other samples do not progress all the way up to the Hvorslev surface on the dry side of the critical state line.

The normalization of Fig. 12-8 is highly satisfactory for clay. The difficulty for sand is that the normal consolidation line, and hence its slope  $\lambda$ ,

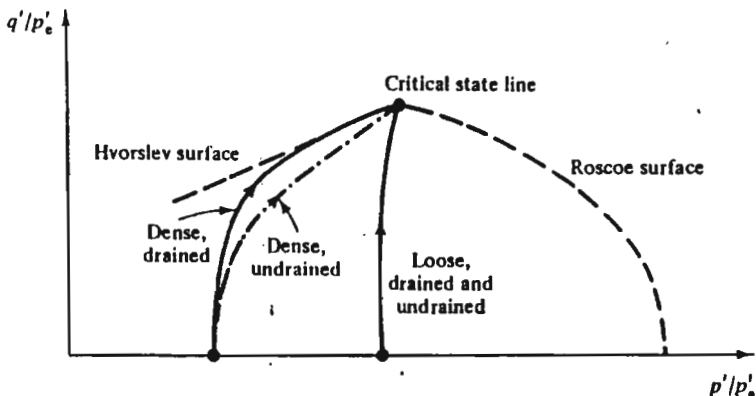


Figure 12-8 Test paths in  $q'/p'_e : p'/p'_e$  space for drained and undrained tests on loose and dense samples of sand

is difficult to establish, as tests have to be performed at stresses larger than those commonly adopted in soil testing. In any case, the slope  $\lambda$  of the normal consolidation line is rather low (typically,  $\lambda = 0.10$ ). The definition of  $p'_o$ ,

$$p'_o = \exp[(N-v)/\lambda], \quad (12-1)$$

also includes the parameter  $N$  which fixes the intercept of the normal consolidation line with the line corresponding to  $p' = 1 \text{ kN m}^{-2}$ ; again the value of  $N$  is difficult to establish with accuracy for sand. We see, therefore, that the term in square brackets on the right-hand side of Eq. (12-1) is uncertain in value, is large (because  $\lambda$  is small), and yet has an exponential effect on the value of  $p'_o$ . It is unsatisfactory, therefore, to use a normalization for sands which relies on the parameter  $p'_o$ .

We know that the behaviour of a sample of sand is influenced most of all by its initial specific volume. It seems reasonable, therefore, to choose a normalization in which the initial specific volume has a dominant influence, and in which the exact position and slope of the normal consolidation line are less crucial. The obvious alternative to the  $p'_o$ -scaling (where we are essentially considering the size of the constant  $v$  section of the state boundary surface) is to use a scaling based on the size of the constant  $p'$  section of the state boundary surface. The difficulty again is that we must then define some equivalent specific volume corresponding to the specific volume on the normal consolidation line at that pressure; difficulties in locating the normal consolidation line for sand make this approach unsatisfactory.

A more satisfactory alternative is to think of a reference constant  $p'$  section of the state boundary surface and then to correct the positions of states in  $v : p'$  space so that they lie on the reference section. The idea is illustrated in Fig. 12-9. The reference section of the state boundary surface is arbitrarily chosen to be at  $p' = 1 \text{ kN m}^{-2}$  to be consistent with our definitions of  $N$  and  $\Gamma$ . Then, on the reference section,  $v = N$  for the normal consolidation line and  $v = \Gamma$  for the critical state line. We wish all states on the critical state line to be represented by a single point ( $v = \Gamma$ ) on the reference section, and all states on the normal consolidation line to be represented by a single point ( $v = N$ ) on the reference section, for, in each case, the behaviour of all such samples will be identical. Similarly, a point such as A, between the normal consolidation line and the critical state line, must appear in the reference section at a value of  $v$  between  $N$  and  $\Gamma$ . The procedure to map A on to the reference section is obvious. Draw a line through A at slope  $\lambda$  (i.e., parallel to both the critical state line and to the normal consolidation line) and the intersection of that line with the reference section, point A', is used to represent point A, and indeed all other points on line A'A. In the same way, the point B maps into the point B'.

We define the value of specific volume on the reference section as  $v_\lambda$ . Then,

$$v_\lambda = v + \lambda \ln(p'), \quad (12-2)$$

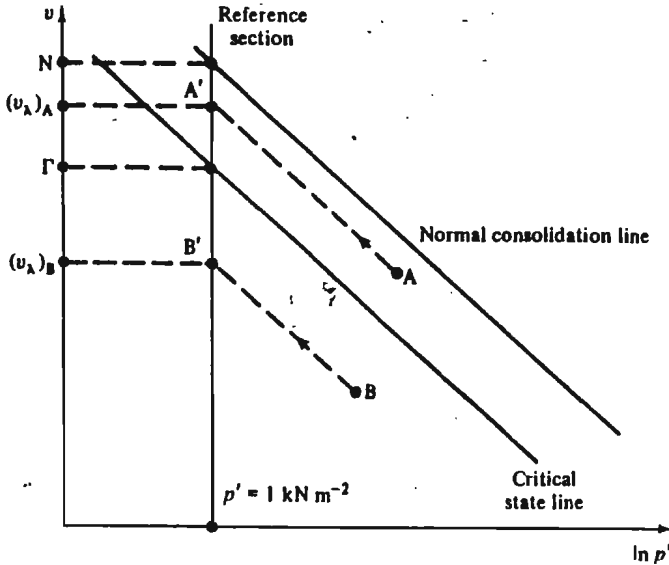


Figure 12-9 The method of correcting points so they lie on the constant  $p'$  reference section

where  $v$  and  $p'$  are the specific volume and mean normal effective pressure at a typical point A and  $v_\lambda$  is the specific volume of the corresponding point A' on the reference section. The parameter  $v_\lambda$  gives a direct measure of the position of a sample in  $v : p'$  space with respect to the critical state line; it depends primarily on the specific volume  $v$  of the sample, and less, because  $\lambda$  is small for sands, on the mean normal pressure.

We have now discussed the mapping of points onto the reference ( $p' = \text{constant}$ ) section of the state boundary surface. We note that  $p' = 1 \text{ kN m}^{-2}$  on the reference section, by definition, and so the scaled deviator stress must be appropriate to that value of  $p'$ . The mean normal stress has been scaled in the ratio  $(1/p')$ , and so it is appropriate to scale the deviator stress by the same factor of  $(1/p')$ . The scaled value of deviator stress to be plotted on the reference section at point A' would, therefore, be  $(q'/p')$ , where  $q'$  and  $p'$  are the stresses at the typical state point A considered.

All points on the critical state line will therefore have  $q'/p' = M$  and all points on the isotropic normal consolidation line will have  $q'/p' = 0$ . A view of the reference section will, therefore, be as shown in Fig. 12-10. The two sections of the state boundary surface, the Hvorslev surface and the Roscoe surface, are separated by the critical state line, while the Roscoe surface joins the critical state line to the normal consolidation line.

We saw in Chapter 11 that the Hvorslev surface was straight for clays in  $q'/p'_0 : p'/p'_0$  space, and had the form

$$q'/p'_0 = g + h(p'/p'_0), \quad (12-3)$$

where  $g$  and  $h$  are soil constants. Equation (12-3) may be rewritten as

$$q'/p' = g(p'_0/p') + h. \quad (12-4)$$

Substitution of Eq. (12-1) into Eq. (12-4) gives

$$q'/p' = g/p' \exp [(N-v)/\lambda] + h \quad (12-5)$$

and, using Eq. (12-2),

$$q'/p' = g/p' \exp [(N/\lambda) - (v_\lambda/\lambda) + \ln p'] + h \quad (12-6)$$

or, using Eq. (11-10),

$$q'/p' = (M-h) \exp [(\Gamma - v_\lambda)/\lambda] + h. \quad (12-7)$$

Thus, if we assume that the Hvorslev surface has the same shape for sands as for clays, we can sketch the Hvorslev surface in the  $q'/p' : v_\lambda$  space of Fig. 12-10 as shown. Of course, there is no guarantee that the Hvorslev surface has precisely the same shape for sands as for clays, but the form of Fig. 12-10 suggests that the maximum observable value of  $q'/p'$  for sand is a function of  $v_\lambda$ . When  $v_\lambda$  is small the sample is heavily overconsolidated and  $q'/p'$  can be high, while, when  $v_\lambda$  is equal to  $\Gamma$ ,  $q'/p'$  cannot exceed  $M$ . These suppositions are in accord with common experience in soil mechanics testing; dense sands give higher values of the angle of internal friction than do loose sands.

The precise form of the state boundary surface for sands can be investigated experimentally, although there is little published data available. We shall quote data from triaxial tests as well as from tests in plane strain conditions to get an indication of the likely shape of the Hvorslev surface.

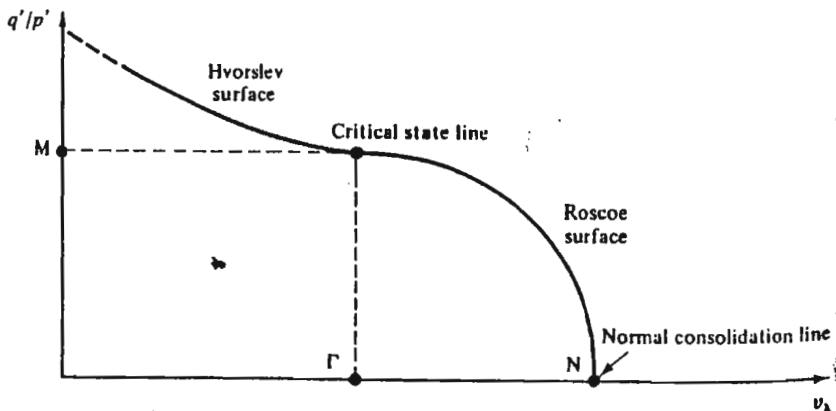


Figure 12-10 The reference section in  $q'/p' : v_\lambda$  space

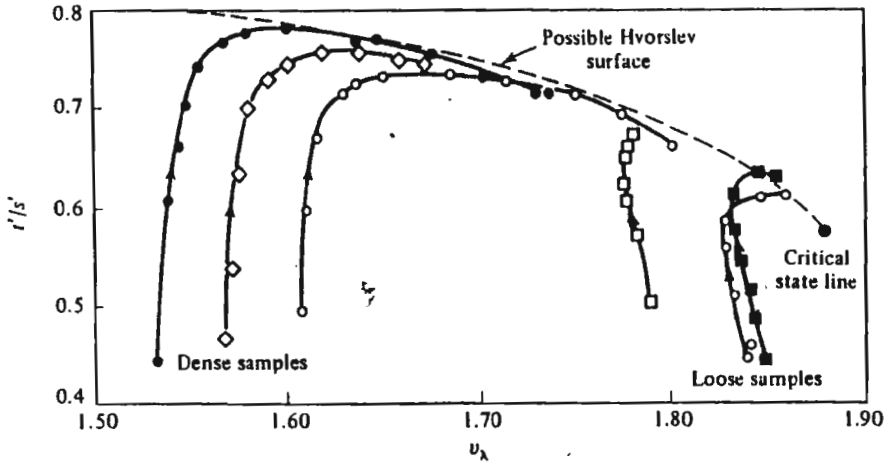


Figure 12-11 Test paths in  $t'/s' : v_\lambda$  space for tests on Leighton Buzzard sand in the simple shear apparatus in which the vertical stress was held constant (after Stroud, 1971)

Nevertheless it has to be accepted that the Hvorslev surface has not yet been precisely defined for sand. Stroud (1971) performed tests in the simple shear apparatus at different stress levels and at different specific volumes. He plotted his results in  $t'/s' : v_\lambda$  space (Fig. 12-11) for, as he was using a plane strain testing device, it is more appropriate to use  $t'$  instead of  $q'$  and  $s'$  instead of  $p'$ . The data from drained tests (Fig. 12-11) defined a state boundary surface which appeared curved in  $t'/s' : v_\lambda$  space.

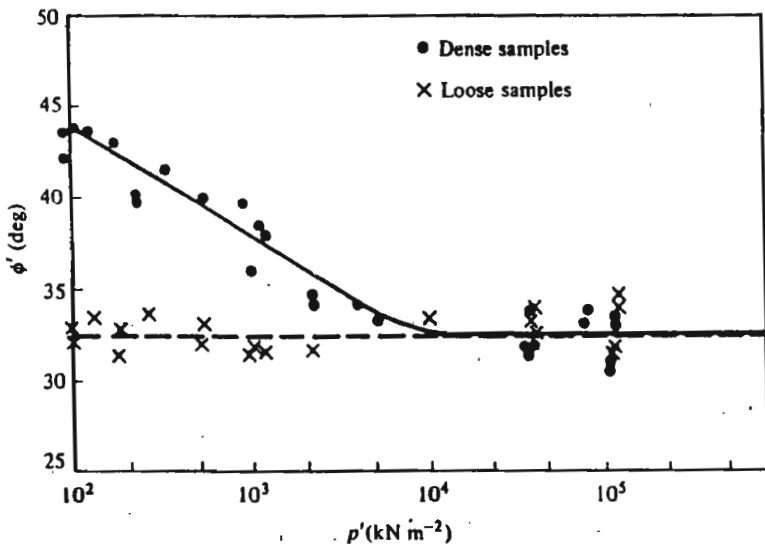


Figure 12-12 Angle of internal friction for Chattahoochee River sand tested at different stress levels in the triaxial apparatus (after Vesic and Clough, 1968)

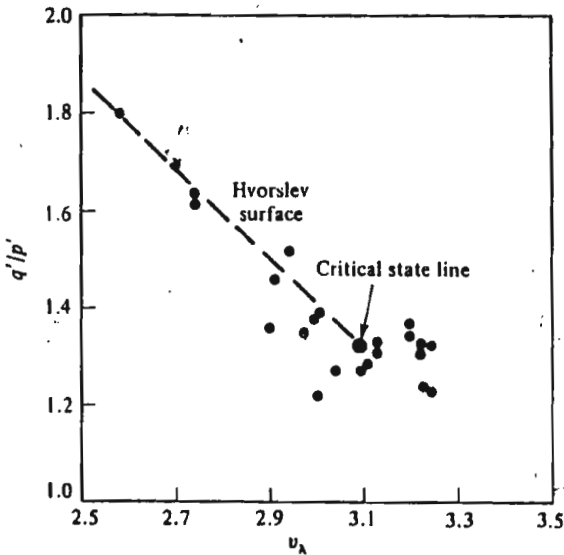


Figure 12-13 The data of Fig. 12-12 replotted in  $q'/p' : v_\lambda$  space. Value of  $\lambda$  taken as 0.175 (data from Vesic and Clough, 1968)

In contrast, an indication that the Hvorslev surface for sands is straight in  $q'/p' : v_\lambda$  space is provided by the data of Vesic and Clough (1968). Vesic and Clough plot the measured angle of internal friction for initially dense and loose samples of Chatahoochee River sand against the logarithm of the mean normal stress in triaxial tests (Fig. 12-12). The same data map into  $q'/p' : v_\lambda$  space as shown in Fig. 12-13. It should also be noted that the failure points for the loose samples all map into a region close to the critical state point in Fig. 12-13.

We note, as for clays, that sand samples will move to the state boundary surface, and then move along the surface as they expand or contract, until they eventually reach the critical state condition. For samples on the right-hand side of the critical state line (i.e.,  $v_\lambda > \Gamma$ ), the maximum value of  $q'/p'$  will be reached at the critical state line, and so we expect failure there.

Samples on the left-hand side of the critical state line (i.e.,  $v_\lambda < \Gamma$ ) have the possibility of exhibiting values of  $q'/p' > M$ . Samples which have low values of  $v_\lambda$  (i.e., they are very dense or the stress level is very low) can resist rather high values of  $q'/p'$ .

**Example 12-1** Calculation of the peak value of  $q'/p'$  for samples of sand at different mean normal stresses and specific volumes

Drained triaxial compression tests have been performed on samples of sand which failed at  $v = 1.5$  (Sample A) and  $v = 1.8$  (Sample B). It was

found that the maximum values of  $q'/p'$  were 1.85 and 1.42, respectively, and both samples had  $p' = 200 \text{ kN m}^{-2}$  at peak. The sand has  $\lambda = 0.03$ . It may be assumed that both samples failed on the dry side of the critical state line.

Estimate the peak value of  $q'/p'$  for samples which fail at (i)  $v = 1.65$ ,  $p' = 3000 \text{ kN m}^{-2}$  (Sample C) and (ii)  $v = 1.5$ ,  $p' = 10 \text{ kN m}^{-2}$  (Sample D).

The value of  $v_\lambda$  is given by Eq. (12-2):

$$v_\lambda = v + \lambda \ln p'$$

For Sample A,

$$v_\lambda = 1.5 + 0.03 \ln(200) = 1.659.$$

For Sample B,

$$v_\lambda = 1.8 + 0.03 \ln(200) = 1.959.$$

For Sample C,

$$v_\lambda = 1.65 + 0.03 \ln(3000) = 1.890.$$

For Sample D,

$$v_\lambda = 1.5 + 0.03 \ln(10) = 1.569.$$

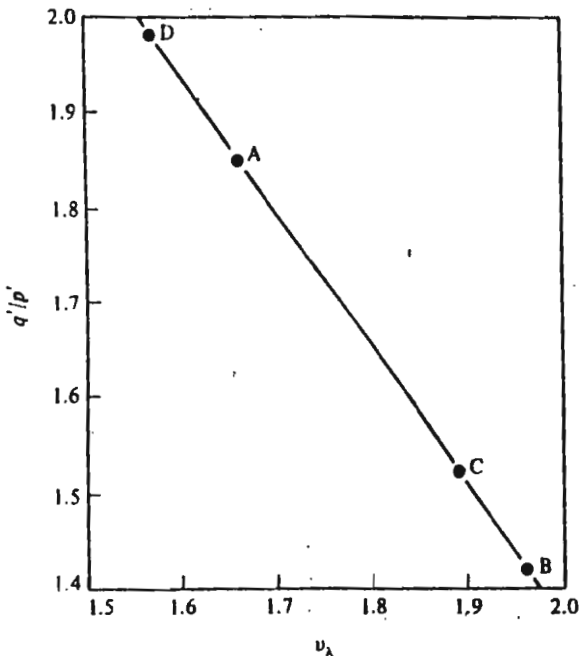


Figure E12-1

Plot the data from Samples A and B in  $q'/p' : v_\lambda$  space, as shown in Fig. E12-1. We shall now assume that the Hvorslev surface is approximately straight in  $q'/p' : v_\lambda$  space and interpolate in Fig. E12-1. Hence, for Sample C,

$$q'/p' = 1.85 - \frac{1.89 - 1.659}{1.959 - 1.659} \times (1.85 - 1.42),$$

$$q'/p' = 1.52.$$

An extrapolation is required for Sample D, and so the estimate of  $q'/p'$  will be less reliable. For Sample D,

$$q'/p' = 1.85 - \frac{1.569 - 1.659}{1.959 - 1.659} \times (1.85 - 1.42),$$

$$q'/p' = 1.98.$$

#### 12-4 THE EFFECT OF DILATION

We have discussed the maximum possible values of  $q'/p'$  that a sand may resist at different states; it is now instructive to consider some simple analogies which help to explain some other factors which influence the mobilized value of  $q'/p'$ .

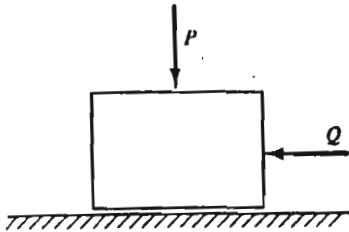
Consider a block resting on a rough plane and acted on by a vertical force  $P$  (Fig. 12-14). If the coefficient of friction between the plane and the block is  $\mu$ , we know that the sideways force  $Q$  must be increased until  $Q = \mu P$  before the block slides horizontally sideways. It seems a reasonable analogy to argue in the same way that at failure of a body of sand, where one block of the soil slides across another block (Fig. 12-14(b)), there would be a constant ratio of the shear stress  $\tau'$  to the effective normal stress  $\sigma'$  on the plane of failure. Thus, by analogy with the purely sideways sliding of the block on the plane, we may write

$$\tau' = \mu \sigma' \quad (12-8)$$

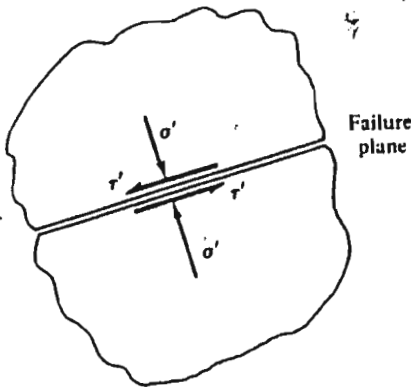
for the behaviour of the sand, though we must note that this relationship applies only for purely sideways movement of one block of soil relative to the other, i.e., for constant volume deformation.

We now consider a second simple analogy: in this case both the bottom of the block and the top of the supporting plane are serrated, as shown in Fig. 12-15. We suppose, as before, that the coefficient of friction between the contacting faces is  $\mu$ . Clearly now, as the block slides sideways, it will also move up at angle  $\alpha$  to the horizontal, so doing work against the vertical force  $P$ . The force  $Q$  will, therefore, have to be sufficient to overcome the friction as well as to supply work to lift the block against  $P$ . The relationship





(a)



(b)

Figure 12-14 (a) Sliding of a block on a rough plane. (b) Sliding of one block of sand with respect to another block of sand

between  $P$  and  $Q$  during sliding can be obtained by finding the sum  $N$  of the normal forces and the sum  $S$  of the shear forces on the planes of contact. We have

$$N = P \cos \alpha + Q \sin \alpha, \quad (12-9)$$

$$S = -P \sin \alpha + Q \cos \alpha. \quad (12-10)$$

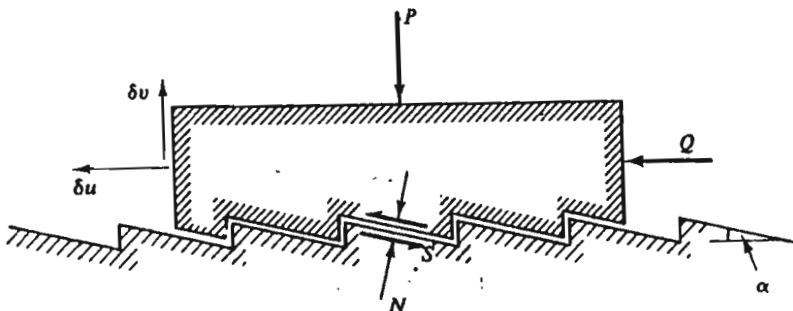


Figure 12-15 Sliding of a serrated block on a serrated plane

Putting  $S = \mu N$  for sliding and substituting gives

$$Q - P \tan \alpha = \mu P + \mu Q \tan \alpha. \quad (12-11)$$

For a small horizontal movement of  $\delta u$ , the block will move upwards by  $\delta v$ , where  $\delta v / \delta u = \tan \alpha$ . Substitution for  $\tan \alpha$  and collection of terms gives

$$\frac{Q}{P} = \frac{\mu + (\delta v / \delta u)}{1 - \mu(\delta v / \delta u)}. \quad (12-12)$$

The ratio  $Q/P$  for sliding of the block now exceeds  $\mu$ , the coefficient of friction between the block and the plane, by an amount which depends on the ratio of vertical to horizontal movement of the block. This analogy can be extended so that it is more relevant for sand undergoing uniform simple shear. Consider a stack (of area  $A$ ) of serrated blocks resting on top of one another (Fig. 12-16), with the stack being sheared under the action of a shear force  $\tau'A$  and a normal force  $\sigma'A$ . Of course, Eq. (12-12) will also

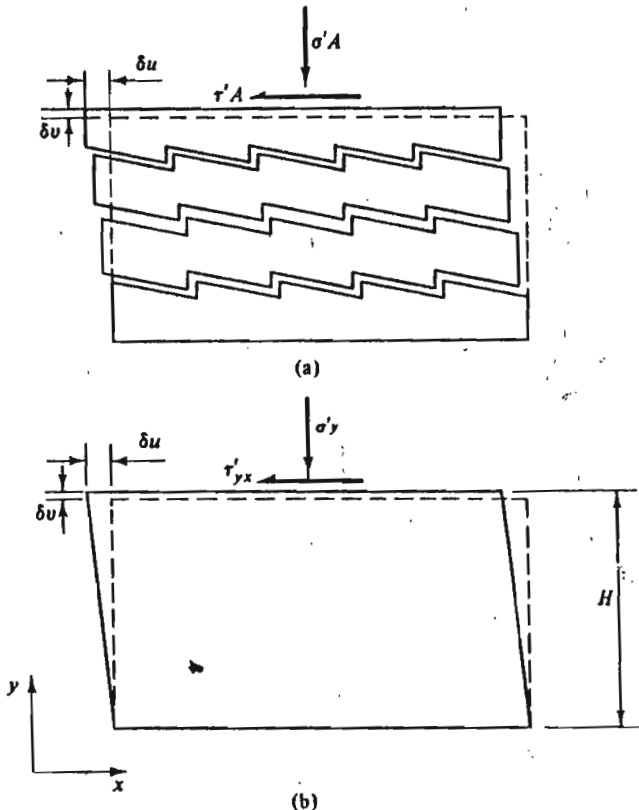


Figure 12-16 Deformation of (a) a stack of serrated blocks and (b) a sample in simple shear

apply for the extended model of Fig. 12-16(a). The corresponding (simple shear) deformation of a sample of sand, of height  $H$ , is indicated in Fig. 12-16(b).

We can note, for the sample of sand, that the ratio  $\delta v/H$ , which is positive for expansion, is equal in magnitude to the (compressive) vertical strain in the sand, but of opposite sign. Because the horizontal strain is zero, the vertical strain is equal to the volumetric strain  $\delta \epsilon_v$ . Similarly, the ratio  $\delta u/H$  is equal to the shear strain  $\delta \gamma_{vx}$ . Thus, if the analogy is pursued further, the term  $\delta v/\delta u$  in Eq. (12-12) may be replaced by  $(-\delta \epsilon_v/\delta \gamma_{vx})$  to give

$$\frac{\tau'_{vx}}{\sigma'_v} = \frac{\mu - (\delta \epsilon_v/\delta \gamma_{vx})}{1 + \mu(\delta \epsilon_v/\delta \gamma_{vx})} \tag{12-13}$$

Equation (12-13) suggests that the ratio between the shear stress and the normal stress in a shear box test on a sand depends on a frictional constant  $\mu$  as well as the ratio between volumetric strain and shear strain, with higher values of  $\tau'_{vx}/\sigma'_v$  occurring for higher ratios of negative volumetric strain (expansion) to shear strain.

An alternative, and perhaps a simpler, hypothesis would be to argue for a sand that the net work crossing the boundaries of a specimen is entirely dissipated in friction. Now, for an increment of horizontal displacement  $\delta u$  in a simple shear deformation, as shown in Fig. 12-16(b), the net work transferred into the specimen during the increment is  $\tau'_{vx} A \delta u - \sigma'_v A \delta v$ . We assume that this work is entirely dissipated in friction, and that the work dissipated in friction is taken to be proportional to a frictional constant  $\mu$ , the normal force  $\sigma'_v A$  and the shear displacement  $\delta u$ . Thus,

$$\tau'_{vx} A \delta u - \sigma'_v A \delta v = \mu \sigma'_v A \delta u. \tag{12-14}$$

Equation (12-14) may be rearranged as

$$\tau'_{vx}/\sigma'_v = \mu + (\delta v/\delta u). \tag{12-15}$$

Again, the ratio  $\tau'_{vx}/\sigma'_v$  depends on a frictional constant ( $\mu$ ) as well as the rate  $(\delta v/\delta u)$  at which the sample dilates (expands) during shear, with higher values of  $\tau'_{vx}/\sigma'_v$  given for higher values of rates of dilation.

An analysis of this form was suggested by Taylor (1948, pp. 345-347).

It is tempting to generalize Eq. (12-15) and to rewrite it in terms of the equivalent invariant parameters as

$$q'/p' = M - (\delta \epsilon_v/\delta \epsilon_s), \tag{12-16}$$

remembering that the sign convention for  $\delta v$  is such that a positive  $\delta v$  gives expansion, i.e., a negative volumetric strain increment  $\delta \epsilon_v$ .

Equation (12-13) is less easy to generalize, partly, at least, because of our reservations about whether the serrated block model can adequately represent deformation behaviour in three dimensions. Nevertheless, it is clear that the model suggests that  $q'/p'$  depends on a frictional constant as well as on the

rate of volume change during shear (say,  $\delta\epsilon_v/\delta\epsilon_s$ ), though in a more complicated way than suggested by Eq. (12-16).

A number of workers have suggested relationships between parameters equivalent to  $q'/p'$  and  $\delta\epsilon_v/\delta\epsilon_s$ . Perhaps the most notable is the stress-dilatancy relationship of Rowe (1962), which has some conceptual similarities with the serrated block model of Fig. 12-16(a) and with Eq. (12-13), and which has much experimental evidence in its support. However, we shall now adopt Taylor's model in its generalized form (Eq. (12-16)), since our discussion will be only qualitative, and the Taylor model has the merit of simplicity.

## 12-5 CONSEQUENCES OF TAYLOR'S MODEL

Equation (12-16) relates the stress ratio  $q'/p'$  to the dilation rate  $\delta\epsilon_v/\delta\epsilon_s$ . In particular, when  $\delta\epsilon_v/\delta\epsilon_s$  is zero (constant volume deformation), we expect that  $q'/p' = M$ . Thus, in data from a drained triaxial test on dense sand (Fig. 12-17) we expect that  $q'/p' = M$  at strains corresponding to the

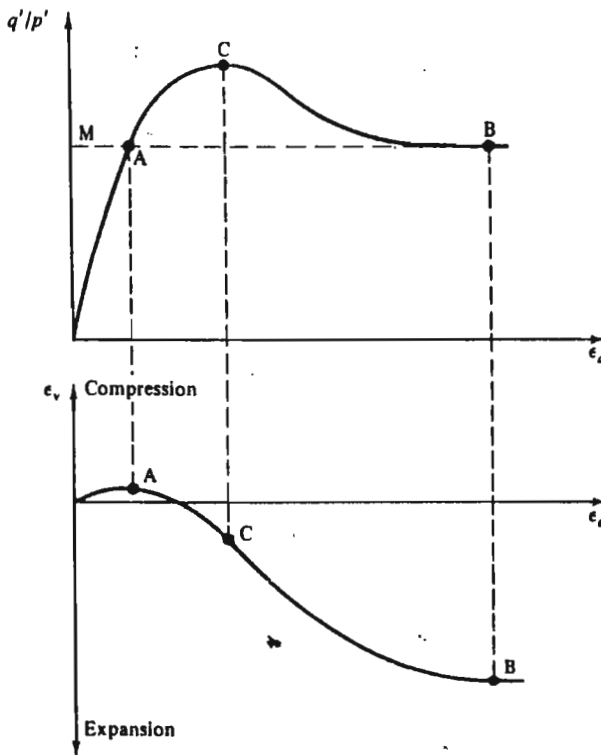


Figure 12-17 Typical  $q'/p' : \epsilon_s$  and  $\epsilon_v : \epsilon_s$  relationships for a drained triaxial test on dense sand

two points (A, B) where the sample is instantaneously deforming at constant volume. For strains less than that at A, the sample contracts and so  $\delta\epsilon_v/\delta\epsilon_a$  is positive. We, therefore, expect that  $q'/p'$  is less than  $M$ . The sample expands continuously between A and B, with the maximum rate of dilation at some point C. It follows, therefore, that  $q'/p'$  would have its maximum value at a strain corresponding to that at C. These ideas are entirely consistent with the data of Fig. 12-1(a). We thus conclude that there is a direct link between the shape of the  $\epsilon_v : \epsilon_a$  curve and the shape of the  $q'/p' : \epsilon_a$  curve.

The curves for a loose sample of sand are sketched in Fig. 12-18.

The link between stress ratio and dilation rate can be shown to be consistent with the form of the Hvorslev surface. Consider a sample at some point A on the Hvorslev surface shown in  $q'/p' : v_\lambda$  space in Fig. 12-19. At A,  $q'/p'$  will be greater than  $M$  and so, by Eq. (12-16), the sample will expand during shear. If it expands,  $v_\lambda$  will increase and the sample will move down the Hvorslev surface towards the critical state line. The same increment of deformation can also be represented in  $q' : p'$  and  $v : p'$  spaces as shown in Fig. 12-20; the constant  $v$  sections of the Hvorslev surface corresponding to the initial and final state points are indicated by lines 1-1 and 2-2 in the  $q' : p'$  plot.

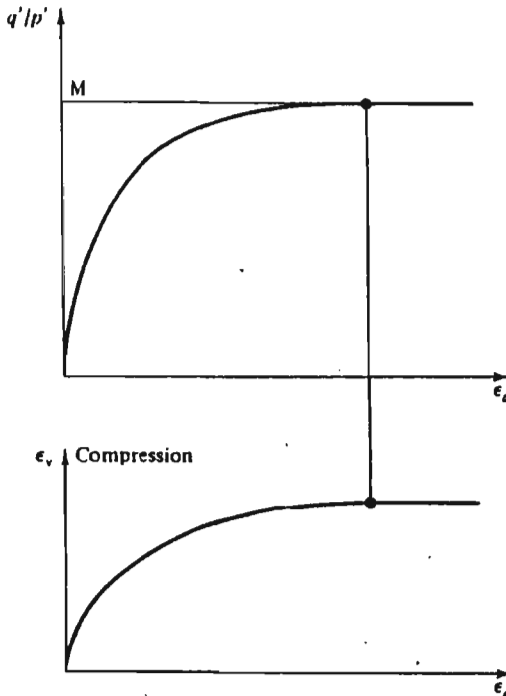


Figure 12-18 Typical  $q'/p' : \epsilon_a$  and  $\epsilon_v : \epsilon_a$  relationships for a drained triaxial test on loose sand

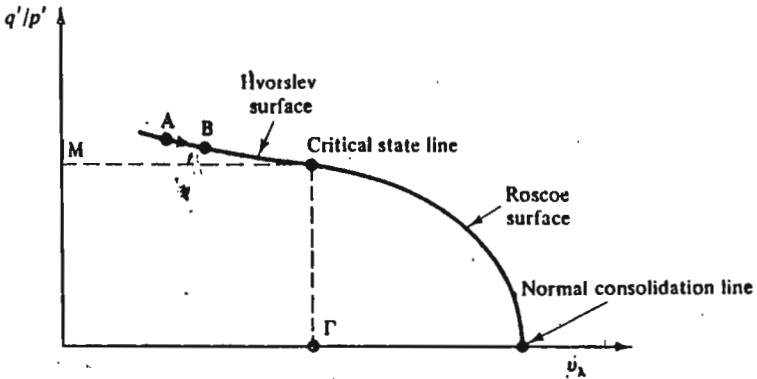


Figure 12-19 The state boundary surface viewed on the reference section

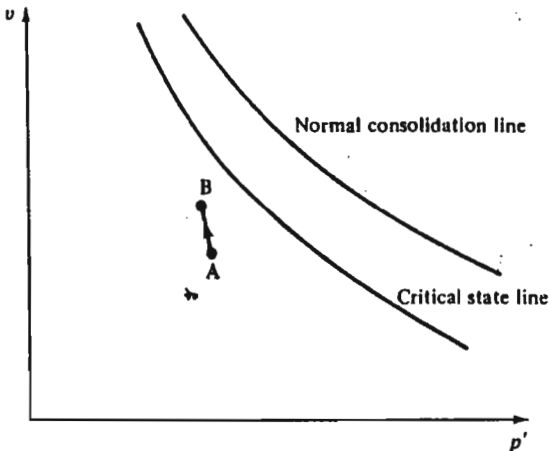
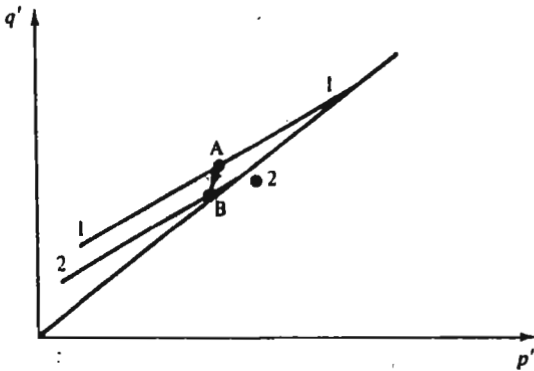


Figure 12-20 The path for an increment of loading of dense sand in  $q' : p$  and  $v : p'$  spaces

The whole stress path can be represented on the reference section, as shown in Fig. 12-21. It is simplest to consider a hypothetical drained test (ABCDE) on a dense sample in which the effective mean normal stress  $p'$  is held constant during the test. Changes in  $v_\lambda$  are then brought about only by changes in specific volume  $v$  of the specimen. For the portion of the test for which  $q'/p'$  remains less than  $M$  (i.e., ABC), the sample will contract and so the test path will move up and to the left in Fig. 12-21. As straining continues,  $q'/p'$  will be greater than  $M$ , and so the sample will expand and move to the right on the plot, following the Hvorslev surface down towards the critical state line. The strains associated with any portion of the test path will increase as the test proceeds, and, when the sample arrives at the critical state, unlimited deformation may occur at constant volume and at constant stresses.

A looser specimen of sand will follow a path (FGE) that shows more initial contraction before the sample eventually arrives at the critical state condition after large deformations.

We have so far considered drained tests. In undrained tests,  $\delta\varepsilon_v/\delta\varepsilon_s = 0$  and, hence, from Eq. (12-16),  $q'/p'$  should always be equal to  $M$ . Thus, on a  $q'/p' : v_\lambda$  plot (Fig. 12-22), the major part of the test path will be a horizontal line BC at  $q'/p' = M$ . However, we appreciate that the sand will deform a little as it mobilizes sufficient shear stresses for  $q'/p'$  to be equal to  $M$ , and so we must expect some small deformations over the path AB. In order that the sample moves towards the critical state at C, the value of  $v_\lambda$  must change from its initial value  $v_{\lambda_0}$ , say, corresponding to a specific volume of  $v_0$  and mean normal stress of  $p'_0$ , to  $\Gamma$  at the critical state when  $p' = p'_u$ . Initially,

$$v_{\lambda_0} = v_0 + \lambda \ln p'_0 \tag{12-17}$$

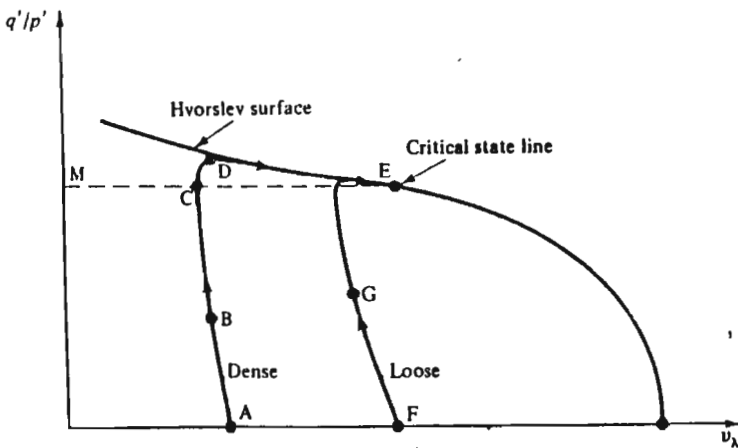


Figure 12-21 Stress paths for drained tests on loose and dense specimens of sand in  $q'/p' : v_\lambda$  space

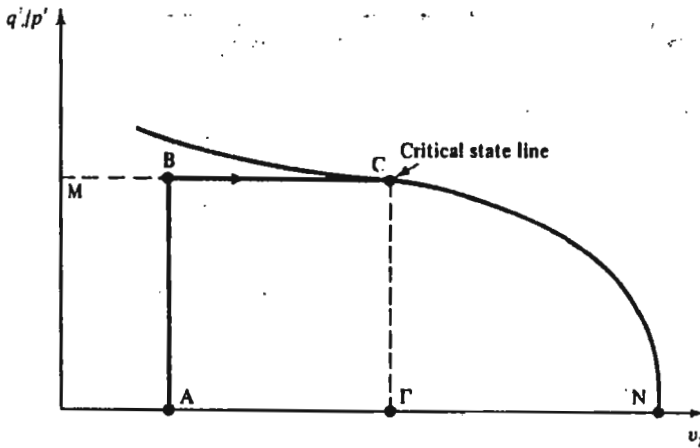


Figure 12-22 The stress path for an undrained test on dense sand in  $q'/p' : v_\lambda$  space

and, at the critical state, where, because the sample is undrained,  $v = v_0$ ,

$$\Gamma = v_0 + \lambda \ln p'_u. \quad (12-18)$$

Subtraction of Eq. (12-17) from Eq. (12-18) gives

$$p'_u/p'_0 = \exp[(\Gamma - v_{\lambda_0})/\lambda] \quad (12-19)$$

Thus, as  $\Gamma > v_{\lambda_0}$ , the mean normal effective stress on the specimen must increase as the sample moves towards the critical state, i.e., there must be a negative pore pressure generated. The value of  $p'_u$  increases exponentially with the difference  $(\Gamma - v_{\lambda_0})$ , and so a dense sample of sand, for which  $\Gamma - v_{\lambda_0}$  is large, will reach the critical state at extremely large values of  $p'_u$ . Conversely, a loose sample of sand, for which  $\Gamma - v_{\lambda_0}$  would be much smaller, would reach the critical state line at rather lower values of  $p'_u$ . The corresponding test paths in  $q' : p'$  and  $v : p'$  space are illustrated in Fig. 12-23. The loose sample follows the path  $A_1 B$  and ends on the critical state with a relatively low negative value of  $u_f$ , while the dense specimen follows the path  $A_2 C$  and reaches C on the critical state line with a high value of  $p'$  and a large negative pore pressure  $u_f$ .

Figure 12.23 indicates that, for sands, the Hvorslev surface should be thought of only as a state boundary surface beyond which samples cannot progress. There is no guarantee that the paths followed during testing will necessarily coincide with the Hvorslev surface, and, indeed, the undrained path is somewhat below the Hvorslev surface; nevertheless, although the failure state may lie below the Hvorslev surface it will not fall below the critical state line.

It should be noted that the interpretation of undrained tests discussed above relies on Eq. (12-16). The equation was developed by assuming that all work which crossed the boundaries of a specimen was dissipated in



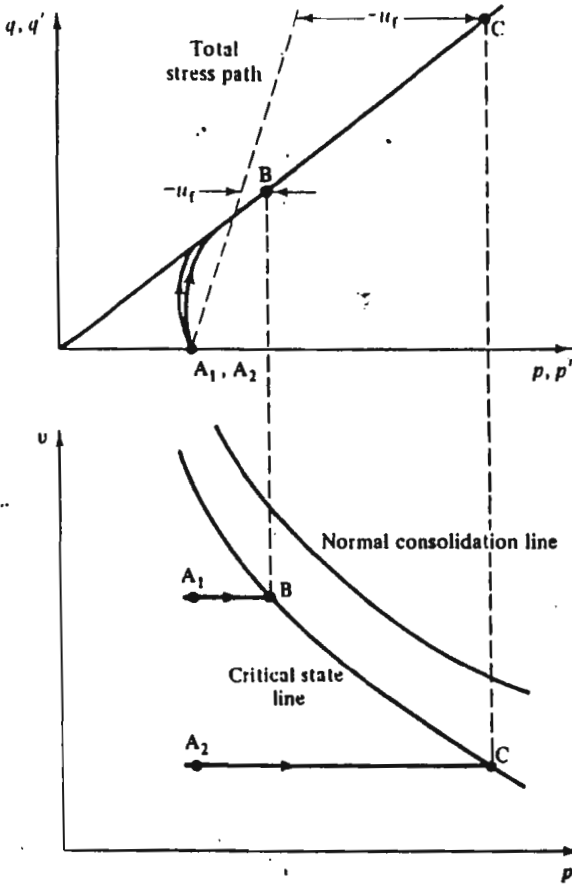


Figure 12-23 Test paths for undrained tests on loose and dense specimens of sand in  $q' : p'$  and  $v : p'$  space

friction. In reality, a certain proportion of the work will be stored in elastic compression of the specimen. For undrained tests, where the volume of the sample remains constant, this has the consequence that there will be some (fairly small) elastic compression of the sample, which must be exactly balanced by some simultaneous dilation of the sand brought about by the increase of  $q'/p'$ . We expect, therefore, that the stress ratio  $q'/p'$  will slightly exceed  $M$  at stages of the test when there is a rapid increase of  $p'$ .

**Example 12-2** Calculation of the ultimate conditions in undrained tests on samples of sand with different specific volumes

Two samples of sand are consolidated to  $p' = p = 200 \text{ kN m}^{-2}$  and subjected to undrained compression tests with the value of  $p$  held

constant. After consolidation, Sample A has  $v = 1.60$  and Sample B has  $v = 1.75$ . The sand has  $\Gamma = 1.93$ ,  $\lambda = 0.03$ , and  $M = 1.42$ . Calculate the stresses when the samples reach their ultimate conditions on the critical state line.

The initial value of  $v_{\lambda}$  is given, from Eq. (12-17), as

$$v_{\lambda_0} = v_0 + \lambda \ln p'_0.$$

Hence, for Sample A,

$$v_{\lambda_0} = 1.60 + 0.03 \ln(200) = 1.7589$$

and, for Sample B,

$$v_{\lambda_0} = 1.75 + 0.03 \ln(200) = 1.9089.$$

The value of  $p'$  at the ultimate condition is

$$p'_u = p'_0 \exp[(\Gamma - v_{\lambda_0})/\lambda].$$

Hence, for Sample A,

$$(p'_u)_A = 200 \exp[(1.93 - 1.7589)/0.03],$$

$$(p'_u)_A = 59\,970 \text{ kNm}^{-2}$$

and, for Sample B,

$$(p'_u)_B = 200 \exp[(1.93 - 1.9089)/0.03],$$

$$(p'_u)_B = 404 \text{ kNm}^{-2}.$$

The value of  $q'$  at the ultimate condition is

$$q'_u = Mp'_u.$$

Hence, for Sample A,

$$(q'_u)_A = 1.42(59\,970)$$

$$(q'_u)_A = 85\,160 \text{ kNm}^{-2}$$

and, for Sample B,

$$(q'_u)_B = 1.42(404)$$

$$(q'_u)_B = 574 \text{ kNm}^{-2}.$$

The value of  $p$  was held constant in each test at  $200 \text{ kNm}^{-2}$  and so the pore pressure  $u$  at the ultimate conditions can be calculated simply as

$$u_u = p - p'_u.$$

Hence, for Sample A,

$$(u_u)_A = 200 - 59\,970$$

$$(u_u)_A = -59\,770 \text{ kNm}^{-2}$$

and, for Sample B,

$$(u_a)_B = 200 - 404$$

$$(u_a)_B = -204 \text{ kNm}^{-2}$$

As cavitation of the pore water occurs at about  $u = -100 \text{ kNm}^{-2}$ , it would be necessary to apply a back pressure to reach the ultimate conditions in either test. The back pressure required for Sample A is impractically high and so the test would have to be terminated before the ultimate conditions were reached.

## 12-6 SUMMARY

1. The shear behaviour of sand may be fitted into the same framework that served for clay.
2. Sand samples are usually on the dry side of the critical state line and their behaviour must, therefore, be compared with heavily overconsolidated clay.
3. A state boundary surface similar to the Hvorslev surface for clays limits the extent of stress paths in  $q' : p' : v$  space, and the shape of the surface is such that sands, like overconsolidated clays, can support values of  $q'/p'$  greater than  $M$ .
4. There is a link between the stress ratio  $q'/p'$  and the rate of dilation ( $-\delta\varepsilon_v/\delta\varepsilon_n$ ) of the sand. The highest values of  $q'/p'$  will be observed for samples which are dense, when they are tested drained at low stress levels, since they will dilate strongly at failure.

## REFERENCES

- Bishop, A. W. and Henkel, D. J. *The Measurement of Soil Properties in the Triaxial Test*, Edward Arnold, London, 1962.
- Cole, E. R. L. The behaviour of soils in the simple shear apparatus. PhD Thesis, University of Cambridge, 1967.
- Eldin, A. K. G. Some fundamental factors controlling the shear properties of sand. PhD Thesis, University of London, 1951.
- Rowe, P. W. The stress-dilatancy relation for static equilibrium of an assembly of particles in contact. *Proc. R. Soc. A*, 264, 500-527, 1962.
- Stroud, M. A. The behaviour of soils in simple shear. PhD Thesis, University of Cambridge, 1971.
- Taylor, D. W., *Fundamentals of Soil Mechanics*. Wiley, New York, 1948.
- Vesic, A. S. and Clough, G. W. Behaviour of granular materials under high stresses. *Proc. Am. Soc. Civil Engrs*, 94, SM3, 661-688, 1968.

## BEHAVIOUR OF SOILS BEFORE FAILURE

### 13-1 INTRODUCTION

In the last three chapters we have introduced the concepts of the critical state line and the state boundary surface for sands and clays. The stress paths followed by soils in drained and undrained tests have been identified, and methods of calculating volumetric strains to the ultimate condition on the critical state line have been described. So far, however, we have not considered the magnitude of the shear strains and we have not considered the stress-strain behaviour of a sample early on in a test.

In order to consider deformations at an early stage of a test, it is necessary, and indeed essential, to make a distinction between elastic and plastic strains and to develop a criterion which determines whether a particular loading path produces elastic or plastic strains. We will also discuss the application of the theories of elasticity and plasticity to the stress-strain behaviour of soil. We shall find that interpretation of soil deformations in terms of these theories gives extra insight into the critical state framework developed in the preceding chapters. It also allows quantitative estimates to be made of the shear and volumetric strains caused by loading.

We go on to discuss the Cam-clay theory, which uses ideas of elasticity and plasticity expressed in quantitative mathematical terms. We have chosen to discuss the original simple Cam-clay theory, which is described by Schofield and Wroth (1968, pp. 134-166) in more detail, because it is simple, it illustrates how the various concepts fit together, and it is the basis for much recent work on the stress-strain behaviour of soil. Nevertheless, readers should be aware that although predictions of the theory are broadly correct, they are unsatisfactory in some respects and the simple theory has been superseded by theories which, although conceptually similar to Cam-clay, are mathematically more complex. The reader must be referred to recent research papers and conferences for an up-to-date account

### 13-2 ELASTIC AND PLASTIC DEFORMATIONS: THE ELASTIC WALL

It is first necessary to make a distinction between elastic (recoverable) and plastic (irrecoverable) strains. This distinction is commonly made in the

discussion of the behaviour of metals. Thus, the behaviour of metal can often be idealized as shown in Fig. 13-1. For uniaxial applied stresses less than  $\sigma_y$ , the deformation is linearly elastic and, if the metal is loaded and unloaded, the strains caused on loading are fully recovered on unloading. However, if the metal is loaded beyond a stress  $\sigma_y$ , additional plastic strains occur and the state of the metal might be represented by point G. When the metal is unloaded it follows path GB and some (elastic) strain is recovered. However, at B, the metal has suffered a large irrecoverable plastic strain. If the metal is reloaded from B the deformation is linearly elastic for applied stresses less than  $\sigma_g$ , which is greater than  $\sigma_y$ . The stresses  $\sigma_y$  and  $\sigma_g$  at which the behaviour of the metal becomes plastic are known as *yield stresses* and an effect of plastic straining from Y to G is to raise the yield stress from  $\sigma_y$  to  $\sigma_g$ ; this effect is known as *strain hardening*. If the metal is loaded beyond G it will eventually fail at F where the stress is  $\sigma_f$ .

For soil, the distinction between recoverable and irrecoverable strain is best illustrated by behaviour during isotropic compression. The normal consolidation line for a clay is indicated by line ABC in Fig. 13-2. If the clay is unloaded from B, it moves along the swelling line BD. If it is reloaded from D, the soil retraces path DB to B, after which additional compressions occur as the sample moves down the normal consolidation line to C. Similarly, if the sample is unloaded from C, it moves back along the swelling line to E. We should note that, at a fixed value of mean normal effective stress, the sample is at a lower specific volume at E than at D, i.e., some irrecoverable (plastic) strain has occurred on the path DBCE. We know that the strains are recoverable along the swelling lines DB and EC, and so the plastic strains must have occurred over path BC, that part of the path that lies on the state boundary surface. There is a direct analogy with the

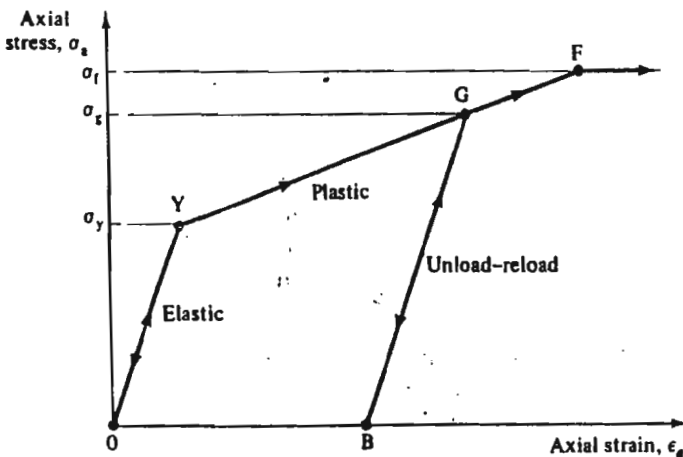


Figure 13-1 Elastic-plastic behaviour of metal

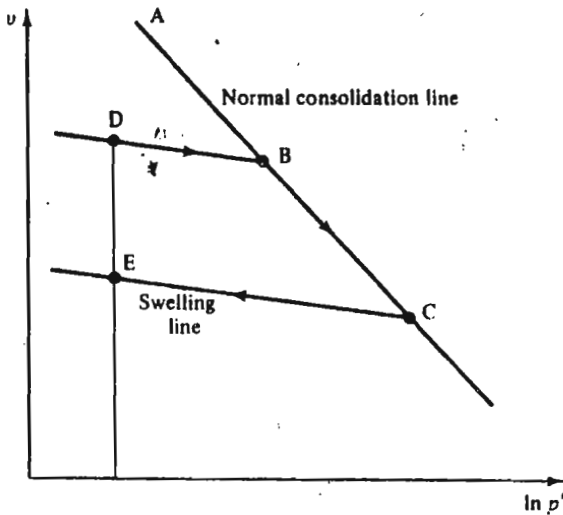


Figure 13-2 Elastic-plastic behaviour of clay in isotropic compression and swelling

occurrence of plastic strains over the path YG for the metal specimen of Fig. 13-1.

We can generalize this observation, and argue for soils that plastic (irrecoverable) strains only occur *when the sample is traversing the state boundary surface*. Thus, for paths below the state boundary surface, the strains are purely elastic and recoverable. This hypothesis leads to some strong limitations on the paths that can be followed by specimens. For example, because irrecoverable (plastic) strain has occurred between points D and E of Fig. 13-2, it means that the test path followed by the specimen must have touched the state boundary surface between D and E. The path DBCE satisfies that requirement because section BC (the normal consolidation line) lies on the Roscoe surface. An alternative path for the specimen to move from D to E is for it to be sheared at constant  $p'$ . Then, in order that the necessary irrecoverable strains occur, the test path must be such that  $q'$  increases so that the test path strikes the Roscoe state boundary surface at G (Fig. 13-3), above D, before the path traverses the state boundary surface to K, above E. As the value of  $q'$  reduces, the sample then deforms only elastically as it moves to E. The value of  $q'$  at G fixes the value of  $q'$  which must be applied to the sample at D (when  $p'$  is held constant) in order to cause irrecoverable deformation.

There is a range of other paths by which the sample could move from D to E; all of them require that the sample moves across the state boundary surface. Conversely, there is a range of paths which may be followed by a sample at D without plastic deformation occurring. All paths that remain on the curved vertical plane above the swelling line BD, but below the state

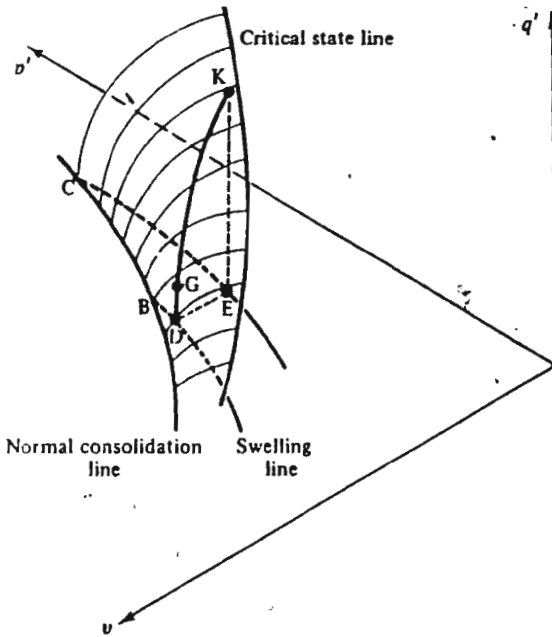


Figure 13-3 The test path from points D to E in  $q' : p' : v$  space

boundary surface, will cause only elastic deformation of the soil; this curved surface, BJIH in Fig. 13-4 is called the *elastic wall*. Of course there is an infinite number of elastic walls, each elastic wall being associated with a particular swelling line.

If the state of a sample is below the state boundary surface, its behaviour is assumed to be elastic and stresses and strains may be related through the theory of elasticity. On the other hand, if the state of a sample lies on the state boundary surface, both plastic and elastic strains may occur and the plastic strains may be calculated from the theory of plasticity. The importance of the distinction between elastic and plastic strains is that elastic strains are relatively small, while plastic strains are relatively large. Thus, if a loading on a soil stratum causes only elastic strains, we expect that the soil deformations would be small. Conversely, soil deformations and settlements will be large if significant amounts of plastic strain occur in the soil stratum.

For the theoretical calculation of soil deformations, the distinction between elastic and plastic strains is important, for the two types of strain are computed completely differently.

### 13-3 CALCULATION OF ELASTIC STRAINS

The behaviour of an ideal isotropic elastic soil was discussed in Sec. 4-11. We began with the generalized form of Hooke's law in Eqs (4-66) and we

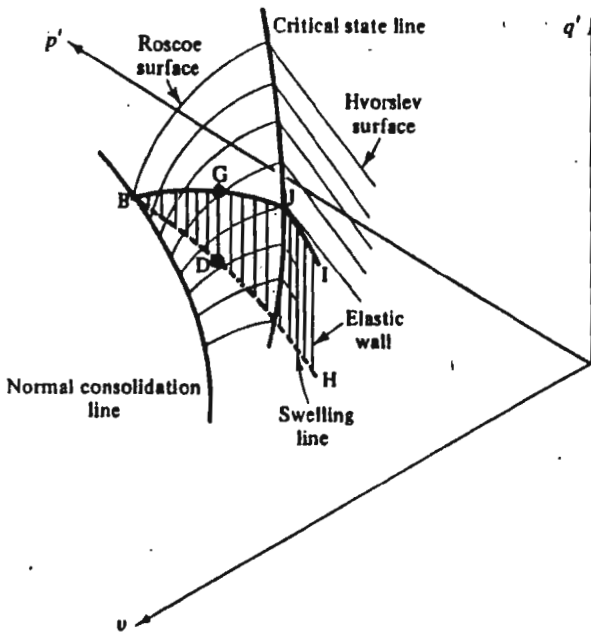


Figure 13-4 The elastic wall

showed that increments of strain could be related to increments of effective stress more conveniently through the use of invariants by Eqs (4-76) and (4-77). These were

$$\delta \varepsilon_v = \frac{1}{K'} \delta p' + 0. \delta q', \quad (13-1)$$

$$\delta \varepsilon_s = 0. \delta p' + \frac{1}{3G'} \delta q', \quad (13-2)$$

where  $K'$ , the elastic bulk modulus, and  $G'$ , the elastic shear modulus, were constants over the appropriate increments of stress and strain. Equations (13-1) and (13-2) show that, for an ideal isotropic elastic soil, volumetric strains are connected with  $p'$  and separated from  $q'$  and shear strains are connected with  $q'$  and separated from  $p'$ .

We have now postulated the existence of the elastic wall BJIH in Fig. 13-4 and suggested that the path of an overconsolidated soil whose state lies below the state boundary surface must remain on a particular elastic wall; consequently, the path followed by a sample of an overconsolidated soil during loading or unloading will follow the line of intersection of the elastic wall and the appropriate drained or undrained loading planes discussed in Section 10.5. Thus, Fig. 13-5 shows the line of intersection DG of the elastic



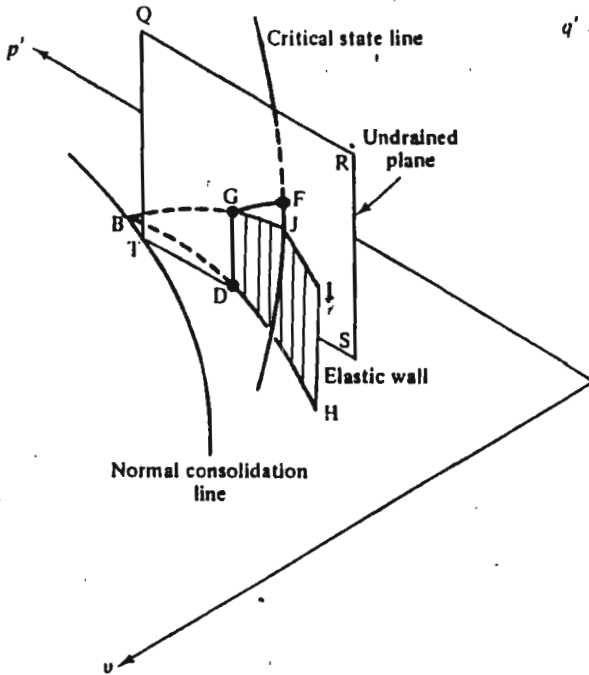


Figure 13-5 Intersection of an elastic wall and an undrained plane

wall and an undrained plane QRST for a constant volume loading or unloading test. The path DG rises vertically from D to G, which is on the state boundary surface. If the sample is loaded beyond G it will suffer plastic strains as its state traverses the state boundary surface along its intersection with the undrained plane towards its ultimate state at F at the intersection of the critical state line and the undrained plane.

For undrained loading of saturated soil, when  $\delta\varepsilon_v = 0$ , Eq. (13-1) has the consequence that

$$\delta p' = 0. \quad (13-3)$$

This confirms that the stress path DG in Fig. 13-5 rises vertically up the intersection of the undrained plane and the elastic wall. It was for this reason that we sketched undrained effective stress paths on overconsolidated samples, in Fig. 11-15 and elsewhere, as being vertical until they reached the state boundary surface.

Figure 13-6 shows the intersection DG of an elastic wall and a drained plane QRST, and this is the path followed by a sample of isotropic elastic soil during loading or unloading in a drained triaxial compression test; the line DG is not straight because the elastic wall is curved in plan and there is a reduction in volume associated with an increase of  $p'$ . It was for this

reason that we showed, in Fig. 11-22 and elsewhere, that there was compression of overconsolidated samples in drained triaxial tests before the sample reached the state boundary surface. If the sample is loaded beyond G (Fig. 13-6), it will suffer plastic strains as its state traverses the state boundary surface along its intersection with the drained plane towards its ultimate state at F, where the critical state line and the drained plane intersect.

We now have sufficient information to calculate the shear and volumetric strains in a sample of ideal isotropic elastic soil as it is loaded or unloaded in drained triaxial compression along DG. The elastic wall is vertically above a swelling line BDF introduced in Chapter 7 and is therefore given by

$$v = v_c - \kappa \ln p' \quad (13-4)$$

or

$$\delta v = -\kappa(\delta p'/p'). \quad (13-5)$$

Hence, from Eq. (4-54),  $\delta \epsilon_v = -\delta v/v$ , we have

$$\delta \epsilon_v = (\kappa/vp') \delta p'. \quad (13-6)$$

Thus, the bulk modulus  $K'$  for the soil is given by

$$K' = vp'/\kappa, \quad (13-7)$$

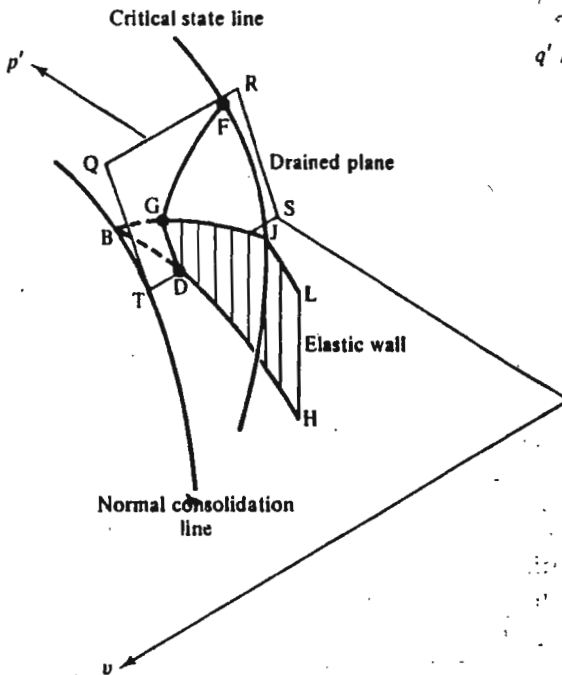


Figure 13-6 Intersection of an elastic wall and a drained plane

and using the result for elastic materials that

$$\frac{G'}{K'} = \frac{E'}{2(1+\nu')} \frac{3(1-2\nu')}{E'} = \frac{3(1-2\nu')}{2(1+\nu')} \quad (13-8)$$

gives

$$G' = \frac{\nu p' 3(1-2\nu')}{\kappa 2(1+\nu')} \quad (13-9)$$

So, from Eq. (13-2),

$$\delta \varepsilon_a = \frac{2\kappa(1+\nu')}{9\nu p'(1-2\nu')} \delta q' \quad (13-10)$$

Equations (13-6) and (13-10) define the stress-strain behaviour of a soil undergoing ideal isotropic elastic deformations during a drained triaxial compression test along a path such as DG in Fig. 13-6. They are also valid for any loading path in which the state of the soil remains below the state boundary surface. In particular, Eqs. (13-6) and (13-10) are valid for any undrained loading path such as DF in Fig. 13-5, in which case  $\delta \varepsilon_v = \delta p' = 0$  and increments of shear strain are related to increments of  $q'$  by Eq. (13-10).

Equation (13-7), together with the definition of bulk modulus  $K'$  in terms of  $E'$  and  $\nu'$ , gives

$$K' = \nu p' / \kappa = E' / 3(1-2\nu') \quad (13-11)$$

and, hence,

$$E' = 3\nu p'(1-2\nu') / \kappa \quad (13-12)$$

Values for  $E'$  and  $\nu'$  may be obtained directly from the results of a drained triaxial compression test in which  $\Delta \sigma'_3 = \Delta \sigma'_r = 0$  and axial and radial strains are measured. From the generalized Hooke's law in Eqs (4-67), putting  $\delta \sigma'_3 = \delta \sigma'_r = 0$

$$E' = \delta \sigma'_a / \delta \varepsilon_a \quad (13-13)$$

$$\nu' = -\delta \varepsilon_r / \delta \varepsilon_a \quad (13-14)$$

In this treatment of elastic behaviour in soils, the value of Young's modulus  $E'$  as given by Eq. (13-12) depends on the current values of  $\nu$  and  $p'$ , on the value of  $\kappa$  which defines the slope of a swelling line as well as on  $\nu'$ . Even though we assume that  $\nu'$  is constant, the value of  $E'$  will not be constant and the soil behaviour, even if it is isotropic and elastic, will not be linear; Eqs (13-6) and (13-10) are, therefore, valid only for increments of loading sufficiently small so that the value of  $E'$  may be assumed to be constant. However, in many cases the change of specific volume  $\nu$  during a loading path which causes only elastic strains, and which therefore, remains on a particular elastic wall, is relatively small and so the value of  $E'/p'$  will remain approximately constant. Hence, we may write

$$E'/p' = 3\nu(1-2\nu')/\kappa \simeq \text{constant} \quad (13-15)$$

Consequently, for a drained loading or unloading test on a soil in the elastic range in which the value of  $p'$  changes during loading, we would expect the stress-strain behaviour to be non-linear. On the other hand, for any undrained loading, or unloading of an isotropic soil in the elastic range  $\delta p' = 0$  and, hence, in theory, the stress-strain behaviour should be linear.

The treatment in this section illustrates a simple, but fairly realistic, approach to the non-linear elastic behaviour of soils; recent work at Cambridge and elsewhere suggests that there are certain additional mathematical and theoretical restrictions on the permissible relationships between the elastic parameters which must be allowed for in a rigorous treatment.

### 13-4 CALCULATION OF ELASTIC STRAINS FOR UNDRAINED LOADING IN TERMS OF TOTAL STRESSES

So far, in accordance with the principle of effective stress, we have quite properly related increments of elastic strain to increments of effective stress. However, for the special case of undrained loading of saturated soil when there is no volume change, it is convenient to relate increments of strain to increments of total stress, ignoring any pore pressures generated. This technique of considering total stresses instead of effective stresses is common in soil mechanics and it is a technique which we will consider again in Chapter 14, in connection with the undrained strength of soils.

For undrained elastic behaviour in terms of total stress, we define an undrained Young's modulus  $E_u$  and an undrained Poisson's ratio  $\nu_u$ . These have the same meanings as  $E'$  and  $\nu'$ , but are defined in terms of total stresses for undrained loading of saturated soil. Hence, by analogy with Eqs (13-13) and (13-14), for an undrained triaxial test with  $\Delta\sigma_3 = \Delta\sigma_r = 0$  we have

$$E_u = \delta\sigma_u / \delta\varepsilon_u, \quad (13-16)$$

$$\nu_u = -\delta\varepsilon_r / \delta\varepsilon_u, \quad (13-17)$$

and the generalized form of Hooke's law for undrained loading in terms of total stresses becomes

$$\left. \begin{aligned} \delta\varepsilon_1 &= (1/E_u) [\delta\sigma_1 - \nu_u \delta\sigma_2 - \nu_u \delta\sigma_3], \\ \delta\varepsilon_2 &= (1/E_u) [\delta\sigma_2 - \nu_u \delta\sigma_3 - \nu_u \delta\sigma_1], \\ \delta\varepsilon_3 &= (1/E_u) [\delta\sigma_3 - \nu_u \delta\sigma_1 - \nu_u \delta\sigma_2]. \end{aligned} \right\} \quad (13-18)$$

Following earlier arguments, the behaviour of an ideal isotropic elastic soil during undrained loading in terms of invariants of total stress is given by

$$\delta\varepsilon_v = \frac{1}{K_u} \delta p + 0 \cdot \delta q, \quad (13-19)$$

$$\delta\varepsilon_s = 0 \cdot \delta p + \frac{1}{3G_u} \delta q, \quad (13-20)$$